

Frank Arthur

Modelling and characterization
of climate, environment,
and human impact during
the Holocene and Eemian
using an Interactive Physical
Downscaling

Dissertation for the
degree of Ph.D
Ecology

Faculty of Technology, Natural
Sciences and Maritime Studies

Frank Arthur

Modelling and characterization of
climate, environment, and human
impact during the Holocene and
Eemian using an Interactive
Physical Downscaling

A PhD dissertation in
Ecology

© 2024 Frank Arthur

Faculty of Technology, Natural Sciences and Maritime Studies
University of South-Eastern Norway
Bø

Doctoral dissertations at the University of South-Eastern Norway no. 199

ISSN: 2535-5244 (print)
ISSN: 2535-5252 (online)

ISBN: 978-82-7206-868-3 (print)
ISBN: 978-82-7206-869-0 (online)



This publication is licensed with a Creative Commons license. You may copy and redistribute the material in any medium or format. You must give appropriate credit, provide a link to the license, and indicate if changes were made. Complete license terms at <https://creativecommons.org/licenses/by-nc-sa/4.0/deed.en>

Cover image: © Animea, Frédéric Durillon. Reproduced with permission
Print: University of South-Eastern Norway

Acknowledgments

This PhD journey has been made possible through the support and contribution of several people. In the first place, I would like to express my deepest gratitude to my supervisor, Hans Renssen for his unwavering support, guidance, and invaluable mentorship throughout the entire journey of my doctoral research. He was available whenever I needed help and the speed at which he provided comments on my manuscript was just amazing. Special thanks to my co-supervisor Didier Roche for being a great supervisor, he helped me with most of the technical stuff related to the iLOVECLIM model and his contribution to reviewing my papers and the dissertation has been very helpful. I am also thankful to Ralph Fyfe, Aurélien Quiquet, Marie José Gaillard and Karl-Johan Lindholm. Their expertise, encouragement, and constructive feedback have been instrumental in shaping this dissertation and in shaping me as a researcher.

I am indebted to the staff of the department (especially Live, Rune, Hanna and Veronica), whose dedication to the project provided me with a stimulating environment to pursue my research. Their support and resources have been instrumental in the successful completion of this dissertation.

I am also immensely thankful to the EU Horizon 2020 (TerraNova) for the funding of this project. I thank all the team members within the project, including the PI's and the 15 Early-Stage PhD Researchers that I have worked with throughout the project. Special thanks to Sjoerd and Ruud for organizing the TAFS meetings.

Again, big thanks go to all the other PhD colleagues/friends (Peter, Rasmus, Daniel, Benedikte, Hanna, Jenny, Tom Robin, Thilde, Nicolas, Jenny Hanssen, Ashlee, Bright, Christian, Ally, Rick, Karolis, Zohreb and Jasmine) for the scientific advice, encouragement, coffee breaks, lunch breaks and parties. You made the PhD life quite relaxed and interesting. I learned a lot from you.

I am grateful to all the participants and co-authors, especially Kailin and Angelina who contributed to this research, without you this work would not have been possible. Their willingness to share their time, data and insights has been crucial to significantly enhance the quality of this dissertation.

I am thankful to all those who have played a role, big or small, in the completion of this dissertation. Your support and encouragement have been invaluable, and I am truly grateful for the opportunity to undertake this research and to contribute to the body of knowledge in my field.

Finally, and most importantly I would like to extend my heartfelt appreciation to my family for their unwavering love, encouragement, and understanding throughout this challenging yet rewarding journey. Thank you very much to my wife Leilat. Her constant believe in me has been the source of my strength. I thank you for your unwavering love, patience and encouragement throughout this journey. Special thanks to my daughter Kaliyah for bringing me joy while pursuing this research work. I will lastly thank my parents and siblings for showing interest in this project and always calling to check up on the progress of the work. Thank you, Joseph, Rebecca, Sandra, Eric and George.

Abstract

Keywords: Holocene, Eemian, Interactive Physical Downscaling, Archaeology, Climate modelling, Scandinavian Fimbulwinter, iLOVECLIM.

The study of the past climate is important as it provides valuable information about how the earth's climate has changed over long timescales and helps scientists to better understand natural climate processes and distinguish them from human-induced changes. The Holocene and Eemian epochs represent critical periods in Earth's climatic history, characterized by distinct climate conditions and significant implications for our understanding of past, present, and future climate dynamics. In this thesis, I employ an interactive physical downscaling to our Earth system model of intermediate complexity (iLOVECLIM) to conduct comprehensive simulations of the Holocene and Eemian climates, to unravel the regional intricacies of these pivotal periods. Utilizing the downscaling approach allows us to increase the resolution of the model from 5.56° to 0.25° latitude-longitude in Europe, enabling a detailed examination of regional climate dynamics, including temperature, precipitation, and vegetation patterns. This thesis includes four papers. Transient simulations using both the standard version of the iLOVECLIM and a version with an interactive physical downscaling were performed for the Eemian and the Holocene epoch, as reported in two separate papers. In addition, we have combined archeological data with our downscaled model to simulate the impact of the 536/540 AD volcanic eruption (the Fimbulwinter) within the Holocene period in Scandinavia. In a final paper, bias correction is applied to the downscaling scheme to correct climate model outputs by performing simulations within (the Mid Holocene, the Last Glacial Maximum, the pre-industrial and the Present day). The comparative analysis of these simulations offers a unique opportunity to assess the impact of varying boundary conditions, such as greenhouse gas concentrations, orbital parameters, and land surface characteristics on regional climate patterns. The results show that the interactive downscaling as expected provides more spatial variability in terms of temperature gradient and precipitation in topographic regions such as the Alps, the Scandes mountains and the Scottish Highlands. The results also agree well with other climate models and captures the magnitude of the temperature and precipitation patterns reconstructed by proxy reconstruction during the Holocene and the Eemian in Europe. For example, the Holocene simulations suggest that the downscaling technique simulates approximately 24% more precipitation than the standard version. The simulation for the Eemian at 127 ka produces a magnitude of temperature ($3 - 4^\circ\text{C}$) and precipitation of ($150 - 300\text{ mm/yr}$) change in the Northern part of Europe relative to pre-industrial which is similar to most reconstructions from proxies. Moreover, our simulations with volcanic eruptions applied in 536 and 540 AD reveal a significant cooling in Scandinavia (ensemble mean -1.1°C), with a sudden decrease in precipitation and a very sharp decline in growing degree days

(GDD0) following the volcanic event. Our results imply that a social shift that was already underway was intensified by this sudden climatic anomaly. In the fourth paper, there was a good agreement between the simulated results and the pollen-based biome reconstruction when bias correction was combined with the downscaling in the mid-Holocene and the pre-industrial. Our results demonstrate that we can simulate paleoclimate and vegetation in better agreement with independent reconstructions when bias correction is applied to simulated climate variables. Our study underscores the significance of downscaling as a valuable tool for unraveling the regional complexities of past climates and their implications for the present and future. The insights gained from this research have the potential to advance our understanding of Earth's climatic evolution, contributing to more robust climate models and enhancing our ability to assess the potential impact of ongoing and future environmental changes on regional climates.

List of papers

Paper 1

Arthur, F., Roche, D. M., Fyfe, R., Quiquet, A., & Renssen, H. (2023). Simulations of the Holocene climate in Europe using an interactive downscaling within the iLOVECLIM model (version 1.1). *Climate of the Past*, 19(1), 87–106. <https://doi.org/10.5194/cp-19-87-2023>.

Paper 2

Arthur, F., Zapolska, A., Roche, D. M., Li, H., Renssen, H.: Modelling the climate of the Eemian in Europe using an Interactive Physical Downscaling (Manuscript).

Paper 3

Arthur, F., Hatlestad, K., Lindholm, K. J., Loftsgarden, K., Löwenborg, D., Solheim, S., Roche, D.M., & Renssen, H. (2024). The impact of volcanism on Scandinavian climate and human societies during the Holocene: Insights into the Fimbulwinter eruptions (536/540 AD). *The Holocene*. <https://doi.org/10.1177/09596836231225718>

Paper 4

Zapolska, A., Vrac, M., Quiquet, A., Extier, T., **Arthur, F.**, Renssen, H., & Roche, D. M. (2023). Improving biome and climate modelling for a set of past climate conditions: evaluating bias correction using the CDF-t approach. *Environmental Research: Climate*, 2(2), 025004. <https://doi.org/10.1088/2752-5295/accbe2>

Abbreviations

GCM	General Circulation Models
EMIC	Earth System Models of Intermediate Complexity
SDM	Statistical Downscaling Models
RCM	Regional Climate Models
PMIP4	Paleoclimate Modelling Intercomparison Project Phase 4
(CMIP6)	Coupled Model Intercomparison Project Phase 6
CRU	Climate Research Unit
MPI-ESM	Max Planck Institute-Earth System Model
HTM	Holocene Thermal Maximum
CDF-t	Cumulative Distribution Function-transform
MH	Mid Holocene
LGM	Last Glacial Maximum
LIG	Last Interglacial

Table of Contents

Acknowledgments	I
Abstract.....	III
List of papers	V
Abbreviations	VII
1 Introduction.....	1
1.1 Objectives of this thesis.....	3
1.1.1 The climate system, its variation and mechanisms underlying climate change.	3
1.2 Climate modelling and proxy-based reconstructions	7
1.2.1 Climate models.....	7
1.2.2 Proxy-based reconstructions.....	11
1.3 Climate forcings during the Holocene and the Eemian.....	12
1.4 Previous modelling studies on the Holocene and Eemian climate	15
1.4.1 The Holocene.....	15
1.4.2 The Eemian	18
1.5 Climate modelling in archaeological studies: The link between volcanic eruption and the Fimbulwinter	20
1.6 The context of this PhD thesis: The TerraNova project.....	23
1.7 The Research Questions of the Thesis	24
2 Methods (Model and simulations).....	25
2.1 The iLOVECLIM climate model	25
2.2 Interactive physical downscaling	26
2.3 Climate model experiments and datasets used	27
2.3.1 Paper 1 – Transient simulations of the Holocene climate	27
2.3.2 Paper 2 – Transient simulations of the Eemian climate.....	28
2.3.3 Paper 3 – Simulation of the impact of volcanic forcing on the climate of the 6th century AD.....	28
2.3.4 Paper 4 – Application of bias correction to simulations of past climate.....	31
3 Summary of Main Results and Discussion.....	33

3.1	The impact of interactive downscaling on the Holocene climate in Europe (Paper 1).....	33
3.2	Modelling the climate during the Eemian in Europe with interactive downscaling (Paper 2)	36
3.3	The impact of volcanism on the Scandinavian climate and human societies during the Holocene (536 and 540 AD) – (paper 3).....	38
3.4	The impact of bias correction on the climate and vegetation (paper 4)	41
4	Conclusion and Future Perspective	45
5	Bibliography	49

1 Introduction

The study of past climates (so-called paleoclimates) is significant in a variety of ways. In addition to being generally interesting to learn about past climates, it also provides information on how climate changes and can be used to identify the processes that regulate the climate from both natural and anthropogenic perspectives (Goose, 2015; Strandberg, 2017). Additionally, it provides an important context for the current climate change. Paleoclimate studies provide valuable insights into Earth's climate history, including the study of long-term climate trends, the identification of natural climate variability, and the understanding of past climate responses to external factors such as volcanic eruptions or changes in solar radiation (Bradley, 2014). There are two main methods to study paleoclimates: numerical models and proxy-based reconstructions.

The past, present, and future climate change are studied using numerical climate models. The two main types of global climate models utilized are known as General Circulation Models (GCMs, McGuffie & Henderson-Sellers, 2005) and Earth system Models of Intermediate Complexity (EMICs, Claussen et al., 2002). These models are evaluated against historical and prehistorical data to increase their predictability power of the future climate. These climate models have been previously used to simulate the past climate, longer back in time (e.g., Zorita et al., 2005; Renssen et al., 2009; Williams et al., 2020; Liu et al., 2021; Otto-Bliesner et al., 2021), and are routinely compared to independent field-based data to assess their performance (Bonfils et al., 2004; Brewer et al., 2007; Bartlein et al., 2011; Mauri et al., 2015). These independent data are often called “proxy data” and are based on natural archives that contain climate information. However, this model-data comparison is often challenging and poses considerable uncertainties due to the disparity in spatial resolution between the simulated climate model outputs and proxy-based paleoclimate reconstructions (Ludwig et al., 2019). In addition, transient multi-millennial simulations with GCMs are still difficult due to the computational cost (for instance, a simulation of the last 11,500 years can take more than 6 months to run). Therefore, EMICs (like our model iLOVECLIM) have been developed that include simplified physics and use less computing time. This makes it possible to run multiple experiments over many thousands of years, which is good for paleoclimate studies because it helps to account for the inherent uncertainties in the modelling and provides a more robust estimate of the past climate which helps to include long-term processes as well (Goosse and Renssen, 2004). However, the computational efficiency of EMICs comes at a cost, as these coarse-resolution models do not include spatial details about the Earth's surface that may be important for climate, such as local topography, lake bodies and vegetation (Quiquet et al., 2018), and use

simplified representations of climatic processes (Claussen et al., 2002). The limitations of current global climate models in bridging the gap between its coarse resolution and regional-to-local scales, where the implications of climate change are of major concern, can be overcome by employing spatial downscaling. Downscaling is aimed at obtaining high-resolution information from coarser-resolution data (Castro et al., 2005). There are two main types of downscaling: statistical and dynamical downscaling (Murphy, 1999). However, there is another type called geographical downscaling which usually deals with land use mapping at the local level for agriculture and economic purposes (Cantelaube et al., 2012).

Statistical downscaling models (SDMs) involve developing statistical relationships between large-scale atmospheric variables (such as those provided by GCMs, e.g., pressure field) and local-scale weather variables such as temperature and precipitation (Lorenz et al., 2016). By analyzing historical data and identifying patterns, statistical downscaling techniques can be used to estimate local weather conditions based on larger-scale information from global or regional models. Dynamical downscaling involves the use of Regional Climate Models (RCMs) to produce high-resolution climate simulations for specific geographic areas. These models take the output from global climate models (GCMs) as input and then use additional data and algorithms to generate detailed climate information at a finer scale. By incorporating topographic features, land use, and other local influences (e.g., Ludwig et al., 2019).

This thesis begins by outlining the fundamentals of climate and the climate system. After that, the principles behind climate models and how climate modelling works from a paleoclimate perspective are highlighted. The thesis continues to outline the importance of paleoclimatology and proxy-based reconstructions. The first part of the thesis ends by describing the past climates of warm periods such as the Holocene (the last 11,500 years) and the Eemian (127,000 to 116,000 yr BP, year before present), which will highlight the forcings and boundary conditions that control these climates. The second part will describe the methods and the climate model tool used for all 4 papers included in the thesis. The next part summarizes the results of the papers included in this thesis with emphasis on climate and archaeological data. Finally, conclusions and future perspectives are made regarding the response of the climate to downscaling as well as the significance of applying downscaling to climate models from a paleoclimate context.

1.1 Objectives of this thesis

The main objective of this thesis is to improve our low-resolution climate model by applying downscaling to be able to capture regional or local climate features that are important for impact assessments at smaller scales. In this study, I therefore, performed transient simulations of the Holocene and Eemian climate in Europe with both the low-resolution version of the iLOVECLIM model and a high-resolution version with downscaling applied. The interactive physical downscaling allows for higher spatial resolution simulations, providing more detailed information on climate patterns, such as temperature and precipitation at local levels which is important for paleoclimate research. A second important objective of this work is to produce downscaled climate data which will be useful for prehistorical and historical climate analysis, allowing researchers to examine past climate conditions at high spatial resolutions and helping in understanding climate variability, detecting long-term trends, and studying historical climate events in more detail. In this thesis, one specific case is explored, focused on the Fimbulwinter event (536/540 AD), a period within the last millennium with a forcing by volcanic eruptions. For this second objective, this thesis also contributes to the improvement of paleoclimatic data quality by applying bias correction to different past climate conditions (i.e., The Last Glacial Maximum, Mid-Holocene, Pre-industrial and Present day).

1.1.1 The climate system, its variation and mechanisms underlying climate change.

Climate as defined by the IPCC (2013) “as the statistical description in terms of the mean and variability of relevant quantities over a period ranging from months to thousands or millions of years”. It is determined by several factors, including temperature, precipitation and prevailing wind patterns. The climate system is very chaotic and dynamic which consists of five key components: the atmosphere (the gaseous cover extending from the Earth’s surface to outer space with a mixture of gasses), the hydrosphere (encompasses all the Earth’s water, i.e. ocean, rivers, lakes, groundwater, etc), the cryosphere (Earth’s frozen water, i.e. sea ice, glaciers, permafrost, ice sheets, etc), the lithosphere (the upper layer of the solid Earth, both continental and oceanic), the biosphere (ecosystems and living organisms), and the interactions between them (IPCC, 2013). The climate system changes over time because of its internal dynamics, as well as external forcings like solar variations and anthropogenic forcings such as the changing composition of the atmosphere and land use change (IPCC, 2013).

Through physical, chemical, and biological processes and feedbacks, these components interact with one another in terms of heat, energy, and momentum. For instance, the distribution of heat is influenced by the heat exchanges between the components of the ocean and atmosphere, primarily through latent heat and related to the hydrological cycle (Fig 1) (IPCC, 2013). In the meantime, numerous feedbacks, for example, those related to albedo, link the various components of the atmosphere and cryosphere together and have an impact on the radiation budget of the climate system (Goosse, 2015). The complexity of the climate system and the interconnections between its various components make climatology an interdisciplinary subject area in which physical and chemical processes regulate the climate of the Earth (McGuffie & Henderson-Sellers, 2005).

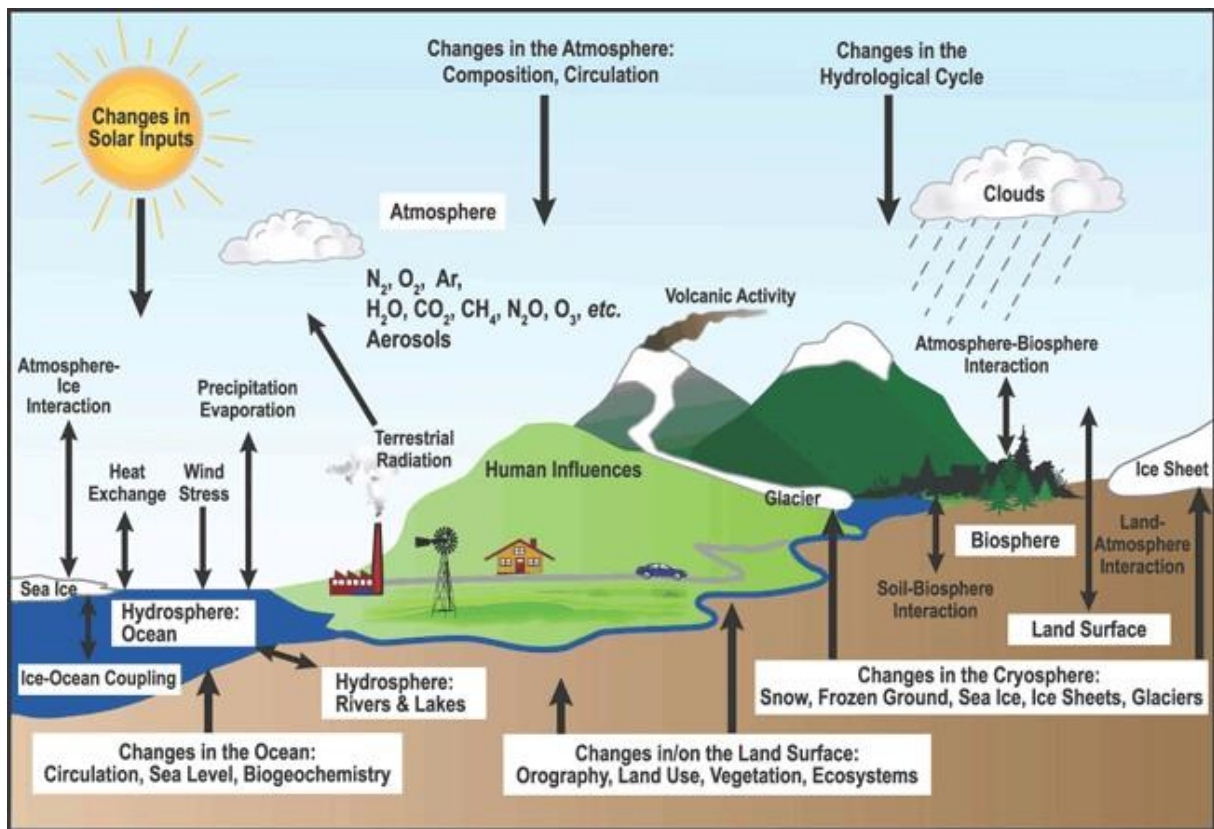


Fig 1: The interactions within the climate system (IPCC, 2013).

The climate system is a complex and dynamic system that is constantly being influenced by a variety of factors. Forcings are factors outside the climate system that drive or control the climate. Feedbacks are factors that transfer changes within the system, and boundary conditions refer to the non-time-dependent features of a system that define its boundaries (Fig 3) (Bakker, 2014). Boundary conditions can also be

factors not considered explicitly in a model and can vary. In general, three external forcings affect the climate system: the amount of solar radiation that reaches the Earth's surface, plate tectonics and the orbital configuration of the Earth (Ruddiman, 2001). On the other hand, the timescale of each of these processes varies greatly. For instance, processes involving clouds, snow, water vapor, sea ice, dust, the upper ocean and aerosols operate on timescales ranging from years to decades (Fig 2. Palaeosens Project members, 2012). There are also decadal timescales that are relevant for sea ice and GHG concentrations and a wide range of decadal to multi-millennial timescales that are important for the deep oceans. Processes related to the carbon cycle and land ice span from centennial to multi-millennial timescales (Fig 2), while processes such as weathering, plate tectonics, and vegetation evolution operate on timescales spanning millions of years (Fig 2).

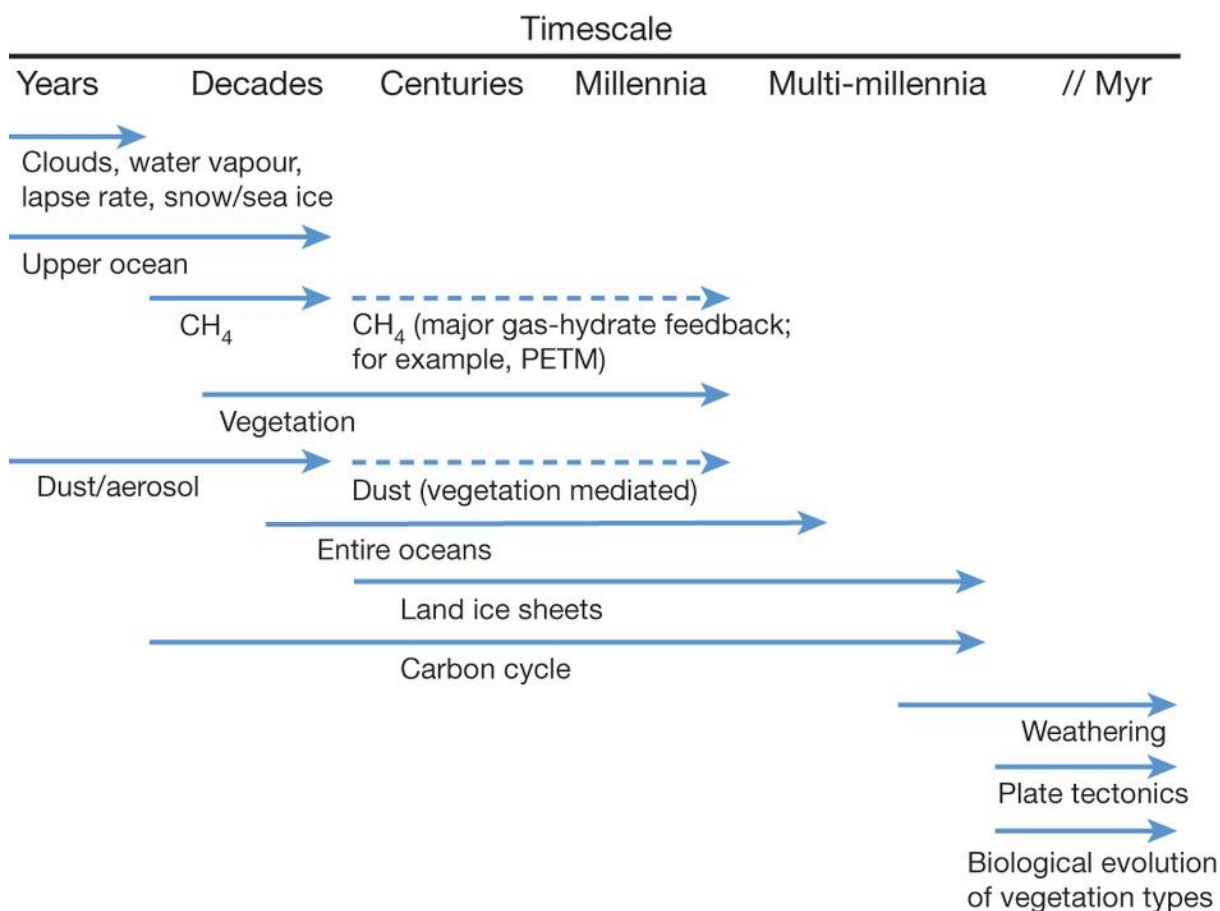


Fig 2: Typical timescales of different processes in the climate system. Figure from Palaeosens Project members (2012).

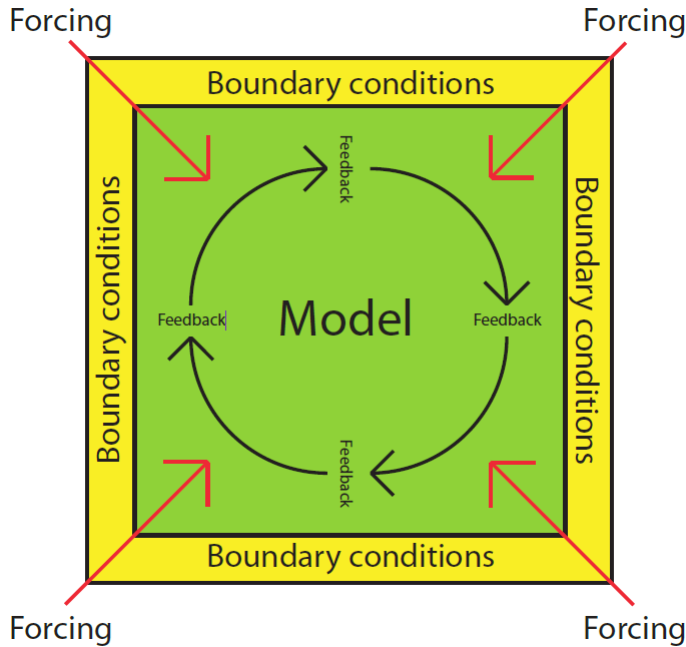


Fig. 3: Schematic showing a general model setup. (Bakker, 2014).

It is possible to determine whether a process qualifies as a boundary condition or as feedback by looking at the timescales of the climate system feedbacks (Palaeosens Project members, 2012). A climatic process can be considered a boundary condition if its timescale is longer than the time scale of interest (Bakker, 2014). In Paleoclimate studies, the same process can be either a forcing, feedback or a boundary condition (Fig 3), depending on the research question and the part of the climate system that is studied (Bakker, 2014). For example, if the atmosphere-ocean system is studied in an AOGCM, then the ice sheets are normally fixed throughout the simulation and are treated as a boundary condition. If the ice sheet is varied through time, then it can be a forcing (Goosse, 2015). However, if the GCM includes an interactive ice sheet model, then it is part of feedbacks in the system since the ice sheets can grow or melt in response to cooling or warming, and thus also affect the climate (Goosse, 2015).

To further explore the distinction between forcings, feedbacks and boundary conditions, we can use the evolution of the climate over millions of years as a reference period. Fig 2 shows the climate forcings: variations in the orbital configuration of the sun; changes in the amount of solar radiation that reaches the Earth's surface; processes related to tectonic movements such as the bathymetry of the ocean and evolution of the topography of continents, weathering and the transfer of heat and material from within the earth into the climate system; and the long-term evolution of vegetation (Bakker, 2014). All other activities within this time range can be considered as climate system feedbacks, and no boundary

condition needs to be set. However, for a time scale of hundreds of thousands of years, bathymetry, topography, weathering, Earth's heat flux and vegetation evolution can be assumed constant and consequently be considered as boundary conditions of the climate system (Bakker, 2014). Global sea level and ice sheet configuration are usually regarded as boundary conditions of the climate system on multi-millennial timescales, thereby ignoring any potential forcings and feedbacks related to it. It is also possible to assume that the deep ocean circulation and the orbits of the sun, moon, earth, and other planets will remain constant across even shorter durations, such as decadal to centennial. (Palaeosens Project members, 2012; Bakker, 2014). Thus, in this case, the only remaining natural climatic forcings are variations in the sun's energy output and the gases released by volcanoes, however, the latter have also been proposed as feedback mechanisms (Huybers and Langmuir, 2009; Bakker, 2014).

1.2 Climate modelling and proxy-based reconstructions

1.2.1 Climate models

An Earth system climate model incorporates detailed physical descriptions of all the five components of the climate system. It considers the complex couplings between these elements, although some components may be simplified or predetermined (Stocker, 2011). The response of the climate system to external forcing agents is challenging to predict due to non-linear processes and varying response timescales of different components (Goosse, 2015). To calculate this response, numerical models specifically designed for studying the climate system are employed (McGuffie and Henderson-Sellers, 2015). These climate models provide a mathematical representation of the underlying physical processes governing climate (Goosse, 2015), using fundamental laws of physics, such as the laws of thermodynamics, fluid dynamics, and radiative transfer (Washington and Parkinson, 2005; McGuffie and Henderson-Sellers, 2015). In essence, climate modelling aims to simulate multiple processes that contribute to the formation of climate patterns. Climate models employ a set of equations to capture the processes and interactions driving Earth's climate, encompassing the atmosphere, oceans, and terrestrial regions. By integrating these various components and their interactions, climate models provide a powerful tool for scientists to study and project future climate conditions (Stocker, 2011). They allow researchers to investigate complex phenomena such as the impact of greenhouse gas emissions, the role of feedback mechanisms, and the response of the climate system to natural and anthropogenic forcing (Goosse, 2015). Through rigorous model evaluation and validation against observed data, scientists can

enhance the accuracy and reliability of climate models, enabling more informed decision-making regarding climate change mitigation and adaptation strategies (IPCC, 2013).

Climate models employ numerical methods to solve budget equations on a computer. To facilitate computation, the equations are discretized into grid boxes that correspond to specific regions within Earth's climate system (Goosse, 2015). These grid boxes interact with each other by exchanging energy, momentum and mass at their boundaries (McGuffie and Henderson-Sellers, 2015). The spatial resolution of a climate model depends on the size of the grid boxes (Fig 4). Climate models can be produced at various spatial resolutions. The higher the resolution, the more detailed the model's simulations will be. GCMs normally have a resolution of 200 km, compared to EMIC's. The size of the grid cells could be reduced to 30 km (today's Regional Climate Models). This would increase the number of cells covering the surface of the Earth, improving spatial resolution. However, higher resolution requires more computational resources and so there is a trade-off between resolution and computational cost. For example, a global climate model at 60 km will require more than 200,000 grid points per level (IPCC, 2013), this increase in the number of grid points will increase drastically the computing time required for the simulation. Fig 4 shows that increasing the number of grid cells can better resolve the complex topography of the Earth's surface (IPCC, 2013), which can lead to more accurate simulations of climate processes. This is because they can better represent the effects of topography on atmospheric circulation, precipitation and temperature. For example, high-resolution models can better simulate the impact of mountain ranges, which can affect the flow of air, and the distribution of precipitation.

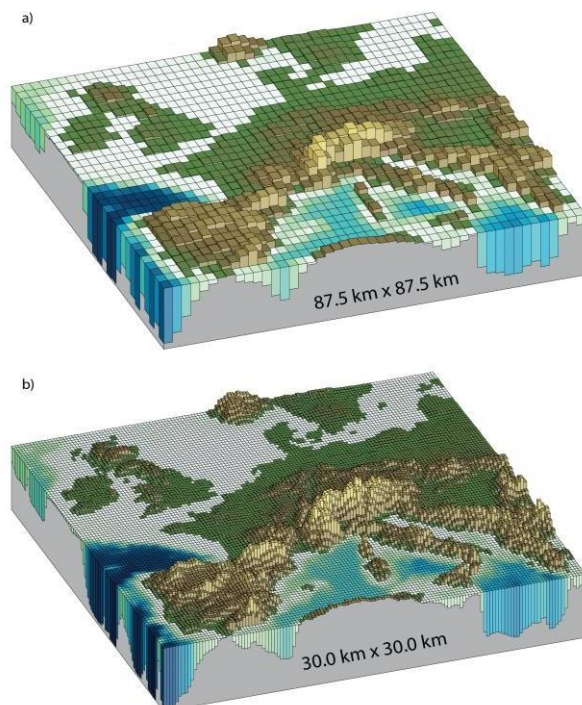


Fig 4: Two examples of higher resolution model surface grids, showing the European topography at a resolution of (a) 87.5×87.5 km and (b) 30.0×30.0 km (IPCC, 2013).

Climate models can simulate the behavior of climate variables in three dimensions and over time (Goosse, 2015). Typically, the calculations are performed at regular intervals (so-called time steps), such as every 30 minutes. For instance, an atmospheric model calculates a range of "weather" variables within each grid cell for every time step, such as temperature, precipitation, evaporation, wind strength, wind direction and air pressure (McGuffie and Henderson-Sellers, 2015).

Although climate models are very useful tools to study the past, present, and future climate, some GCM's coarse resolution prevents them from accounting for fine-scale climatic variability and change. It is therefore important to develop models that can improve the spatial resolution in climate modelling. Coarse-resolution GCMs omit many of the processes involving local terrain, vegetation, and hydrology that regulate regional climate (Fig 5). Several of these processes may be involved implicitly in the establishment of statistical relationships between the large and local scales (Fig 5).

Statistical downscaling uses statistical relationships between large-scale climate variables and local-scale climate variables to estimate the local-scale climate from the large-scale climate (Zorita and von Storch, 1999). Dynamical downscaling usually uses a Regional Climate Model (RCM) to simulate the climate of a specific region at a higher resolution than the GCM that provides the boundary conditions for the RCM (Ludwig et al., 2019). Another solution that can be used in the context of dynamical downscaling is grid stretching, as applied with the GCM from the Laboratoire de Meteorologie Dynamique (LMD), which involves increasing the number of grid points in a particular region, effectively reducing the grid spacing and allows for a more detailed representation of the underlying physical process (Krinner and Genthon, 1997). In this work, I have applied a new downscaling approach (an interactive physical downscaling), which is computationally inexpensive and more interactive with the low-resolution version of the iLOVECLIM model. The idea behind the downscaling process is to reproduce the model physics on a high spatial resolution to explicitly resolve the effects of small-scale processes for the past climate (Quiquet et al., 2018). This downscaling approach takes into consideration the topography in any region (in my case Europe) and provides detailed spatial information in regions such as the Alps, the Scandes mountains and the Scottish Highlands. The Interactive downscaling can provide more detailed information about the climate of a specific region. The interactive downscaling resolves atmospheric and surface processes occurring at the sub-grid scale while Statistical downscaling bases its estimate of the future on the observed climate. (Von Storch et al., 2020).

One disadvantage of Dynamical downscaling is that the results are subject to biases inherent in the RCMs being used and these biases can arise from the simplifications and parameterizations within the model, potentially affecting the accuracy of the downscaled climate information (Wilby et al., 2009). For Statistical downscaling, it assumes that the statistical relationships between large-scale and local-scale variables remain constant over time. This can be a limitation when dealing with non-stationary climate processes, such as trends and changes in variability (Wilby et al., 2009). The choice of which downscaling method to use depends on the specific application.

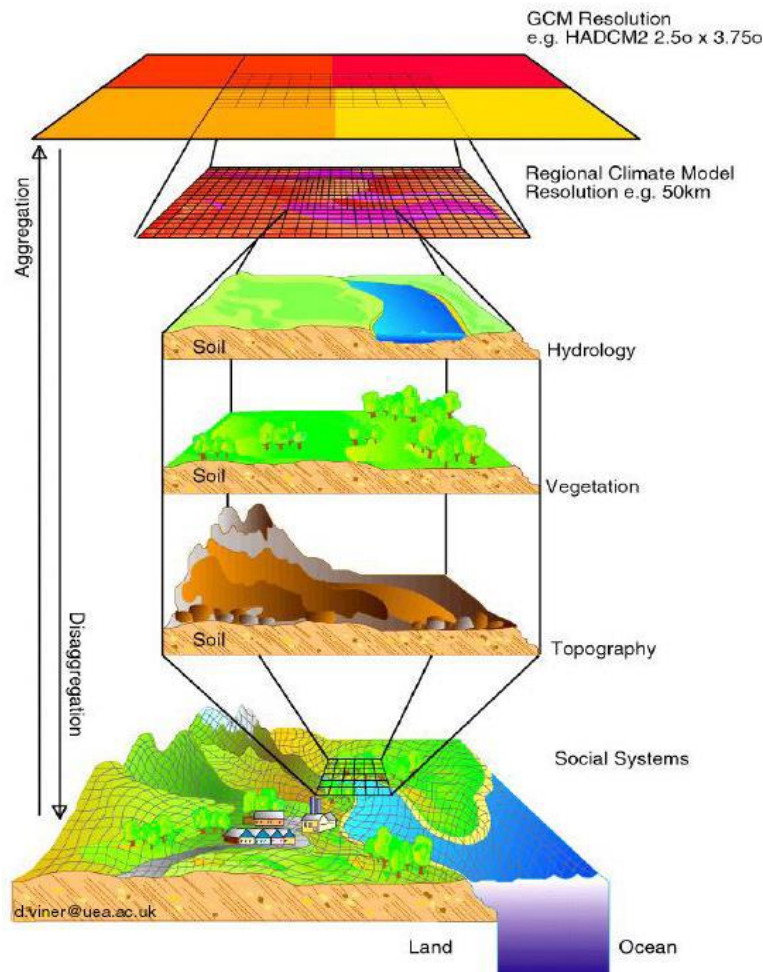


Fig 5: The dynamical spatial downscaling concept as applied in an RCM (Viner, 2012).

1.2.2 Proxy-based reconstructions

The field of paleoclimatology plays a crucial role in understanding climate systems dynamics at various time scales as it provides valuable insights into climatic conditions that occurred thousands of years ago (Goosse, 2015). Since direct measurements are not possible for such distant periods, scientists rely on proxies (indirect imprints left behind by past climate phenomena) to reconstruct and interpret past climatic conditions (Roberts, 2014). According to Bradley (2014), a proxy is a natural archive that has been affected by the climate and may be used to reconstruct a climatic relevant parameter that describes the climate in the past. For example, certain organisms like diatoms, foraminifera (forams), and corals serve as important climate proxies (Dowsett, 2007). By studying the abundance, distribution, and composition of these organisms in sediment or rock formations, scientists can gain knowledge about

past environmental variables such as sea surface temperatures, salinity, and nutrient availability (Goosse, 2015). In addition to biological proxies, various geological and ice-based proxies are utilized (Bradley, 2014). For instance, ice cores extracted from ice sheets and glaciers provide valuable information about past atmospheric composition and temperature variations (Brook, 2007). By analyzing the gas bubbles, isotopes, and chemical composition of the ice cores, scientists can reconstruct past atmospheric conditions and changes in greenhouse gas concentrations over time (Steig et al., 2013).

Tree rings also serve as important proxies for studying past climates. The width, density, and isotopic composition of tree rings can indicate variations in temperature, precipitation and drought conditions throughout a tree's lifetime (Roberts, 2014). By examining tree ring patterns in ancient or preserved wood samples, researchers can reconstruct past climate variations on annual to multi-decadal timescales (Goosse, 2015). Other proxies used in paleoclimatology include packrat middens, which are fossilized remains of plant material collected by packrats in their nests (Cronin, 2010). These middens preserve a record of past vegetation and climate conditions. Sediment cores from lakes, oceans, and terrestrial environments also provide valuable information about past climate through the analysis of sediment composition, microfossils, and geochemical signatures (Seppä et al., 2001; Davis et al., 2003; Cronin, 2010). By combining and analyzing various proxy records from different sources and regions, paleoclimatologists can reconstruct past climate patterns and gain insights into long-term climate variability, natural climate drivers, and the response of the Earth's climate system to external forcing factors (Goosse, 2015). These reconstructions contribute to our understanding of climate dynamics and provide an important context for evaluating modelling, and projecting future climate changes (Cronin, 2010; Bradley, 2014; Goosse, 2015).

1.3 Climate forcings during the Holocene and the Eemian

The Holocene and the Eemian are the two most recent warm periods (interglacials) during the Quaternary. The study of the Holocene and the Eemian climates are of interest because they allow us to investigate how the Earth's climate system responds to the changes in forcing relative to the present day (Otto-Bliesner et al., 2017). The climate during the Holocene has generally been characterized by a relatively stable and warm period, allowing human civilization to flourish (Gupta, 2004). The main variation in forcing from the present was the change in three astronomical parameters (eccentricity, obliquity, and precession of the equinoxes) (also referred to as orbital forcing, ORB) which determines the latitudinal and seasonal distribution of incoming solar radiation (Berger, 1978). The continental

layouts were extremely similar to those of the present day, and greenhouse gas (GHG) concentrations were comparable to those of the pre-industrial era (Otto-Bliesner et al., 2017). During the Holocene, the orbital induced insolation in summer (JJA) decreased by 30 W/m^2 in the Northern Hemisphere (Fig 6) (Berger, 1978). The Holocene temperatures have also been impacted by radiative forcing due to the variations in the concentration of greenhouse gases (GHGs) in the atmosphere. The cumulative influence of GHGs, which are dominated by CO_2 , increased rapidly from the start of the Holocene onward by 10 ka, reaching a peak of -0.3 W/m^2 in comparison to the pre-industrial period (Schilt et al. 2010). This was then followed by a little decline to a minimum at 7 thousand years before the present (ka), before progressively rising until 0 ka (Fig 6) (Schilt et al. 2010). Another natural forcing during the Holocene is represented by volcanic eruptions, which caused decadal to inter-annual variability (Bradley, 2003).

The two main climate forcings in the Eemian are the amount of insolation received by Earth and atmospheric GHG concentrations. The Eemian insolation variations are more pronounced than those of the Holocene because of differences in orbital configuration between the two interglacial periods (Fig 7) (Otto-Bliesner et al., 2017). Variations in the astronomical configuration led to changes in the amount of insolation that the Earth receives. For the Eemian period, the anomalies are almost negligible when averaged globally. On the other hand, this contrasts with the variations in the distribution across various latitudes and seasons (Berger, 1978). During the early stages of the Eemian (between 127 – 123 ka), the amount of summer insolation anomaly (June at 65°N) received in the NH was more than 60 W/m^2 (Fig 7). The variations in insolation throughout the Southern Hemisphere (SH) summer exhibit a sharp minimum between 126 and 123 ka, whereas, during the late Eemian, insolation values are slightly above the present day.

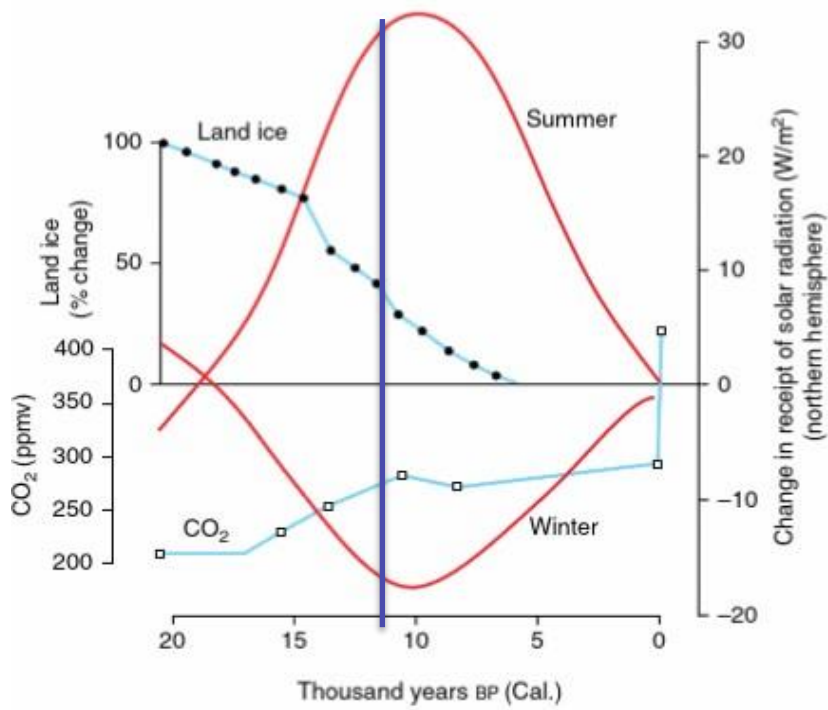


Fig. 6: Overview of forcings during the last 20 thousand years CO₂ concentration, land ice and received solar radiation for the Northern Hemisphere. The blue line marks the start of the Holocene at 11.5 ka (Roberts, 2014).

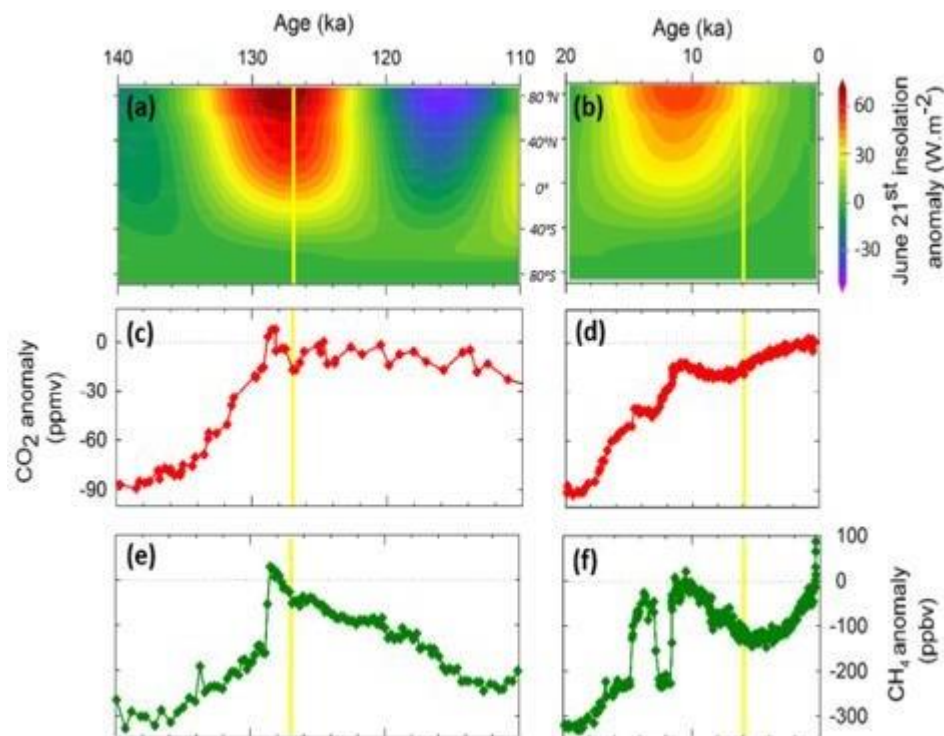


Fig. 7: Forcing and climatic records across the Eemian (left) and the Holocene (right) (Figure from Otto-Bliesner et al., 2017). The yellow lines indicate the early Eemian at (127 ka, left) and the mid-Holocene (6 ka, right). Insolation changes in a and b due to changes in astronomical parameters (Berger, 1978). Levels of CO₂ (c and d) (Siegenthaler et al., 2005; Schneider et al., 2013) and CH₄ (e and f) in the atmosphere based on ice cores (Loulergue et al., 2008).

1.4 Previous modelling studies on the Holocene and Eemian climate

1.4.1 The Holocene

Several modelling studies have been done in the past for the Holocene, the Eemian and various time slices within these periods (e.g., the Mid Holocene (MH) at 6 ka and 127 ka). Most of these studies used state-of-the-art GCMs while other studies utilized high-resolution models (RCMs).

The Paleoclimate Modelling Intercomparison Project Phase 4 (PMIP4) and the Coupled Model Intercomparison Project Phase 6 (CMIP6) have shown a lot of interest in the MH, the Eemian and other past climate periods because these periods are well archived with paleoenvironmental data. For some years now, numerous climate models have contributed to PMIP's aims to understand climate system responses to different forcings and the results have been compared with prehistorical climates to assess the effectiveness of current numerical models in simulating climate change (Braconnot et al., 2007; Hargreaves et al., 2013; Kageyama et al., 2013; Otto-Bliesner et al., 2017; Williams et al., 2020). One of the key findings from the PMIP4/CMIP6 simulations is that the MH was substantially warmer than the pre-industrial climate. For example, Williams et al. (2020) simulate a warming of about 2 °C during the MH relative to the pre-industrial era in Europe, while the ensemble mean temperature anomalies within PMIP4 (15 climate models) of the MH relative to the pre-industrial analyzed by Brierley et al. (2020) was about +2 to +4 °C, which was particularly pronounced in the Northern Hemisphere. The annual precipitation anomalies in Europe during the MH were between (+200 and +400mm/yr) wetter than pre-industrial era (Williams et al., 2020). However, there are some disagreements between the different PMIP4 models about the magnitude of the warming. The disagreement between the different modelling studies is likely due to several factors, including the different designs of climate models and the different methods that are used to analyze the data. Despite the disagreement between the different modelling studies, there is a consensus that the MH climate was warmer and wetter than the preindustrial climate (Brierley et al., 2020).

Recently there has been simulation of the Holocene climate with high resolution models (e.g., Strandberg et al., 2014; Russo and Cubasch 2016; Badder et al., 2020; Russo et al., 2022). For instance, using the RCM model COSMO-CLM, Russo and Cubasch (2016) applied a dynamical downscaling for various time slices of the middle to late Holocene in Europe. Their findings demonstrate that their RCM can replicate a climatology that is quite realistic when compared to high-resolution instrumental gridded datasets from the Climate Research Unit (CRU). Badder et al. (2020) explored the Holocene temperature conundrum, which has led to conflicting results in reconstructions of global mean annual temperature evolution using the MPI-ESM (Max Planck Institute-Earth System Model). The study uses data from a transient climate model simulation to perform a spatiotemporal analysis of annual temperature variability during the Holocene and finds that both a global cooling trend and a warming trend occur. According to their findings, the simulated cooling mode is driven by fluctuations in the seasonal cycle of Arctic Sea ice, due to volcanic eruption and orbital forcings, the findings also show that the tropics are where the warming is most evident because of the increase of incoming radiation. The effects of

anthropogenic deforestation on the climate in Europe during the Holocene period (6 ka and 0.2 ka) were simulated using the Regional Climate Model RCA3 by Strandberg et al. (2014). The results reveal that deforestation's effects depend on local climate and vegetation characteristics. At ~6 ka, deforestation was generally small, but some areas showed significant temperature differences (0.5–1 °C) and at ~0.2 ka, extensive deforestation led to significant temperature differences in Europe in both winter and summer (Strandberg et al., 2014). Deforestation reduces temperatures in southern Europe due to the albedo effect, which is most prominent in the region. The difference in temperatures during the summer ranges from -1 °C in south-western Europe to +1 °C in eastern Europe due to deforestation (Strandberg et al., 2014). This study concurs with a recent work by Dallmeyer et al. (2023), which compares the LPJ-GUESS dynamic vegetation model (high spatial resolution), with pollen-based reconstruction (based on the REVEALS model), and Holocene tree cover changes in Europe. Both models show a significant increase in tree cover (70-85%) during the mid-Holocene and a decrease closer to the pre-industrial era (Dallmeyer et al., 2023). However, REVEALS' decline begins earlier than the climate model result, suggesting anthropogenic deforestation occurs earlier than recommended land usage (Nikulina et al., 2024). The study also reveals that land usage was the primary cause of forest decrease during the mid-and late-Holocene (Dallmeyer et al., 2023).

Transient simulations of the Holocene using the iLOVECLIM model have previously been done by several authors (e.g., Renssen et al., 2005; 2006; 2009; 2012; Zhang et al., 2018; Li et al., 2020). Renssen et al. (2006) performed a transient simulation of the Holocene (the last 9000 years), forced with total solar irradiance (TSI), greenhouse gas concentrations and variations in orbital parameters. The goal of their study was to investigate how TSI fluctuations on a decadal to centennial-scale affect Holocene climate variability (Renssen et al., 2006). The results indicate that negative TSI anomalies increase the likelihood of reduced deepwater formation in the Nordic Seas, leading to increased sea ice expansion and cooling (Renssen et al., 2006). Also, summers in the Holocene were cooler before 7 ka due to the Laurentide ice sheet's influence and the ice sheet's high surface albedo, which delayed the Holocene Thermal Maximum (HTM) in Europe by thousands of years (Renssen et al., 2009). Renssen et al. (2012) later showed that the timing of the HTM falls between 9 ka and 5 ka in almost all regions studied. The HTM occurs between 7 and 6 ka in most regions of Europe and NE North America, while the earliest known HTM (occurred before 8 ka BP) over regions like the Central Arctic Ocean, areas of the tropical Pacific and Atlantic Oceans, Northern Africa, the Middle East, and Northwest America (Renssen et al., 2012). In both hemispheres, the HTM was most pronounced at high latitudes, where the model's highest

temperature anomaly compared to the preindustrial level was 5 °C. However, the weakest signal was simulated over low-latitude continents (0.5 –1.5 °C) and oceans (less than 0.5 °C) (Renssen et al., 2012).

Recently, Zhang et al. (2018) analyzed four Holocene transient simulations in the Northern Hemisphere performed with the LOVECLIM, HadCM3, CCSM3, and FAMOUS climate models (model-model comparison). The findings show similar trends of early Holocene warming (between 10 -7 ka), warming in the mid-Holocene and a gradual drop to pre-industrial winter temperatures across, northern Canada Greenland and northeastern Europe. At 4 ka, the simulated annual mean temperature begins to rise gradually by about 2 °C, and then it remains at the 0-ka value. However, inconsistent temperatures are seen in the Arctic, eastern Siberia, and Alaska, rendering the Holocene temperature changes in these areas uncertain. Their study shows that the variations in model responses are likely due to the physics, resolution, and sensitivities of the models (Zhang et al., 2018).

1.4.2 The Eemian

Several climate studies in the Eemian have been conducted with most findings concluding with an annual mean increasing temperature for the high northern latitudes, intensification of the monsoons, and summer warming over the continents (Brewer et al., 2009; Lunt et al., 2013; Bakker et al., 2013; Bakker, 2014; Brierley et al., 2020; Otto-Bliesner et al., 2021). Numerous Eemian modelling studies conducted equilibrium experiments, transient experiments, and model-data comparisons to examine various characteristics of the climate. For example, Kasper et al. (2007) investigated the effects of the different orbital configurations of the Eemian as compared to the present day with two equilibrium experiments (125 ka and 115 ka), focusing on modifications to North Atlantic storm trajectories. The simulations showed a significant change in Northern Hemisphere winter storm tracks, with the North Atlantic storm track strengthening and extending further east at 125 ka. This led to increased winter precipitation in northern Europe, while weaker changes were simulated at 115 ka. Born et al. (2009) examined equilibrium climate models' responses to insolation changes between 126 and 115 ka, and the results show that a significant drop in summer insolation at high northern latitudes between 126 and 115 ka led to an increase in the export of Arctic Sea ice.

Bakker et al. (2013) performed an intercomparison analysis of transient simulations in the Eemian with seven different climate models. The objective was to ascertain the overall transient temperature response to the Eemian forcings and to determine the most important feedback in the simulations. The results show a strong July temperature evolution in the Northern Hemisphere (NH), depicted by the model inter-comparison, with a maximum temperature of 0.3 to 5.3 °C above pre-industrial occurring between 130 and 125 ka. There is only a July temperature maximum in the Southern Hemisphere (SH), -1.3 to 2.5 °C at approximately 128 ka, when variations in the amounts of greenhouse gases are considered. The simulations indicate that the insolation changes during the summer and winter affected the temperatures in almost all latitudes. However, two main exceptions are NH high-latitude winter temperature variations, which are mostly dependent on models, and SH mid- to high-latitude winter temperature changes, which seem to be significantly impacted by variations in GHG concentrations (Bakker et al., 2013).

The effect of the interaction between climate and vegetation in the Eemian over the Sahara was investigated by Li et al. (2020) using the iLOVECLIM model. The Sahara had a comparatively high vegetation cover (more than 70%) in the early Eemian, according to the results, and after 123 ka, there was an acceleration of desertification. Peak rates of desertification occur at 122 ka in response to a sharp drop in July insolation at 20 °N. The early Eemian experiments with dynamical vegetation showed a doubling in the amount of precipitation (~60 cm/yr) compared to the simulations with fixed pre-industrial vegetation, moreover, the inclusion of dynamic vegetation increases surface temperatures in North Africa by roughly 2.5 °C (Li et al., 2020). The study concludes that the effect of Sahara vegetation feedback accounts for about 30% of the global vegetation effect on high-latitude warming (Li et al., 2020).

The evaluation results of 17 climate models in the Eemian by the PMIP4/CMIP6 projects are presented by Otto-Bliesner et al. (2021). The lig127k experiments (for 127 ka) aim to investigate climatic responses to stronger orbital forcing than the mid-Holocene experiment. These models range in equilibrium climate sensitivity (ECS) from 1.8 to 5.6 °C. In contrast to the CMIP6piControl, the seasonal feature of insolation anomalies causes significant warming in the summer throughout the continents of the Northern Hemisphere in the lig127k ensemble, as well as a significant decrease in minimum sea ice in the Arctic. The results of the multi-model ensemble show increased summer monsoonal precipitation in the Northern Hemisphere and decreased precipitation in the Southern Hemisphere, as expected given the bigger insolation anomalies at 127 ka than 6 ka (Otto-Bliesner et al., 2021). The 17 CMIP6 models

used in the lig127k experiment have shown that the continents warmed during the JJA and cooled during the DJF due to variations in seasonal insolation. Both the Arctic and the Southern Ocean show annual positive temperature anomalies in the lig127k simulations. The large spread across the models in their simulations of Arctic Sea ice highlights the necessity for a more comprehensive understanding of the atmospheric and ocean feedbacks, which vary throughout the lig127k ensemble.

The above overview of some previous studies in the Holocene and the Eemian indicates the interest of the paleoclimate community in these periods. Most of these studies employ coarse-resolution GCMs due to computational restrictions, making it difficult to resolve small-scale processes in the atmosphere and the land surface and further rendering comparison with proxy data very problematic. On the other hand, other studies that utilized high-resolution RCMs conducted only snapshot experiments. The novelty in this present study is that a physical interactive downscaling approach with a high resolution of (0.25° latitude-longitude) has been employed to simulate the transient Holocene and the Eemian climates for the first time in Europe. The downscaling tool is numerically cheap, and the results are comparable with proxy-based reconstruction due to the spatial variability.

1.5 Climate modelling in archaeological studies: The link between volcanic eruption and the Fimbulwinter

Climate models with high spatial resolution are becoming increasingly accessible, which enables us to investigate how the past climate affected society on a scale that is relevant to archaeological data. The archaeological record provides an opportunity to investigate the complex interaction between environmental and human systems under various climate regimes and at various spatial and temporal scales (Burke et al., 2021). The study of climate within archaeology provides a much-needed long-term perspective to climate studies by identifying the factors that assisted human resilience in the past and applying the knowledge to the present (Burke et al., 2021). The cultural diversity represented in the archaeological record is one of its benefits. One example of a climate impact on humans that can be studied using climate models is the effect of strong volcanic eruptions during the late Holocene.

Proxy-based reconstructions of volcanic eruptions have been extensively utilized to understand climate variability (Sigl et al., 2015), demonstrating that in the recent past, volcanism was a major natural driver of climatic fluctuations. Volcanic eruptions can release sulfur into the stratosphere, which has a

substantial effect on the climate of Earth. This sulfur is released in the form of sulfur dioxide (SO₂) and hydrogen sulfide (H₂S), which combine to form sulfate aerosols (Helama et al., 2018). Once these volcanic sulfate aerosol emissions reach the stratosphere, they disperse globally, scatter and reflect solar energy while absorbing infrared radiation (Fig 8) (Robock, 2000; Oppenheimer, 2011). This causes a cooling of the Earth's surface and a net decrease in radiation reaching the surface (Fig 8). The immediate effects of this radiative forcing, such as post-eruption surface cooling in summer and a decrease in sunlight reaching the biosphere are well understood, and documented over the modern instrumental period (Robock, 2000; Gao et al., 2007; Oppenheimer, 2011).

Volcanic forcings, one of the significant natural climate forcings plays an important role in shaping the earth's climate throughout history. The mid-6th century AD is regarded as a turning point in Scandinavian history due to the enormous amount of settlement abandonment, decline, social restructuring, and material upheaval that occurred during this time (Gräslund and Price, 2012; Löwenborg, 2012; Price and Gräslund, 2015). These changes have drawn more attention in recent years, and research has connected them to a sudden cooling event that occurred in the Northern Hemisphere between 536 and 540 AD and was linked to catastrophic volcanism (Toohey et al., 2016; van Dijk et al., 2023).

The evidence for the connection of the 536 and 540 AD to volcanism comes from studies of known volcanic eruptions from historical sources before 630 AD, with the most notable volcanic event being in 536 AD and a second explosive eruption following in 540 AD (e.g., Stothers and Rampino, 1983). According to Gräslund (2008), a layer of dust caused the sky to become dull, causing at least two years without summer (also known as the *Fimbulwinter* after an Old Norse myth), which caused severe crop failures throughout Scandinavia. Most studies suggest that there was a reduction in plant productivity. According to Helama et al. (2018), the cumulative effects of a changing climate and decreased agricultural productivity affected people's health on a large scale, leading to famine and lowering societies' resistance to plague outbreaks like the Justinian plague that occurred around the same time (Büntgen et al., 2016, 2020; Price and Gräslund, 2015).

Several studies have recently analyzed the effects of the 536 AD volcanic eruption on Scandinavian society and climate from an archaeological perspective (e.g., Axboe, 1999; Baillie, 1999; Keys, 1999; Gunn, 2000; Gräslund, 2008; Gräslund & Price, 2012; Arrhenius, 2023). Even documented records of the events at 536 AD coincide with the optical characteristics of stratospheric sulfate aerosols produced by volcanic eruptions (Robock, 2000; Arjava, 2005; Gräslund and Price, 2012). According to Toohey et al. (2016), the two eruptions of 536 and 540 AD also resulted in nearly a decade of surface cooling and the largest volcanic forcing in the last 2000 years.

The effect of these two eruptions on climate has been studied using climate models by changing the volcanic aerosol forcing in a model. For example, van Dijk et al. (2023) studied the impact of volcanic eruptions in the mid-6th century on climate and society in Scandinavia (focusing on southern Norway) with the MPI-ESM. The study indicates that during the average growing season in southern Norway, there was a maximum surface cooling of up to 3.5°C. The study reveals that the volcanic cooling led to reduced productivity and site abandonment in the western coast and mountainous areas, while the Oslofjord area showed less crisis. The impact on agriculture and society was regional, with varying levels of disaster impact on the society (van Dijk et al., 2023). This result agrees with an earlier study in the Northern Hemisphere by Toohey et al. (2016). Their Earth system model simulations show peak anomalies in Arctic Sea ice extents that span decades, with peak NH mean temperatures exceeding -2°C (Toohey et al., 2016). The cooling is interpreted as having a likely impact on agricultural production in Europe, with multiple years of significant decreases in crop production across Scandinavia.

However, these studies have not yet explored in detail the societal impacts on specific regions within Scandinavia. In this PhD project, large archaeological datasets are used in a large time span within specific study regions in both Sweden and Norway, and climate simulations are run for the first time with the iLOVECLIM model (using an interactive downscaling). The climate model has a high spatial resolution that allows for a meaningful comparison with archaeological data on a regional scale. Another novelty employed in our approach is that we have run the climate simulations with both volcanic eruptions and without volcanic eruptions to analyze the real impact of the volcanic eruption during the Fimbulwinter. Again, the combination of archaeological C14 dated records and the climate simulations allows us to analyze the effect that volcanic eruption had on human societies in Scandinavia. We have performed 10 ensemble experiments by using different initial conditions and control runs to simulate the changes in temperature, precipitation and crop production.

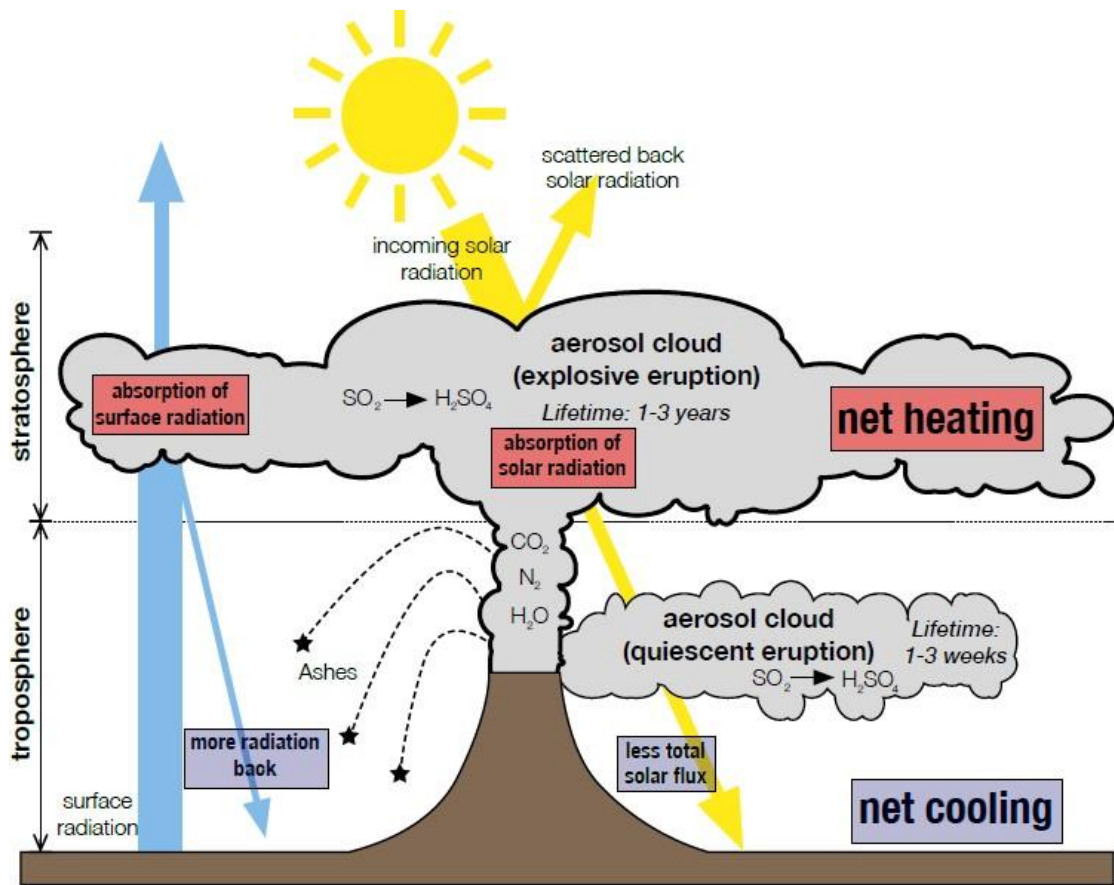


Fig 8: Schematic representation of volcanic inputs and their impacts (Robock, 2000).

1.6 The context of this PhD thesis: The TerraNova project.

This dissertation, on ‘Modelling and characterization of climate, environment, and human impact during the Eemian and the Holocene using an interactive physical downscaling’ is part of a project funded by the European Union within the context of the EU’s Horizon 2020 program (TerraNova). TerraNova is an interdisciplinary EU project, that combines humanities and science to map the past landscape histories and land use strategies (<https://cordis.europa.eu/project/id/813904>, <https://www.terranovaltn.eu>). Through 15 PhD dissertations, the project aims to explore the land use changes and the effects of natural forcing through the Holocene and Anthropocene, to better understand human impact on the

environment. The Eemian is also studied as a reference state of Europe without the disruptive impact of modern humans. A key tool in understanding the effects of land use changes and natural forcing is climate modelling. Climate models simulate climatic patterns and interrelations and can be used to project the future or understand the past climate. For this thesis, the iLOVECLIM 1.2 earth system model with downscaling has been used to simulate the climate data. TerraNova is an interdisciplinary project that facilitates collaboration with others, so involvement with other groups and disciplines. For example, this PhD project collaborated with the climate modelling group at VU Amsterdam, the Archeology Department at Uppsala University, the group working on pollen-based vegetation reconstruction at Linnaeus University and the French National Center for Scientific Research CNRS. One of the overarching goals of TerraNova is to create a first-of-its-kind digital atlas of Europe that incorporates historical human population trends, plant and environmental disturbances, animal evolution, and climate change. This dissertation contributes to the climate data that has been used in the atlas.

1.7 The Research Questions of the Thesis

The research questions summarized for all the 4 papers to be answered in this study include:

- *What is the impact of downscaling on the climate patterns during the past climate (Holocene, Eemian) in Europe? (Paper 1 and 2).*
- *Can we see evidence of the impact of downscaling for the relationship between patterns of climate due to the impact of volcanic eruptions and ^{14}C records? (Paper 3).*
- *What is the benefit of employing numerically inexpensive interactive downscaling for paleoclimate studies? (Paper 1, 2 and 3).*
- *Within the framework of palaeoclimate modelling, is it possible to develop a technique for correcting climatic biases? If so, what are the advantages and limitations? (Paper 4).*

2 Methods (Model and simulations)

2.1 The iLOVECLIM climate model

In all the climate model simulations reported in this thesis, I have used the iLOVECLIM model. The iLOVECLIM model (Roche et al., 2014) is a three-dimensional model that represents the atmosphere in a simplified manner compared to GCMs. iLOVECLIM is substantially faster than coupled GCMs due to its simplicity and lower spatial resolution (Goosse et al., 2010; Kitover et al., 2015). iLOVECLIM is built upon the LOVECLIM 1.2 model code, and both share the same elements of the climate system. We use a version which includes the following components: the atmospheric model ECBilt (Opsteegh et al., 1998), the sea ice-ocean component CLIO (Goosse and Fichefet, 1999), and the terrestrial vegetation model VECODE (Brovkin et al., 1997).

The model has been used to successfully simulate certain significant past and future climates. For instance, the Holocene (e.g., Renssen et al., 2007), the Last Glacial Maximum, LGM (e.g., Timmermann et al., 2004; Roche et al., 2007), the last millennium (e.g., Goosse et al., 2005), the last deglaciation (e.g., Timm et al., 2008), and the 21st century (e.g., Schaeffer et al., 2002; Driesschaert et al., 2007). The atmospheric component (ECBilt) models the dynamical processes in the atmosphere using the quasi-geostrophic potential vorticity equation and three vertical levels at 800, 500, and 200 hPa (Opsteegh et al., 1998). In addition to the quasi-geostrophic equations, an estimate of the neglected terms in the vorticity and thermodynamic equations is incorporated as a forcing that varies temporally and spatially runs on a global spectral grid that is truncated at T21, representing a horizontal resolution of about 5.6° latitude and 5.6° longitude. This resolution allows for a reasonable representation of large-scale atmospheric patterns and interactions within the model's simulations. The oceanic component of the model, CLIO (Goosse et al., 2010), is a three-dimensional free-surface ocean general circulation model that has been coupled with a full sea ice model (Goosse and Fichefet, 1999), with a horizontal resolution of 3 degrees by 3 degrees latitude–longitude and divided into 20 vertical layers to represent the vertical structure of the ocean. This vertical discretization enables the model to capture vertical mixing processes and the distribution of temperature, salinity, and other properties throughout the water column. VECODE shares the same grid as ECBilt and has three different plant functional types (PFTs): trees, grass, and desert. Each of these PFTs has unique physical characteristics for evapotranspiration, albedo and surface roughness. These properties influence the energy and water exchanges between the land surface and the atmosphere, impacting regional climate patterns and feedback processes within the model.

2.2 Interactive physical downscaling

An interactive (physical) downscaling for temperature and precipitation was applied in the coupled iLOVECLIM model, as described by Quiquet et al. (2018). The original ECBilt's T21 grid was downscaled to a European domain that spans from 13.875 degrees west to 49.875 degrees east and 35.125 degrees north to 71.875 degrees north, with a resolution of 0.25 degrees latitude and longitude (Fig 9). The main aim of the downscaling method is to explicitly account for the sub-grid orography by reproducing part of only the model physics (the vertical part) of ECBilt on a higher spatial scale. To achieve this, artificial vertical layers were incorporated, allowing for the computation of variables such as temperature and precipitation for each atmospheric time step at various altitudes within the sub-grid orography (Quiquet et al., 2018). A conventional method was used where the "large-scale" fields (on the native grid) represent the average or sum of the computations made on the sub-grid. During runtime, the downscaling is done at each model time step. The precipitation at the coarse resolution is the sum of the sub-grid precipitation due to the two-way coupling between the coarse grid and the sub-grid, which provides consistency. The reader is referred to Quiquet et al. (2018) for more information, including the physics employed in the downscaling and for temperature in the model.

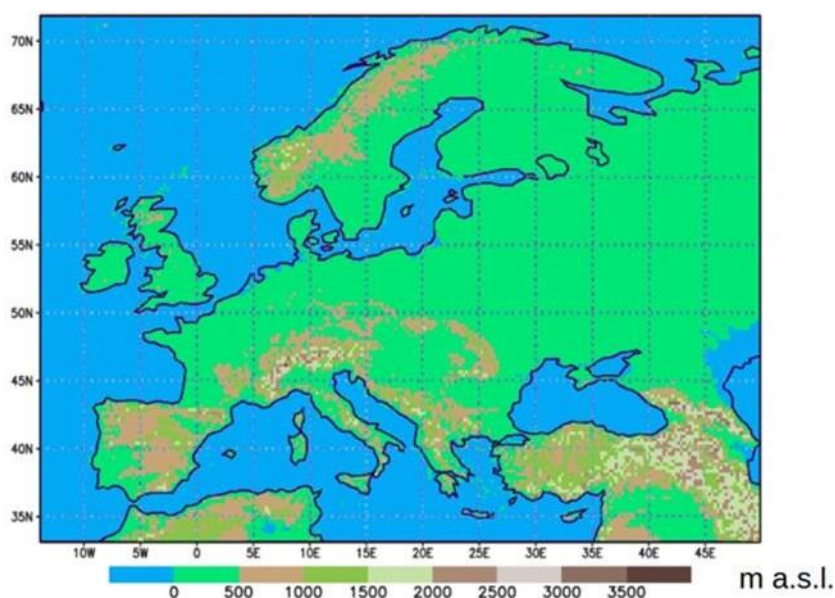


Fig 9. The sub-grid utilized for the interactive downscaling, (The European grid topographic plot).

2.3 Climate model experiments and datasets used

2.3.1 Paper 1 – Transient simulations of the Holocene climate

iLOVECLIM-1.1 (Roche et al., 2014) was used to simulate the transient evolution of the climate over the last 11.5 ka. Two simulations were done (11.5K_Standard and 11.5K_Down). On the low-resolution T21 grid, the experiment 11.5K_Standard is run using the model's standard version. The second experiment (11.5K_Down) computes temperature and precipitation on a regional sub-grid in Europe using downscaling on the quasi-geostrophic T21 grid. The forcings used for the simulations include astronomical forcing (Berger, 1978) and varying annual atmospheric trace gas concentrations of CO₂, CH₄, and N₂O (Raynaud et al., 2000). The simulations were designed to use fixed ice sheet configurations with pre-industrial levels of aerosol content and the solar constant (Table 1). During the Holocene, the changing latitudes, and seasons of the incoming solar radiation at the top of the atmosphere are caused by astronomical forcing and the levels of CO₂, CH₄, and N₂O based on ice cores as explained earlier in the introduction.

Table 1: The Experimental set-up for the simulations (From Arthur et al., 2023)

	Simulations	
Model	iLOVECLIM (standard version)	iLOVECLIM (downscaling)
Component	Ocean, sea ice, atmosphere, vegetation	
Atmospheric resolution (lat × long)	5.6° × 5.6°	0.25° × 0.25°
Oceanic component resolution	3° × 3°	
Prescribed forcings and reference	Orbital forcings (Berger, 1978) GHG (Schilt et al., 2010; Raynaud et al., 2000) Ice sheets, fixed	
Initial condition	Equilibrium experiment at 11.5 ka (1 kyr)	
Duration of experiment	11.5 kyr	

2.3.2 Paper 2 – Transient simulations of the Eemian climate

Two different experiments were performed for this study with the iLOVECLIM model. Similar to paper 1, A transient experiment over the Eemian (127 ka – 116 ka) was performed with fully coupled dynamical vegetation VECODE. Then downscaling was applied to the model to perform a similar transient simulation over Europe from 127 ka – 116 ka (EEM_Down). Both simulations were done starting from an equilibrium run (128 ka for 3000 years). The orbital forcings and greenhouse gas concentrations of CO₂, CH₄, and N₂O used in the transient simulations were the same as those used in the PMIP4 protocol (Otto-Bliesner et al., 2017).

2.3.3 Paper 3 – Simulation of the impact of volcanic forcing on the climate of the 6th century AD

2.3.3.1 *Experimental setup*

In this study, iLOVECLIM-1.1 (Quiquet et al., 2018) has been applied with downscaling to perform ensemble experiments with volcanic eruptions and without volcanic eruptions to simulate the climate from 1 AD to 1000 AD. Atmospheric trace gas concentrations of CO₂, CH₄, N₂O (Raynaud et al., 2000) and orbital forcings (eccentricity, obliquity, and precession) (Berger, 1978) were used as forcings for the simulations. The simulations were run in four separate groups. There are 10 ensemble members in each simulation. These simulations are (VOLC_50, VOLC_1000, NOVOLC_50, and NOVOLC_1000). VOLC_50 includes 10 equilibrium simulations, run for 50 years with the same forcings at 1 AD, with volcanic eruptions included, but different starting conditions. Each simulation's initial conditions are generated from the previous ensemble run. The setup of NOVOLC_50 is identical to that of VOLC_50, except that, it was run under different initial conditions and without any volcanic eruptions. The simulations VOLC_50 and NOVOLC_50 were done to create various climate states that would serve as the starting point or initial conditions for the 10 ensemble transient simulations (VOLC_1000 and NOVOLC_1000). Volcanic eruptions were applied from year 1 AD to year 1000 AD (1000-year run) in the transient experiment (VOLC_1000). The volcanic forcing was applied through aerosol content in the atmosphere. All 10 ensemble members had the same climate forcings, but the initial conditions were different as they were generated from the VOLC_50 simulations. The set-up of NOVOLC_1000 is identical to that of VOLC_1000 except that it was run under different initial conditions and without any volcanic eruptions derived from NOVOLC_50. (See Table 2 for the volcanic forcings applied). Because

of how chaotic the climate system is, analyzing a single-member simulation can produce uncertainty related to internal climate variability. However, a 10-member ensemble simulation with varied initial conditions but the same atmospheric physics, dynamics, and forcings were used, making the 10-members evolve differently. Thus, the 10 members' range gives us an estimate of the internal variability. The average response to the volcanic forcing is represented by the ensemble means as the noise of each of the ten ensemble members is effectively canceled out by the average over them, revealing a common results signal.

2.3.3.2 *The Volcanic forcings applied in the iLOVECLIM Model.*

The eVOLV2K datasets were employed to simulate our 536 and 540 AD eruptions. A detailed description of this volcanic forcing dataset can be found elsewhere (Sigl et al., 2016; Toohey & Sigl, 2017; Jungclaus et al., 2017). The table shows the sulfur injection and the global radiative forcings that were used at the various latitudes in our iLOVECLIM model.

Table 2: The stratospheric sulfur injection and volcanic forcing for the eruptions in AD 536 and 540 utilized in this study (eVolv2k; Toohey and Sigl, 2017).

Eruption Year	Eruption month	Eruption Latitude	Sulfur injection (Tg)	Global Forcing (Wm^{-2})
536	<i>Jan – Dec</i>	NH extratropics	18.8	-11.3
540	<i>Jan – Dec</i>	Tropics	31.8	-19.1

2.3.3.3 *Archaeological Radiocarbon ¹⁴C Datasets*

Datasets were carefully chosen to examine the consequences of the volcanic event on inland and coastal regions of Scandinavia because the main goal of paper 3 is to investigate the effects of the so-called Fimbulwinter on different regions of Scandinavia. As a result of the meticulous work of earlier researchers, it provided an opportunity to make use of extensive ¹⁴C databases in the study areas. One crucial dataset utilized in the study was the ¹⁴C archaeological record for the Dalarna region of central Sweden. Previous research conducted by Hatlestad et al. (2021) had already utilized this database, and the current study reanalyzed it, building upon their findings. Additionally, a substantial ¹⁴C database was used for southern coastal Sweden, encompassing Skåne and Blekinge, which was added in Friman and Lager (2022), and the analysis was reoriented following those changes to meet the study goals. Over 12,238 dated records over the last 10,000 years are included in the datasets. However, the analysis is restricted to the first millennium AD given the unique focus of this study on the 536/540 AD volcanic event. This dataset included data from various regions, with 1,555 records from Norway, 2,461 records from Sweden, and a total of 1,894 unique sites. The dataset was organized to capture three distinct climatic transitions in the regions under investigation. These transitions were defined as follows: (i) before the volcanic event, (ii) during the Fimbulwinter aftermath, and (iii) the subsequent climate recovery period.

Study area for paper 3 (Southern Fennoscandia)

This study focuses on some specific regions in Sweden and Norway. Within the Swedish study area, two unique biomes were explored 1) the inland boreal forest of Dalarna, and 2) the temperate southern coastal area of Skåne (Fig 10). The topography of Dalarna is very diverse, ranging from the Scandinavian mountains in the west to the flat plains with esker markings that lead to the Baltic Sea in the east. The climate is characterized by subarctic cold winters and relatively mild summers (Holm, 2012). The topography of Dalarna is varied and offers diverse natural landscapes (Persson et al., 2011). Skåne, located in the coastal part of Sweden, is a region renowned for its diverse topography. The region features expansive plains, particularly in the central and southern areas (Persson et al., 2011). These fertile lowlands, known as the "Skåne Plain", are renowned for their agricultural productivity. The flat terrain, combined with rich soil and a favorable climate, has made Skåne a significant agricultural hub in Sweden. The plains are adorned with fields of crops, such as wheat and barley. Skåne enjoys a temperate maritime climate, influenced by its proximity to the Baltic Sea and the Gulf Stream. The other study region (Southern Norway) is between latitudes 57.9° and 62.3° N. As in Sweden, the research area has been divided into two main sections: 1) the inland, which includes the highland/mountain region,

and 2) the coast. There is a subarctic climate in Norway's highlands and mountainous areas, which is characterized by moderately cold temperatures, moderate precipitation, and a wide range of weather conditions throughout the farming year (Svensson, 1998; Holm et al., 2005; Loftsgarden, 2019). Winters are long and cold, with average temperatures often dropping below freezing. In some areas, temperatures can reach extreme lows, especially at higher altitudes. Summers are relatively short, and temperatures are cool to mild, with average highs ranging from 10 to 20 °C (Holm et al., 2005).

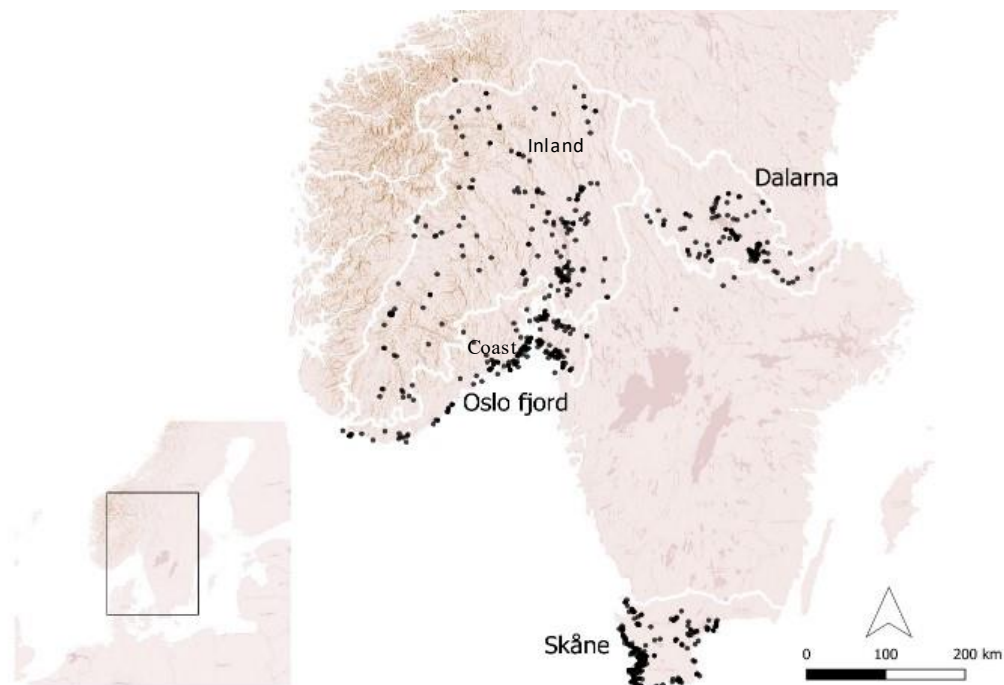


Figure 10: The inland and coastal study regions (white outline) of Norway and Sweden, as well as locations for the 4,016 radiocarbon dates (black points) used in this analysis (Arthur et al., 2024).

2.3.4 Paper 4 – Application of bias correction to simulations of past climate

This PhD project contributed mainly to this paper coordinated by Angelina Zapolska and the VU team, by providing climate model results from the Holocene as discussed in paper 1. So, this paper 4 can be seen as an application of the downscaled results.

This study used a bias correction technique developed by Vrac et al. (2012) based on the cumulative distribution function-transform (CDF-t). This technique is used in climate modelling to adjust the distribution of simulated climate data to match the distribution of observed climate data and reconstructed proxy data (Vrac et al., 2012). Previous studies have used the CDF-t method for downscaling (Michelangeli et al., 2009; Lavaysse et al., 2012; Vigaud et al., 2013) and bias correction (Mesta and Kentel, 2022) to adjust climate model outputs to better match observed data. However, this technique has not been validated for past periods with proxy data, which is the purpose of this work. Therefore, this study evaluates CDF-t as a bias correction tool solely for three distinct climatic periods: pre-industrial (PI, 0 ka BP, taken at 1750 AD), mid-Holocene (MH, 6 ka BP), and Last Glacial Maximum (LGM, 21 ka BP).

To assess the performance of the CDF-t bias correction approach, different groups of simulations were performed for each of the distinct periods, the simulations hereafter are Present Day (PD), PI, MH and the LGM. Each of the simulations was performed with the low resolution of the model (5.56°) and with downscaling applied (0.25°).

3 Summary of Main Results and Discussion

The results of the four papers included in this thesis indicate that interactive downscaling applied to the iLOVECLIM model improves the model's ability to simulate high spatial variability in topographic regions and provides detailed climate information of temperature gradient and precipitation in the Holocene and the Eemian. The downscaling can yield extremely valuable local-scale information, as it is commensurate with archaeological data, which is useful for studying the impact of natural forcings (such as the effect of volcanic eruption) on human society.

3.1 The impact of interactive downscaling on the Holocene climate in Europe (Paper 1)

The study (paper 1) presents the results of the iLOVECLIM model simulation of the Holocene climate in Europe, comparing the standard version of the model (11.5K_Standard) with an interactive downscaling version (11.5K_Down) (Arthur et al., 2023). The downscaling technique provides more detailed and spatially varied results, particularly in regions with elevated topography such as the Scandes mountains, the Alps, the Scottish Highlands, and the Pyrenees. The downscaling improves the representation of the impact of topography on temperature and precipitation patterns (Fig 11 &12). In terms of the temperature evolution during the Holocene, both versions of the model show a similar trend, with warmer conditions in the mid-Holocene (2 °C) compared to the pre-industrial era (Fig 11). However, the downscaled version (11.5K_Down) provides a more realistic representation of temperature gradients in mountainous regions, such as the Alps and the Scandes mountains (Fig 11). Positive temperature anomalies relative to the pre-industrial era are recorded in central and south-western Europe, ranging between (0.5 °C and 1 °C) at 6 ka.

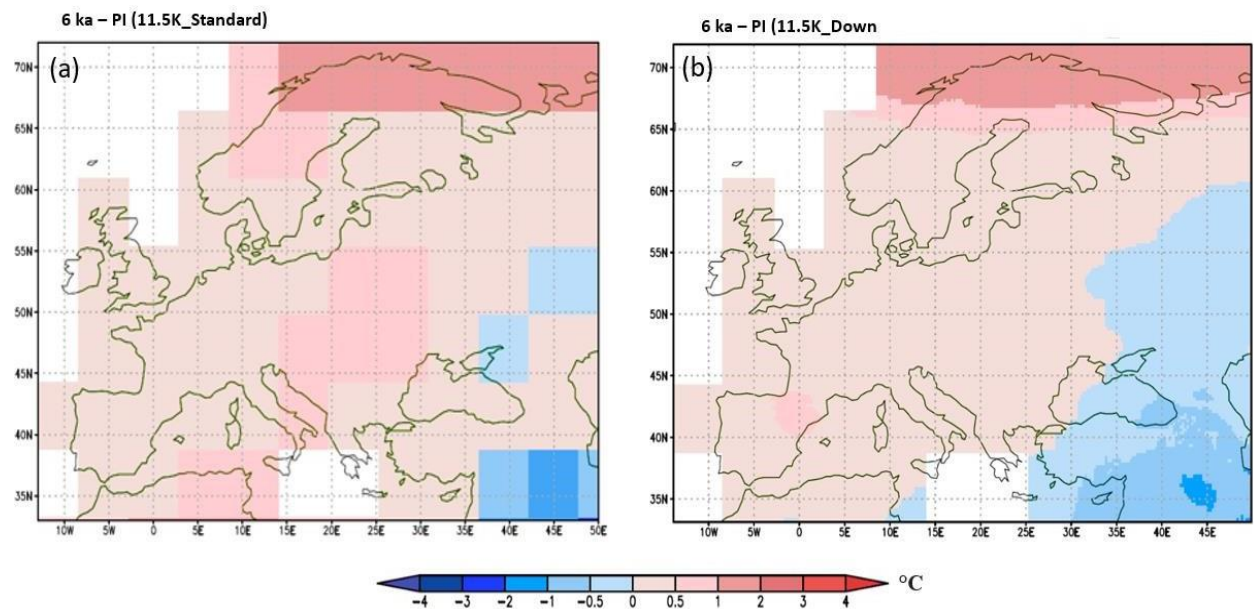


Fig 11: Mean annual temperature anomalies relative to pre-industrial mean (in °C) simulated by the iLOVECLIM, showing spatial variability in Europe at 6 ka BP for 11.5 K_Standard and 11.5 K_Down.

For precipitation, the downscaled version (11.5K_Down) produces higher precipitation values in general, particularly in mountainous regions, and captures detailed information, resulting in a more realistic representation of the impact of topography on precipitation patterns (Fig. 12). The downscaling's principal effect is to enhance precipitation in elevated regions (such as the Scandes mountains and the Alps), which accounts for the higher precipitation anomalies in these mountainous regions (Arthur et al., 2023). In most topographically complex areas of Europe, experiment 11.5K_Down is generally wetter than 11.5K_Standard. (Fig. 12). However, in less elevated areas, 11.5K_Standard is typically wetter than 11.5K_Down. According to the downscaled version 11.5K_Down, precipitation in the Alps doubled as compared to the standard version.

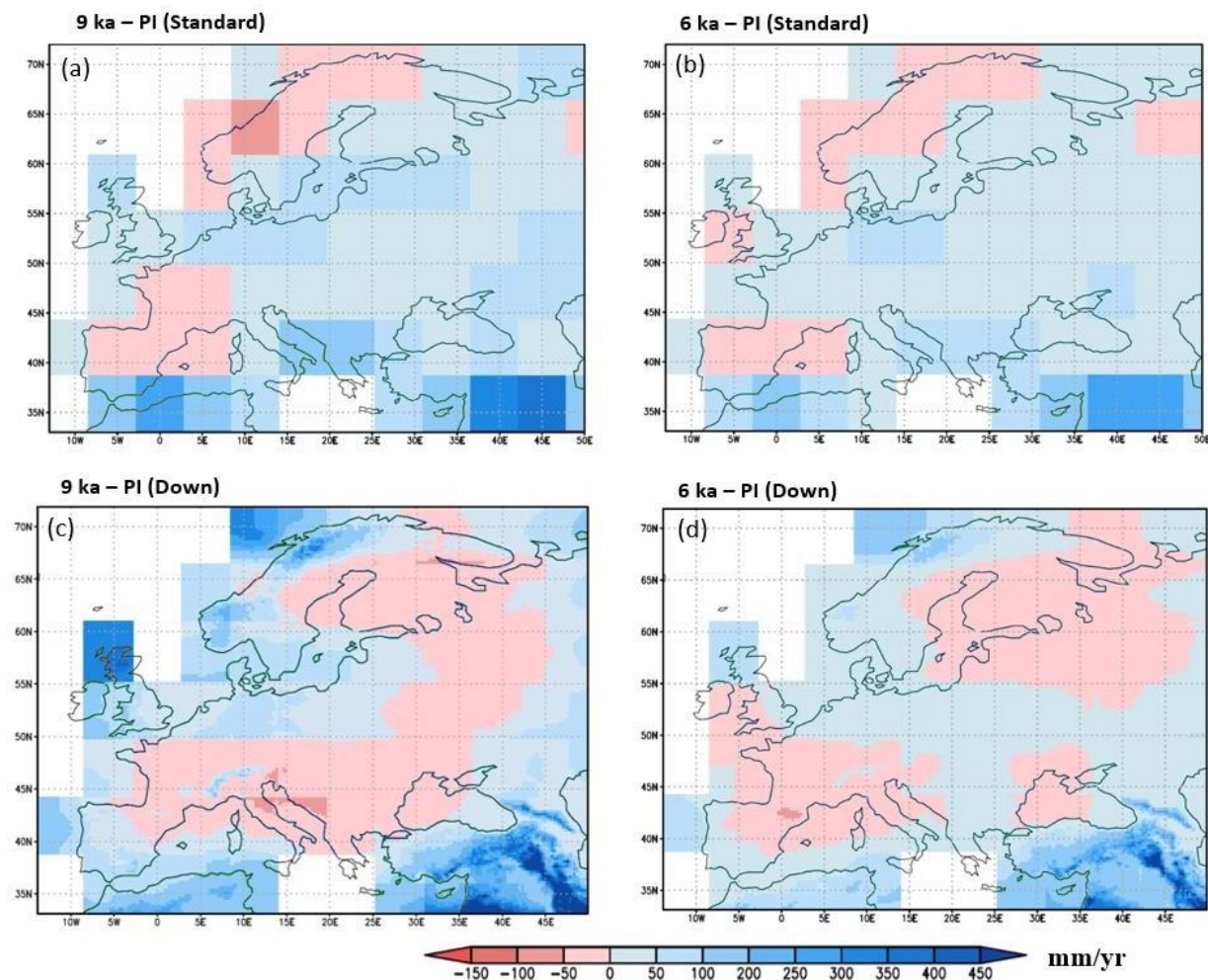


Fig 12: Mean annual precipitation anomalies relative to pre-industrial mean (in mm/yr) simulated by the iLOVECLIM, showing spatial variability in Europe for 9 ka BP (a, c) and 6 ka BP (b, d) for 11.5 K_Standard and 11.5 K_Down.

The performance of the downscaling technique is evaluated by making a comparison between the downscaled results with other climate models and proxy data. The comparison reveals better agreement in terms of temperature and precipitation patterns in Europe as compared to the standard version of the model. For example; Scandinavia (Harrison et al., 1996; Seppä and Birks, 2001; Bjune et al., 2005; Mauri et al., 2015), the Italian Alps (Harrison et al., 1996; Mauri et al., 2015; Furlanetto et al., 2018) and the Mediterranean region (Kuhnt et al., 2008; Bartlein et al., 2011; Roberts et al., 2011; Magny et al., 2013; Guiot and Kaniewski, 2015; Mauri et al., 2015; Sadori et al., 2016; Peyron et al., 2017; Finné et al., 2019). The findings can be used to replicate the various regional responses that some proxy-based

reconstructions have shown, such as the wetter conditions in northern and southern Europe during the mid-Holocene in comparison to pre-industrial values.

The study highlights the importance of using downscaling techniques in paleoclimate research as they provide a more realistic representation of local conditions and facilitate accurate comparisons with proxy data. The downscaling approach employed in this study offers a cost-effective method for conducting multi-millennial simulations and has the potential to improve our knowledge of past climate variability.

3.2 Modelling the climate during the Eemian in Europe with interactive downscaling (Paper 2)

The comparison of the simulated annual mean temperature and precipitation anomalies relative to pre-industrial by both EEM_Down and EEM_Standard show several notable similarities and differences in terms of magnitude and patterns of change depending on the region in Europe. Generally, both simulations highlight the warmer temperature during the Eemian compared to pre-industrial. However, as expected, the EEM_Down provides more detailed information with spatial variability than the EEM_Standard.

Both versions of the model agree on a clear North-South temperature gradient in Europe, with the largest temperature difference relative to pre-industrial (reaching +3°C) seen at 127 ka in Northernmost Europe (Fig. 13). In Southern Europe, this difference is much smaller and even becomes slightly negative, signifying cooler conditions than the pre-industrial era. This temperature gradient becomes less clear later in the Eemian, reflecting the orbitally forced change in summer insolation (see Fig. 7). Comparing the two model versions, the temperature gradient is more expressed in EEM_Down, with warmer conditions in northern Scandinavia and western Europe than EEM_Standard, (Fig 13).

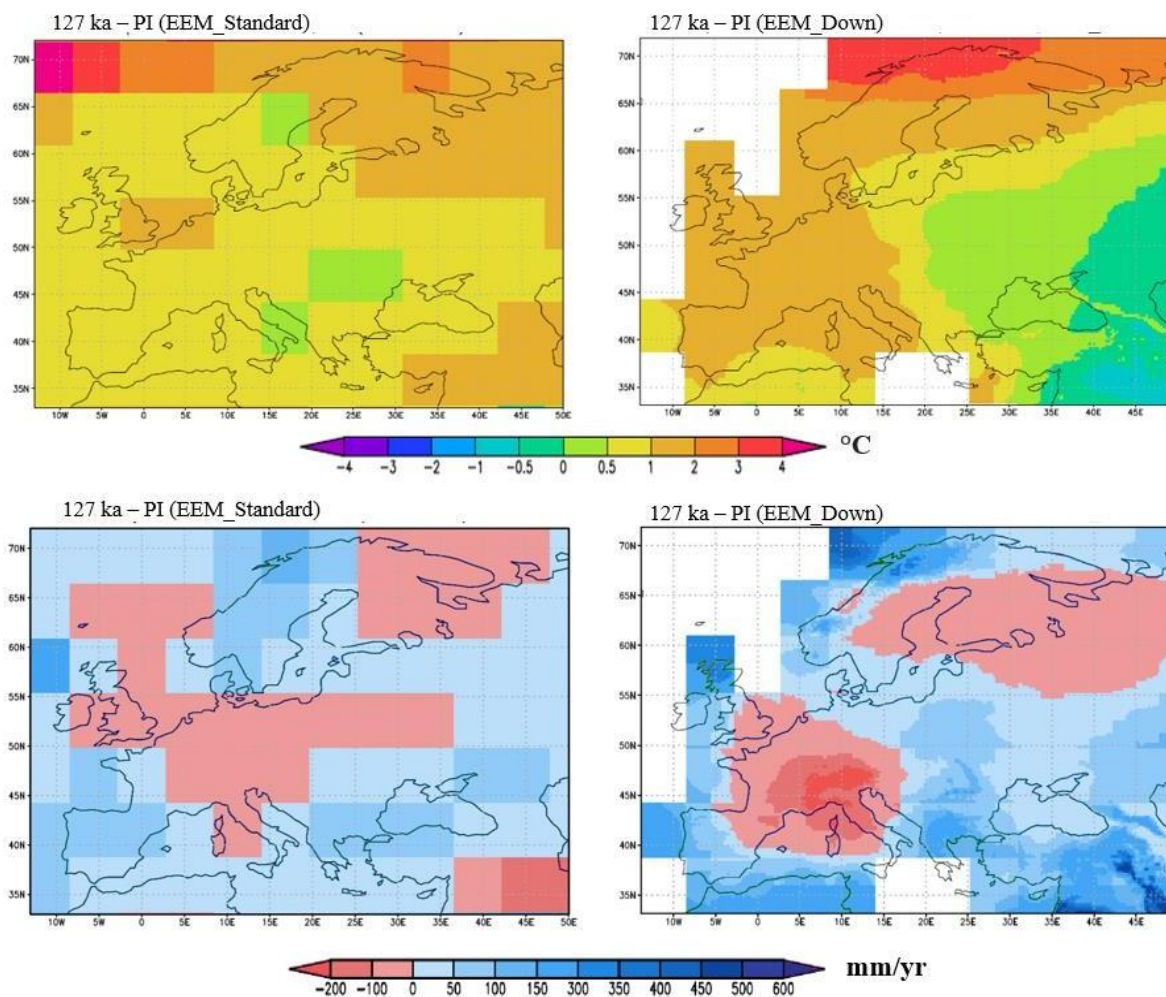


Fig. 13: Simulated mean annual temperature (top in $^{\circ}\text{C}$) and precipitation (bottom in mm/yr) anomalies (relative to the pre-industrial mean) showing spatial distribution in Europe for 127 ka, for EEM_Standard (Left figures) and EEM_Down (Right figures).

The precipitation results of EEM_Standard do not show a clear spatial structure in Fig 13, with basically all changes within -100 to +100 mm/yr , whereas EEM_Down clearly shows a pattern with some areas that are wetter than preindustrial and some regions being drier. There is a wet-dry-wet pattern relative to pre-industrial that has a NW-SE direction, with the Atlantic coast (Iberia, Ireland, Scotland, Scandinavian coast) being wetter, then a zone with drier conditions stretching from France and northern Italy towards the northeast (Finland and Northern Russia), and finally wetter conditions in the southeastern part of the domain. The dry zone is interrupted by slightly wetter conditions in central Europe. This wet-dry-wet pattern in the result of EEM_Down is clearest at 127ka and becomes weaker

later in the Eemian. At this time, the Atlantic coast and the southeastern part of the domain receive more than 300 mm/yr more precipitation than at pre-industrial.

The EEM_Down model accurately reproduces temperature and precipitation anomalies across Europe at 127 ka, with 3-4 °C anomalies in agreement with Capron et al. (2017) and Turney and Jones (2010). Scussolini et al. (2019) conducted comprehensive proxy-based reconstructions, revealing that southern and eastern Europe were wetter than pre-industrial, with precipitation anomalies above 200 mm/yr. The EEM_Down simulations agree with these reconstructions in Italy but disagree with France. Brewer et al. (2008) found a traditional three-part division of the Eemian climate evolution, with an early optimum followed by gradual cooling, followed by a sharp drop in temperatures and precipitation. Wilcox et al. (2020) found that temperatures were up to 4.3 °C warmer during the Eemian than in the present-day. The simulated early Eemian in EEM_Down suggests maximum annual warming in northern Europe, which agrees well with the simulated mean of several models analyzed by Lunt et al. (2013) and the CMIP6-PMIP4 lig127 k simulations as well.

3.3 The impact of volcanism on the Scandinavian climate and human societies during the Holocene (536 and 540 AD) – (paper 3)

The climate simulations with iLOVECLIM show diverse patterns of temperature, precipitation, and Growing Degree Days (GDD0) changes during the volcanic period, with variations observed between the inland and coastal regions in Scandinavia. The mean ensemble temperature anomalies during the volcanic eruption period (536-541 AD) with respect to the simulations without volcanic eruption show a regional decrease of -1°C. The ensemble member 7 yields more regionally varied temperature anomalies (-1 to -1.5 °C inland and -0.25 to -0.5 °C coastally) than the ensemble mean and ensemble member 1 (-1.5°C) (Fig 14). Precipitation results are usually similar between regions, with negative anomalies of up to -25 mm/yr observed and a few areas in Norway showing a reduction in precipitation with anomalies of up to -50 mm/yr (Fig. 14).

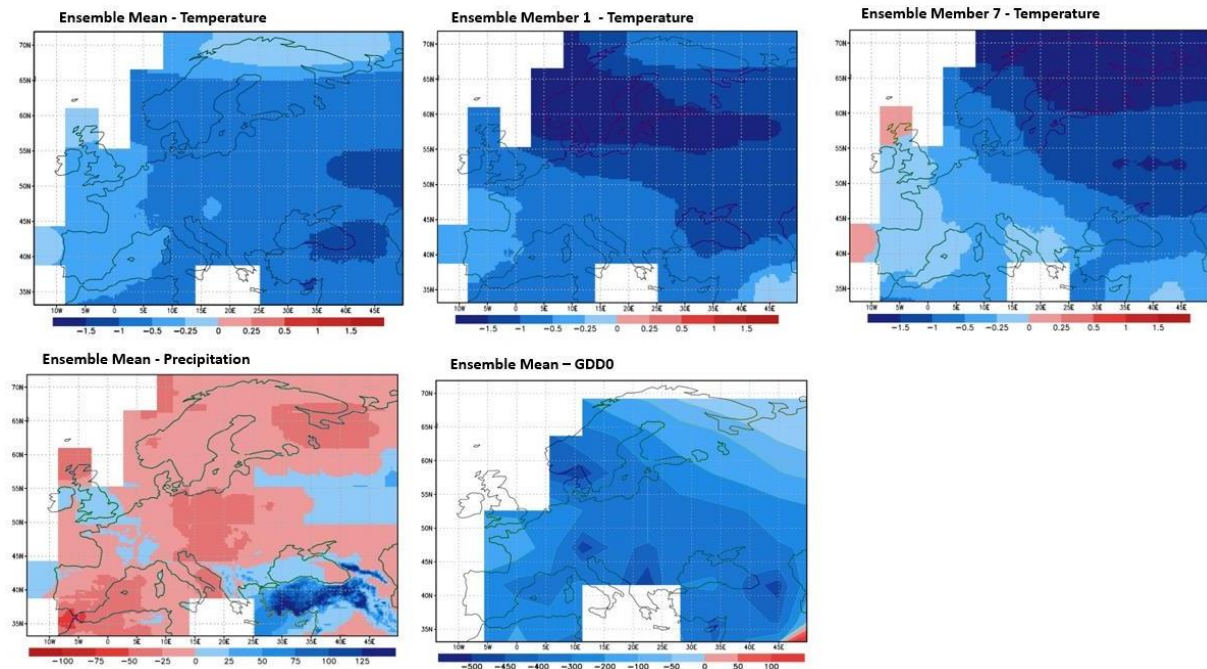


Fig. 14: Ensemble mean temperature anomalies (in °C) during the volcanic eruption (536-541 AD) relative to NOVOLC_1000) and Ensemble members 1 and 7 temperature anomalies (in °C) during the volcanic eruption (536-541 AD) relative to NOVOLC_1000 ensemble member 1 and 7 (top figures). The figures (down) show ensemble mean precipitation (in mm/yr) and Growing Degree Days (in °C/days) during the volcanic eruption (536-541 AD) relative to the NOVOLC_1000 simulations.

Transition II in Norway's land use mark permutation tests reveals two minor settlement hotspots, Coastal Sweden and Inland Sweden, with local growth rates accelerating during the event. Iron production trends were positive, with Coastal Sweden becoming a major iron production hotspot after the volcanic eruption. Local growth rates suggest increased activity during Transition II (Fig 15). However, the rate of local growth in the area suggests that during Transition II, there was an increase in the production of iron, hunting, agriculture and other activities (Arthur et al., 2024).

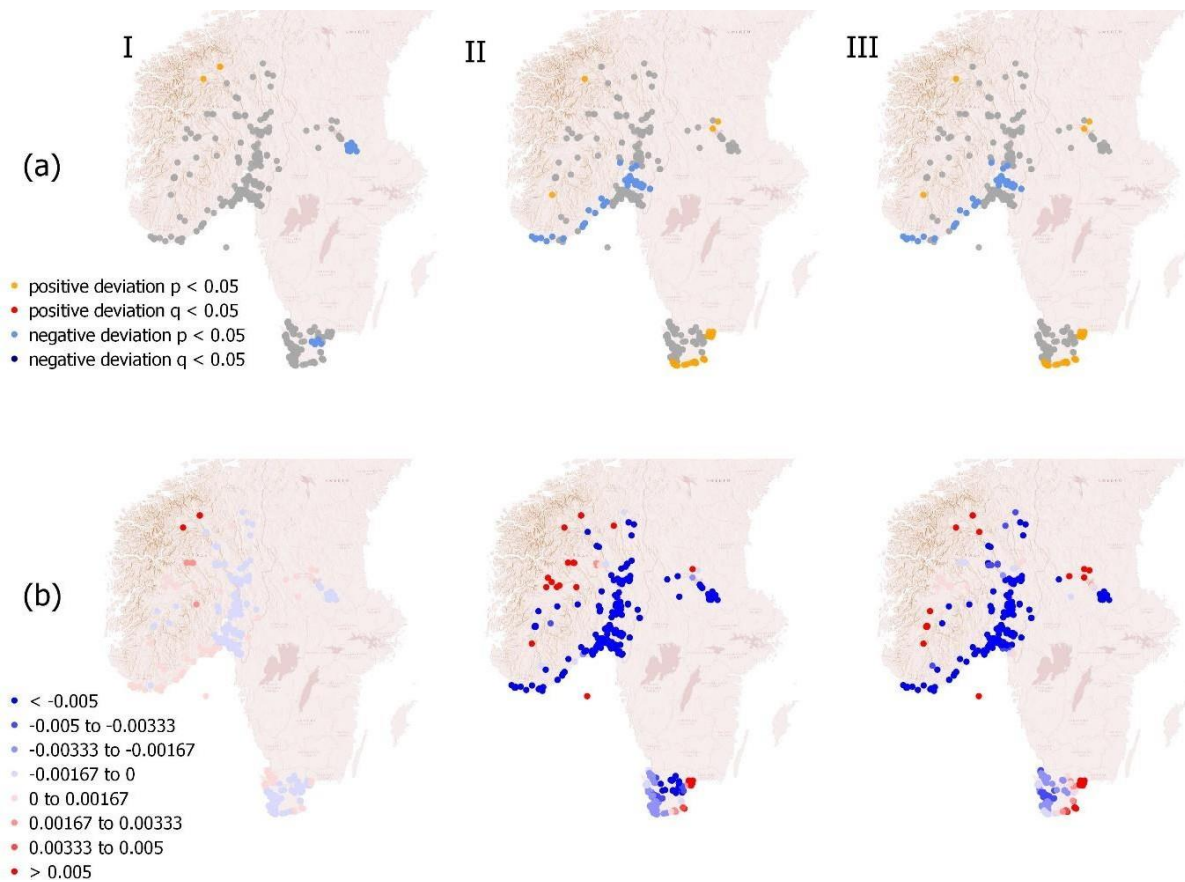


Fig 15: for ‘settlement’ across three (3) transitions: (I) 450-500 to 500-550 AD, (II) 500-550 to 550-600 AD, (III) 550-600 to 650 AD; a) depicts a spatial permutation test showing ‘hot and cold’ spots of growth with p-value and q-value deviations; b) shows local geometric growth rates; So (a) is representing the strength of the changes over the whole area (or all the C14 samples in Scandinavia), with orange *p-values* indicating a positive significant deviation from a permuted null, meaning those areas had more than expected demographic (or population or C14 observation) intensity. The red *q-value* indicates a ‘truer’ positive significance, as this is a test for false discovery rates (a way to further test for type-1 errors - rejecting the null when it should not be rejected). Oppositely, the light blue *p-value* indicates a negative significant deviation (or a loss of population), and the dark blue *q-value* indicates a ‘truer’ negative significance.

(b) represents local mean geometric growth rates, meaning the changes seen between periods (transition I, II, III) at each location (point). The darker blue indicates the most negative growth and the reddest with the most positive growth.

The 536/540 AD volcanic event in Norway led to a substantial reduction in GDD0, which had an impact on crop growth and productivity, especially in the Oslofjord region. Our analysis showed a slight increase in agriculture before and during the event in the archaeological data, followed by a drop during the period of climate recovery. However, the region's unique environmental risks, such as topography and latitude may have pushed it past a critical limit, contributing to an inevitable decline in activity (Arthur et al., 2024). This ongoing transformation may have been accelerated by the volcanic event. There was a drastic reduction in modelled GDD0, temperature, and precipitation in inland Norway as well. According to our climate model, the volcanic eruption in 536/540 AD had a minor climatological impact on Inland Sweden. Although there was a decline in modelled GDD0, temperature, and precipitation, the area's distinct geography, favourable microclimates and a variety of land use probably made it more likely to succeed during the Fimbulwinter. After the eruption, iron production continued in inland Sweden, proving that trading was still a practical means of reducing environmental risk.

3.4 The impact of bias correction on the climate and vegetation (paper 4)

This work is led by Angelina Zapolska, and I provided the Mid-Holocene and pre-industrial climate data to support it. The results of applying the CDF-t method monthly are compared on a yearly basis to the pre-industrial (PI) climate and show that the monthly-based approach resulted in higher correlation and an improved preservation of monthly differences in precipitation and temperature compared to the observations (Zapolska et al., 2023).

The performance of the bias-corrected model in reproducing temperatures of past climate conditions was evaluated using paleotemperature reconstructions. There was a considerable improvement in the agreement between the model and the reconstructions for the mid-Holocene (MH) period on the high-resolution grid over Europe and on a global T21 grid (Fig 16). However, there was no significant improvement for the Last Glacial Maximum (LGM) period. The study reveals a reduction in the well-known, widespread biases in the iLOVECLIM model. The impact of the bias correction on the simulated biome distribution was also analyzed by comparing it with pollen-based vegetation reconstructions

(BIOME6000). It was revealed that the bias-corrected model better matched the reconstructions for the PI and MH periods, particularly on the high-resolution grid over Europe (Fig 16).

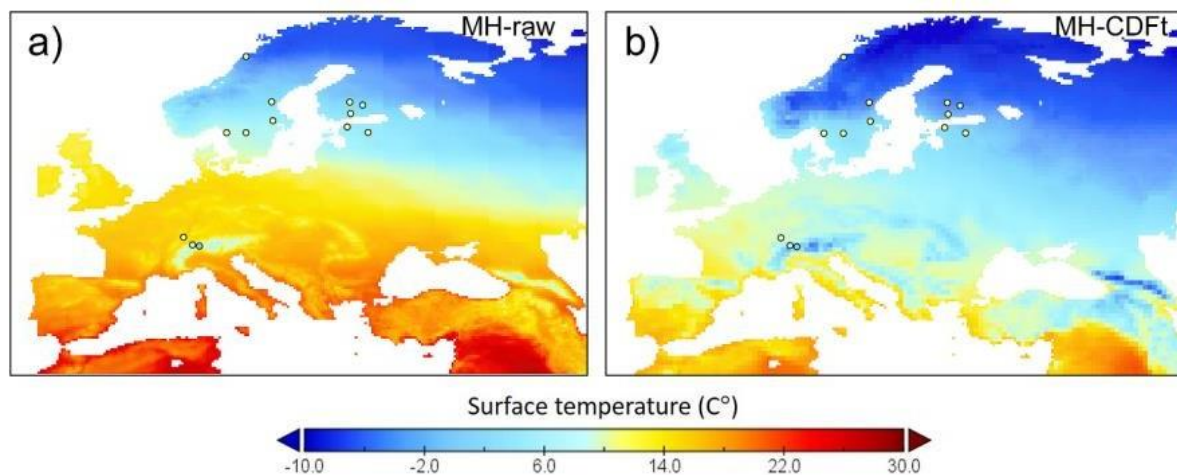


Fig 16: Simulated temperature values for MH (gridded map) and proxy-based temperature values resampled to the high-resolution grid, (data points in circles, Kaufman et al., 2020) (a) before bias correction (MH-raw) and (b) after bias correction (MH-CDF-t) on the high-resolution grid (Zapolska et al., 2023).

The performance of the bias correction is evaluated using both an inverse approach (comparing modelled temperatures with proxy-based temperature reconstructions) and a forward approach (comparing modelled biome distribution with pollen-based biome reconstructions). The inverse approach showed improved agreement between modelled temperatures and reconstructions for the MH. The limitation of this study includes the coarse resolution of the T21 grid that was used for the downscaling and the importance of spatial distribution and continuity of reconstruction data. Despite these limitations, the CDF-t method showed potential for improving the representation of climate and vegetation conditions in the periods studied. Overall, the results demonstrate that the CDF-t bias correction method effectively reduces model biases and improves the agreement between the simulated and reconstructed climate variables. However, the performance of the method depends on the availability and quality of paleoclimate and vegetation data, as well as the resolution of the model. In conclusion, the study emphasized the significance of bias correction in paleoclimate modelling to enhance the accuracy of climate simulations. The CDF-t method provides a promising approach for addressing biases and improving the agreement between modelled and reconstructed data. Further

research and refinements are needed to better understand the limitations and potential of bias correction techniques in paleoclimates modelling.

4 Conclusion and Future Perspective

In these 4 studies, an interactive physical downscaling has been applied to the coarse resolution of the iLOVECLIM model to increase its spatial resolution from 5.56° to 0.25° latitude–longitude in Europe. Transient simulations of the Holocene and the Eemian have been performed with both the low-resolution version and a version with downscaling applied (papers 1 and 2). The downscaling method has been combined with ¹⁴C archaeological data to study the local impact of volcanic eruption on human society in Scandinavia during the fimbulwinter, 536/540 AD (paper 3). Bias correction is then combined with downscaling to correct the biases associated with the model from a paleoclimate perspective (paper 4). Based on the objectives and results of these studies, the following research questions outlined earlier in the thesis have been answered.

- *What is the impact of downscaling on the climate patterns during the past climate (Holocene, Eemian) in Europe?*

To evaluate the effects of downscaling on the climate model, the spatial and temporal temperature and precipitation results of the low-resolution grid are compared with the high-resolution grid. According to the findings, downscaling significantly increases the spatial variability and provides detailed local information compared to the coarse resolution of the standard model, especially in topographic regions (such as the Alps and the Scandes). The downscaling results also agree better with other climate models and proxy-based reconstruction as compared to the standard version.

- *Can we see evidence of the impact of downscaling for the relationship between patterns of climate due to the impact of volcanic eruptions and ¹⁴C records?*

When comparing the correlation between the downscaled climate simulations and the archaeological data, there was a clear difference between the two main regions studied. Land use and demography in Sweden remained mostly stable, and even increased inland after the volcanic event, even though the climate in Scandinavia deteriorated. In contrast, land use and demography declined along the coast of Norway. However, the study was unable to conclusively link the 536/540 AD event to shifts in demography and land use in some of the areas.

- *What is the benefit of employing numerically inexpensive interactive downscaling for paleoclimate studies?*

A numerically inexpensive tool that can run multi-millennial simulations at a kilometric scale has been demonstrated in these studies. The downscaling method is quite simple, yet it managed to obtain a good level of agreement with proxy data. The downscaling technique is suitable for long-term simulations since it requires just a modest amount of computer power. Theoretically, it can be used and expanded in future research to any resolution higher than the T21 grid. The downscaling scheme was able to resolve the small-scale features of the climate system, such as the distribution of land and the topography, making it suitable for comparison with local paleoclimate studies. A good method for comparing climate models with proxy data is downscaling since the simulations are more equipped to match the spatial description of the proxy data. The downscaling's enhanced capacity to provide detailed information in topographical areas is crucial, given that proxy records are frequently obtained at highly elevated regions where the most complex climate archives (such as ice core, pollen records, etc) are retrieved,

- *Within the framework of palaeoclimate modelling, is it possible to develop a technique for correcting climatic biases? If so, what are the advantages and limitations?*

The CDF-t methodology for correcting palaeoclimate modelling biases is described in this study and tested its capacity to execute bias correction of the iLOVECLIM model's simulated variables. Three-time periods (PI, MH, and LGM), as well as two spatial resolutions (5.625° and 0.25° latitude-longitude), were used to test the robustness of the methodology. The application of the CDF-t approach to the simulated values was able to significantly increase the agreement between the simulated and proxy reconstruction data, regardless of the limitations of both the forward and inverse accuracy evaluation. The study concludes that using the CDF-t technique is effective in reducing biases in climate model simulations, particularly for large-scale features such as the mean climate, and is computationally efficient, making it suitable for large datasets and computationally intensive climate models.

Future Perspective

The following recommendations are suggested for future research related to modelling the past climate using downscaling.

- The downscaling in these studies is now focused on annual mean temperatures and precipitation results, but in the Holocene and Eemian, the seasonality was more expressed than today. So, it would be interesting to see studies with the downscaling technique also to seasonal results, or even shorter timescales (days or weeks) because events such as volcanic eruptions can have a strong short-term effect. Again, further studies should evaluate/test this downscaling approach in other regions than Europe.
- The computation of the atmospheric dynamics in iLOVECLIM is still done at the coarse grid scale. As a result, the fine-scale structure of the wind patterns, which may have an impact on the temperature and precipitation, is not considered. Future improvements to the model could include downscaling both the atmospheric physics and the atmospheric dynamics. This will however be computationally expensive, but a different approach would be to use the native grid wind direction to weigh the nearby sub-grid precipitation, which will require less computation.
- The first CDF-t approach-based bias correction of paleoclimate modelling was presented in paper 4. The suggested methodology needs to be evaluated on more different time periods of the past with diverse Earth system models of intermediate complexity to further evaluate the use of the CDF-t application in paleoclimates modelling.
- In paper 4, no appreciable improvement in pollen-based reconstructions was found during the LGM, which was likely due to the limitations of data that was used to characterize the glacial environment. Further study is required for the LGM because the results were mostly influenced by limited data points in the reconstructions.
- The impact of the volcanic eruption during the 536/540 AD (paper 3) can further be explored by investigating if there is a potential for a future fimbulwinter-type event, and if so, which regions could be more affected considering the present-day demography in Europe.
- Future studies should take into consideration the Lag time when comparing society and climate records (paper 3). Human society changes can take longer to manifest in the archaeological record, delaying the appearance of responses to environmental factors. Several research projects are currently ongoing to overcome this issue (e.g., Heitz et al., 2021; Kim et al., 2021). One of the techniques is to do significance tests on the relationship between variations in population

development and climatic events. Researchers can better comprehend how climate events relate to societal developments by considering these lag time effects.

5 Bibliography

Arjava, A. (2005). The Mystery Cloud of 536 CE in the Mediterranean Sources. *Dumbarton Oaks Papers*, 59, 73. <https://doi.org/10.2307/412875.1>.

Arrhenius, B. (2023). Helgö in the shadow of the dust veil 536-37. *The Journal of Archaeology and Ancient History*, 5, 1–15. <https://doi.org/10.33063/jaah.vi5.122>.

Arthur, F., Hatlestad, K., Lindholm, K. J., Loftsgarden, K., Löwenborg, D., Solheim, S., Roche D. M., & Renssen, H. (2024). The impact of volcanism on Scandinavian climate and human societies during the Holocene: Insights into the Fimbulwinter eruptions (536/540 AD). *The Holocene*. <https://doi.org/10.1177/09596836231225718>.

Arthur, F., Roche, D. M., Fyfe, R., Quiquet, A., & Renssen, H. (2023). Simulations of the Holocene climate in Europe using an interactive downscaling within the iLOVECLIM model (version 1.1). *Climate of the Past*, 19(1), 87–106. <https://doi.org/10.5194/cp-19-87-2023>.

Axboe, M. (1999). The year 536 and the Scandinavian gold hoards. *Medieval Archaeology*, 43. 186-188.

Bader, J., Jungclaus, J., Krivova, N., Lorenz, S., Maycock, A., Raddatz, T., Schmidt, H., Toohey, M., Wu, C. J., & Claussen, M. (2020). Global temperature modes shed light on the Holocene temperature conundrum. *Nature Communications*, 11(1). <https://doi.org/10.1038/s41467-020-18478-6>

Baillie, MG. (1999). Exodus to Arthur: catastrophic encounters with comets. BT Batsford Ltd, London.

Bakker, P. (2014). Modelling the climate of the Last Interglacial: The evolution of the Last Interglacial climate and its sensitivity to melting of the Greenland Ice Sheet, an investigation through model inter-comparison and model-data comparison. [PhD-Thesis - Research and graduation internal, Vrije Universiteit Amsterdam].

Bakker, P., Stone, E. J., Charbit, S., Gröger, M., Krebs-Kanzow, U., Ritz, S. P., Varma, V., Khon, V., Lunt, D. J., Mikolajewicz, U., Prange, M., Renssen, H., Schneider, B., & Schulz, M. (2013). Last

interglacial temperature evolution – a model inter-comparison. *Climate of the Past*, 9(2), 605–619. <https://doi.org/10.5194/cp-9-605-2013>.

Bartlein, P. J., Harrison, S. P., Brewer, S., Connor, S., Davis, B. A. S., Gajewski, K., Guiot, J., Harrison-Prentice, T. I., Henderson, A., Peyron, O., Prentice, I. C., Scholze, M., Seppä, H., Shuman, B., Sugita, S., Thompson, R. S., Vial, A. E., Williams, J., & Wu, H. (2010). Pollen-based continental climate reconstructions at 6 and 21 ka: a global synthesis. *Climate Dynamics*, 37(3–4), 775–802. <https://doi.org/10.1007/s00382-010-0904-1>.

Berger, A. L. (1978). Long-Term Variations of Caloric Insolation Resulting from the Earth's Orbital Elements. *Quaternary Research*, 9(2), 139–167. [https://doi.org/10.1016/0033-5894\(78\)90064-9](https://doi.org/10.1016/0033-5894(78)90064-9).

Bjune, A. E., Bakke, J., Nesje, A., & Birks, H. J. (2005). Holocene mean July temperature and winter precipitation in western Norway inferred from palynological and glaciological lake-sediment proxies. *The Holocene*, 15(2), 177–189. <https://doi.org/10.1191/0959683605hl798rp>.

Bonfils, C., de Noblet-Ducoudré, N., Guiot, J., & Bartlein, P. (2004). Some mechanisms of mid-Holocene climate change in Europe, inferred from comparing PMIP models to data. *Climate Dynamics*, 23(1), 79–98. <https://doi.org/10.1007/s00382-004-0425-x>.

Born, A., Nisancioglu, K. H., & Braconnot, P. (2009). Sea ice induced changes in ocean circulation during the Eemian. *Climate Dynamics*, 35(7–8), 1361–1371. <https://doi.org/10.1007/s00382-009-0709-2>.

Braconnot, P., Otto-Bliesner, B., Harrison, S., Joussaume, S., Peterchmitt, J.-Y., Abe-Ouchi, A., Crucifix, M., Driesschaert, E., Fichet, Th., Hewitt, C. D., Kageyama, M., Kitoh, A., Laine, A., Loutre, M.-F., Marti, O., Merkel, U., Ramstein, G., Valdes, P., Weber, S. L., Yu, Y., & Zhao, Y. (2007). Results of PMIP2 coupled simulations of the Mid-Holocene and Last Glacial Maximum – Part 1: experiments and large-scale features. *Climate of the Past*, 3, 261–277. <https://doi.org/10.5194/cp-3-261-2007>.

Bradley, R. S., Hughes, M. K., & Diaz, H. F. (2003). Climate in Medieval Time. *Science*, 302(5644), 404–405. <https://doi.org/10.1126/science.1090372>.

Bradley, R.S. (2014). *Paleoclimatology: Reconstructing Climates of the Quaternary* (3rd edition). Elsevier/Academic Press, San Diego. 675pp (ISBN: 9780123869135).

Brewer, S., Guiot, J., & Torre, F. (2007). Mid-Holocene climate change in Europe: a data-model comparison. *Climate of the Past*, 3(3), 499–512. <https://doi.org/10.5194/cp-3-499-2007>.

Brewer, S., Guiot, J., Sánchez-Goñi, M., & Klotz, S. (2008). The climate in Europe during the Eemian: a multi-method approach using pollen data. *Quaternary Science Reviews*, 27(25–26), 2303–2315. <https://doi.org/10.1016/j.quascirev.2008.08.029>.

Brierley, C. M., Zhao, A., Harrison, S. P., Braconnot, P., Williams, C. J. R., Thornalley, D. J. R., Shi, X., Peterschmitt, J.-Y., Ohgaito, R., Kaufman, D. S., Kageyama, M., Hargreaves, J. C., Erb, M. P., Emile-Geay, J., D'Agostino, R., Chandan, D., Carré, M., Bartlein, P. J., Zheng, W., Zhang, Z., Zhang, Q., Yang, H., Volodin, E. M., Tomas, R. A., Routson, C., Peltier, W. R., Otto-Bliesner, B., Morozova, P. A., McKay, N. P., Lohmann, G., Legrande, A. N., Guo, C., Cao, J., Brady, E., Annan, J. D., & Abe-Ouchi, A. (2020). Large-scale features and evaluation of the PMIP4-CMIP6 *midHolocene* simulations, *Climate of the Past*, 16, 1847–1872. <https://doi.org/10.5194/cp-16-1847-2020>.

Brook, E. J. (2007). Ice Core Methods: Overview. In Elias, S. A., editor, *Encyclopedia*.

Brovkin, V., Ganopolski, A., & Svirezhev, Y. (1997). A continuous climate-vegetation classification for use in climate-biosphere studies. *Ecological Modelling*, 101(2–3), 251–261. [https://doi.org/10.1016/s0304-3800\(97\)00049-5](https://doi.org/10.1016/s0304-3800(97)00049-5).

Büntgen, U., Arseneault, D., Boucher, É., Churakova, O. V., Gennaretti, F., Crivellaro, A., Hughes, M. K., Kirilyanov, A. V., Klippel, L., Krusic, P. J., Linderholm, H. W., Ljungqvist, F. C., Ludescher, J., McCormick, M., Myglan, V. S., Nicolussi, K., Piermattei, A., Oppenheimer, C., Reinig, F., Sigl, M., Vaganov, E. A., & Esper, J. (2020). Prominent role of volcanism in Common Era climate variability and human history. - *Dendrochronologia*, 64, 125757. <https://doi.org/10.1016/j.dendro.2020.125757>.

Büntgen, U., Myglan, V. S., Ljungqvist, F. C., McCormick, M., Di Cosmo, N., Sigl, M., Jungclaus, J., Wagner, S., Krusic, P. J., Esper, J., Kaplan, J. O., de Vaan, M. A. C., Luterbacher, J., Wacker, L., Tegel, W., & Kirilyanov, A. V. (2016). Cooling and societal change during the Late Antique Little Ice Age from 536 to around 660 AD. *Nature Geoscience*, 9(3), 231–236. <https://doi.org/10.1038/ngeo2652>.

Burke, A., Peros, M. C., Wren, C. D., Pausata, F. S. R., Riel-Salvatore, J., Moine, O., de Vernal, A., Kageyama, M., & Boisard, S. (2021). The archaeology of climate change: The case for cultural diversity. *Proceedings of the National Academy of Sciences of the United States of America*, 118(30), e2108537118. <https://doi.org/10.1073/pnas.2108537118>.

Cantelaube, P., Jayet, P., Carré, F., Bamps, C., & Zakharov, P. (2012). Geographical downscaling of outputs provided by an economic farm model calibrated at the regional level. *Land Use Policy*, 29(1), 35–44. <https://doi.org/10.1016/j.landusepol.2011.05.002>.

Castro, C. L., Pielke, R. A., & Leoncini, G. (2005). Dynamical downscaling: Assessment of value retained and added using the Regional Atmospheric Modeling System (RAMS). *Journal of Geophysical Research: Atmospheres*, 110(D5). <https://doi.org/10.1029/2004jd004721>.

Capron, E., Govin, A., Feng, R., Otto-Bliesner, B., & Wolff, E. (2017). Critical evaluation of climate syntheses to benchmark CMIP6/PMIP4 127 ka Last Interglacial simulations in the high-latitude regions. *Quaternary Science Reviews*, 168, 137–150. <https://doi.org/10.1016/j.quascirev.2017.04.019>.

Claussen, M., Mysak, L. A., Weaver, A. J., Crucifix, M., Fichet, T., Loutre, M.-F., Weber, S. L., Alcamo, J., Alexeev, V. A., Berger, A., Calov, R., Ganopolski, A., Goosse, H., Lohmann, G., Lunkeit, F., Mokhov, I. I., Petoukhov, V., Stone, P., & Wang, Z. (2002). Earth system models of intermediate complexity: closing the gap in the spectrum of climate system models, *Climate Dynamics*, 18, 579–586. <https://doi.org/10.1007/s00382-001-0200-1>.

Cronin, T. M. (2010). *Paleoclimates: Understanding Climate Change Past and Present*. Columbia University Press. <http://www.jstor.org/stable/10.7312/cron14494>.

Dallmeyer, A., Poska, A., Marquer, L., Seim, A., & Gaillard, M.-J. (2023). The challenge of comparing pollen-based quantitative vegetation reconstructions with outputs from vegetation models – a European perspective, *Climate of the Past*, 19, 1531–1557. <https://doi.org/10.5194/cp-19-1531-2023>.

Davis, B., Brewer, S., Stevenson, A., & Guiot, J. (2003). The temperature of Europe during the Holocene reconstructed from pollen data. *Quaternary Science Reviews*, 22(15–17), 1701–1716. [https://doi.org/10.1016/s0277-3791\(03\)00173-2](https://doi.org/10.1016/s0277-3791(03)00173-2).

Dowsett, H. J. (2007). Paleooceanography, Biological Proxies: Planktic foraminifera. In Elias, S. A., editor, *Encyclopedia of Quaternary Science*, pages 1678 – 1682. Elsevier, Oxford.

Driesschaert, E., Fichet, T., Goosse, H., Huybrechts, P., Janssens, I., Mouchet, A., Munhoven, G., Brovkin, V., & Weber, S. L. (2007). Modeling the influence of Greenland ice sheet melting on the Atlantic meridional overturning circulation during the next millennia. *Geophysical Research Letters*, 34(10). <https://doi.org/10.1029/2007gl029516>.

Finné, M., Woodbridge, J., Labuhn, I., & Roberts, C. N. (2019). Holocene hydro-climatic variability in the Mediterranean: A synthetic multi-proxy reconstruction. *The Holocene*, 29(5), 847–863. <https://doi.org/10.1177/0959683619826634>.

Friman, B., & Lagerås, P. (2022). From Neolithic Boom-and-Bust to Iron Age Peak and Decline: Population and Settlement Dynamics in Southern Sweden Inferred from Summed Radiocarbon Dates. *European Journal of Archaeology*, 26(2), 168–188. <https://doi.org/10.1017/ea.2022.43>.

Furlanetto, G., Ravazzi, C., Pini, R., Vallè, F., Brunetti, M., Comolli, R., Novellino, M. D., Garozzo, L., & Maggi, V. (2018). Holocene vegetation history and quantitative climate reconstructions in a high-elevation oceanic district of the Italian Alps. Evidence for a middle to late Holocene precipitation increase. *Quaternary Science Reviews*, 200, 212–236. <https://doi.org/10.1016/j.quascirev.2018.10.001>.

Gao, C., Oman, L., Robock, A., & Stenchikov, G. L. (2007). Atmospheric volcanic loading derived from bipolar ice cores: Accounting for the spatial distribution of volcanic deposition. *Journal of Geophysical Research*, 112(D9). <https://doi.org/10.1029/2006jd007461>.

Goosse, H. (2015). *Climate System Dynamics and Modelling*. Cambridge University Press.

Goosse, H., & Fichefet, T. (1999). Importance of ice-ocean interactions for the global ocean circulation: A model study. *Journal of Geophysical Research Oceans*, 104(C10), 23337–23355. <https://doi.org/10.1029/1999jc900215>.

Goosse, H., Brovkin, V., Fichefet, T., Haarsma, R., Huybrechts, P., Jongma, J., Mouchet, A., Selten, F., Barriat, P.-Y., Campin, J.-M., Deleersnijder, E., Driesschaert, E., Goelzer, H., Janssens, I., Loutre, M.-F., Morales Maqueda, M. A., Opsteegh, T., Mathieu, P.-P., Munhoven, G., Pettersson, E. J., Renssen, H., Roche, D. M., Schaeffer, M., Tartinville, B., Timmermann, A., & Weber, S. L. (2010). Description of the Earth system model of intermediate complexity LOVECLIM version 1.2, *Geoscience Model Development*, 3, 603–633. <https://doi.org/10.5194/gmd-3-603-2010>.

Goosse, H., Renssen, H., Timmermann, A., & Bradley, R. S. (2005). Internal and forced climate variability during the last millennium: a model-data comparison using ensemble simulations. *Quaternary Science Reviews*, 24(12–13), 1345–1360. <https://doi.org/10.1016/j.quascirev.2004.12.009>.

Gräslund, B. (2007). Fimbulvintern, Ragnarök och klimatkrisen år 536-537 e.Kr. *Saga och sed: Kungl. Gustav Adolfs akademis årsbok*. 93-123.

Gräslund, B., & Price, N. (2012). Twilight of the gods? The ‘dust veil event’ of AD 536 in critical perspective. *Antiquity*, 86(332), 428–443. <https://doi.org/10.1017/s0003598x00062852>.

Guiot, J., & Kaniewski, D. (2015). The Mediterranean Basin and Southern Europe in a warmer world: what can we learn from the past? *Frontiers in Earth Science*, 3. <https://doi.org/10.3389/feart.2015.00028>.

Gunn, J.D. (2000). AD 536 and its 300-year aftermath - The Years Without Summer: Tracing AD 536 and Its Aftermath. Ed. J. D. Gunn. (BAR, International Series), 872, Oxford. 5ñ20.

Gupta, A.K. (2004). Origin of agriculture and domestication of plants and animals linked to early Holocene climate amelioration. *Current Science*, 87. 54–59.

Hargreaves, J. C., Annan, J. D., Ohgaito, R., Paul, A., & Abe-Ouchi, A. (2013). Skill and reliability of climate model ensembles at the Last Glacial Maximum and mid-Holocene. *Climate of the Past*, 9(2), 811–823. <https://doi.org/10.5194/cp-9-811-2013>.

Harrison, S. P., Yu, G., & Tarasov., P. E. (1996). Late Quaternary Lake-Level Record from Northern Eurasia. *Quaternary Research*, 45(2), 138–159. <https://doi.org/10.1006/qres.1996.0016>.

Hatlestad, K., Wehlin, J., & Lindholm, K. J. (2021). Coping with Risk. A Deep-Time Perspective on Societal Responses to Ecological Uncertainty in the River Dalälven Catchment Area in Sweden. *Land*, 10(8), 883. <https://doi.org/10.3390/land10080883>.

Heitz, C., Laabs, J., Hinz, M., Hafner., A. (2021). Collapse and Resilience in Prehistoric Archaeology: Questioning Concepts and Causalities in Models of Climate-Induced Societal Transformations. In: Erdkamp, P., Manning, J.G., Verboven, K. (eds) *Climate Change and Ancient Societies in Europe and the Near East*. Palgrave Studies in Ancient Economies. Cham Palgrave Macmillan, pp.127–199. https://doi.org/10.1007/978-3-030-81103-7_5.

Helama, S., Arppe, L., Uusitalo, J., Holopainen, J., Mäkelä, H. M., Mäkinen, H., Mielikäinen, K., Nöjd, P., Sutinen, R., Taavitsainen, J. P., Timonen, M., & Oinonen., M. (2018). Volcanic dust veils from sixth century tree-ring isotopes linked to reduced irradiance, primary production and human health. *Scientific Reports*, 8(1). <https://doi.org/10.1038/s41598-018-19760-w>.

Holm, I., Innselset., S. M., & Oye, I. (eds) (2005). *Utmark: The Outfield as Industry and Ideology in the Iron Age and the Middle Ages*. Bergen: UBAS. University of Bergen Archaeological Series International. Available at: <http://opac.regesta-imperii.de/id/1024317> (accessed 20 July 2023).

Holm, O. (2012). *Självägarområdenas egenart: Jämtland och andra områden i Skandinavien med småskaligt jordäggande 900-1500*. Diss. Stockholm: Stockholm University.

Huybers, P., & Langmuir, C. (2009). Feedback between deglaciation, volcanism, and atmospheric CO₂. *Earth and Planetary Science Letters*, 286(3–4), 479–491. <https://doi.org/10.1016/j.epsl.2009.07.014>.

IPCC. (2013): *Climate Change 2013: The Physical Science Basis. Contribution of Working Group I to the Fifth Assessment Report of the Intergovernmental Panel on Climate Change* [Stocker, T.F., D. Qin, G.-K. Plattner, M. Tignor, S.K. Allen, J. Boschung, A. Nauels, Y. Xia, V. Bex and P.M. Midgley (eds.)]. Cambridge University Press, Cambridge, United Kingdom and New York, NY, USA, 1535 pp.

Jungclauss, J. H., Bard, E., Baroni, M., Braconnot, P., Cao, J., Chini, L. P., Egorova, T., Evans, M., González-Rouco, J. F., Goosse, H., Hurrett, G. C., Joos, F., Kaplan, J. O., Khodri, M., Klein Goldewijk, K., Krivova, N., LeGrande, A. N., Lorenz, S. J., Luterbacher, J., Man, W., Maycock, A. C., Meinshausen, M., Moberg, A., Muscheler, R., Nehrbass-Ahles, C., Otto-Bliesner, B. I., Phipps, S. J., Pongratz, J., Rozanov, E., Schmidt, G. A., Schmidt, H., Schmutz, W., Schurer, A., Shapiro, A. I., Sigl, M., Smerdon, J. E., Solanki, S. K., Timmreck, C., Toohey, M., Usoskin, I. G., Wagner, S., Wu, C.-J., Yeo, K. L., Zanchettin, D., Zhang, Q., & Zorita, E. (2017). The PMIP4 contribution to CMIP6 – Part 3: The last millennium, scientific objective, and experimental design for the PMIP4 *past1000* simulations, *Geoscientific Model Development*, 10, 4005–4033. <https://doi.org/10.5194/gmd-10-4005-2017>.

Kageyama, M., Albani, S., Braconnot, P., Harrison, S. P., Hopcroft, P. O., Ivanovic, R. F., Lambert, F., Marti, O., Peltier, W. R., Peterschmitt, J.-Y., Roche, D. M., Tarasov, L., Zhang, X., Brady, E. C., Haywood, A. M., LeGrande, A. N., Lunt, D. J., Mahowald, N. M., Mikolajewicz, U., Nisancioglu, K. H., Otto-Bliesner, B. L., Renssen, H., Tomas, R. A., Zhang, Q., Abe-Ouchi, A., Bartlein, P. J., Cao, J., Li, Q., Lohmann, G., Ohgaito, R., Shi, X., Volodin, E., Yoshida, K., Zhang, X., & Zheng, W. (2017). The PMIP4 contribution to CMIP6 – Part 4: Scientific objectives and experimental design of the PMIP4-CMIP6 Last Glacial Maximum experiments and PMIP4 sensitivity experiments, *Geoscientific Model Development*, 10, 4035–4055. <https://doi.org/10.5194/gmd-10-4035-2017>, 2017.

Kageyama, M., Braconnot, P., Bopp, L., Mariotti, V., Roy, T., Woillez, M.-N., Caubel, A., Foujols, M.-A., Guilyardi, E., Khodri, M., Lloyd, J., Lombard, F., & Marti, O. (2013). "Mid-Holocene and Last

Glacial Maximum climate simulations with the IPSL model. Part II: model-data comparisons." *Climate Dynamics*, 40, 2469-2495. doi: 10.1007/s00382-012-1499-5.

Kaspar, F., Spanghel, T., & Cubasch, U. (2007). Northern hemisphere winter storm tracks of the Eemian interglacial and the last glacial inception. *Climate of the Past*, 3(2), 181–192. <https://doi.org/10.5194/cp-3-181-2007>.

Keys, D. (2000). *Catastrophe: A quest for the origins of the modern world*. New York: Ballantine Pub.

Kim, H., Lee, G. A., & Crema, E. R. (2021). ‘Bayesian analyses question the role of climate in Chulmun demography’, *Scientific Reports*, 11(1), pp. 1–10. DOI: 10.1038/s41598-021-03180-4.

Kitover, D. C., van Balen, R., Roche, D. M., Vandenberghe, J., & Renssen, H. (2015). Advancement toward coupling of the VAMPER permafrost model within the Earth system model *iLOVECLIM* (version 1.0): description and validation, *Geoscientific Model Development*, 8, 1445–1460. <https://doi.org/10.5194/gmd-8-1445-2015>.

Krinner, G., & Genthon, C. (1997). The Antarctic surface mass balance in a stretched grid general circulation model. *Annals of Glaciology*, 25, 73–78. <https://doi.org/10.3189/s0260305500013823>.

Kuhnt, T., Schmiiedl, G., Ehrmann, W., Hamann, Y., & Andersen, N. (2008). Stable isotopic composition of Holocene benthic foraminifers from the Eastern Mediterranean Sea: Past changes in productivity and deep-water oxygenation. *Paleogeography, Palaeoclimatology, Paleoecology*, 268(1–2), 106–115. <https://doi.org/10.1016/j.palaeo.2008.07.010>.

Lavaysse, C., Vrac, M., Drobinski, P., Lengaigne, M., & Vischel, T. (2012). Statistical downscaling of the French Mediterranean climate: assessment for present and projection in an anthropogenic scenario. *Natural Hazards and Earth System Sciences*, 12(3), 651–670. <https://doi.org/10.5194/nhess-12-651-2012>.

Li, H., Renssen, H., & Roche, D.M. (2020). Modeling climate-vegetation interactions during the last interglacial: The impact of biogeophysical feedbacks in North Africa. *Quaternary Science Reviews*, 249. doi: 10.1016/j.quascirev.2020.106609.

Loftsgarden, K. (2020). Mass Production and Mountain Marketplaces in Norway in the Viking and Middle Ages. *Medieval Archaeology*, 64(1), 94–115. <https://doi.org/10.1080/00766097.2020.1754662>.

Loftsgarden, K. (2019). The Prime Movers of iron production in the Norwegian Viking and Middle Ages. *Fornvannen-Journal of Swedish Antiquarian Research*, 114(2). 75–87.

Lorenz, D. J., Nieto-Lugilde, D., Blois, J. L., Fitzpatrick, M. C., & Williams, J. W. (2016). Downscaled and debiased climate simulations for North America from 21,000 years ago to 2100AD. *Scientific Data*, 3(1). <https://doi.org/10.1038/sdata.2016.48>.

Loulergue, L., Schilt, A., Spahni, R., Masson-Delmotte, V., Blunier, T., Lemieux, B., Barnola, J. M., Raynaud, D., Stocker, T. F., & Chappellaz, J. (2008). Orbital and millennial-scale features of atmospheric CH₄ over the past 800,000 years. *Nature*, 453(7193), 383–386. <https://doi.org/10.1038/nature06950>.

Löwenborg, D. (2012). An Iron Age Shock Doctrine. *The Journal of Archaeology and Ancient History*, (4), 1–29. DOI: 10.33063/jaah.vi4.120.

Ludwig, P., Gómez-Navarro, J. J., Pinto, J. G., Raible, C. C., Wagner, S., & Zorita, E. (2018). Perspectives of regional paleoclimate modeling. *Annals of the New York Academy of Sciences*, 1436(1), 54–69. <https://doi.org/10.1111/nyas.13865>.

Lunt, D. J., Abe-Ouchi, A., Bakker, P., Berger, A., Braconnot, P., Charbit, S., Fischer, N., Herold, N., Jungclaus, J. H., Khon, V. C., Krebs-Kanzow, U., Langebroek, P. M., Lohmann, G., Nisancioglu, K. H., Otto-Bliesner, B. L., Park, W., Pfeiffer, M., Phipps, S. J., Prange, M., Rachmayani, R., Renssen, H., Rosenbloom, N., Schneider, B., Stone, E. J., Takahashi, K., Wei, W., Yin, Q., & Zhang, Z. S. (2013). A multi-model assessment of last interglacial temperatures, *Climate of the Past*, 9, 699–717. <https://doi.org/10.5194/cp-9-699-2013>.

Magny, M., Combourieu-Nebout, N., de Beaulieu, J. L., Bout-Roumazeilles, V., Colombaroli, D., Desprat, S., Francke, A., Joannin, S., Ortu, E., Peyron, O., Revel, M., Sadori, L., Siani, G., Sicre, M. A., Samartin, S., Simonneau, A., Tinner, W., Vannièrè, B., Wagner, B., Zanchetta, G., Anselmetti, F., Brugiapaglia, E., Chapron, E., Debret, M., Desmet, M., Didier, J., Essallami, L., Galop, D., Gilli, A., Haas, J. N., Kallel, N., Millet, L., Stock, A., Turon, J. L., & Wirth, S. (2013). North–south palaeohydrological contrasts in the central Mediterranean during the Holocene: tentative synthesis and working hypotheses, *Climate of the Past*, 9, 2043–2071. <https://doi.org/10.5194/cp-9-2043-2013>.

Mauri, A., Davis, B., Collins, P., & Kaplan, J. (2015). The climate of Europe during the Holocene: a gridded pollen-based reconstruction and its multi-proxy evaluation. *Quaternary Science Reviews*, *112*, 109–127. <https://doi.org/10.1016/j.quascirev.2015.01.013>.

McGuffie, K., & Henderson-Sellers, A. (2014). *The Climate Modelling Primer*. John Wiley & Sons.

Mesta, B., & Kentel, E. (2021). Superensembles of raw and bias-adjusted regional climate models for Mediterranean region, Turkey. *International Journal of Climatology*, *42*(4), 2566–2585. <https://doi.org/10.1002/joc.7381>.

Michelangeli, P. A., Vrac, M., & Loukos, H. (2009). Probabilistic downscaling approaches: Application to wind cumulative distribution functions. *Geophysical Research Letters*, *36*(11). <https://doi.org/10.1029/2009gl038401>.

Murphy, J. (1999). An Evaluation of Statistical and Dynamical Techniques for Downscaling Local Climate. *Journal of Climate*, *12*(8), 2256-2284. [https://doi.org/10.1175/1520-0442\(1999\)012<2256:AEOSAD>2.0.CO;2](https://doi.org/10.1175/1520-0442(1999)012<2256:AEOSAD>2.0.CO;2).

Myhre, A. (2015). *Klima, energi og miljø* (2. utg. ed.). Oslo: Universitetsforl.

Nikulina, A., MacDonald, K., Zapolska, A., Serge, M. A., Roche, D. M., Mazier, F., Davoli, M., Svenning, J. C., van Wees, D., Pearce, E. A., Fyfe, R., Roebroeks, W., & Scherjon, F. (2024). Hunter-gatherer impact on European interglacial vegetation: A modelling approach. *Quaternary Science Reviews*, *324*, 108439. <https://doi.org/10.1016/j.quascirev.2023.108439>.

Oppenheimer, C. (2011). *Eruptions that Shook the World*. Cambridge University Press.

Opsteegh, J. D., Haarsma, R. J., Selten, F. M., & Kattenberg, A. (1998). ECBILT: a dynamic alternative to mixed boundary conditions in ocean models. *Tellus A: Dynamic Meteorology and Oceanography*, *50*(3), 348. <https://doi.org/10.3402/tellusa.v50i3.14524>.

Otto-Bliesner, B. L., Brady, E. C., Zhao, A., Brierley, C. M., Axford, Y., Capron, E., Govin, A., Hoffman, J. S., Isaacs, E., Kageyama, M., Scussolini, P., Tzedakis, P. C., Williams, C. J. R., Wolff, E., Abe-Ouchi, A., Braconnot, P., Ramos Buarque, S., Cao, J., de Vernal, A., Guarino, M. V., Guo, C., LeGrande, A. N., Lohmann, G., Meissner, K. J., Menviel, L., Morozova, P. A., Nisancioglu, K. H., O’ishi, R., Salas y Méliá, D., Shi, X., Sicard, M., Sime, L., Stepanek, C., Tomas, R., Volodin, E., Yeung,

N. K. H., Zhang, Q., Zhang, Z., & Zheng, W. (2021). Large-scale features of Last Interglacial climate: results from evaluating the *lig127k* simulations for the Coupled Model Intercomparison Project (CMIP6)–Paleoclimate Modeling Intercomparison Project (PMIP4), *Climate of the Past*, 17, 63–94. <https://doi.org/10.5194/cp-17-63-2021>.

Otto-Bliesner, B. L., Park, W., Pfeiffer, M., Phipps, S. J., Prange, M., Rachmayani, R., Renssen, H., Rosenbloom, N., Schneider, B., Stone, E. J., Takahashi, K., Wei, W., Yin, Q., & Zhang, Z. S. (2013). A multi-model assessment of last interglacial temperatures, *Climate of the Past*, 9, 699–717. <https://doi.org/10.5194/cp-9-699-2013>.

Otto-Bliesner, B., Braconnot, P., Harrison, S. P., Lunt, D. J., Abe-Ouchi, A., Albani, S., Bartlein, P. J., Capron, E., Carlson, A. E., Dutton, A., Fischer, H., Goelzer, H., Govin, A., Haywood, A., Joos, F., Legrande, A. N., Lipscomb, W. H., Lohmann, G., Mahowald, N., Nehrbass-Ahles, C., Pausata, F. S. R., Peterschmitt, J. Y., Phipps, S., Renssen, H., & Zhang, Q. (2017). The PMIP4 contribution to CMIP6 – Part 2: Two Interglacials, Scientific Objective and Experimental Design for Holocene and Last Interglacial Simulations. *Geoscientific Model Development*, 10, 3979–4003.

PALAEOSSENS Project Members. Making sense of palaeoclimate sensitivity. (2012). *Nature*, 491, 683–691. <https://doi.org/10.1038/nature11574>.

Persson G., Sjökvist E., Åström S., Eklund D., Andréasson J., Johnell A., Asp M., Olsson J., & Nerheim S. (2011). Klimatanalys för Skåne län. SMHI rapport nr 2011-52.

Peyron, O., Combourieu-Nebout, N., Brayshaw, D., Goring, S., Andrieu-Ponel, V., Desprat, S., Fletcher, W., Gambin, B., Ioakim, C., Joannin, S., Kotthoff, U., Kouli, K., Montade, V., Pross, J., Sadori, L., & Magny, M. (2017). Precipitation changes in the Mediterranean basin during the Holocene from terrestrial and marine pollen records: a model–data comparison. *Climate of the Past*, 13(3), 249–265. <https://doi.org/10.5194/cp-13-249-2017>.

Price, N., & Gräslund, B. (2015). Excavating the Fimbulwinter? Archaeology, geomorphology the climate event(s) of AD 536. In: Felix Riede (ed.) Past Vulnerability, Volcanic eruptions and human vulnerability in traditional societies past and present, *Aarhus University Press*, Aarhus. pp 109-320.

Quiquet, A., Roche, D. M., Dumas, C., & Paillard, D. (2018). Online dynamical downscaling of temperature and precipitation within the *iLOVECLIM* model (version 1.1). *Geoscience Model Development*, 11, 453–466. <https://doi.org/10.5194/gmd-11-453-2018>.

Raynaud, D., Barnola, J. M., Chappellaz, J., Blunier, T., Indermühle, A., & Stauffer, B. (2000). The ice record of greenhouse gases: a view in the context of future changes. *Quaternary Science Reviews*, 19(1–5), 9–17. [https://doi.org/10.1016/s0277-3791\(99\)00082-7](https://doi.org/10.1016/s0277-3791(99)00082-7).

Renssen, H., Goosse, H. & Fichet, T. (2007). Simulation of Holocene cooling events in a coupled climate model. *Quaternary Science Reviews*, 26. 2019-2026.

Renssen, H., Goosse, H., & Muscheler, R. (2006). Coupled climate model simulation of Holocene cooling events: oceanic feedback amplifies solar forcing. *Climate of the Past*, 2(2), 79–90. <https://doi.org/10.5194/cp-2-79-2006>.

Renssen, H., Goosse, H., Fichet, T., Brovkin, V., Driesschaert, E., & Wolk, F. (2004). Simulating the Holocene climate evolution at northern high latitudes using a coupled atmosphere-sea ice-ocean-vegetation model. *Climate Dynamics*, 24(1), 23–43. <https://doi.org/10.1007/s00382-004-0485-y>.

Renssen, H., Seppä, H., Crosta, X., Goosse, H., & Roche, D. (2012). Global characterization of the Holocene Thermal Maximum. *Quaternary Science Reviews*, 48, 7–19. <https://doi.org/10.1016/j.quascirev.2012.05.022>.

Renssen, H., Seppä, H., Heiri, O., Roche, D. M., Goosse, H., & Fichet, T. (2009). The spatial and temporal complexity of the Holocene thermal maximum. *Nature Geoscience*, 2(6), 411–414. <https://doi.org/10.1038/ngeo513>.

Roberts, N. (2014). *The Holocene*. John Wiley & Sons.

Roberts, N., Brayshaw, D., Kuzucuoğlu, C., Perez, R., & Sadori, L. (2011). The mid-Holocene climatic transition in the Mediterranean: Causes and consequences. *The Holocene*, 21(1), 3–13. <https://doi.org/10.1177/0959683610388058>.

Robock, A. (2000). Volcanic eruptions and climate. *Reviews of Geophysics*, 38(2), 191–219. <https://doi.org/10.1029/1998rg000054>.

Roche, D. M., Dokken, T. M., Goosse, H., Renssen, H., & Weber, S. L. (2007). Climate of the Last Glacial Maximum: sensitivity studies and model-data comparison with the LOVECLIM coupled model. *Climate of the Past*, 3(2), 205–224. <https://doi.org/10.5194/cp-3-205-2007>.

Roche, D. M., Dumas, C., Bügelmayr, M., Charbit, S., & Ritz, C. (2014). Adding a dynamical cryosphere to iLOVECLIM (version 1.0): coupling with the GRISLI ice-sheet model. *Geoscientific Model Development*, 7(4), 1377–1394. <https://doi.org/10.5194/gmd-7-1377-2014>.

Ruddiman, W. F. (2003). The anthropogenic greenhouse era began thousands of years ago, *Climate Change*, 61. 261 – 293.

Russo, E., & Cubasch, U. (2016). Mid-to-late Holocene temperature evolution and atmospheric dynamics over Europe in regional model simulations. *Climate of the Past*, 12(8), 1645–1662. <https://doi.org/10.5194/cp-12-1645-2016>.

Russo, E., Fallah, B., Ludwig, P., Karremann, M., & Raible, C. C. (2022). The long-standing dilemma of European summer temperatures at the mid-Holocene and other considerations on learning from the past for the future using a regional climate model. *Climate of the Past*, 18, 895–909. <https://doi.org/10.5194/cp-18-895-2022>.

Sadori, L., Giraudi, C., Masi, A., Magny, M., Ortu, E., Zanchetta, G., & Izdebski, A. (2016). Climate, environment and society in southern Italy during the last 2000 years. A review of the environmental, historical and archaeological evidence. *Quaternary Science Reviews*, 136, 173–188. <https://doi.org/10.1016/j.quascirev.2015.09.020>.

Schaeffer, M., Selten, F. M., Opsteegh, J. D., & Goosse, H. (2002). Intrinsic limits to predictability of abrupt regional climate change in IPCC SRES scenarios. *Geophysical Research Letters*, 29(16), 14–1. <https://doi.org/10.1029/2002gl015254>.

Schilt, A., Baumgartner, M., Schwander, J., Buiron, D., Capron, E., Chappellaz, J., Loulergue, L., Schüpbach, S., Spahni, R., Fischer, H., & Stocker, T. F. (2010). Atmospheric nitrous oxide during the last 140,000 years. *Earth and Planetary Science Letters*, 300(1–2), 33–43. <https://doi.org/10.1016/j.epsl.2010.09.027>.

Schneider, R., Schmitt, J., Köhler, P., Joos, F., & Fischer, H. (2013). A reconstruction of atmospheric carbon dioxide and its stable carbon isotopic composition from the penultimate glacial maximum to the last glacial inception. *Climate of the Past*, 9(6), 2507–2523. <https://doi.org/10.5194/cp-9-2507-2013>.

Scussolini, P., Bakker, P., Guo, C., Stepanek, C., Zhang, Q., Braconnot, P., Cao, J., Guarino, M. V., Coumou, D., Prange, M., Ward, P. J., Renssen, H., Kageyama, M., Otto-Bliesner, B., & Aerts, J. C. J. H. (2019). Agreement between reconstructed and modeled boreal precipitation of the Last Interglacial. *Science advances*, 5(11), eaax7047. <https://doi.org/10.1126/sciadv.aax7047>.

Seppä, H., & Birks, H. J. (2001). July mean temperature and annual precipitation trends during the Holocene in the Fennoscandian tree-line area: pollen-based climate reconstructions. *The Holocene*, 11(5), 527–539. <https://doi.org/10.1191/095968301680223486>.

Siegenthaler, U., Stocker, T. F., Monnin, E., Lüthi, D., Schwander, J., Stauffer, B., & Jouzel, J. (2005). Stable Carbon Cycle-Climate Relationship During the Late Pleistocene. *Science*, 310(5752), 1313–1317. <https://doi.org/10.1126/science.1120130>.

Sigl, M., Winstrup, M., McConnell, J.R., Welten, K.C., Plunkett, G., Ludlow, F., Büntgen, U., Caffee, M., Chellman, N., Dahl-Jensen, D., Fischer, H., Kipfstuhl, S., Kostick, C., Maselli, O.J., Mekhaldi, F., Mulvaney, R., Muscheler, R., Pasteris, D.R., Pilcher, J.R., Salzer, M., Schüpbach, S., Steffensen, J.P., Vinther, B.M., & Woodruff, T.E. (2015) “Timing and climate forcing of volcanic eruptions for the past 2,500 years,” *Nature*, 523(7562), 543–549. <https://doi.org/10.1038/nature14565>.

Steig, E. J., Ding, Q., White, J. W. C., Küttel, M., Rupper, S. B., Neumann, T. A., Neff, P. D., Gallant, A. J. E., Mayewski, P. A., Taylor, K. C., Hoffmann, G., Dixon, D. A., Schoenemann, S. W., Markle, B. R., Fudge, T. J., Schneider, D. P., Schauer, A. J., Teel, R. P., Vaughn, B. H., & Korotkikh, E. (2013). Recent climate and ice-sheet changes in West Antarctica compared with the past 2,000 years. *Nature Geoscience*, 6(5), 372–375. <https://doi.org/10.1038/ngeo1778>.

Stocker, T. (2011). *Introduction to Climate Modelling*. Springer Science & Business Media.

Stothers, R. B., & Rampino, M. R. (1983). Historic volcanism, European dry fogs, and Greenland acid precipitation, 1500 B.C. to A.D. 1500. *Science*, 222(4622), 411–413. [doi:10.1126/science.222.4622.411](https://doi.org/10.1126/science.222.4622.411).

Strandberg, G. (2017). Modelling regional climate-vegetation interactions in Europe: A palaeo perspective (PhD dissertation, Department of Meteorology, Stockholm University). Retrieved from <https://urn.kb.se/resolve?urn=urn:nbn:se:su:diva-140536>.

Strandberg, G., Kjellström, E., Poska, A., Wagner, S., Gaillard, M.-J., Trondman, A.-K., Mauri, A., Davis, B. A. S., Kaplan, J. O., Birks, H. J. B., Bjune, A. E., Fyfe, R., Giesecke, T., Kalnina, L., Kangur, M., van der Knaap, W. O., Kokfelt, U., Kuneš, P., Latalowa, M., Marquer, L., Mazier, F., Nielsen, A. B., Smith, B., Seppä, H., & Sugita, S. (2014). Regional climate model simulations for Europe at 6 and 0.2 k BP: sensitivity to changes in anthropogenic deforestation. *Climate of the Past*, 10, 661–680. doi:10.5194/cp-10-661-2014.

Svensson, E. (1998). *Människor i utmark*. [Doctoral Thesis (monograph), Historical Archaeology]. Almqvist & Wiksell International.

Timm, O., Timmermann, A., Abe-Ouchi, A., Saito, F., & Segawa, T. (2008). On the definition of seasons in paleoclimate simulations with orbital forcing. *Paleoceanography*, 23(2). <https://doi.org/10.1029/2007pa001461>.

Timmermann, A., Justino, F., Jin, F. F., Krebs, U., & Goosse, H. (2004). Surface temperature control in the North and tropical Pacific during the last glacial maximum. *Climate Dynamics*, 23(3–4), 353–370. <https://doi.org/10.1007/s00382-004-0434-9>.

Toohey, M., & Sigl, M. (2017). Volcanic stratospheric sulfur injections and aerosol optical depth from 500 BCE to 1900 CE. *Earth System Science Data*, 9(2), 809–831. DOI:10.5194/essd-9-809-2017.

Toohey, M., Krüger, K., Sigl, M., Stordal, F., & Svensen, H. (2016). Climatic and societal impacts of a volcanic double event at the dawn of the Middle Ages. *Climatic Change*, 136(3-4), 401–412, DOI:10.1007/s10584-016-1648-7.

Turney, C. S. M., & Jones, R. T. (2010). Does the Agulhas Current amplify global temperatures during super-interglacials? *Journal of Quaternary Science*, 25, 839–843. doi:10.1002/Jqs.1423.

van Dijk, E., Mørkestøl Gundersen, I., de Bode, A., Høeg, H., Loftsgarden, K., Iversen, F., Timmreck, C., Jungclaus, J., and Krüger, K. (2023). Climatic and societal impacts in Scandinavia following the 536 and 540 CE volcanic double event. *Climate of the Past*, 19, 357–398. <https://doi.org/10.5194/cp-19-357-2023>.

Vigaud, N., Vrac, M., & Caballero, Y. (2012). Probabilistic downscaling of GCM scenarios over southern India. *International Journal of Climatology*, 33(5), 1248–1263. <https://doi.org/10.1002/joc.3509>.

Viner, D. (2012). Spatial Downscaling. Retrieved from <http://www.cccsn.ec.gc.ca/?page=downscaling>. (last assessed: 20th August 2021).

Von Storch, H., Feser, F., Stendel, M., Xu, Y., Laprise, R., & Takayabu, I. (2020). Modelling, Simulating and Forecasting Regional Climate and Weather. *Frontiers. Media SA*.

Vrac, M., Drobinski, P., Merlo, A., Herrmann, M., Lavaysse, C., Li, L., & Somot, S. (2012). Dynamical and statistical downscaling of the French Mediterranean climate: uncertainty assessment. *Natural Hazards and Earth System Sciences*, 12(9), 2769–2784. <https://doi.org/10.5194/nhess-12-2769-2012>.

Washington, W. M., & Parkinson, C. (2005). Introduction to Three-Dimensional Climate Modeling. University Science Books.

Wilcox, P. S., Honiat, C., Trüssel, M., Edwards, R. L., & Spötl, C. (2020). Exceptional warmth and climate instability occurred in the European Alps during the Last Interglacial period. *Communications Earth & Environment*, 1(1). <https://doi.org/10.1038/s43247-020-00063-w>.

Wilby, R. L., Troni, J., Biot, Y., Tedd, L., Hewitson, B. C., Smith, D. M., & Sutton, R. T. (2009). “A review of climate risk information for adaptation and development planning.” *International Journal of Climatology*, 29(9). 1193-1215.

Williams, C. J. R., Guarino, M. V., Capron, E., Malmierca-Vallet, I., Singarayer, J. S., Sime, L. C., Lunt, D. J., & Valdes, P. J. (2020). CMIP6/PMIP4 simulations of the mid-Holocene and Last Interglacial using HadGEM3: comparison to the pre-industrial era, previous model versions and proxy data. *Climate of the Past*, 16(4), 1429–1450. <https://doi.org/10.5194/cp-16-1429-2020>.

Zapolska, A., Vrac, M., Quiquet, A., Extier, T., Arthur, F., Renssen, H., & Roche, D. M. (2023). Improving biome and climate modelling for a set of past climate conditions: evaluating bias correction using the CDF-t approach. *Environmental Research Climate*, 2(2), 025004. <https://doi.org/10.1088/2752-5295/accbe2>.

Zhang, Y., Renssen, H., Seppä, H., & Valdes, P. J. (2018). Holocene temperature trends in the extratropical Northern Hemisphere based on inter-model comparisons. *Journal of Quaternary Science*, 33(4), 464–476. <https://doi.org/10.1002/jqs.3027>.

Zorita, E. & von Storch, H. (1999). The analog method as a simple statistical downscaling technique: comparison with more complicated methods. *Journal of Climate*, 12(8). 2474-2489.

Zorita, E. (2005). Natural and anthropogenic modes of surface temperature variations in the last thousand years. *Geophysical Research Letters*, 32(8). <https://doi.org/10.1029/2004gl021563>.

Paper 1

Arthur, F., Roche, D. M., Fyfe, R., Quiquet, A., & Renssen, H. (2023). Simulations of the Holocene climate in Europe using an interactive downscaling within the iLOVECLIM model (version 1.1). *Climate of the Past*, *19*(1), 87–106. <https://doi.org/10.5194/cp-19-87-2023>.



Simulations of the Holocene climate in Europe using an interactive downscaling within the iLOVECLIM model (version 1.1)

Frank Arthur¹, Didier M. Roche^{2,3}, Ralph Fyfe⁴, Aurélien Quiquet³, and Hans Renssen¹

¹Department of Natural Sciences and Environmental Health, University of South-Eastern Norway, Bø, Norway

²Faculty of Science, Cluster Earth and Climate, Vrije Universiteit Amsterdam, Amsterdam, the Netherlands

³Laboratoire des Sciences du Climat et de l'Environnement, LSCE/IPSL, CEA-CNRS-UVSQ, Université Paris-Saclay, Gif-sur-Yvette, France

⁴School of Geography, Earth and Environmental Sciences, University of Plymouth, Plymouth, UK

Correspondence: Frank Arthur (frank.arthur@usn.no)

Received: 24 February 2022 – Discussion started: 16 March 2022

Revised: 29 November 2022 – Accepted: 10 December 2022 – Published: 10 January 2023

Abstract. This study presents the application of an interactive downscaling in Europe using iLOVECLIM (a model of intermediate complexity), increasing its atmospheric resolution from 5.56 to 0.25° kilometric. A transient simulation using the appropriate climate forcings for the entire Holocene (11.5–0 ka BP) was done for both the standard version of the model and with an interactive downscaling applied. Our results show that simulations from downscaling present spatial variability that agrees better with proxy-based reconstructions and other climate models as compared to the standard model. The downscaling scheme simulates much higher (by at least a factor of 2) precipitation maxima and provides detailed information in mountainous regions. We focus on examples from the Scandes mountains, the Alps, the Scottish Highlands, and the Mediterranean. The higher spatial resolution of the downscaling provides a more realistic overview of the topography and gives local climate information, such as precipitation and temperature gradient, that is important for paleoclimate studies. With downscaling, we simulate similar trends and spatial patterns of the precipitation changes reconstructed by other proxy studies (for example in the Alps) as compared to the standard version. Our downscaling tool is numerically cheap, implying that our model can perform kilometric, multi-millennial simulations and is suitable for future studies.

1 Introduction

Numerical climate models are used to study past, present, and future climate change, and two types of global climate models are primarily used, the so-called general circulation models (GCMs) and Earth system models of intermediate complexity (EMICs). GCMs and EMICs simulate the climate of the Earth by applying mathematical equations to describe the atmospheric, oceanic, and land interactions or feedbacks. These climate models are evaluated with past climate data to ensure that their sensitivity to climate change is realistic and thus improve their ability to project future climate change. GCMs and EMICs have been used to simulate the past climate. Examples are the Last Glacial Maximum (LGM, e.g. Liu et al., 2021), the Holocene (e.g. Claussen et al., 2002; Renssen et al., 2009; Renssen and Osborn, 2003; Schmidt et al., 2004; Otto-Bliesner et al., 2006), and the Last Millennium (e.g. Crowley, 2000; Jones et al., 2001; Zorita et al., 2005). These paleoclimate simulations have been routinely compared with proxy-based paleo data to evaluate their performance (Masson et al., 1999; Bonfils et al., 2004; Brewer et al., 2007; Bartlein et al., 2011). However, the difference in spatial resolution between the simulated climate model results and proxy-based paleo reconstructions makes this comparison problematic and usually poses some uncertainties (Renssen et al., 2001; Ludwig et al., 2019). Transient simulations of the Holocene with GCMs are still currently a challenge due to the numerical cost (it can take more than 4–

5 months). Therefore, EMICs (like iLOVECLIM) have simplified physics and are computationally more efficient, making it feasible to perform large ensemble experiments at a multi-millennial timescale, which is an advantage to paleoclimate studies. EMICs can explicitly simulate the interaction between all the components of an Earth system model and simulate the transient and equilibrium climate sensitivity (Claussen et al., 2002). Still, EMICs' representation of the large-scale atmospheric moisture content and other processes produced by local-scale features such as mountains ranges, water bodies, and forests is quite poor and thus affects the dynamics of these sub-components that rely on the global atmospheric water cycle (Quiquet et al., 2018). This implies that many of the processes that govern the local climate (vegetation, hydrology, and topography) are not well represented in most coarse-resolution EMICs.

This limitation of global climate models can be overcome by applying spatial downscaling, a primary tool in meteorology and climate studies. Downscaling can establish a relationship between large-scale atmospheric processes and the local scale to derive information at a fine spatial resolution (Castro et al., 2005). There are two approaches of downscaling used to resolve this coarse-resolution–fine-resolution variance: statistical and dynamical downscaling (Murphy, 1999). Statistical downscaling models (SDMs) involve creating an empirical relationship between historical large-scale atmospheric characteristics (such as pressure fields) and local climate variables (temperature, precipitation, etc.) and applying these statistical relationships to the output of large-scale global variables (GCMs/EMICs) to simulate the local climate variables (e.g. Stoner et al., 2013). The main types of SDMs are “weather typing” methods, which are based on conditioning the simulations of small-scale data on recurrent weather types over a specific region (e.g. Willems and Vrac, 2011), “transfer functions”, which link large-scale atmospheric conditions and local-scale data directly (e.g. Vrac et al., 2007), and “stochastic weather generators” that generate local-scale time series from their possibly conditional probability density functions (e.g. Olsson et al., 2009). There are some studies related to statistical downscaling in a paleo perspective. For example, Latombe et al. (2018) simulated the climate of the Last Glacial Maximum (23–19 ka BP) over western Europe by statistically downscaling the temperature and precipitation time series outputs from a GCM with a generalized additive model (GAM). Lorenz et al. (2016) performed a transient paleoclimate simulation with statistical downscaling for North America spanning the period between 21 ka BP and 2100 CE at 0.5° spatial resolution. Their study provides datasets that offer a standard collection of climate simulations that may be used to model the impact of past and future climate change on biodiversity.

Dynamical downscaling is the technique used by global models to simulate the land–atmosphere interaction process by considering the sub-grid, orography, and other conditions over a local scale (Feser et al., 2011). Dynamical down-

scaling is thus aimed at increasing the spatial resolution (horizontally and vertically) by simulating the regional sub-component of the climate from global models (Ludwig et al., 2019). In contrast, statistical downscaling only assumes constant statistical relationships between large- and local-scale processes. These relationships may not be valid for conditions very different from the present, such as in the early Holocene. Conversely, since it is based on physical laws, dynamical downscaling can be applied to any period and gives more comprehensive information for some specific regions, particularly if precipitation is highly influenced by local topography (Gómez-Navarro et al., 2011; Wang et al., 2015; Raible et al., 2017; Quiquet et al., 2018). However, there may be some uncertainties and limitations in the use of dynamical spatial downscaling. The uncertainties of downscaled temperature and precipitation usually depend on the errors associated with the large-scale model, such as its physical parameterization (Murphy, 1999; Feser et al., 2011), the model's simplification or limitation, and the biases associated with the model's atmospheric circulation (Quiquet et al., 2018).

Comparing paleoclimate model results at a high spatial resolution with proxy-based data informs meaningful interpretation (Bonfils et al., 2004; Russo and Cubasch, 2016; Ludwig et al., 2019). Dynamical downscaling has been applied to both present and future climate analyses to give an improved estimate of future climate change (e.g. Jacob et al., 2007). According to Jacob et al. (2014), regional (dynamical) downscaling better represents the physical processes that trigger precipitation and provides more realistic outputs in complex regions when compared to outputs from low-resolution models. Despite these advantages, applying dynamical downscaling in paleoclimate studies is still limited, with the main reason being that it is computationally intensive and costly to run long-term climate simulations with downscaling. Still, there is good potential, as comparing paleoclimate simulations with proxy-based reconstructions is more meaningful at a high spatial resolution.

Some attempts have been made in the past to simulate high-resolution climate in a paleo-perspective. Examples are available for the LGM (Yokoyama et al., 2000; Strandberg et al., 2011; Hofer et al., 2012; Ludwig et al., 2016) and the Little Ice Age/Medieval Warm Period over arid central Asia (Fallah et al., 2016). The Last Millennium over the Iberian Peninsula was studied with a Regional Climate Model (RCM) of 30 km spatial resolution to evaluate the significance of the internal variability of temperature and precipitation at regional scales (Gómez-Navarro et al., 2011). Renssen et al. (2001) also applied an RCM to simulate the European climate during the Younger Dryas cold period (12.9–11.7 ka BP). In addition, Gómez-Navarro et al. (2013) performed a higher-resolution RCM simulation in Europe spanning from 1500–1990 CE, and their results compared to observed Climate Research Unit (CRU) datasets show an improvement in the climate model most particularly in areas of complex topography. In a different study, the same

results were compared with empirical proxy-based reconstructions (Gómez-Navarro et al., 2015), and the results show regional mean biases, particularly for summer temperature and winter precipitation. These biases were similar to biases found relative to CRU observational data in their earlier study (e.g. Gómez-Navarro et al., 2013). Russo and Cubasch (2016) present a dynamical downscaling for different time slices of middle-to-late Holocene in Europe using the RCM model COSMO-CLM. Comparison of their results with observed CRU data show that their RCM can reproduce a realistic climatology. The same model was recently applied by Russo et al. (2022) to analyse summer temperatures of the mid-Holocene in Europe and to understand the potential causes of the discrepancy between results of climate model simulations and pollen-based reconstruction (Russo et al., 2022). Moreover, Velasquez et al. (2021) applied dynamical downscaling to the LGM climate of Europe and utilized the land and atmospheric components of GCM (CCSM4), RCM (WRF), and dynamic vegetation model simulations to study the significance of land–atmospheric response for the European climate. The results from the study suggest that the regional climate is significantly influenced by the LGM land cover (Velasquez et al., 2021).

The Holocene (11.5–0 ka BP) is a significant period for studying the climate evolution and variability to improve our knowledge of the climate system. The period is well known and archived with proxy data (e.g. Masson et al., 1999; Bonfils et al., 2004; Braconnot et al., 2007; Wanner et al., 2008; Mauri et al., 2015). It is also a period used to evaluate how climate models respond to the variations in insolation in response to astronomical forcing (Fischer and Jungclauss, 2011). In the early Holocene, the astronomical forcing was very different from today because of changes in three astronomical parameters (eccentricity, obliquity, and precession) that alter the amount and distribution of incoming solar energy at the top of the atmosphere (Berger, 1978). According to Berger (1978), during the early Holocene at 11 ka BP, the Northern Hemisphere received about 30 W m^{-2} more insolation during boreal summer than at present, which caused the climate to be relatively warm during the early to middle Holocene. This relatively high summer insolation resulted in the reorganization of various variables of the climate system, such as the melting of the ice sheets (including the Fennoscandia Ice Sheet, FIS and Laurentide Ice Sheet, LIS) and the associated freshwater release in different regions during the early Holocene (Briner et al., 2016; Zhang et al., 2016).

Within the Holocene, the mid-Holocene (MH, 6 ka BP) is a time slice that was characterized by relatively warm conditions in the Northern Hemisphere, associated with the astronomically forced summer insolation. Other forcings were similar to pre-industrial values, including atmospheric greenhouse gas concentration levels (Bartlein et al., 2011). The MH is very well documented, offering the opportunity to study this warm condition and long growing season in re-

gions such as Europe. Pollen-based climatic variables such as surface temperature over Europe (Mauri et al., 2015) show that the climate system also responded to other large-scale complex processes such as the orography or land–surface interactions with the atmosphere and atmospheric circulation (Bonfils et al., 2004). Previous climate model studies, when compared to proxy data for the mid-Holocene, suggest that some climate models simulate a cooler and wetter climate in southern Europe during winter but with a very weak signal (e.g. Brewer et al., 2007; Brayshaw et al., 2011). However, there is a poor agreement for southern Europe between proxy-based reconstructions of summer temperature and almost all climate models. Climate models show warming in summer in the Mediterranean region at 6 ka BP relative to the pre-industrial era (e.g. Masson et al., 1999; Mauri et al., 2014; Fischer and Jungclauss, 2011; Russo and Cubasch, 2016; Brierley et al., 2020). This model response is tightly connected to the insolation change at mid-Holocene, with summer insolation being higher and winter insolation being lower. The modelled MH temperatures reflect this, including over the Mediterranean region, while continental-scale reconstructions from pollen records show large cooling during summer over the Mediterranean region (Davis et al., 2003; Mauri et al., 2015).

Several modelling groups have recently performed transient modelling simulations of the Holocene. For instance, Bader et al. (2020) used the Max Planck Institute for Meteorology Earth System Model (MPI-ESM 2) to run two different global Holocene transient simulations for temperature which span from 6000 BCE to 1850 CE. Their results conclude with one simulation showing global cooling during the late Holocene, while the other simulation shows global warming in the late Holocene. The results also indicate that the warming is most conspicuous in the tropics. Paleoclimate proxies indicate that the Northern Hemisphere summer temperature was warmer during the first part of the Holocene than the pre-industrial era, primarily because the perihelion occurred during the boreal summer. However, most global-scale proxy-based reconstructions are inconsistent with long-term warming simulated by climate models in response to ice sheet retreat and rising greenhouse gas concentration throughout the Holocene epoch, a discrepancy termed the “Holocene temperature conundrum” (Liu et al., 2014). While reconstructions show a cooling trend, model results suggest a warming trend. Accordingly, one of the most striking differences between climate reconstructions and climate model simulations is the direction of global temperature change in the Holocene. Furthermore, the accuracy of LGM and Holocene paleoclimate simulations depends on detailed knowledge of paleoclimate boundary conditions, which may not be independent from proxies.

Within this study, we present a simulation of the transient Holocene climate evolution during the last 11.5–0 ka BP in Europe (Fig. 1), performed with both the standard version of the iLOVECLIM model (Roche et al., 2014) and a version

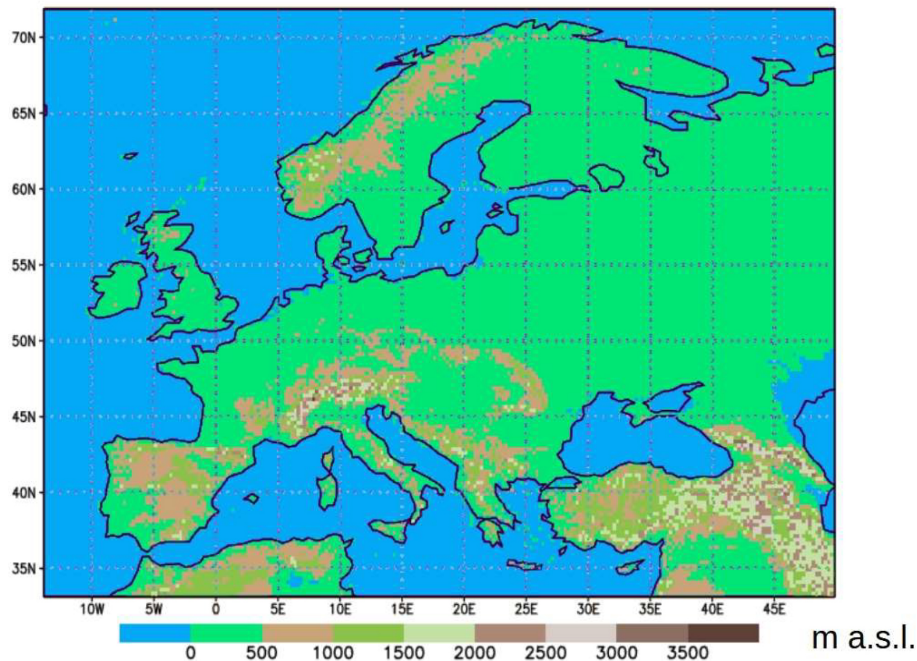


Figure 1. The topography of Europe as included in the interactive downscaling.

with an interactive downscaling (Quiquet et al., 2018). The downscaling is performed at each model time step, and it is consistent between the two grids, with the precipitation at the coarse resolution interacting with the sub-grid. The spatial resolution in Europe is increased from 5.6° latitude \times 5.6° longitude to 0.25° latitude \times 0.25° longitude. Our general objective is to examine the impact of the downscaling on the model results and evaluate if the model (with downscaling) simulates the climate during the Holocene in better agreement with other climate models and proxy data. Thus, our main goal is to evaluate the benefits of using downscaling in paleo-climate simulation. In addition, we will assess the impact of the model resolution on their sensitivity at high spatial resolution. We wish to provide a comprehensive and consistent overview of the climate system at a fine resolution during the Holocene.

We will answer the following questions in this paper.

- i. What is the impact of downscaling on the precipitation patterns during the Holocene in different regions in Europe?
 - ii. Do the high-resolution results of precipitation in the mountainous regions (e.g. the Alps, the Scandes, and the Scottish Highlands) produce Holocene climate patterns that compare more favourably to proxy data and other climate models when compared with the low-resolution results?
1. What is the advantage of using cheap numerically interactive downscaling for paleoclimate research?

2 Model, simulations, and methods

2.1 The iLOVECLIM model

The iLOVECLIM model (version 1.0) (Roche et al., 2014) is a three-dimensional model with a simplified representation of the atmosphere relative to GCMs. This simplification and its lower spatial resolution make iLOVECLIM much faster than coupled GCMs (Goosse et al., 2010; Kitover et al., 2015). It is a fork of the LOVECLIM 1.2 model code (Goosse et al., 2010), and these share their main climate system components. Here we apply a version that includes the following components: the atmospheric model ECBilt (Opsteegh et al., 1998), the sea ice ocean component CLIO (Coupled Large-scale Ice-Ocean model, Goosse and Fichefet, 1999), and the terrestrial vegetation model VECODE (Brovkin et al., 1997).

Our model version is a direct follow-up of the ECBilt–CLIO–VECODE coupled climate model and has been successfully used to simulate some key past and future climates, for example the LGM (e.g. Timmermann et al., 2004; Roche et al., 2007), the last deglaciation (e.g. Timm et al., 2008), the Holocene (e.g. Renssen et al., 2005a, b), the last millennium (e.g. Goosse et al., 2005a, b), and the 21st century (e.g. Schaeffer et al., 2002, 2004; Driesschaert et al., 2007). The atmospheric component (ECBilt) includes three vertical levels at 800, 500, and 200 hPa and applies the quasi-geostrophic potential vorticity equation to model the dynamical processes in the atmosphere (Opsteegh et al., 1998). It runs on a global spectral grid truncated at T21 that represents a horizontal resolution of 5.6° latitude and 5.6° lon-

gitude. Another component of the model, CLIO (Goosse et al., 2010), is a three-dimensional free-surface ocean general circulation model that has been coupled with a full sea ice model (Goosse and Fichefet, 1999). It has a horizontal resolution of 3° by 3° latitude–longitude and 20 layers in the vertical. VECODE runs on the same grid as ECBilt and includes three different plant functional types (PFTs): trees, grass, and desert or bare soil, each with different physical properties for evapotranspiration, surface roughness, and albedo. The vegetation fraction (v) is calculated by the sum of the tree fraction (f) and grass fraction (g) (Goosse et al., 2010).

2.2 Interactive downscaling

In this study, we apply an interactive downscaling presented by Quiquet et al. (2018) for precipitation and temperature in the coupled iLOVECLIM model. The downscaling is done from the original ECBilt's T21 grid towards a European domain between 13.875° W and 49.875° E in longitude and 35.125 and 71.875° N in latitude, with a resolution of 0.25° in latitude–longitude. The basic idea behind the downscaling process is to reproduce the model physics of ECBilt (not the dynamics) on a higher spatial resolution so that the sub-grid orography is explicitly considered. To do so, we use artificial vertical layers so that variables such as temperature and precipitation formation can be computed at any altitude in the sub-grid orography for each atmospheric time step (Quiquet et al., 2018). We follow a conservative approach in which the “large-scale” fields (on the native grid) are the sum or mean of what is computed on the sub-grid. First, the downscaling is performed at each model time step during run time. Secondly, there is a two-way coupling between the coarse grid and the sub-grid which ensures consistency (the precipitation at the coarse resolution is the sum of the sub-grid precipitation). As such, there is a strong difference with standard offline downscaling techniques. The results from Quiquet et al. (2018) show that, in comparison to the standard version of the model, the downscaling improves the vertical distribution of temperature (for example, with a more realistic profile in mountainous regions) and the precipitation distribution in mountainous regions. However, the results also suggest that the downscaling is not able to correct the biases of the large-scale native model, which are mostly driven by the model's simplification, or the atmospheric circulation, which is not downscaled (Quiquet et al., 2018).

To apply interactive downscaling in the model, the temperature and moisture variables on the vertically extended native (ECBilt) grid are recomputed in the model. The computation is done on the 11 vertical levels of the grid (10, 250, 500, 750, 1000, 1250, 1500, 2000, 3000, 4000, and 5000 m) (Quiquet et al., 2018) by using the equations required for the vertically extended grid defined by Haarsma et al. (1997). The atmospheric boundary layer is not well represented in the ECBilt, hence the heat and moisture fluxes at the Earth surface are computed based on an idealized vertical pro-

file (Quiquet et al., 2018). The temperatures are computed based on hydrostatic equilibrium and the ideal gas law at the 650 and 350 hPa horizon, with the assumption that the atmosphere is isothermal above 200 hPa. Above 500 hPa, the atmosphere is assumed dry (Goose et al., 2010). The temperatures and precipitation at the sub-grid orography are then computed from the climate variables obtained or computed from the vertically extended artificial grids (Quiquet et al., 2018). For detailed information, such as an explanation of the physics applied on the downscaling in the model, the reader is referred to Quiquet et al. (2018).

2.3 Experimental set-up

We applied iLOVECLIM-1.0 (Roche et al., 2014) and iLOVECLIM-1.1 (Quiquet et al., 2018) to simulate the transient evolution of the climate during the last 11.5 kyr (Table 1). Two experiments were performed (hereafter 11.5 K_Standard and 11.5 K_Down). The experiment 11.5 K_Standard is performed with the standard version of the model on the low-resolution T21 grid. The second experiment (11.5 K_Down) is when downscaling has been applied to the quasi-geostrophic T21 grid to compute the temperature and precipitation on the regional sub-grid in Europe (Fig. 1). We forced the simulations with orbital forcings (Berger, 1978) and atmospheric trace gas concentrations of CO_2 , CH_4 , and N_2O (Raynaud et al., 2000), which vary annually for the 11.5–0 ka BP simulation period. Constant ice sheet configurations were prescribed for the experiments, while the solar constant and aerosol levels were kept fixed at pre-industrial levels. During the Holocene, the astronomical forcing determines variations in terms of seasons and latitudes of the incoming solar radiation at the top of the atmosphere. For example, at 65° N, the summer insolation is reduced by 30 W m^{-2} throughout the Holocene epoch (Fig. 2). The ice-core-based levels of CO_2 , CH_4 , and N_2O represent 1 W m^{-2} variability in radiative forcing (Schilt et al., 2010). This greenhouse gas (GHG) forcing was at its maximum level at 10 ka BP and then started decreasing to a low value at 8 ka BP before rising again during the last 6 kyr to pre-industrial values (Fig. 2). The experiments were initialized with a state derived from an experiment that was run for 1000 years until equilibrium with 11.5 ka BP astronomical parameters, greenhouse gas levels, and ice sheets.

We present the results of precipitation and temperature as anomalies relative to the pre-industrial period at the end of our simulations and compare our downscaled results (11.5 K_Down) with the results of the standard version (11.5 K_Standard).

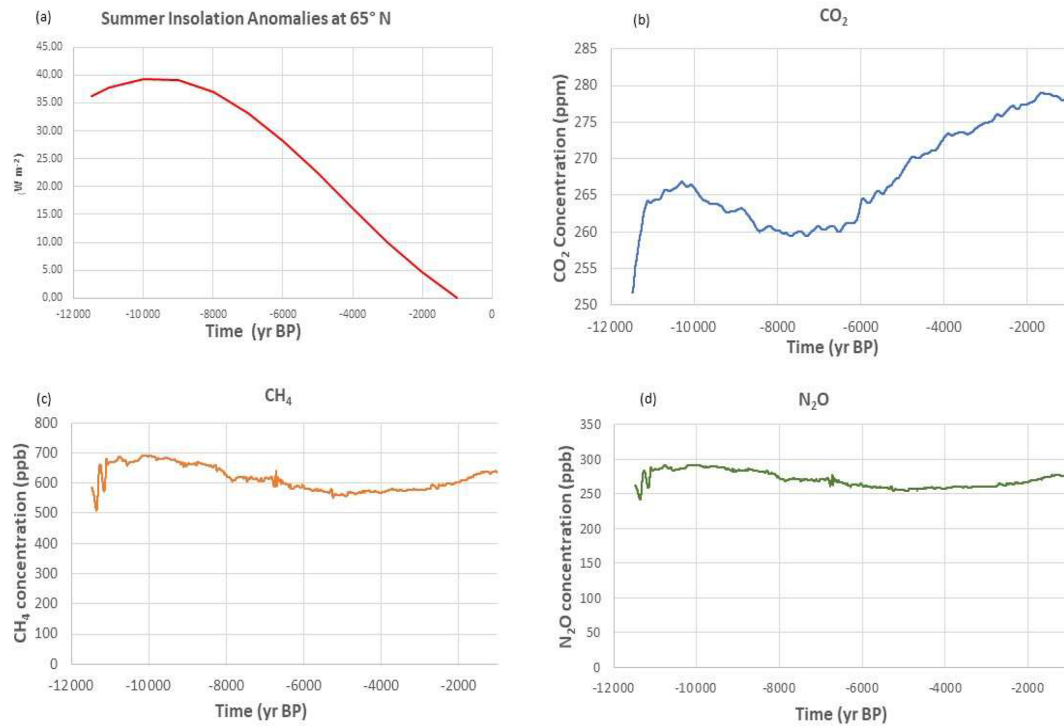


Figure 2. Climate forcings used in the experiment GHG forcings (Raynaud et al., 2000) and summer (July) insolation at 65° N during the Holocene (Berger, 1978).

Table 1. Summary of the main features of the model and experimental set-up.

	Simulations	
Model	iLOVECLIM (standard version)	iLOVECLIM (downscaling)
Component	Ocean, sea ice, atmosphere, vegetation	
Atmospheric resolution (lat × long)	5.6° × 5.6°	0.25° × 0.25°
Oceanic component resolution	3° × 3°	
Prescribed forcings and reference	Orbital forcings (Berger, 1978) GHG (Schilt et al., 2010; Raynaud et al., 2000) Ice sheets, fixed	
Initial condition	Equilibrium experiment at 11.5 ka (1 kyr)	
Duration of experiment	11.5 kyr	

3 Results

3.1 Spatial distribution of annual temperature anomalies and annual precipitation anomalies in Europe

Simulated annual temperature anomalies relative to the pre-industrial era at 11.5K_Down and 11.5K_Standard (Fig. 3) show some similarities in terms of their spatial patterns. However, as expected more details are visi-

ble in 11.5K_Down than in 11.5K_Standard. The downscaling produces local temperature changes visible on the high-resolution grid (11.5K_Down), particularly in northern Scandinavia and the Alps, at both 9 and 6 ka BP (Fig. 3d and e). Simulated annual temperature anomalies for 11.5K_Down and 11.5K_Standard were warm at both 9 and 6 ka BP, with annual temperature anomalies (relative to the pre-industrial era) of up to 4°C for 9 ka BP and 2°C for 6 ka BP. Central Europe and south-western Eu-

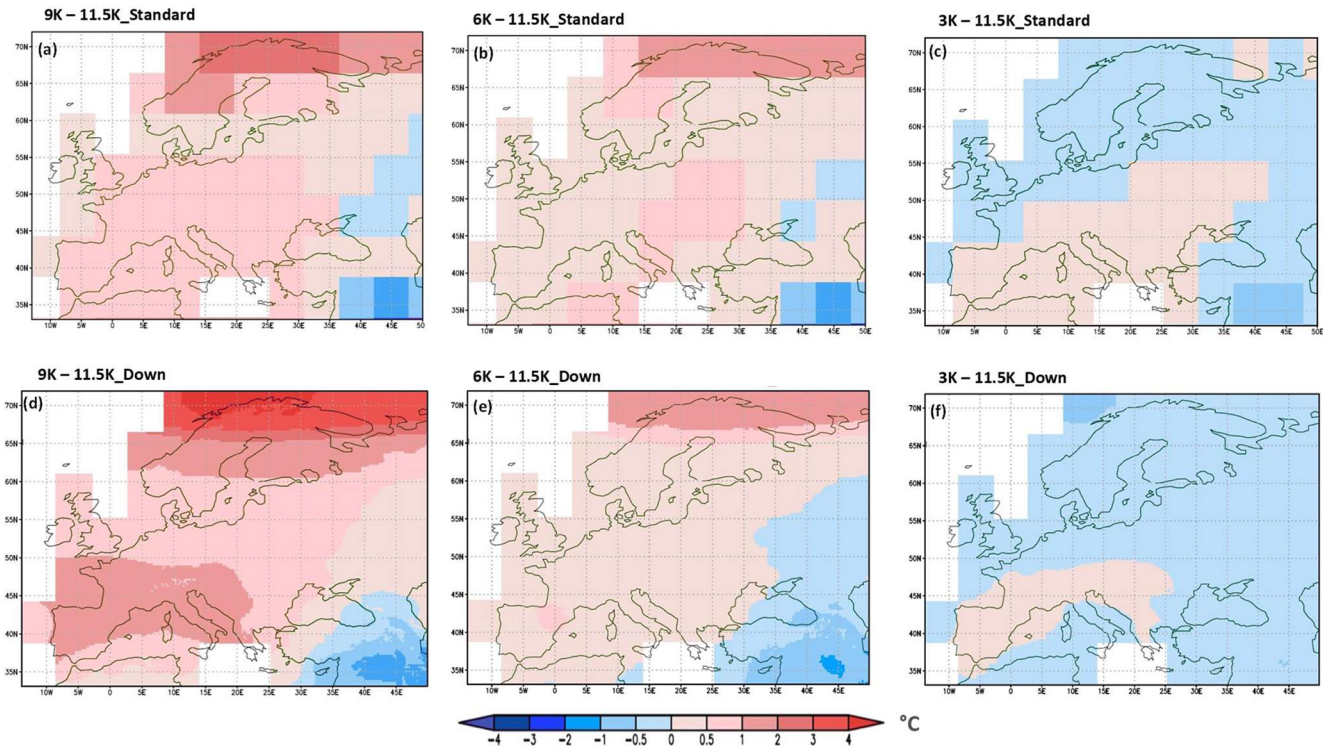


Figure 3. Simulated mean annual temperature anomalies (results minus the pre-industrial mean) showing spatial distribution in Europe for 9 ka BP (a, d), 6 ka BP (b, e) and 3 ka BP (c, f) for 11.5 K_Standard and 11.5 K_Down.

Europe have positive temperature anomalies relative to the pre-industrial era, reaching between 0.5 and 1 °C at 9 ka BP. Only southern Turkey has negative temperature anomaly up to −2 °C at 9 ka BP. During the mid-Holocene, northern Scandinavia was 2 °C warmer than the pre-industrial era, whereas northern Europe was relatively warm, with an annual temperature anomaly of 0.5 °C. The south-eastern corner of the domain was cool, with a negative annual temperature anomaly of −1 °C at 6 ka BP. At 3 ka BP, most regions in Europe were cooler than the pre-industrial era, except for the south-western area, which had a positive surface temperature anomaly of up to 0.5 °C. The latitudinal pattern during the mid-Holocene shows that the warming was stronger at high latitudes than mid-latitudes.

These spatial patterns in our results during the mid-Holocene appears to agree with PMIP4- and CMIP6-related work analysed by Williams et al. (2020), who found mean annual temperature anomalies between 1 and 2 °C warmer than the pre-industrial era in Europe, which is similar to our results. Our model simulates cooler conditions in south-eastern Europe but slightly higher temperatures in the south-west compared to the pre-industrial era, which contradicts the cool conditions in the south-west suggested by Brewer et al. (2007) based on reconstructions of proxy data. Reconstructions of mean annual temperature in the mid-Holocene by Wu et al. (2007) reveal a similar pattern in some regions

to our results, showing intense cooling in southern Europe and warming over northern and central Europe. However, our model simulates a similar magnitude of warming relative to the pre-industrial era over northern Scandinavia, which is more in agreement with Mauri et al. (2015).

Overall, the native grid (T21/11.5_Standard) is still seen in the 11.5 K_Down model results in many regions for all time slices. This is because the main impact of the downscaling is to physically compute the climate variables that are related to temperature in accordance with the sub-grid topography for the given coarse-grid information

The simulated mean precipitation anomalies show that 11.5 K_Down provides more spatial detail than 11.5 K_Standard and better considers the impact of topography on precipitation (Fig. 4). The results reveal that 11.5 K_Down drastically increases the spatial variability of the model in topographic regions when compared to 11.5 K_Standard. For instance, our 11.5 K_Down experiment provides a more detailed view in the Scandes mountains, the Alps, the Scottish Highlands, and the Pyrenees. The Scandes mountains are characterized by wetter than pre-industrial conditions at 9 and 6 ka BP for the 11.5 K_Down but relatively dry conditions at 9, 6, and 3 ka BP compared to the pre-industrial era for 11.5 K_Standard (Fig. 4). The annual precipitation anomaly in the Scandes mountains at 9 ka BP was about 250 mm yr^{−1} for 11.5 K_Down,

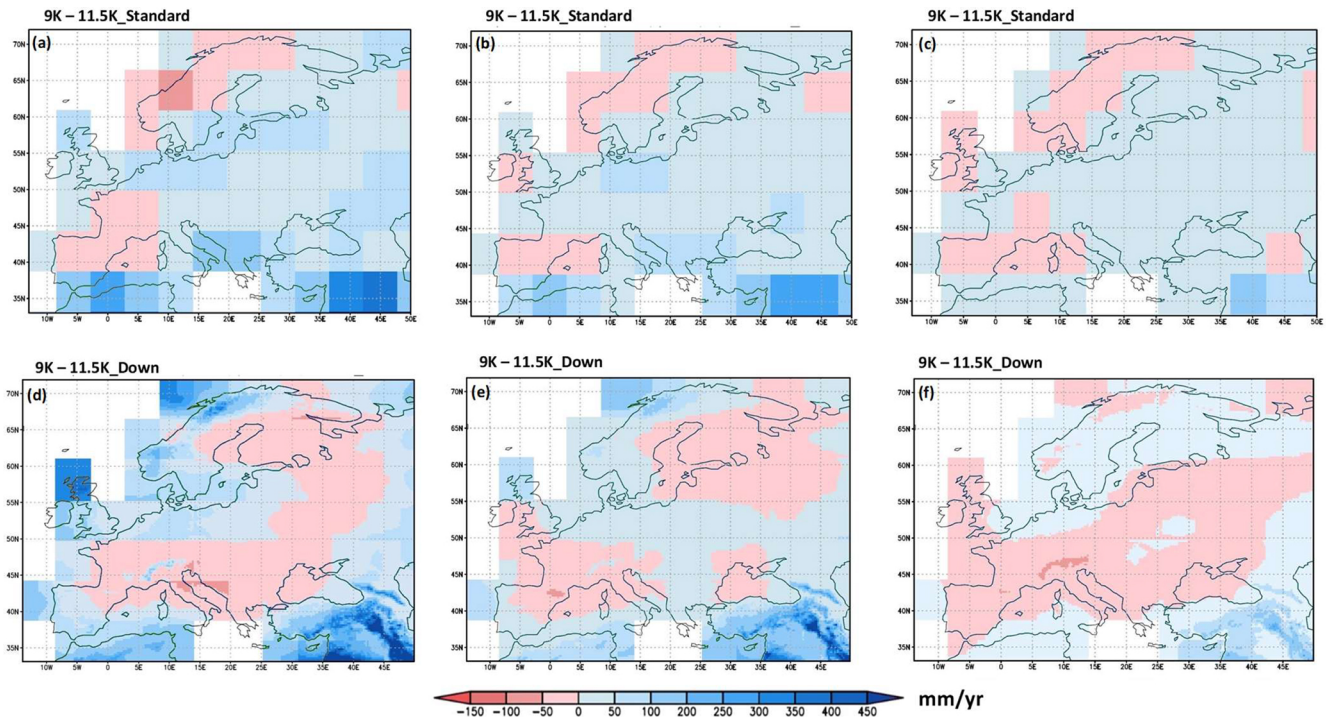


Figure 4. Simulated mean annual precipitation anomalies (in mm yr^{-1} , results minus the pre-industrial mean) showing spatial distribution in Europe for 9 ka BP (a, d), 6 ka BP (b, e), and 3 ka BP (c, f) for 11.5 K_Standard and 11.5 K_Down.

while the 11.5K_Standard has a mean annual precipitation anomaly of -50 mm yr^{-1} . The annual mean precipitation anomaly relative to the pre-industrial era in the mid-Holocene (6 ka BP) was up to 50 and -50 mm yr^{-1} in Scandinavia for 11.5 K_Down and 11.5 K_Standard, respectively. In the Alps, the Pyrenees, and the Massif Central, the 11.5 K_Down simulated annual precipitation anomalies at 9 ka BP were up to 150 mm yr^{-1} higher than the pre-industrial era, and this detailed information is not seen in 11.5 K_Standard (Fig. 4). Even at 6 ka BP, our 11.5 K_Down precipitation provides additional information in the Alps, with an annual precipitation anomaly up to 50 mm yr^{-1} . The Scottish Highlands show precipitation that is about 350 to 400 mm yr^{-1} wetter than the pre-industrial era in the early Holocene (9 ka BP) for 11.5 K_Down. However, it was about 50 mm yr^{-1} drier than the pre-industrial era in the late Holocene (3 ka BP) for both the 11.5 K_Down and 11.5 K_Standard experiments in the Scottish Highlands. The Scottish Highlands were still up to 100 mm yr^{-1} wetter in the mid-Holocene than the pre-industrial era for 11.5 K_Down; this was approximately 50 % less in 11.5 K_Standard, which shows precipitation anomalies between 50 and 100 mm yr^{-1} . The mountain ranges thus drastically affect the local precipitation anomalies, eventually changing the sign of the standard model (e.g. the downscaled Alps and the Scandes most of the time are in opposition with the standard model, as wetter regions becomes drier and drier regions becomes wetter).

The higher precipitation anomalies in these mountainous regions are due to the impact of the downscaling, as the primary effect of the downscaling is to increase precipitation in elevated areas (e.g. the Scandes mountains and the Alps). The results with downscaling provide details of the precipitation that better reflect the effect of the underlying topography. In general, experiment 11.5 K_Down is relatively wet compared to 11.5 K_Standard in most topographically complex regions in Europe.

The simulated annual mean precipitation anomalies with respect to the pre-industrial era for the 11.5 K_Down grid reproduce some of the major large-scale structures in Europe. For instance, the annual precipitation anomalies of 11.5 K_Down show a pattern characterized by a relatively dry zone in central Europe, which splits wetter areas south and east of the Mediterranean (Morocco, Algeria, Turkey, and the Middle East) from wetter north-western Europe, especially at 9 and 6 ka BP (Fig. 4). At 9 ka BP, southwestern Iberia and southern Turkey were wetter, with precipitation anomalies ranging from 100 to 400 mm yr^{-1} and showing more spatial details. This is generally true for 11.5 K_Standard, but the spatial details do not provide much information compared to the 11.5 K_Down grid. North-western Europe has precipitation anomalies of about 50 to 300 mm yr^{-1} at 9 ka BP. In contrast, the dry zone in central Europe is characterized by a negative precipitation anomaly of up to -50 mm yr^{-1} at 9 ka BP. The impact of the down-

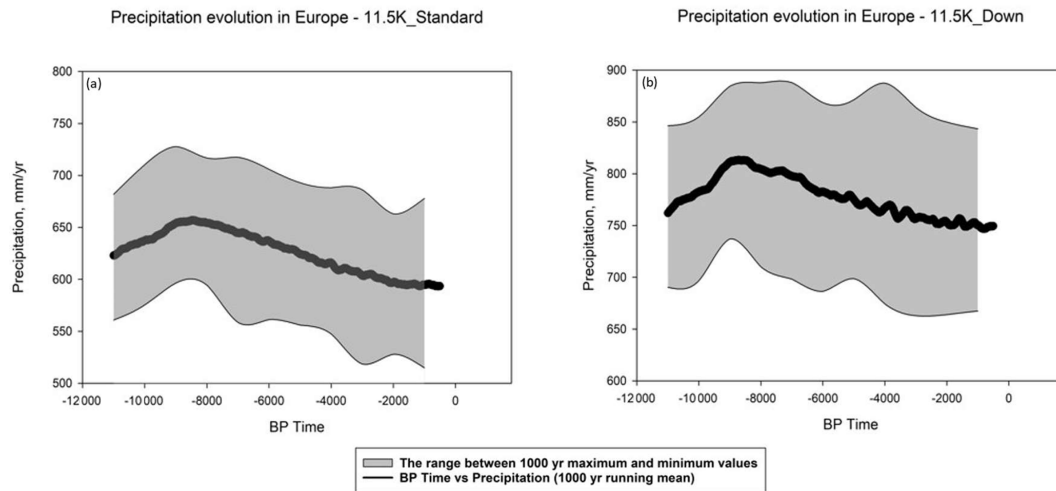


Figure 5. Annual precipitation evolution in Europe during the Holocene for both 11.5K_Standard (a) and 11.5K_Down (b). Grey-shaded areas represent the range between the maximum and minimum precipitation values in the transient simulations, and the black curve shows the 1000-year running mean of precipitation (in mm yr^{-1}).

scaling is seen in the results, as the downscaling reproduces some local topographical features in these regions. The results in 11.5K_Down suggest that northern Italy was about 50 mm yr^{-1} drier relative to the pre-industrial era. However, in 11.5K_Standard, northern Italy was relatively up to 50 mm yr^{-1} wetter than the pre-industrial era. Other regions, such as north-eastern Europe (especially western Russia) were generally dry (about -50 mm yr^{-1}) throughout the Holocene for the 11.5K_Down grid at 9 and 6 ka BP but were relatively wet (up to 50 mm yr^{-1}) for 11.5K_Standard. The Iberian Peninsula was between 50 and 100 mm yr^{-1} wetter than pre-industrial at 9 ka BP in the 11.5K_Down grid, but up to -50 mm yr^{-1} drier than the pre-industrial era for the simulated 11.5K_Standard.

3.2 Temporal trends in annual precipitation for the Holocene in Europe

In most areas, applying an interactive downscaling leads to an increase in precipitation compared to the standard experiment. The average precipitation in Europe for the entire Holocene was 775 and 624 mm yr^{-1} for 11.5K_Down and 11.5K_Standard, respectively. Consequently, this shows about a 24% increase in precipitation for the whole of Europe when downscaling is applied. In both experiments, it was generally wetter in the early and middle Holocene than the pre-industrial era, especially between 10 and 7 ka BP. For the 11.5K_Down model, precipitation generally rises from 762 mm yr^{-1} at 11 ka BP to its maximum peak value of 822 mm yr^{-1} between 9 and 8.5 ka BP and slightly decreases after 7.5 ka BP to 746 mm yr^{-1} in the late Holocene (Fig. 5). This precipitation trend in the Holocene is similar to 11.5K_Standard. Precipitation was about 622 mm yr^{-1} at 11 ka BP for 11.5K_Standard, then rises steadily to

666 mm yr^{-1} between 9 and 8.5 ka BP, before declining gradually to 593 mm yr^{-1} towards the pre-industrial era. The mid-Holocene was 32 mm yr^{-1} wetter than the pre-industrial era in the 11.5K_Down. The precipitation has a decreasing trend towards the pre-industrial era.

3.3 Regional annual precipitation evolution for the Holocene (Scandes mountains, Alps, and Scottish Highlands)

One of our objectives in this study is to evaluate our model's performance for regions with elevated topography. We compare the precipitation from reconstructed proxy data over the Alps, the Scandes mountains, and the Scottish Highlands with our model results.

3.3.1 Scandes mountains

Compared to 11.5K_Standard, our 11.5K_Down produces about twice as much precipitation in the Scandes mountains, with an opposite long-term trend. In the downscaled version, precipitation rises gradually from 1233 mm yr^{-1} at 11 ka BP to its maximum peak of 1469 mm yr^{-1} around 9 ka BP (Fig. 6), after which precipitation started declining gradually to 1 ka BP. This contrasts with 11.5K_Standard, which has rising precipitation trend from 525 mm yr^{-1} at 11 ka BP to the pre-industrial level of 637 mm yr^{-1} (Fig. 6a). In addition, there is a clear maximum peak at 9 ka BP in 11.5K_Down that is absent in 11.5K_Standard.

3.3.2 Alps

Similar to the Scandes mountains, there is a doubling of the precipitation in 11.5K_Down when compared to

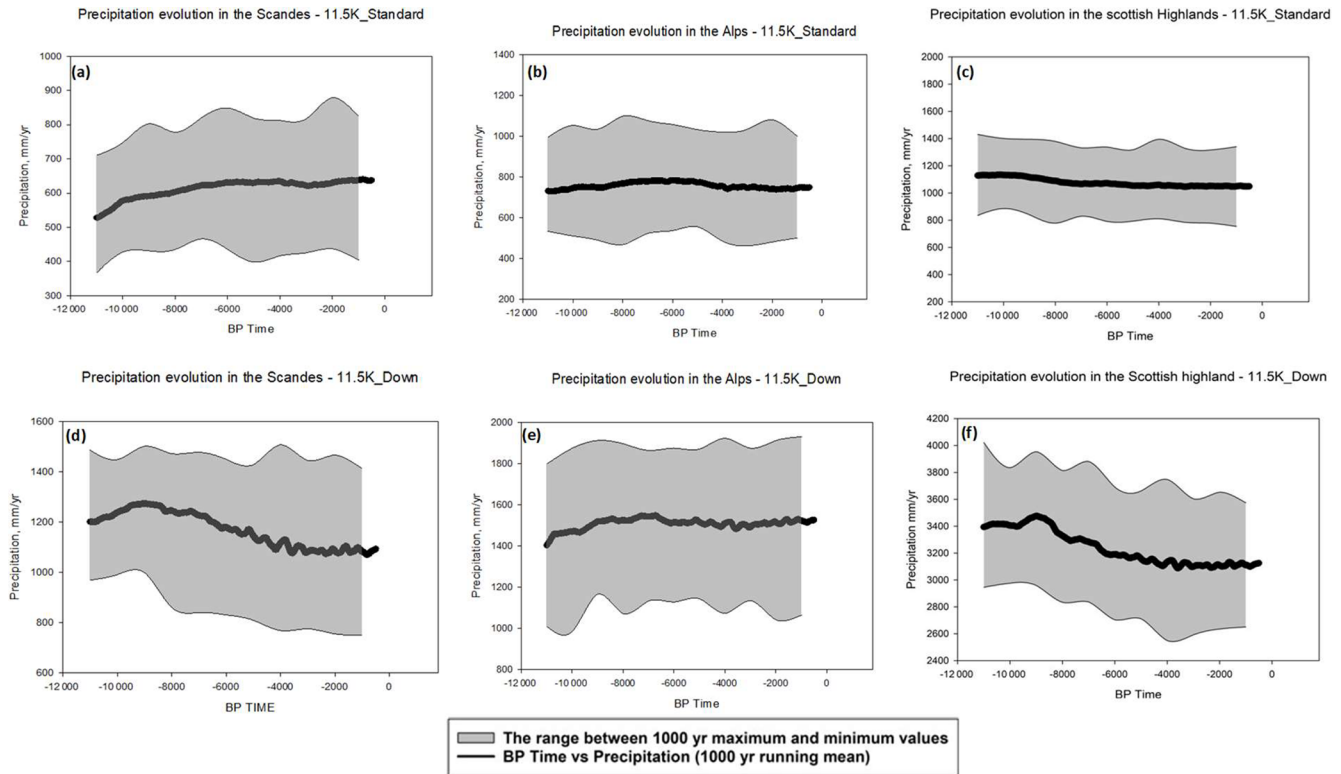


Figure 6. Regional annual precipitation evolution during the Holocene in some mountainous regions in Europe for both 11.5 K_Standard and 11.5 K_Down in the Scandes mountains (a, d), Alps (b, e), and Scottish Highlands (c, f). Grey-shaded areas represent the range between the maximum and minimum values in the transient simulations, and the black curve shows the 1000-year running mean of precipitation (in mm yr^{-1}).

11.5 K_Standard in the Alps. The trends for both experiments are similar, with reduced precipitation in the early Holocene and a flat trend afterwards (Fig. 6). The precipitation trend in the Alps for 11.5 K_Down shows that these mountains were drier in the early Holocene when compared to the pre-industrial era, with the late Holocene showing a flat trend towards the pre-industrial era. Thus, there is higher precipitation in the late Holocene than the early Holocene for 11.5 K_Down. The figure for 11.5 K_Down shows a slight increase in precipitation in the early Holocene towards 7 ka BP, followed by a slight dip and stable trend towards the pre-industrial era. For 11.5 K_Standard, the precipitation rise from 11 ka BP was quite steady and stable to the late Holocene with less variability when compared to 11.5 K_Down.

3.3.3 Scottish Highlands

In the Scottish Highlands, the 11.5 K_Down model simulates the highest average precipitation in Europe, with a Holocene mean value of 3238 mm yr^{-1} , compared to 1077 mm yr^{-1} for 11.5 K_Standard. Thus, the downscaled result is about 3 times higher than the 11.5 K_Standard. Generally, precipitation rises from 11.5 ka BP to its maximum peak aver-

age of 3474 mm yr^{-1} around 8.7 ka BP and declines gradually through the rest of the Holocene for 11.5 K_Down (Fig. 6f). Compared to pre-industrial, 11.5 K_Down simulates wetter conditions in the early and middle Holocene, but after 3.6 ka BP the model simulates a stable trend. The precipitation pattern for 11.5 K_Standard is quite different from 11.5 K_Down. The 11.5 K_Standard experiment shows a gradual decline towards the pre-industrial era, while the decrease in 11.5 K_Down is more pronounced with its maximum peak at a different time.

4 Discussion

The precipitation values simulated by 11.5 K_Down clearly show the influence of topography, since the highest values of above 400 mm yr^{-1} are produced in mountainous regions such as the Scandes, Scotland, and the Alps, which have a much higher elevation. The basic effect of the interactive downscaling is to redistribute precipitation in a physically consistent way based on topography (Quiquet et al., 2018). In most cases, 11.5 K_Standard is wetter than 11.5 K_Down in less elevated regions (Fig. 4). For example, some parts of central Europe are relatively dry in 11.5 K_Down at 9 ka BP but are relatively wet in 11.5 K_Standard. Since the topog-

raphy in 11.5 K_Down is more realistic, the spatial pattern obtained and the distribution with the downscaling is better than in the standard version. Thus, downscaling reproduces local features of these mountain regions described in the results, with higher precipitation in agreement with what is known from modern observations. The annual and selected regional precipitation trends presented in the results reveal that all the selected regions in the 11.5 K_Standard experiment present less precipitation. In comparison, 11.5 K_Down simulates much higher precipitation, coinciding with topography variations.

Our 11.5 K_Down simulation represents climate at a regional scale closer to the spatial scale of proxy data than our 11.5 K_Standard experiment. The improvement resulting from the downscaling technique will impact the comparison of our results with other climate model simulations and proxy-based reconstructions, especially because the latter are influenced by local conditions that are more realistically represented in the model. Previous model–data comparisons have revealed that General Circulation Models (GCMs) have great difficulty simulating key Holocene climate features, particularly trends in southern Europe (Mauri et al., 2014). One important factor could be the coarse resolution of GCMs (about 200–600 km) relative to the regional and local climate represented by proxy records. Thus, these models may not be able to account for a fine-scale variability of local features such as complex topography. To evaluate the performance of our model, we have compared our 11.5 K_Down and 11.5 K_Standard annual precipitation results for some regions in Europe with available proxy data and other simulated climate models. Some studies suggest that proxy-based reconstructions could be biased towards the growing season (Bader et al., 2020). However, studies using inverse vegetation modelling have found no evidence for seasonal biases in pollen-based reconstructions (Davis, 2017; Chevalier et al., 2020). For example, Davies (2017) shows comparisons with modern analogue technique (MAT) and inverse modelling (IVM) of proxy-based reconstructions for the mid-Holocene in the Mediterranean, and their findings show no significant difference in the methods, which implies no evidence of bias in the MAT. Given these results, we did not consider any impact of a seasonal bias.

The trend for precipitation reconstructions of Mauri et al. (2015) in the Alps shows an increase in precipitation from the early to middle Holocene, similar to our 11.5 K_Down experiment, but do not show such a significant increasing trend (Fig. 7a). In terms of the precipitation temporal trend, our 11.5 K_Down agrees with lake-level reconstructions by Harrison et al. (1996) that suggest no clear Holocene trend in lake-level records derived from some high-altitude sites (above 1000 m) in the Alps such as Landos and Rousses. Although our model simulations do not match perfectly with the proxy-based reconstructions of Mauri et al. (2015), the downscaled trend with reduced precipitation in the early Holocene is in better agreement with the

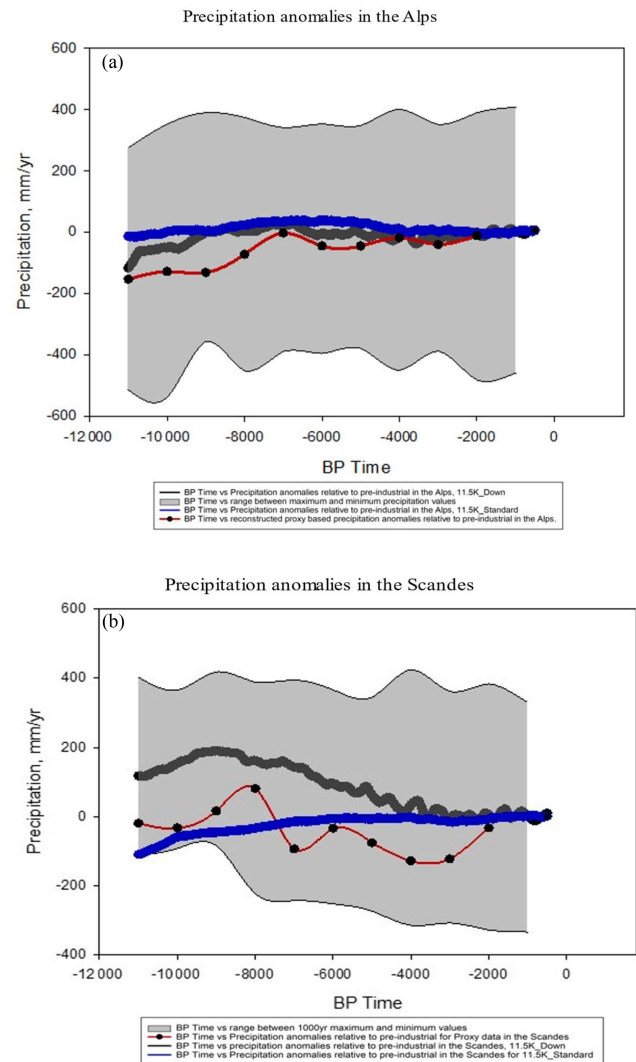


Figure 7. Comparison between simulated annual precipitation anomalies from iLOVECLIM and pollen-based reconstructions from Mauri et al. (2015) in the Alps (a) and the Scandes mountains (b). The red line shows proxy reconstructions, while the blue and black lines show the standard and downscaling simulations, respectively. Grey-shaded areas represent the range between the maximum and minimum precipitation values in the simulations, and the black curve shows the 1000-year running mean of precipitation anomalies relative to the pre-industrial era (in mm yr^{-1}).

proxy-based precipitation trend than our standard version. The same is true for the Scandes mountains (Fig. 7b), where the downscaled results show a maximum in precipitation between 10 and 8 ka BP, followed by a decreasing trend, in agreement with the proxy-based reconstructions (Mauri et al., 2015). To provide an example of the advantages of the applied downscaling, we assess the performance of the simulations at a high-elevation site in the Italian Alps (Armentarga peat bog, 2345 m a.s.l.) with proxy data reconstructions based on pollen data (Furlanetto et al., 2018).

The 11.5 K_Down and the reconstructions show a middle to late Holocene precipitation increase (Fig. 9b). The level of Holocene precipitation reconstructed by Furlanetto et al. (2018) for the high-elevation region is between 1100 and 1600 mm yr⁻¹, which is lower than but closely agrees with our 11.5 K_Down simulation that simulates precipitation between 1500 and 1750 mm yr⁻¹ (Fig. 9b). Their reconstructions thus suggest that precipitation in this elevated topographic region was higher than the 650 mm yr⁻¹ simulated by our 11.5 K_Standard (Fig. 9a), which supports the higher values that can be seen in the 11.5 K_Down simulations. It is therefore likely that the 11.5 K_Standard result is less realistic than 11.5 K_Down in oceanic mountain regions. The 11.5 K_Standard result of 650 mm yr⁻¹ is more appropriate for precipitation of the surrounding lowlands, which would be expected as the standard experiment does not take into consideration the topography in this site in the Alps.

Comparing our 11.5 K_Down version with the 11.5 K_Standard version of the simulations for the Scandes mountains, 11.5 K_Down shows that the early Holocene (10–5 ka BP) was a wetter period that is followed by drier conditions in the late Holocene, while the 11.5 K_Standard result is characterized by flat precipitation pattern with no significant trend (Fig. 6). Similar to the Alps, proxy data support our results with downscaling, as proxy-based precipitation reconstructions from Scandinavia suggest a more humid and wet early Holocene, followed by a dry middle to late Holocene (Seppä and Birks, 2001; Bjune et al., 2005; Harrison et al., 1996). For example, the pollen-based climate reconstructions by Seppä and Birks (2001) in Scandinavia have a similar trend as our 11.5 K_Down results, showing enhanced precipitation in the early Holocene that decreased steadily towards the late Holocene. This pattern is not seen in the 11.5 K_Standard simulations. Bjune et al. (2005) reconstructed winter precipitation based on Holocene glacier behaviour and show drier conditions in Scandinavia from 11.5 to 8 ka BP, a wetter period from 8 to 4 ka BP, followed by a drier period after 4 ka BP to the pre-industrial era. The pattern of their results thus agrees with the 11.5 K_Down simulation (Fig. 6). Moreover, pollen-inferred precipitation anomalies from Mauri et al. (2015) show that the spatial pattern in their precipitation in the Scandes mountains is similar to our downscaling experiment presented in Fig. 4. Consequently, our 11.5 K_Down results are in better agreement with the proxy-based reconstructions than our 11.5 K_Standard in most available studies and shows that downscaling also provides a more realistic representation of the hydroclimate in Scandinavia. However, it should be noted that our model simulations assumed present-day topography and did not correct precipitation for post-glacial isostatic uplift in the Scandes mountains, potentially leading to an overestimation of precipitation in the Scandes earlier in the Holocene.

The comparison with proxy-based reconstructions in our third region, the Scottish Highlands, is hampered by the un-

availability of suitable records. However, a comparison to modern data makes clear that the downscaling results are much more representative of the precipitation in the high-altitude Scottish Highlands than the standard results. Our precipitation values in this region for the high resolution were overestimated by the model, but we can have some confidence that 11.5 K_Down also represents the Holocene precipitation conditions better than 11.5 K_Standard due to the spatial variability.

We also compared our 11.5 K_Down results with studies in the Mediterranean. This region is very sensitive to changes in humidity, and during the early and middle Holocene period the dominant controlling factor on the Mediterranean ecosystem was precipitation rather than temperature (Magny et al., 2013; Mauri et al., 2015; Peyron et al., 2017). For instance, Brayshaw et al. (2011) used the HadSM3 global climate model, which was dynamically downscaled to about 50 km using a regional climate model (HadRM3), to simulate enhanced precipitation for time slices during the Holocene in the Mediterranean. This is consistent with the results of our 11.5 K_Down high-resolution model, which simulates wetter conditions during most of the Holocene relative to pre-industrial values (Fig. 4). Their regional climate model simulations show that some coastal areas, particularly in the north-eastern Mediterranean, received more precipitation at 9 and 6 ka BP (Brayshaw et al., 2011). This agrees with the high-resolution model that simulates higher precipitation above 450 mm yr⁻¹ around the Balkans and southern Turkey. The 11.5 K_Down results also show a contrasting pattern between different regions in the Mediterranean, with the southern and eastern Mediterranean being wet and the western–central part being dry (Fig. 4), particularly during the early to middle Holocene. This pattern is similar to reconstructions based on proxy data, such as lake levels, pollen data, and stable isotopes. All these data show that throughout the Holocene, climate conditions in the Mediterranean region varied spatially and temporally (e.g. Mauri et al., 2015; Sadori et al., 2016; Cheddadi and Khater, 2016). For instance, an east–west division during the Holocene is also observed in the Mediterranean region from lake-level reconstructions (Magny et al., 2013), marine and terrestrial pollen records (Guiot and Kaniewski, 2015), and speleothem isotopes (Roberts et al., 2011). Specifically, the simulated wetter mid-Holocene conditions in 11.5 K_Down agree with the high precipitation reconstructed at 6 ka BP (Bartlein et al., 2011; Guiot and Kaniewski, 2015; Mauri et al., 2015; Kuhnt et al., 2008). In the mid-Holocene, precipitation values 100–500 mm yr⁻¹ higher than the pre-industrial levels were reconstructed in the Mediterranean by Bartlein et al. (2011), in agreement with the high-resolution simulation (Fig. 4). Pollen-based reconstructions by Peyron et al. (2017) suggest dry early to middle Holocene conditions in northern Italy, similar to the downscaling simulations. The synthetic multi-proxy reconstructions of Finné et al. (2019) for the Holocene in the Mediterranean show a longer period of wet-

ter conditions in the east and south as compared to the northern and central areas of the Mediterranean. This was especially clear before 8.7 ka BP. Their study also reveals that the driest period in the eastern Mediterranean was at 3 ka BP, whereas Italy remained wetter around this time (Finné et al., 2019). Comparing their work with our 11.5 K_Down, we can see some similarities. For instance, at 3 ka BP, the eastern Mediterranean was the driest compared to the early and middle Holocene, and these drier conditions agree with the reconstructions from their study.

As shown above, we can compare our high-resolution results with paleo-reconstructions in these complex mountainous terrains in Europe due to the spatial variability attained from the downscaling. Compared to other studies, we find that the downscaled precipitation simulations are consistently in line with some European regions. Europe experienced multiple climate changes of various magnitudes over the Holocene, and regions within the continent experienced those changes differently. Based on our results, we can reproduce the different regional responses presented by some proxy-based reconstructions, for instance in northern and southern Europe we find wetter conditions from the early to middle Holocene relative to pre-industrial values (Fig. 4), similar to the proxy-based reconstructions reported by Mauri et al. (2015).

We have compared our results with some of the climate models from the Paleoclimate Modelling Intercomparison Project 4 (PMIP4). For example, Williams et al. (2020) simulated a mid-Holocene climate in Europe that was wetter than the pre-industrial era, with precipitation anomalies between 200 and 400 mm yr⁻¹. The magnitude of the simulated anomalies of their study is similar to the proxy reconstructions of Bartlein et al. (2011), with proxy-based anomalies between 200 and 400 mm yr⁻¹. Comparing the 11.5 K_Down simulations to Williams et al. (2020), we find that our results agree with some regions but are in contrast with some other regions. For example, at 6 ka BP, our model simulates wetter conditions relative to the pre-industrial era, with anomalies above 200 mm yr⁻¹ in the eastern Mediterranean. However, our model simulates drier conditions in the eastern part of Europe towards Russia, which is in contradiction with their studies. The mid-Holocene mean annual precipitation results of the PMIP4 ensembles in the mid-Holocene studied by Brierley et al. (2020) show positive precipitation anomalies in the Mediterranean similar to our 11.5 K_Down results. However, the PMIP4 ensemble mean does not capture the slight increase in precipitation in northern and central Europe and much wetter conditions in the Mediterranean as reconstructed for the mid-Holocene by Bartlein et al. (2011). Our simulations suggest slightly drier conditions in north-eastern Europe in agreement with the PMIP4 ensembles. Previous studies suggest that the persistent mismatch between model simulations and reconstructions is usually due to the biases in the pre-industrial control (Harrison et al., 2015). As studied by Brierley et al. (2020) in

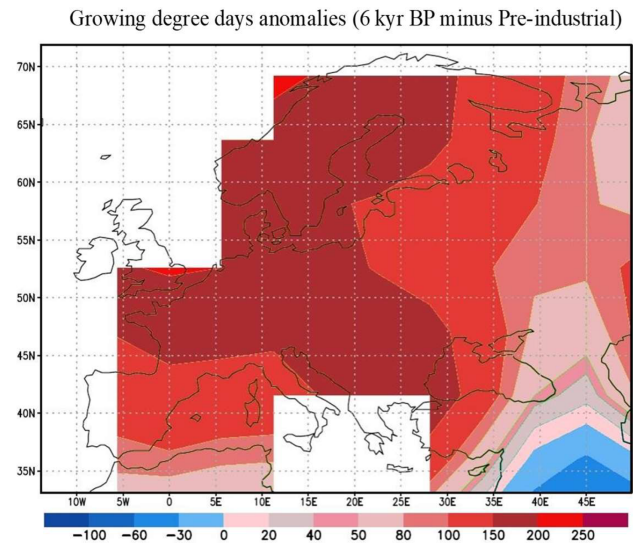


Figure 8. Simulated mid-Holocene growing degree days above 0 °C (GDD0) expressed as degree day anomalies (°C) relative to the pre-industrial era.

the PMIP4 (15 ensemble simulations), different climate models would usually give different results, but this may have no impact on the general conclusions.

One important variable for describing past climate is the intensity of the growing season as expressed by growing degree days above 0 °C (GDD0). Our model simulates more optimal conditions for plant growth at 6 ka BP relative to pre-industrial values in some parts of central Europe and northern Europe, most particularly in Scandinavia (Fig. 8) between 150 and 200 degree days. The growing degree days decrease in southern and eastern Europe, with a vast decrease in Turkey, Russia, Spain, and Italy. The model simulations fit well with the proxy-based reconstructions of Mauri et al. (2015), which show an increase in growing season intensity in Scandinavia and a decrease in southern Europe, particularly in Turkey (shown in the Supplement of Mauri et al., 2015). Jiang et al. (2018) analysed the growing season over ice-free land for the mid-Holocene based on numerical simulations from 28 PMIP 2 and 3 models. Their results show a latitude-varying difference in the mid-Holocene relative to the pre-industrial era. For example, 24 out of their 28 analysed PMIP model results indicate that growing season prolonged from the northern middle to high latitudes (above 50° N) and shortened between 20 and 50° N, similar to our results. It is well documented that the most important forcing for the mid-Holocene is the orbitally induced incoming solar radiation at the top of the atmosphere in the Northern Hemisphere (Berger, 1978), which is stronger in summer than in the pre-industrial era. The longer growing seasons in the north are a response to this orbital forcing. This was also found by Bartlein et al. (2011), who reconstructed the mid-Holocene changes in growing degree days using subfos-

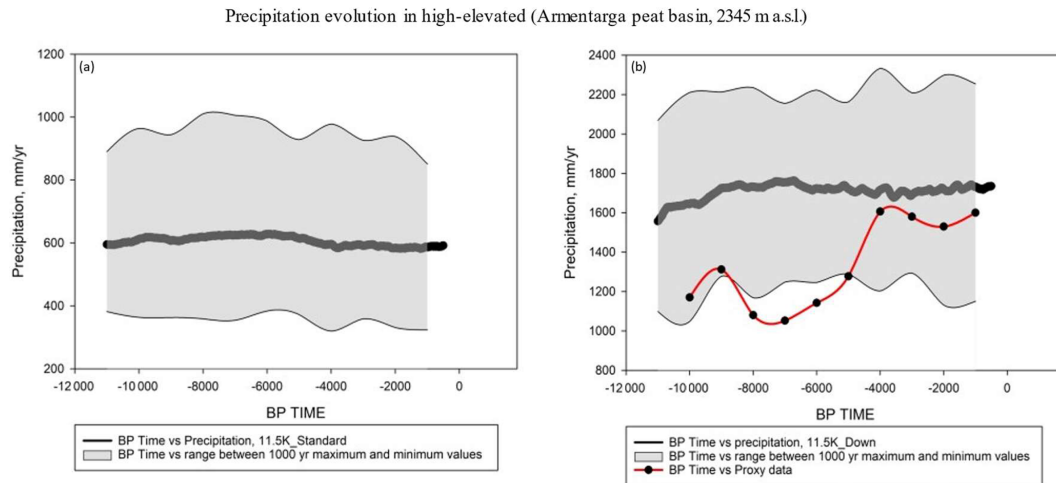


Figure 9. Simulated annual precipitation evolution with the standard version of the model (a) and interactive downscaling plotted with proxy-based reconstructions (Furlanetto et al., 2018), (b) at a high-elevation Armentarga peat site ($46^{\circ}2'26.642''$ N; $9^{\circ}52'44.263''$ E) in the central Alps (2345 m a.s.l.). The black line shows the 1000-year running mean of precipitation evolution during the Holocene (in mm yr^{-1}), while the light grey areas represent the range between the maximum and minimum values in the simulations. The red line shows the proxy-based reconstructions at the site.

sil pollen and plant macrofossil data. Their results show an increase in growing degree warmth over northern Europe and a decrease over southern Europe most particularly around the Mediterranean. The study by Bartlein et al. (2011) was supported with previous reconstructions based on different approaches, for instance through inverse modelling (Wu et al., 2007), a modern analogue method based on lake-level data (Cheddadi et al., 1996), and climate calibration from different plant functional types (Tarasov et al., 1999). Our model simulations agree with these proxy-based reconstructions in most regions in Europe.

The high resolution in our simulations shows spatial details for precipitation in the Holocene. In terms of climate impact studies, such local-scale information achieved from downscaling can be very useful. However, with our high-resolution simulations, only the physical part of precipitation is downscaled. The main reason precipitation increases over the mountains with the downscaling is simply because it is colder at high elevation and cold air cannot contain much humidity and thus rains out. However, since we see more of the topography, it is better represented in the model (Quiquet et al., 2018). We argue that such high-resolution climate modelling can be very useful to paleoclimatologists for model–data comparison at the local scale. For example, if a scientist studying paleoclimate data retrieves data from high-elevation region such as the Alps or the Scandes mountains, then it would be highly useful to get information on the gradients in precipitation and temperature provided by a high-resolution (regional) climate model. It is probable that these regional proxy data have been impacted by these gradients, hence it can be expected that the spatial scale of the high-resolution

(regional) climate model will be in better agreement with the proxy data than the coarse-resolution (global) model.

The interactive downscaling method that we have used for this study is relatively simplified since only the atmospheric physics are downscaled according to the sub-grid orography. The atmospheric dynamics remains computed at the coarse grid scale. As such, the fine-scale structure of the wind pattern that could affect the precipitation and temperature is not accounted for. For example, high precipitation on windward slopes and equally low precipitation on leeward slopes cannot be reproduced. One way to improve the model in future development would be to downscale the atmospheric dynamics in addition to the atmospheric physics. However, this will require heavy developments given the spectral nature of the atmospheric grid. An alternative solution would be to weigh the local sub-grid precipitation using the native grid wind direction. To do so, we could use some pre-computed index based on the normal vector of the sub-grid orography surface. Also, as discussed earlier, the downscaling tends to redistribute the precipitation according to the elevation with an increase in precipitation at high elevation and a respective drying at low elevation. As a result, although the pattern of precipitation appears better reproduced, there is an overestimation of the precipitation in most high-elevation regions (e.g. Scottish Highlands). This bias is a direct consequence of the physics of precipitation in iLOVECLIM where the precipitation is mostly the result of the local humidity. In the model, when this humidity reaches a critical fraction of the water vapour saturation, rain or snow is produced. Since the saturation is non-linearly linked to temperature, for a given humidity the precipitation rate is much higher at high elevation where the temperature is colder. On top of this aspect,

the original model biases can also largely explain the biases of the downscaled version. For example, iLOVECLIM has a large warm bias at the global scale that favours a humid atmosphere.

5 Conclusions

In this study, we have applied an interactive downscaling to our low-resolution iLOVECLIM model in Europe, increasing its resolution from 5.56 to 0.25° latitude–longitude. To our knowledge, this is the first time downscaling has been applied for Holocene transient experiments. A transient simulation for the entire Holocene (11.5–0 ka BP) was done for both the standard version of the model and with downscaling being applied. We have answered the following research questions in this paper.

- *What is the impact of dynamical downscaling on the precipitation patterns during the Holocene in different complex regions in Europe?* We have compared the spatial and temporal annual precipitation results of the low-resolution grid with the high-resolution grid to analyse the impact of downscaling on the model. Our results suggest that when downscaling is applied for precipitation, it drastically increases the spatial variability particularly in high-elevation regions as compared to the coarse resolution of the standard model.
- *Are the high-resolution results of precipitation in the mountainous regions (e.g. the Alps, the Scandes mountains, and the Scottish Highlands) producing more realistic Holocene climate when compared with the low-resolution grid and other proxy data?* We have shown that the high-resolution simulation presents a better agreement with proxy-based reconstructions and other climate model studies as compared to the coarse (low-resolution) grid, particularly in the Mediterranean and mountainous regions in Europe. The downscaling scheme simulates much higher (by at least a factor of 2) precipitation maxima and provides detailed information in the Scandes mountains and the Alps. By comparing our 11.5 K_Down and 11.5 K_Standard simulations with published proxy-based reconstructions, 11.5 K_Down simulates the magnitude of the precipitation changes reconstructed by other proxy studies (for example high-elevation sites) in close agreement, and there is good agreement for the overall trend and spatial pattern in 11.5 K_Standard. The different patterns of change, such as wetter conditions in northern and southern Europe, are captured well by our 11.5 K_Down model. Overall, precipitation was higher during the early Holocene than the late Holocene in most regions in Europe when compared to the pre-industrial era.

- *What is the advantage of using a numerically cheap interactive downscaling in paleoclimate research?* Paleoclimatologists would like to have very high-resolution model runs covering the last million years or more. We have shown a numerically cheap tool that is able to perform multi-millennial simulations at a kilometre scale, and even with a low resolution and a simple downscaling scheme, we achieve relatively good model–data agreement. The downscaling technique is moderately computationally demanding, making it appropriate for long-term integration. It can hypothetically be applied and extended in further studies to any resolution higher than the T21 grid. Our downscaling produces more detailed precipitation information suitable for comparison with regional paleoclimate studies. In addition, the downscaling simulations are better suited to match proxy data in terms of spatial representation, making the downscaling a useful approach for comparisons between climate models and proxy data. The downscaling's improved ability to resolve complex topography areas is very important since proxy records are often obtained from high altitudes, where the most sensitive climate archives (such as trees, sediments, and ice cores) are found.

Code availability. The iLOVECLIM source code is accessible at <http://www.elic.ucl.ac.be/modx/elic/index.php?id=289> (UCL, 2021). The developments on the iLOVECLIM source code are hosted at <http://forge.ipsl.jussieu.fr/ludus> (IPSL, 2021); due to copyright restrictions they cannot be publicly accessed. Request for access can be made by contacting Didier M. Roche (didier.roche@lsce.ipsl.fr). For this study, we used the model at revision 1147.

Data availability. Data sets are available at <https://doi.org/10.23642/usn.19354082.v2> (Arthur et al., 2022).

Author contributions. All authors designed the study. FA performed the simulations and wrote the manuscript with contributions of HR, RF, DMR. and AQ. The model results were analysed and interpreted by all authors.

Competing interests. The contact author has declared that none of the authors has any competing interests.

Disclaimer. Publisher's note: Copernicus Publications remains neutral with regard to jurisdictional claims in published maps and institutional affiliations.

Acknowledgements. We thank Marie José Gaillard, who provided input in setting up this work. We also thank Heikki Seppä and Basil Davis, who assisted us with proxy-based reconstructions. Finally, we want to give special thanks to the editor (Laurie Menviel) and the two anonymous reviewers for their comments and suggestions, which helped to improve the paper.

Financial support. The research is financed through the European Union's Horizon 2020 research and innovation programme within the TERRANOVA project, no. 813904. The paper only reflects the views of the authors, and the European Union cannot be held responsible for any use which may be made of the information contained therein.

Review statement. This paper was edited by Laurie Menviel and reviewed by two anonymous referees.

References

- Arthur, F., Roche, D., Fyfe, R., Quiquet, A., and Renssen, H.: Replication data for: Simulations of the Holocene climate in Europe using an interactive downscaling within the iLOVECLIM model (version 1.1), University of South-Eastern Norway [data set], <https://doi.org/10.23642/usn.19354082.v2>, 2022.
- Bader, J., Jungclaus, J., Krivova, N., Lorenz, S., Maycock, A., Raddatz, T., Schmidt, H., Toohey, M., Wu, C. J., and Claussen, M.: Global temperature modes shed light on the Holocene temperature conundrum, *Nat. Commun.*, 11, 4726, <https://doi.org/10.1038/s41467-020-18478-6>, 2020.
- Bartlein, P. J., Harrison, S., Brewer, S., Connor, S., Davis, B., Gajewski, K., Guiot, J., Harrison-Prentice, T., Henderson, A., and Peyron, O.: Pollen-based continental climate reconstructions at 6 and 21 ka: a global synthesis, *Clim. Dynam.*, 37, 775–802, <https://doi.org/10.1007/s00382-010-0904-1>, 2011.
- Berger, A. L.: Long-term variations of daily insolation and Quaternary climatic changes, *J. Atmos. Sci.*, 35, 2362–2367, [https://doi.org/10.1175/1520-0469\(1978\)035<2362:LTVODI>2.0.CO;2](https://doi.org/10.1175/1520-0469(1978)035<2362:LTVODI>2.0.CO;2), 1978.
- Bjune, A. E., Bakke, J., Nesje, A., and Birks, H. J. B.: Holocene mean July temperature and winter precipitation in western Norway inferred from palynological and glaciological lake-sediment proxies, *Holocene*, 15, 177–189, <https://doi.org/10.1191/0959683605hl798rp>, 2005.
- Bonfils, C., de Noblet, N., Guiot, J., and Bartlein, P.: Some Mechanisms of mid-Holocene climate change in Europe, inferred from comparing PMIP models to data, *Clim. Dynam.*, 23, 79–98, <https://doi.org/10.1007/s00382-004-0425-x>, 2004.
- Braconnot, P., Otto-Bliesner, B., Harrison, S., Joussaume, S., Peterchmitt, J.-Y., Abe-Ouchi, A., Crucifix, M., Driesschaert, E., Fichefet, Th., Hewitt, C. D., Kageyama, M., Kitoh, A., Laine, A., Loutre, M.-F., Marti, O., Merkel, U., Ramstein, G., Valdes, P., Weber, S. L., Yu, Y., and Zhao, Y.: Results of PMIP2 coupled simulations of the Mid-Holocene and Last Glacial Maximum – Part I: experiments and large-scale features, *Clim. Past*, 3, 261–277, <https://doi.org/10.5194/cp-3-261-2007>, 2007.
- Brayshaw, D. J., Rambeau, C. M. C., and Smith, S. J.: Changes in the Mediterranean climate during the Holocene: insights from global and regional climate modelling, *Holocene*, 21, 15–31, <https://doi.org/10.1177/0959683610377528>, 2011.
- Brewer, S., Guiot, J., and Torre, F.: Mid-Holocene climate change in Europe: a data-model comparison, *Clim. Past*, 3, 499–512, <https://doi.org/10.5194/cp-3-499-2007>, 2007.
- Brierley, C. M., Zhao, A., Harrison, S. P., Braconnot, P., Williams, C. J. R., Thornalley, D. J. R., Shi, X., Peterschmitt, J.-Y., Ohgaito, R., Kaufman, D. S., Kageyama, M., Hargreaves, J. C., Erb, M. P., Emile-Geay, J., D'Agostino, R., Chandan, D., Carré, M., Bartlein, P. J., Zheng, W., Zhang, Z., Zhang, Q., Yang, H., Volodin, E. M., Tomas, R. A., Routson, C., Peltier, W. R., Otto-Bliesner, B., Morozova, P. A., McKay, N. P., Lohmann, G., Legrande, A. N., Guo, C., Cao, J., Brady, E., Annan, J. D., and Abe-Ouchi, A.: Large-scale features and evaluation of the PMIP4-CMIP6 mid-Holocene simulations, *Clim. Past*, 16, 1847–1872, <https://doi.org/10.5194/cp-16-1847-2020>, 2020.
- Briner, J. P., McKay, N. P., Axford, Y., Bennike, O., Bradley, R. S., de Vernal, A., Fisher, D., Francus, P., Fréchet, B., Gajewski, K., Jennings, A., Kaufman, D. S., Miller, G., Rouston, C., and Wagner, B.: Holocene climate change in Arctic Canada and Greenland, *Quaternary Sci. Rev.*, 147, 340–364, <https://doi.org/10.1016/j.quascirev.2016.02.010>, 2016.
- Brovkin, V., Ganapolski, A., and Svirezhev, Y.: A continuous climate-vegetation classification for use in climate-biosphere studies, *Ecol. Model.*, 101, 251–261, [https://doi.org/10.1016/S0304-3800\(97\)00049-5](https://doi.org/10.1016/S0304-3800(97)00049-5), 1997.
- Castro, C. L., Pielke Sr., R. A., and Leoncini, G.: Dynamical downscaling: Assessment of value retained and added using the Regional Atmospheric Modelling System (RAMS), *J. Geophys. Res.*, 110, D05108, <https://doi.org/10.1029/2004JD004721>, 2005.
- Cheddadi, R. and Khater, C.: Climate change since the last glacial period in Lebanon and the persistence of Mediterranean species, *Quaternary Sci. Rev.*, 150, 146–157, <https://doi.org/10.1016/j.quascirev.2016.08.010>, 2016.
- Cheddadi, R., Yu, G., Guiot, J., Harrison, S., and Prentice, I.: The climate of Europe 6000 years ago, *Clim. Dynam.*, 13, 1–9, <https://doi.org/10.1007/s003820050148>, 1996.
- Chevalier, M., Davis, B. A. S., Heiri, O., Seppä, H., Chase, B. M., Gajewski, K., Lacourse, T., Telford, R. J., Finsinger, W., Guiot, J., Kühl, N., Maezumi, S. Y., Tipton, J. R., Carter, V. A., Brussel, T., Phelps, L. N., Dawson, A., Zanon, M., Vallé, F., Nolan, C., Mauri, A., de Vernal, A., Izumi, K., Holmström, L., Marsicek, J., Goring, S., Sommer, P. S., Chaput, M., and Kupriyanov, D.: Pollen-based climate reconstruction techniques for late Quaternary studies, *Earth Sci. Rev.*, 210, 103384, <https://doi.org/10.1016/j.earscirev.2020.103384>, 2020.
- Claussen, M., Mysak, L. A., Weaver, A. J., Crucifix, M., Fichefet, T., Loutre, M.-F., Weber, S. L., Alcamo, J., Alexeev, V. A., Berger, A., Calov, R., Ganapolski, A., Gooose, H., Lohmann, G., Lunkeit, F., Mokhov, I. I., Petoukhov, V., Stone, P., and Wang, Z.: Earth system models of intermediate complexity: closing the gap in the spectrum of climate system models, *Clim. Dynam.*, 18, 579–586, <https://doi.org/10.1007/s00382-001-0200-1>, 2002.
- Crowley, T. J.: Causes of climate change over the past 1000 years, *Science*, 289, 270–277, <https://doi.org/10.1126/science.289.5477.270>, 2000.

- Davis, B., Brewer, S., Stevenson, A., and Guiot, J.: The temperature of Europe during the Holocene reconstructed from pollen data, *Quaternary Sci. Rev.*, 22, 1701–1716, [https://doi.org/10.1016/S0277-3791\(03\)00173-2](https://doi.org/10.1016/S0277-3791(03)00173-2), 2003.
- Davis, B. A. S.: The Pollen-Climate Methods Intercomparison Project (PC-MIP), workshop report, *Past Global Changes Magazine*, <https://doi.org/10.22498/pages.25.3.161>, 2017.
- Driesschaert, E., Fichet, T., Goosse, H., Huybrechts, P., Janssens, I., Mouchet, A., Munhoven, G., Brovkin, V., and Weber, S. L.: Modelling the influence of the Greenland ice sheet melting on the Atlantic meridional overturning circulation during the next millennia, *Geophys. Res. Lett.*, 34, L10707, <https://doi.org/10.1029/2007GL029516>, 2007.
- Fallah, B., Sahar, S., and Ulrich, C.: Westerly jet stream and past millennium climate change in Arid Central Asia simulated by COSMO-CLM model, *Theor. Appl. Climatol.*, 124, 1079–1088, <https://doi.org/10.1007/s00704-015-1479-x>, 2016.
- Feser, F., Rocker, B., von Storch, H., Winterfeldt, J., and Zahn, M.: Regional Climate Models add Value to Global Model Data: A Review and Selected Examples, *B. Am. Meteorol. Soc.*, 92, 1181–1192, 2011.
- Finné, M., Woodbridge, J., Labuhn, I., and Roberts, C. N.: Holocene hydro-climatic variability in the Mediterranean: A synthetic multi-proxy reconstruction, *Holocene*, 29, 847–863, <https://doi.org/10.1177/0959683619826634>, 2019.
- Fischer, N. and Jungclauss, J. H.: Evolution of the seasonal temperature cycle in a transient Holocene simulation: orbital forcing and sea-ice, *Clim. Past*, 7, 1139–1148, <https://doi.org/10.5194/cp-7-1139-2011>, 2011.
- Furlanetto, G., Ravazzi, C., Pini, R., Vallè, F., Brunetti, M., Comolli, R., Novellino, M. D., Garozzo, L., and Maggi, V.: Holocene vegetation history and quantitative climate reconstructions in a high-elevation oceanic district of the Italian Alps. Evidence for a middle to late Holocene precipitation increase, *Quaternary Sci. Rev.*, 200, 212–236, <https://doi.org/10.1016/J.Quascirev.2018.10.001>, 2018.
- Gómez-Navarro, J. J., Montávez, J. P., Jerez, S., Jiménez-Guerrero, P., Lorente-Plazas, R., González-Rouco, J. F., and Zorita, E.: A regional climate simulation over the Iberian Peninsula for the last millennium, *Clim. Past*, 7, 451–472, <https://doi.org/10.5194/cp-7-451-2011>, 2011.
- Gómez-Navarro, J. J., Montávez, J. P., Wagner, S., and Zorita, E.: A regional climate palaeosimulation for Europe in the period 1500–1990 – Part 1: Model validation, *Clim. Past*, 9, 1667–1682, <https://doi.org/10.5194/cp-9-1667-2013>, 2013.
- Gómez-Navarro, J. J., Bothe, O., Wagner, S., Zorita, E., Werner, J. P., Luterbacher, J., Raible, C. C., and Montávez, J. P.: A regional climate palaeosimulation for Europe in the period 1500–1990 – Part 2: Shortcomings and strengths of models and reconstructions, *Clim. Past*, 11, 1077–1095, <https://doi.org/10.5194/cp-11-1077-2015>, 2015.
- Goosse, H. and Fichet, T.: Importance of ice-ocean interactions for the global ocean circulation: A model study, *J. Geophys. Res.*, 104, 23337–23355, <https://doi.org/10.1029/1999JC900215>, 1999.
- Goosse, H., Crowley, T., Zorita, E., Ammann, C., Renssen, H., and Driesschaert, E.: Modelling the climate of the last millennium: What causes the differences between simulations?, *Geophys. Res. Lett.*, 32, L06710, <https://doi.org/10.1029/2005GL022368>, 2005a.
- Goosse, H., Renssen, H., Timmermann, A., and Bradley, R. S.: Internal and forced climate variability during the last millennium: a model-data comparison using ensemble simulations, *Quaternary Sci. Rev.*, 24, 1345–1360, <https://doi.org/10.1016/j.quascirev.2004.12.009>, 2005b.
- Goosse, H., Brovkin, V., Fichet, T., Haarsma, R., Huybrechts, P., Jongma, J., Mouchet, A., Seltén, F., Barriat, P.-Y., Campin, J.-M., Deleersnijder, E., Driesschaert, E., Goelzer, H., Janssens, I., Loutre, M.-F., Morales Maqueda, M. A., Opsteegh, T., Mathieu, P.-P., Munhoven, G., Pettersson, E. J., Renssen, H., Roche, D. M., Schaeffer, M., Tartinville, B., Timmermann, A., and Weber, S. L.: Description of the Earth system model of intermediate complexity LOVECLIM version 1.2, *Geosci. Model Dev.*, 3, 603–633, <https://doi.org/10.5194/gmd-3-603-2010>, 2010.
- Guiot, J. and Kaniewski, D.: The Mediterranean Basin and Southern Europe in a warmer world: what can we learn from the past?, *Front. Earth Sci.*, 3, 28, <https://doi.org/10.3389/feart.2015.00028>, 2015.
- Haarsma, R. J., Seltén, F. M., Opsteegh, J. D., Lenterink, G., and Liu, Q.: ECBILT: A coupled atmosphere ocean sea-ice model for climate predictability studies, KNMI technical report, the Netherlands, https://cdn.knmi.nl/system/data_center_publications/files/000/066/085/original/techrap.pdf?1495620503 (last access: 25 October 2022), 1997.
- Harrison, S. P., Yu, G., and Tarasov, P.: Late Quaternary lake-level record from northern Eurasia, *Quatern. Res.*, 45, 138–159, <https://doi.org/10.1006/qres.1996.0016>, 1996.
- Harrison, S. P., Bartlein, P., Izumi, K., Li, G., Annan, J., Hargreaves, J., Braconnot, P., and Kageyama, M.: Evaluation of CMIP5 palaeo-simulations to improve climate projections, *Nat. Clim. Change*, 5, 735–743, <https://doi.org/10.1038/nclimate2649>, 2015.
- Hofer, D., Raible, C. C., Dehnert, A., and Kuhlemann, J.: The impact of different glacial boundary conditions on atmospheric dynamics and precipitation in the North Atlantic region, *Clim. Past*, 8, 935–949, <https://doi.org/10.5194/cp-8-935-2012>, 2012.
- IPSL: LUDUS Framework, <https://forge.ipsl.jussieu.fr/ludus>, last access: 22 December 2021.
- Jacob, D., Bärring, L., Christensen, O. B., Christensen, J. H., de Castro, M., Déqué, M., Giorgi, F., Hagemann, S., Hirschi, M., Jones, R., Kjellström, E., Lenderink, G., Rockel, B., Sánchez, E., Schär, C., Seneviratne, S. I., Somot, S., Van Ulden, A., and van den urk, B.: An inter-comparison of regional climate models for Europe: model performance in present-day climate, *Climatic Change*, 81, 31–52, <https://doi.org/10.1007/s10584-006-9213-4>, 2007.
- Jacob, D., Petersen, J., Eggert, B., Alias, A., Christensen, O. B., Bouwer, L. M., Braun, A., Colette, A., Déqué, M., Georgievski, G., Georgopoulou, E., Gobiet, A., Menut, L., Nikulin, G., Haensler, A., Hempelmann, N., Jones, C., Keuler, K., Kovats, S., and Yiuou, P.: EURO-CORDEX: new high-resolution climate change projections for European impact research, *Reg. Environ. Change*, 14, 563–578, <https://doi.org/10.1007/s10113-013-0499-2>, 2014.

- Jiang, D., Sui, Y., Lang, X., and Tian, Z.: Last glacial maximum and mid-Holocene thermal growing season simulations, *J. Geophys. Res.-Atmos.*, 123, 11466–11478, <https://doi.org/10.1029/2018JD028605>, 2018.
- Jones, P., Osborn, T., and Briffa, K.: The evolution of climate over the last millennium, *Science*, 292, 662–667, <https://doi.org/10.1126/science.1059126>, 2001.
- Kitover, D. C., Van Balen, R., Roche, D. M., Vandenberghe, J., and Renssen, H.: Advancement toward coupling of the VAMPER permafrost model within the Earth system model iLOVECLIM (version 1.0): description and validation, *Geosci. Model Dev.*, 8, 1445–1460, <https://doi.org/10.5194/gmd-8-1445-2015>, 2015.
- Kuhnt, T., Schmiedl, G., Ehrmann, W., Hamann, Y., and Andersen, N.: Stable isotopic composition of Holocene benthic foraminifers from the Eastern Mediterranean Sea: Past changes in productivity and deep water oxygenation, *Palaeogeogr. Palaeoclimatol.*, 268, 105–113, <https://doi.org/10.1016/j.palaeo.2008.07.010>, 2008.
- Latombe, G., Burke, A., Vrac, M., Levavasseur, G., Dumas, C., Kageyama, M., and Ramstein, G.: Comparison of spatial downscaling methods of general circulation model results to study climate variability during the Last Glacial Maximum, *Geosci. Model Dev.*, 11, 2563–2579, <https://doi.org/10.5194/gmd-11-2563-2018>, 2018.
- Liu, Z., Zhu, J., Rosenthal, Y., Zhang, X., Otto-Bliesner, B. L., Timmermann, A., Smith, R. S., Lohmann, G., Zheng, W., and Timm, O. E.: The Holocene temperature conundrum, *P. Natl. Acad. Sci. USA*, 111, E3501–E3505, <https://doi.org/10.1073/pnas.1407229111>, 2014.
- Liu, Z., Otto-Bliesner, B. L., Clark, P. U., Lynch-Stieglitz, J., and Russell, J. M.: SynTRACE-21: Synthesis of Transient Climate Evolution of the last 21,000 years, *PAGES Mag.*, 29, 13–15, <https://doi.org/10.22498/pages.29.1.13>, 2021.
- Lorenz, D. J., Nieto-Lugilde, D., Blois, J. L., Fitzpatrick, M. C., and Williams, J. W.: Downscaled and debiased climate simulations for North America from 21,000 years ago to 2100 AD, *Sci. Data*, 3, 1–19, <https://doi.org/10.1038/sdata.2016.48>, 2016.
- Ludwig, P., Schaffernicht, E. J., Shao, Y., and Pinto, J. G.: Regional atmospheric circulation over Europe during the Last Glacial Maximum and its links to precipitation, *J. Geophys. Res.-Atmos.*, 121, 2130–2145, <https://doi.org/10.1002/2015JD024444>, 2016.
- Ludwig, P., Gómez-Navarro, J. J., Pinto, J. G., Raible, C. C., Wagner, S., and Zorita, E.: Perspectives of regional paleoclimate modelling, *Ann. N. Y. Acad. Sci.*, 1436, 54–69, <https://doi.org/10.1111/nyas.13865>, 2019.
- Magny, M., Combourieu-Nebout, N., de Beaulieu, J. L., Bout-Roumazeilles, V., Colombaroli, D., Desprat, S., Francke, A., Joannin, S., Ortu, E., Peyron, O., Revel, M., Sadori, L., Siani, G., Sicre, M. A., Samartin, S., Simonneau, A., Tinner, W., Vanni re, B., Wagner, B., Zanchetta, G., Anselmetti, F., Brugiapaglia, E., Chapron, E., Debret, M., Desmet, M., Didier, J., Essallami, L., Galop, D., Gilli, A., Haas, J. N., Kallel, N., Millet, L., Stock, A., Turon, J. L., and Wirth, S.: North–south palaeohydrological contrasts in the central Mediterranean during the Holocene: tentative synthesis and working hypotheses, *Clim. Past*, 9, 2043–2071, <https://doi.org/10.5194/cp-9-2043-2013>, 2013.
- Masson, V., Cheddadi, R., Braconnot, P., Joussaume, S., Texier, D., and participants, P. M. I. P.: Mid-Holocene climate in Europe: what can we infer from PMIP model data?, *Clim. Dynam.*, 15, 163–182, <https://doi.org/10.1007/s003820050275>, 1999.
- Mauri, A., Davis, B. A. S., Collins, P. M., and Kaplan, J. O.: The influence of atmospheric circulation on the mid-Holocene climate of Europe: a data–model comparison, *Clim. Past*, 10, 1925–1938, <https://doi.org/10.5194/cp-10-1925-2014>, 2014.
- Mauri, A., Davis, B., Collins, P., and Kaplan, J.: The climate of Europe during the Holocene: a gridded pollen-based reconstruction and its multi-proxy evaluation, *Quaternary Sci. Rev.*, 112, 109–127, 2015.
- Murphy, J.: An evaluation of statistical and dynamical techniques for downscaling local climate, *J. Climate*, 12, 2256–2284, [https://doi.org/10.1175/1520-0442\(1999\)012<2256:AEOSAD>2.0.CO;2](https://doi.org/10.1175/1520-0442(1999)012<2256:AEOSAD>2.0.CO;2), 1999.
- Olsson, J., Berggren, K., Olofsson, M., and Viklander, M.: Applying climate model precipitation scenarios for urban hydrological assessment: a case study in Kalmar City, Sweden, *Atmos. Res.*, 92, 364–375, <https://doi.org/10.1016/j.atmosres.2009.01.015>, 2009.
- Opsteegh, J. D., Haarsma, R. J., Selten, F. M., and Kattenberg, A.: ECBILT: a dynamic alternative to mixed boundary conditions in ocean models, *Tellus A*, 50, 348–367, <https://doi.org/10.1034/j.1600-0870.1998.t01-1-00007.x>, 1998.
- Otto-Bliesner, B. L., Brady, E. C., Tomas, R., Levis, S., and Kothavala, Z.: Last Glacial Maximum and Holocene climate in CCSM3, *J. Climate*, 19, 2526–2544, 2006.
- Peyron, O., Combourieu-Nebout, N., Brayshaw, D., Goring, S., Andrieu-Ponel, V., Desprat, S., Fletcher, W., Gambin, B., Ioakim, C., Joannin, S., Kotthoff, U., Kouli, K., Montade, V., Pross, J., Sadori, L., and Magny, M.: Precipitation changes in the Mediterranean basin during the Holocene from terrestrial and marine pollen records: a model–data comparison, *Clim. Past*, 13, 249–265, <https://doi.org/10.5194/cp-13-249-2017>, 2017.
- Quiquet, A., Roche, D. M., Dumas, C., and Paillard, D.: Online dynamical downscaling of temperature and precipitation within the iLOVECLIM model (version 1.1), *Geosci. Model Dev.*, 11, 453–466, <https://doi.org/10.5194/gmd-11-453-2018>, 2018.
- Raible, C. C., B renbold, O., and G mez-Navarro, J. J.: Drought indices revisited–improving and testing of drought indices in a simulation of the last two millennia for Europe, *Tellus A*, 69, 1296226, <https://doi.org/10.1080/16000870.2017.1296226>, 2017.
- Raynaud, D., Barnola, J.-M., Chappellaz, J., Blunier, T., Indermuhle, A., and Stauffer, B.: The ice record of greenhouse gases: a view in the context of future changes, *Quaternary Sci. Rev.*, 19, 9–17, [https://doi.org/10.1016/S0277-3791\(99\)00082-7](https://doi.org/10.1016/S0277-3791(99)00082-7), 2000.
- Renssen, H. and Osborn, T. J.: Investigating Holocene climate variability: data-model comparisons, *PAGES News*, 11, 32–33, 2003.
- Renssen, H., Isarin, R., Jacob, D. J., Podzun, R., and Vandenberghe, J.: Simulation of the Younger Dryas climate in Europe using a regional climate model nested in an AGCM: preliminary results, *Global Planet. Change*, 30, 41–57, [https://doi.org/10.1016/S0921-8181\(01\)00076-5](https://doi.org/10.1016/S0921-8181(01)00076-5), 2001.
- Renssen, H., Goosse, H., Fichefet, T., Brovkin, V., Driesschaert, E., and Wolk, F.: Simulating the Holocene climate evolution at northern high latitudes using a coupled atmosphere sea ice–ocean–vegetation model, *Clim. Dynam.*, 24, 23–43, <https://doi.org/10.1007/s00382-004-0485-y>, 2005a.

- Renssen, H., Goosse, H., and Fichet, T.: Contrasting trends in North Atlantic deep-water formation in the Labrador and Nordic Seas during the Holocene, *Geophys. Res. Lett.*, 32, L08711, <https://doi.org/10.1029/2005GL022462>, 2005b.
- Renssen, H., Seppä, H., Heiri, O., Roche, D. M., Goosse, H., and Fichet, T.: The spatial and temporal complexity of the Holocene thermal maximum, *Nat. Geosci.*, 2, 411–414, <https://doi.org/10.1038/ngeo513>, 2009.
- Roberts, N., Brayshaw, D., Kuzucuoglu, C., Perez, R., and Sadori, L.: The mid-Holocene climatic transition in the Mediterranean: Causes and consequences, *Holocene*, 21, 3–13, <https://doi.org/10.1177/0959683610388058>, 2011.
- Roche, D. M., Dokken, T. M., Goosse, H., Renssen, H., and Weber, S. L.: Climate of the Last Glacial Maximum: sensitivity studies and model-data comparison with the LOVECLIM coupled model, *Clim. Past*, 3, 205–224, <https://doi.org/10.5194/cp-3-205-2007>, 2007.
- Roche, D. M., Dumas, C., Bügelmayr, M., Charbit, S., and Ritz, C.: Adding a dynamical cryosphere to iLOVECLIM (version 1.0): coupling with the GRISLI ice-sheet model, *Geosci. Model Dev.*, 7, 1377–1394, <https://doi.org/10.5194/gmd-7-1377-2014>, 2014.
- Russo, E. and Cubasch, U.: Mid-to-late Holocene temperature evolution and atmospheric dynamics over Europe in regional model simulations, *Clim. Past*, 12, 1645–1662, <https://doi.org/10.5194/cp-12-1645-2016>, 2016.
- Russo, E., Fallah, B., Ludwig, P., Karremann, M., and Raible, C. C.: The long-standing dilemma of European summer temperatures at the mid-Holocene and other considerations on learning from the past for the future using a regional climate model, *Clim. Past*, 18, 895–909, <https://doi.org/10.5194/cp-18-895-2022>, 2022.
- Sadori, L., Giraudi, C., Masi, A., Magny, M., Ortu, E., Zanchetta, G., and Izdebski, A.: Climate, environment, and society in southern Italy during the last 2000 years. A review of the environmental, historical and archaeological evidence, *Quaternary Sci. Rev.*, 136, 173–188, <https://doi.org/10.1016/j.quascirev.2015.09.020>, 2016.
- Schaeffer, M., Selten, F. M., Opsteegh, J. D., and Goosse, H.: Intrinsic limits to predictability of abrupt regional climate change in IPCC SRES scenarios, *Geophys. Res. Lett.*, 29, 14–1–14–4, <https://doi.org/10.1029/2002GL015254>, 2002.
- Schaeffer, M., Selten, F., Goosse, H., and Opsteegh, T.: On the influence of location of high-latitude ocean deep convection and Arctic sea-ice on climate change projections, *J. Climate*, 17, 4316–4329, <https://doi.org/10.1175/3174.1>, 2004.
- Schilt, A., Baumgartner, M., Schwander, J., Buiron, D., Capron, E., Chappellaz, J., Loulergue, L., Schüpbach, S., Spahni, R., Fischer, H., and Stocker, T. F.: Atmospheric nitrous oxide during the last 140,000 years, *Earth Planet. Sc. Lett.*, 300, 33–43, <https://doi.org/10.1016/j.epsl.2010.09.027>, 2010.
- Schmidt, G. A., Shindell, D. T., Miller, R. L., Mann, M. E., and Rind, D.: General circulation modelling of Holocene climate variability, *Quaternary Sci. Rev.*, 23, 2167–2181, <https://doi.org/10.1016/j.quascirev.2004.08.005>, 2004.
- Seppä, H. and Birks, H. J. B.: July mean temperature and annual precipitation trends during the Holocene in the Fennoscandian tree-line area: pollen-based climate reconstructions, *Holocene*, 11, 527–539, <https://doi.org/10.1191/095968301680223486>, 2001.
- Stoner, A. M. K., Hayhoe, K., Yang, X. and Wuebbles, D. J.: An asynchronous regional regression model for statistical downscaling of daily climate variables, *Int. J. Climatol.*, 33, 2473–2494, <https://doi.org/10.1002/joc.3603>, 2013.
- Strandberg, G., Brandefelt, J., Kjellström, E., and Smith, B.: High-resolution regional simulation of last glacial maximum climate in Europe, *Tellus A*, 63, 107–125, <https://doi.org/10.1111/j.1600-0870.2010.00485.x>, 2011.
- Tarasov, P. E., Guiot, J., Cheddadi, R., Andreev, A. A., Bezusko, L. G., Blyakharchuk, T. A., Dorofeyuk, N. I., Filimonova, L. V., Volkova, V. S., and Zernitskaya, V. P.: Climate in northern Eurasia 6000 years ago reconstructed from pollen data, *Earth Planet. Sc. Lett.*, 171, 635–645, [https://doi.org/10.1016/S0012-821X\(99\)00171-5](https://doi.org/10.1016/S0012-821X(99)00171-5), 1999.
- Timm, O., Timmermann, A., Abe-Ouchi, A., Saito, F., and Segawa, T.: On the definition of seasons in paleoclimate simulations with orbital forcing, *Paleoceanography*, 23, PA2221, <https://doi.org/10.1029/2007PA001461>, 2008.
- Timmermann, A., Justino, F., Jin, F. F., and Goosse, H.: Surface temperature control in the North and tropical Pacific during the last glacial maximum, *Clim. Dynam.*, 23, 353–370, <https://doi.org/10.1007/s00382-004-0434-9>, 2004.
- UCL: LOVECLIM, Université catholique de Louvain [code], <http://www.elic.ucl.ac.be/modx/elic/index.php?id=289>, last access: 22 December 2021.
- Velasquez, P., Kaplan, J. O., Messmer, M., Ludwig, P., and Raible, C. C.: The role of land cover in the climate of glacial Europe, *Clim. Past*, 17, 1161–1180, <https://doi.org/10.5194/cp-17-1161-2021>, 2021.
- Vrac, M., Marbaix, P., Paillard, D., and Naveau, P.: Non-linear statistical downscaling of present and LGM precipitation and temperatures over Europe, *Clim. Past*, 3, 669–682, <https://doi.org/10.5194/cp-3-669-2007>, 2007.
- Wang, J., Swati, F. N. U., Stein, M. L., and Kotamarthi, V. R.: Model performance in spatiotemporal patterns of precipitation: New methods for identifying value added by a regional climate model, *J. Geophys. Res.-Atmos.*, 120, 1239–1259, <https://doi.org/10.1002/2014JD022434>, 2015.
- Wanner, H., Beer, J., Bütikofer, J., Crowley, T. J., Cubasch, U., Flückiger, J., Goosse, H., Grosjean, M., Joos, F., Kaplan, J. O., Küttel, M., Müller, S. A., Prentice, I. C., Solomina, O., Stocker, T. F., Tarasov, P. E., Wagner, M., and Widmann, M.: Mid- to late Holocene climate change – an overview, *Quaternary Sci. Rev.*, 27, 1791–1828, <https://doi.org/10.1016/j.quascirev.2008.06.013>, 2008.
- Willems, P. and Vrac, M.: Statistical precipitation downscaling for small-scale hydrological impact investigations of climate change, *J. Hydrol.*, 402, 193–205, <https://doi.org/10.1016/j.jhydrol.2011.02.030>, 2011.
- Williams, C. J. R., Guarino, M.-V., Capron, E., Malmierca-Vallet, I., Singarayer, J. S., Sime, L. C., Lunt, D. J., and Valdes, P. J.: CMIP6/PMIP4 simulations of the mid-Holocene and Last Interglacial using HadGEM3: comparison to the pre-industrial era, previous model versions and proxy data, *Clim. Past*, 16, 1429–1450, <https://doi.org/10.5194/cp-16-1429-2020>, 2020.

- Wu, H., Guiot, J., Brewer, S., and Guo, Z.: Climatic changes in Eurasia and Africa at the last glacial maximum and mid-Holocene: Reconstruction from pollen data using inverse vegetation modelling, *Clim. Dynam.*, 29), 211–229, <https://doi.org/10.1007/s00382-007-0231-3>, 2007.
- Yokoyama, Y., Lambeck, K., De Deckker, P., Johnston, P., and Fifield, L. K.: Timing of the Last Glacial Maximum from observed sea-level minima, *Nature*, 406, 713–716, <https://doi.org/10.1038/35021035>, 2000.
- Zhang, Y., Renssen, H., and Seppä, H.: Effects of melting ice sheets and orbital forcing on the early Holocene warming in the extratropical Northern Hemisphere, *Clim. Past*, 12, 1119–1135, <https://doi.org/10.5194/cp-12-1119-2016>, 2016.
- Zorita, E., González-Rouco, J. F., von Storch, H., Montávez, J. P., and Valero, F.: Natural and anthropogenic modes of surface temperature variations in the last thousand years, *Geophys. Res. Lett.*, 32, 755–762, <https://doi.org/10.1029/2004GL021563>, 2005.

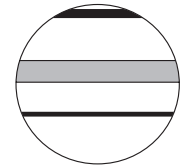
Paper 2

Arthur, F., Zapolska, A., Roche, D. M., Li, H., Renssen, H.: Modelling the climate of the Eemian in Europe using an Interactive Physical Downscaling (Manuscript).

Not available online

Paper 3

Arthur, F., Hatlestad, K., Lindholm, K. J., Loftsgarden, K., Löwenborg, D., Solheim, S., Roche, D.M., & Renssen, H. (2024). The impact of volcanism on Scandinavian climate and human societies during the Holocene: Insights into the Fimbulwinter eruptions (536/540 AD). *The Holocene*. <https://doi.org/10.1177/09596836231225718>



The impact of volcanism on Scandinavian climate and human societies during the Holocene: Insights into the Fimbulwinter eruptions (536/540 AD)

The Holocene
1–15

© The Author(s) 2024



Article reuse guidelines:

sagepub.com/journals-permissions

DOI: 10.1177/09596836231225718

journals.sagepub.com/home/hol



Frank Arthur,¹  Kailin Hatlestad,²  Karl-Johan Lindholm,² 
Kjetil Loftsgarden,³  Daniel Löwenborg,²  Steinar Solheim,³ 
Didier M Roche^{4,5} and Hans Rensen¹ 

Abstract

Recent paleoclimatic research has revealed that volcanic events around 536–540 AD caused severe, short-term global cooling. For this same period, archeological research from various regions evidences significant cultural transformation. However, there is still a lack of understanding of how human societies responded and adapted to extreme climate variability and new circumstances. This study focuses on the effects of the 536/540 AD volcanic event in four Scandinavian regions by exploring the shift in demographic and land use intensity before, during, and after this abrupt climate cooling. To achieve this, we performed climate simulations with and without volcanic eruptions using a dynamically downscaled climate model (iLOVECLIM) at a high resolution (0.25° or ~25 km). We integrated the findings with a comprehensive collection of radiocarbon dates from excavated archeological sites across various Scandinavian regions. Our Earth System Model simulates pronounced cooling (maximum ensemble mean -1.1°C), an abrupt reduction in precipitation, and a particularly acute drop in growing degree days (GDD0) after the volcanic event, which can be used to infer likely impacts on agricultural productivity. When compared to the archeological record, we see considerable regional diversity in the societal response to this sudden environmental event. As a result, this study provides a more comprehensive insight into the demographic chronology of Scandinavia and a deeper understanding of the land-use practices its societies depended on during the 536/540 AD event. Our results suggest that this abrupt climate anomaly amplified a social change already in progress.

Keywords

archeology, climate modeling, Scandinavian Fimbulwinter, spatial analysis, summed probability distribution of radiocarbon dates (^{14}C), volcanic eruption

Received 13 August 2023; revised manuscript accepted 29 November 2023

Introduction

There is still a lack of clear understanding of the immediate impact of volcanism on the climate and the people during the late ancient societies throughout Europe. In our study, we analyze an extensive set of radiocarbon dates from excavated archeological sites from several regions of Scandinavia, providing detailed information on societal changes, and combine this with paleoclimate simulations performed with a high-resolution (0.25° or ~25 km) climate model to examine the impact of volcanism on Scandinavia in the 6th century AD. Although the link between climate and volcanism has been studied widely (e.g. Goosse and Rensen, 2004; Jones et al., 2005; McGregor and Timmermann, 2011; Robock, 2000; Schmidt et al., 2004; Schneider et al., 2009; Timmreck et al., 2010), these studies have not empirically explored the societal impacts (Iversen, 2016; Pfister, 2010; Solheim and Iversen, 2019). Our study traces the climatological effects of the 536/540 AD volcanic eruption and the human response to it using a comparative analysis of the ^{14}C archeological record and a downscaled climate model.

Our analysis compares responses between Sweden and Norway's coastal and inland regions', focusing on spatiotemporal changes in land use. Combining climate and archeological data

poses a challenge due to differing spatial scales, as climate models capture large-scale processes and archeological materials reflect local landscape contexts. To address this, we thus utilize an

¹Department of Natural Sciences and Environmental Health, University of South-Eastern Norway, Norway

²Department of Archaeology and Ancient History, Uppsala University, Sweden

³The Museum of Cultural History, University of Oslo, Norway

⁴Earth and Climate Cluster, Faculty of Science, Vrije Universiteit Amsterdam, The Netherlands

⁵Laboratoire des Sciences du Climat et de l'Environnement, LSCE/IPSL, CEA-CNRS-UVSQ, Université Paris-Saclay, France

Corresponding authors:

Frank Arthur, Department of Natural Sciences and Environmental Health, University of South-Eastern Norway, Gullbringvegen 36, Bø 3800, Norway.
Email: Frank.Arthur@usn.no

Kailin Hatlestad, Department of Archaeology and Ancient History, Uppsala University, Thunbergsvägen 3G, Uppsala 751 05, Sweden.
Email: Kailin.Hatlestad@arkeologi.uu.se

Earth System Model (iLOVECLIM) that is a downscaled climate model with a high spatial resolution (25 km) to provide fine-scale local climate information, including temperature gradient and precipitation distribution, to match regional archeological data more closely. Additionally, we categorized ^{14}C records into general land use categories to evaluate adaptive strategies to climate variability. This integrative approach for climate and archeological data helps discern regional effects of the volcanic event on land use and society.

We aim to investigate how massive volcanic eruptions around 536 and 540 AD influenced the coping strategies of Late ancient European societies in response to sudden environmental changes caused by climate cooling. To guide our research, we have formulated the following research questions:

- (i) *What is the impact of the 536/540 volcanic event on Scandinavian society?*
- (ii) *Can we see evidence for a relationship between patterns of climate and ^{14}C records? Can we identify the volcanic event as a leading signal to change in the archeological record?*
- (iii) *Did the 536/540 event result in changes to land use or regional spatial intensity? If so, what does this indicate about the region's ability to cope with abrupt climate risk?*

Background

Proxy-based reconstructions of volcanic eruptions have widely been used to understand climate variability (Hegerl et al., 2006; Masson-Delmotte et al., 2013; Sigl et al., 2015). These reconstructions have demonstrated that volcanism has been a principal natural driver of climatic variation in the recent past (Schurer et al., 2014). Explosive volcanic eruptions inject sulfur into the stratosphere, leading to the formation of sulfate aerosols from gases like sulfur dioxide (SO_2) and hydrogen sulfide (H_2S) (Helama et al., 2018). These aerosols disperse globally, scattering and reflecting incoming solar energy while absorbing infrared radiation, resulting in a net reduction reaching the Earth's surface and subsequent cooling. The short-term impacts of this radiative forcing are well-documented, including post-eruption surface cooling in summer and the reduction of the amount of sunlight reaching the Earth's surface (Helama et al., 2018). A volcanic eruption's impact on climate is influenced by eruption latitude and eruption season (Toohey et al., 2013). In general, the climate is more affected by tropical eruptions than extratropical ones (Schneider et al., 2009). Tropical eruptions disperse volcanic aerosols to both hemispheres, eventually reaching both poles, and this leads to more prolonged and pronounced impacts compared to extra-tropical eruptions (Zhuo et al., 2021). Yet, short-term temperature decreases due to increased aerosols can be more pronounced in the tropics and at lower latitudes where the sun's energy is typically more intense (Timmreck, 2012).

However, recent studies by Toohey et al. (2019) have found extratropical volcanic eruptions to have a stronger cooling effect than tropical eruptions, citing previous models' tendencies to overestimate volcanic forcings. Their results are supported by current studies from Zhuo et al. (2021) using a fully coupled atmosphere–ocean model, MPI-ESM, which demonstrates stronger cooling in the extratropical hemispheres. These high latitude volcanic eruptions can affect atmospheric circulation, altering precipitation and temperature distribution patterns, lead to a long-term impact on regional climate variability and seasonality (Robock, 2000). For example, strong northern high-latitude volcanic (NHV) eruptions, such as the Laki eruption in 1978, are known to have weakened the Asian and African monsoons, contributing to severe famine in these regions (Oman et al., 2006).

Archeological research into mid-sixth century Scandinavia increasingly links the periods' significant settlement abandonment, reorganization, and material transformation with a brief and abrupt cooling event which followed an explosive volcanic event between 536 and 540 AD (Axboe, 2001; Gräslund, 2007; Gräslund and Price, 2012; Guillet et al., 2020; Gundersen, 1970; Herschend, 2009; Löwenborg, 2023; Price and Gräslund, 2015; Sigl et al., 2013; Toohey et al., 2016; van Dijk et al., 2023; Zachrisson, 2011). The connection to volcanism is established through historical research on known volcanic eruptions before 630 AD (e.g. Stothers and Rampino, 1983), with notable events taking place in 536 and 540 AD. Written accounts of the 536 AD events align with the optical features of stratospheric sulfate aerosol generated from volcanic eruptions (Arjava, 2005; Gräslund and Price, 2012; Robock, 2000). Furthermore, Toohey et al. (2016) argue that the double eruptions of 536 and 540 AD caused the largest decadal volcanic forcing in the last 2000 years, leading to over a decade of surface cooling. Recent ice core evidence has established the origin of the 536 AD volcanic eruption; Larsen et al. (2008) found two sulfate signals in Greenland ice cores around 536 AD separated by about 4 years. They associated the second sulfate peak, a possible tropical eruption, with the 540 AD event. With advances in climate reconstructions based on paleoecological proxies, there has been a growing interest in simulating the Northern Hemisphere climate during the 536/540 event for comparison against contemporaneous changes in the archeological record (Dull et al., 2019; Toohey et al., 2016; van Dijk et al., 2022, 2023).

Previous studies that have examined the impact of the volcanic event of 536 AD on Scandinavian climate and society from an archeological perspective generally cite negative effects (Arrhenius, 2013; Axboe, 1999; Baillie, 1999; Gräslund, 2007; Gräslund and Price, 2012; Gunn, 2000; Høiland-Nielsen, 2006; Keys, 2000; Solheim and Iversen, 2019). Gräslund (2007) proposed that a layer of dust dimmed the sky, leading to two or more years without summer known as the *Fimbulwinter* after an Old Norse myth, resulting in widespread crop failures in Scandinavia (Bellows, 2004). Dendrochronological analysis of Irish oak by Baillie (1994) also indicated reduced plant productivity in the mid-sixth century. Helama et al. (2018) and other researchers suggest that the cascading effects of deteriorating climate and reduced agricultural productivity had significant impacts on human health and led to famine, reducing societies' resilience to plague outbreaks like the Justinian plague during the same period (Büntgen et al., 2016, 2020; Iversen, 2016; Keller et al., 2019; Price and Gräslund, 2015; Sigl et al., 2015; Stothers, 1984, 1999; Tvaauri, 2013). However, these studies do not account for the spatiotemporal heterogeneity of climatic effects and societal response.

Regional setting

Our Swedish study areas include two biomes: (1) the inland boreal forest of Dalarna and (2) the temperate southern coastal area of Skåne and Blekinge (Figure 1). Dalarna experiences marked seasonal variation with cold winters and moderate summers. Its topography also varies from mountains in the west to flat plains in the east, interspersed with bogs and lakes providing milder microclimates (Holm, 2012). In contrast, southern Sweden has a temperate oceanic climate with mild winters, stronger winds, and less temperature variation along the coast (Persson et al., 2012). This region has relatively high rainfall, with peak levels in autumn. The landscape is generally flat, including coastal plains, hills, and low-lying areas, making it one of Scandinavia's most productive arable farming regions due to its mild climate and fertile soils (Skoglund, 2022).

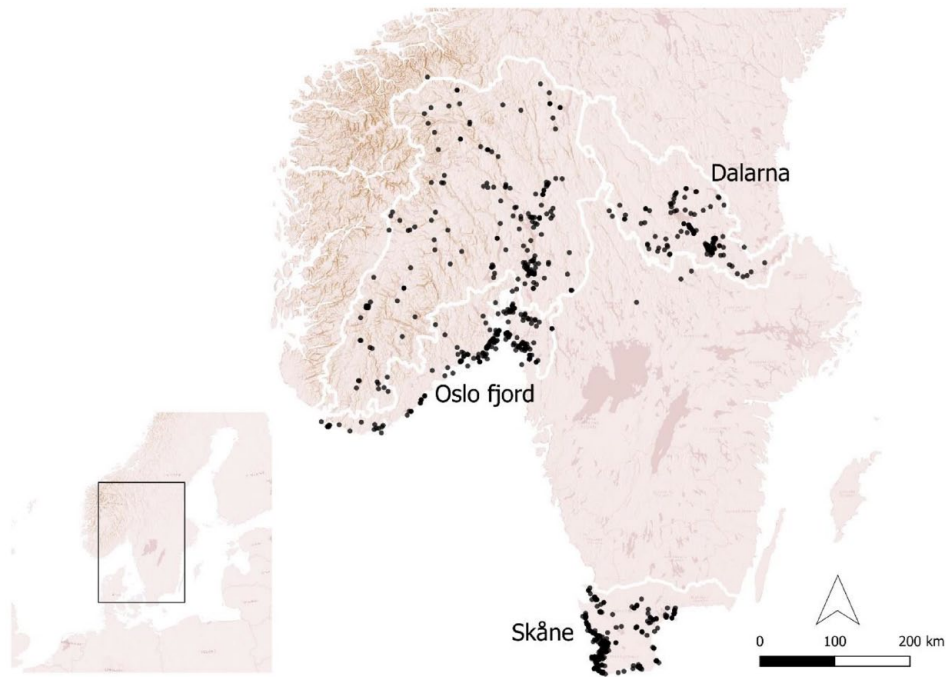


Figure 1. Map showing inland and coastal study regions (white outline) of Norway and Sweden, as well as locations for the 4016 radiocarbon dates (black points) used in this analysis.

Our research area in Norway spans latitudes 57.9°–62.3°N (Figure 1) and it is also divided into (1) inland, which includes highland/mountain regions, and (2) coastal areas. The division into “coastal” and “inland” regions is based on their distinct climates and topography. The coastal region experiences a humid climate with mild winters; the most fertile areas are found along the Oslo fjord and inland Lake Mjøsa. The inland experiences a rain shadow effect that limits rainfall and produces significant temperature fluctuations between seasons. The lower-lying parts of the inland consist of dense forests and bogs, while the elevated areas include alpine and sub-alpine regions. The inland provided valuable resources during the Iron Age for pastures, hunting, trapping, and iron production, while sufficient arable land was still essential for farming (Holm et al., 2005; Loftsgarden, 2019; Svensson, 1998).

Methods

The iLOVECLIM model

iLOVECLIM (hereafter version 1.1) (Quiquet et al., 2018) is a three-dimensional model classified under Earth system models of intermediate complexity, EMICs (Claussen et al., 2002), due to its simplified representation of the atmosphere relative to Global Circulation Models (GCMs). As a result of its efficient description of climate dynamics, iLOVECLIM is substantially faster than coupled GCMs. (Goosse et al., 2010; Kitover et al., 2015). iLOVECLIM is a code fork of the LOVECLIM 1.2 model (Goosse et al., 2010) and shares the main climate system components. The version applied in our study includes the atmospheric model ECBilt (Opsteegh et al., 1998), Coupled Large-scale Ice-Ocean model CLIO (Goosse and Fichefet, 1999), and the terrestrial vegetation and carbon allocation model VECODE (Brovkin et al., 1997). The reader is referred to the supplementary information for more details about the components of the model and how it has been used previously to simulate some past climate periods.

In this study, we utilized a dynamically downscaled version of the coupled iLOVECLIM model to enhance its spatial resolution for temperature and precipitation (Quiquet et al., 2018). This

downscaling procedure allowed for a higher spatial variability in simulating the Holocene climate in Europe, leading to better alignment with proxy-based reconstructions compared to the standard model (Arthur et al., 2023). For a more detailed explanation of the physics applied to the dynamical downscaling in the model, please refer to (Quiquet et al., 2018).

Set-up and simulations

We conducted ensemble experiments, both with and without volcanic forcings, using the iLOVECLIM-1.1 model (Quiquet et al., 2018) to simulate the evolution of the climate from 1 to 1000AD. We forced the simulations with orbital forcings to represent variations in eccentricity, obliquity, and precession (Berger, 1978) and atmospheric trace gas concentrations of CO₂, CH₄, and N₂O (Raynaud et al., 2000). Constant ice sheet configurations were prescribed for the experiments. Four different simulation groups were performed, referred to as VOLC_50, VOLC_1000, NOVOLC_50, and NOVOLC_1000, and each consisting of 10 ensemble members. For instance, VOLC_50 consists of 10 equilibrium experiments which were run for 50 years with the same forcings at 1AD, including volcanic eruptions but different initial conditions. Each initial condition of the simulation is derived from the previous ensemble run. The NOVOLC_50 simulation shares the same setup as VOLC_50 but excludes volcanic eruptions and uses different initial conditions. VOLC_50 and NOVOLC_50 were run to establish distinct climate states that serve as the initial conditions for our 10 ensemble transient simulations (VOLC_1000 and NOVOLC_1000). VOLC_1000 is a transient experiment with volcanic eruptions applied from 1 to 1000AD (1000-year run) using the same climate forcings for all 10 ensemble members but with different initial conditions derived from the VOLC_50 simulations (see Supplementary Information, Table S1, for specific volcanic forcings applied for 536/540AD). On the other hand, NOVOLC_1000 is a transient experiment without volcanic eruptions applied over the same period, with the same climate forcings for all 10 ensemble members but with different initial conditions derived from the NOVOLC_50 simulations.

To account for uncertainties associated with internal climate variability due to the chaotic nature of the climate system, we employed a 10-member ensemble simulation. Each member has identical atmospheric physics, dynamics, parameters, and forcings but starts with different initial conditions, resulting in diverse evolutions. The range covered by the 10 members provides an estimate of the internal variability. However, the ensemble mean represents the average response to the volcanic forcing, as the averaging over the ten members effectively mitigates the individual members' noise and reveals a common signal among them. We present the results of the volcanic eruption simulations as anomalies with respect to the experiment without volcanic eruptions. This approach highlights the impact of volcanism on the climate in our regions of interest.

Volcanic forcings

The volcanic forcing set named eVolv2k, used for the 536 and 540AD eruptions in VOLC_1000, is described in detail elsewhere (Jungclauss et al., 2017; Sigl et al., 2015; Toohey and Sigl, 2017). The eVolv2k database includes estimates of the magnitudes of the volcanic stratospheric sulfur injection (VSSI) events and their source of eruption (latitudes) from 500 BCE to 1900 CE, based on the measurements from the Antarctica and Greenland ice cores. In the iLOVECLIM model, the stratospheric sulfate loading is derived from ice core deposition using the model from Gao et al. (2008). The sulfate loadings are then converted into an equivalent total solar irradiance (TSI) anomaly through the aerosol optical depth (AOD) by a linear scaling (Mairesse, 2013), where volcanism is considered a negative anomaly of TSI (W/m^2) in the iLOVECLIM model (Mairesse, 2013).

In the model, volcanic forcing can be applied in four different latitudinal bands: extra-tropical and tropical bands, separately in both hemispheres. For this study, we focus on the double eruption of 536/540AD. The 536AD eruption is assigned to the Northern Hemisphere extra-tropical band, and the 540AD eruption to the tropical band in the model (Toohey and Sigl, 2017). The volcanic forcings for other periods in the simulations (1–1000AD without 536/540) are prescribed in the iLOVECLIM model from Goosse et al. (2010).

Spatial-temporal analysis of archeological radiocarbon (^{14}C) data

Using summed probability distributions (SPD) of radiocarbon dates to study large-scale demographic and environmental processes is an established method across various disciplines. It has evolved from the time-series analysis methods of researchers like Deacon (1974) and Geyh (1980), who used radiocarbon dates as proxies for demographic and environmental change, respectively (see Carleton and Groucutt (2021) for a history of the approach's development). Following these earlier research contributions, Rick's "Dates as Data" (Rick, 1987), emerged as a pivotal work, frequently referenced for using radiocarbon dating as proxies to explore temporal developments in human activity.

In the past three decades, significant advancements in calibration programs and computing technology have enhanced the utilization of SPDs of radiocarbon dates. However, longstanding debate about the reliability of the technique remains (Brown, 2015; Carleton and Groucutt, 2021; Williams, 2012). Critics contend that relying on a qualitative assessment or "eyeballing" of SPDs lacks statistical rigor and introduces subjective inferences (Crema, 2022). They argue that such approaches may mask systematic and random errors, including issues related to sample size, sampling intensity bias, taphonomic loss, calibration, and measurement error, potentially leading to misinterpretations (Crema, 2022). To address imperfect data in archeology and

palaeosciences, computational statistical analysis has emerged as a valuable approach to enhance the robustness of interpretations and conclusions drawn from radiocarbon date distributions (Crema, 2022; Shennan et al., 2013).

For our analyses, we employ a quantitative approach using the *rcarbon* package (version 1.5.0) from the R programming environment. This package offers a statistical framework for the aggregate analysis of ^{14}C data, accounting for systematic and random errors inherent in ^{14}C analysis through its provided functions (Crema and Bevan, 2021). We compared regional summed probability distributions (SPDs) against a logistical growth model as well as compared regional and categorized land use SPDs against one another (see Crema, 2022 for a detailed description). This approach, following methods from previous works (Brown and Crema, 2021; Crema et al., 2016, 2017; Riris and Arroyo-Kalin, 2019; Shennan et al., 2013; Timpson et al., 2014), requires first calibrating and binning ^{14}C samples based on temporal proximity ($h=50$; see Fig. S15 for sensitivity analysis). Binning attempts controls for sampling intensity bias (Crema, 2022). Next, we generated normalized SPDs from the observed data, and fit them to a logistical growth model and conducted mark permutation tests between our regions and land uses. Null hypothesis testing takes into account calibration effects by creating an expected range of SPDs, or a 95% critical envelope, through the Monte-Carlo method ($n_{sim}=1000$) that addresses sampling errors (Crema and Bevan, 2021).

Our spatial analysis, also utilized a permutation test, *sptest()*, from the *rcarbon* package, where spatial positions of sites are shuffled randomly, and departures from the permuted null are calculated with *p*-values and false discovery rates (*q*-values) to assess the significance of these departures (Brown and Crema, 2021; Crema et al., 2017; Crema and Bevan, 2021). Our spatial analysis was based on a bandwidth of 25 km, comparable to the resolution of the iLOVECLIM climate simulation.

Archeological radiocarbon ^{14}C datasets

Throughout our analysis, we reuse existing data and utilize open-source software, highlighting the significance of and advocating for FAIR data practices (e.g. Wilkinson et al., 2016). Through the diligent efforts of previous researchers, we gained access to rich ^{14}C databases in our study regions (see Acknowledgments) and reoriented our analyses to compare the effects of the volcanic event and the so-called *Fimbulwinter* on topographically and economically diverse regions of inland and coastal Sweden and Norway. This approach facilitates comparative analysis, shedding light on how environmental impacts may have influenced regional land use.

These datasets contain over 12,238 dated records spanning most of the Holocene. However, due to our study's specific focus on the 536/540 volcanic event, we restricted our examination to the first millennium AD, enabling the establishment of demographic and land use patterns in the region across three climatic transitions: (1) before the volcanic event, (2) during the *Fimbulwinter*, and (3) the subsequent climate recovery period. This filtering process resulted in a dataset of 4016 Scandinavian records (see Figure 1; Norway $n=1555$, Sweden $n=2461$, sites $n=1894$). With our substantial sample size and a focus on general trends, we have confidence that the impact of any individual source of error is minimal and does not significantly affect our research outcomes (Riris and Arroyo-Kalin, 2019; Shennan et al., 2013; Timpson et al., 2014).

Land use categorization

Our research aims to understand past human responses to environmental risks through not only the spatiotemporal analysis of

population trends, but also categories of land use. Our extensive ^{14}C datasets, we have been able to assign each ^{14}C record in our database to a general land use category that considers the context of artifacts, features, and site type associated with the sample. As land use activities vary greatly over time and space, our categorizations are intentionally broad and high-level and aim to represent cultural changes and adaptations to external factors. Grouping the data into inclusive categories helps reduce noise in the material and facilitates our exploration of general patterns in response to climatic events. Despite our extensive dataset, challenges arise due to the disproportionate representation of certain sites or structures in the records. For instance, remains from iron production in specific inland regions of Norway between AD 600 and 700 to 1350 and cooking pits, particularly abundant between AD 200 and 600, may skew the data due to their visibility and higher dating frequency (Gundersen et al., 2019; Larsen, 2009; Loftsgarden, 2020; Rundberget, 2013). The land use categories are adapted from Hatlestad et al. (2021) and are informed by the data discussion on cultural change in the categories and contextual associations are as follows:

- *Settlement*: Postholes, hearths, cooking pits, foundations, cellar pits, pit houses, longhouses, floor layers, remnant fields, urban plots, and ovens are examples of the features that were, when found in combination, interpreted as settlements in study area archeological site reports;
- *Iron production*: Bloomeries, charcoal production sites, slag, roasting features, forging pits, casting pits;
- *Agriculture*: cultivation terraces, clearance cairns, fences, enclosures, irrigation ditches, and flax processing sites as agriculture features;
- *Hunting*: pitfall traps, high altitude/melting glacier hunting finds
- *Other*: all other dates that did not meet the criteria for the above categories

Results

Climate results

Simulated ensemble mean temperature change during the volcanic period (536–541 AD) relative to the NOVOLC_1000 experiment show pronounced cooling in Scandinavia and the whole of Europe (Figure 2b), with a maximum ensemble mean cooling of -1.1°C reached after the eruption. The inland and coastal areas of Norway, Dalarna, and southern Sweden exhibit temperature change of up to -1°C relative to the simulation without volcanic forcing (Figure 2b). The ensemble mean represents the average response to the volcanic forcing, effectively canceling out the noise of the individual ensemble members; the “real” climate signal observed in proxy data reflects both internal variability and external forcings like volcanic eruptions. Consequently, the ensemble mean representing the forced response should not be the sole focus when comparing model results with proxy data.

Consistency between the model and data implies that the proxy signal should lie within the simulated climate range of the ensemble set, which includes both the forced response and internal variability (Goosse and Renssen, 2004). In this context, the climatic signal observed in proxies is similar to the results of a specific ensemble member. To assess the full range of climate responses, we consider two ensemble members (1 and 7) that exhibit relatively large climate change during the volcanic forcing. Figure 2d and f show temperature changes for the double eruption event relative to NOVOLC_1000 for ensemble members 1 and 7, respectively.

Ensemble member 1 indicates temperature decreased by more than -1.5°C during the eruption in most regions of Norway and Sweden. For ensemble member 7, temperature anomalies fall below -1.5°C , with inland Norway and central Sweden experiencing changes between -1°C and -1.5°C relative to NOVOLC_1000. In southern Norway and Sweden, temperature changes ranged from -0.25°C to -0.5°C for ensemble member 7 (Figure 2f).

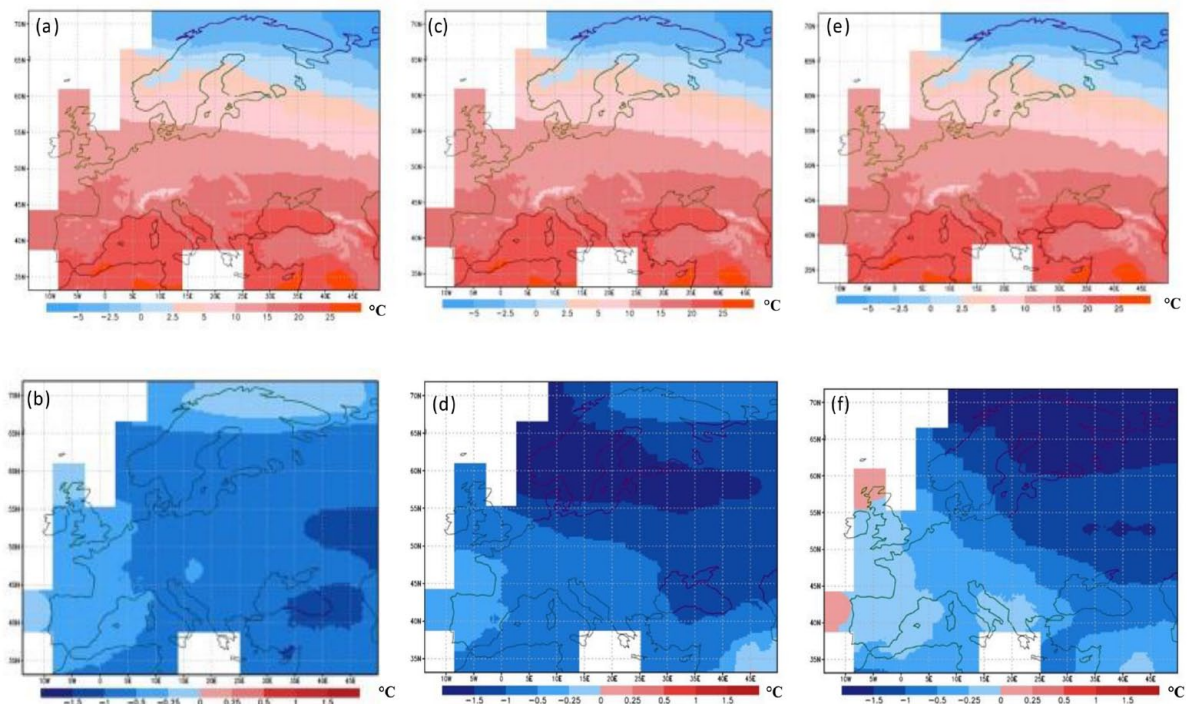


Figure 2. (a) Shows the ensemble mean temperature (all 10 ensemble members) simulated without volcanic eruption, averaged from 1 to 1000 AD as reference period; (b) Ensemble mean temperature change during the volcanic eruption (536–541 AD) relative to the ensemble mean temperature without volcanic eruption. While (c) and (e) show ensemble member 1 and 7 temperatures respectively without volcanic eruption, averaged from 1 to 1000 AD as reference period. (d) and (f) show ensemble member 1 and 7 temperature change respectively, during the volcanic eruption (536–541 AD) relative to ensemble member 1 and 7 simulated without volcanic eruption (i.e. the reference period).

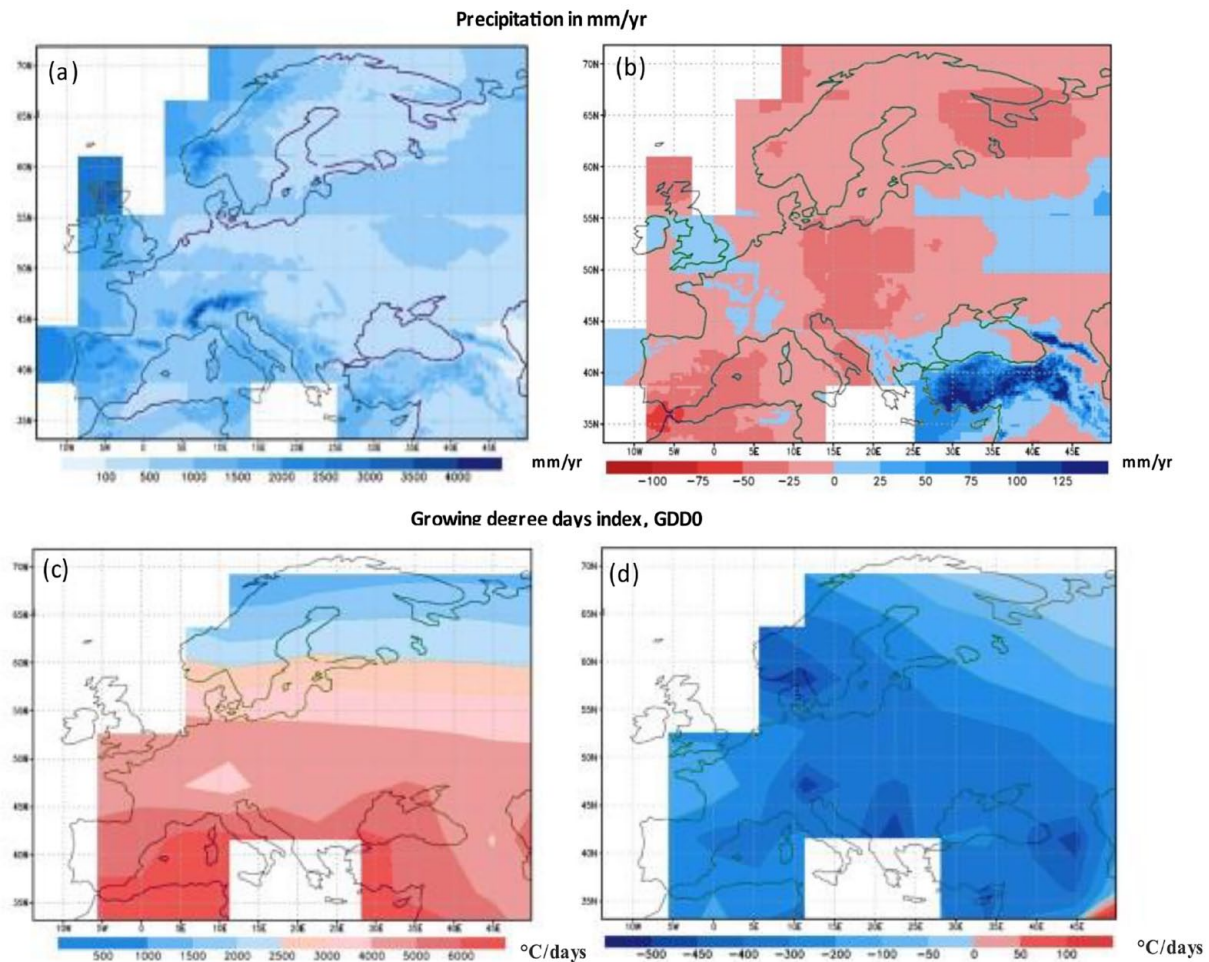


Figure 3. Showing (a) Ensemble mean precipitation simulated without volcanic eruption, averaged from 1 to 1000 AD (NOVOLC_1000) as reference period; (b) Ensemble mean precipitation change during the volcanic eruption (536–541 AD) relative to NOVOLC_1000; (c) Growing Degree Days index (GDD0) simulated without volcanic eruption, averaged from 1 to 600 AD and (d) Growing Degree Days index change during the eruption period (536–541 AD) relative to the GDD0 without volcanic eruption expressed as °C-days.

Precipitation also responded to the significant explosive volcanic eruption with a decrease in most European regions. Figure 3a shows the model ensemble mean spatial patterns of precipitation averaged from 1 to 1000 AD (without volcanic eruption), while Figure 3b shows the ensemble mean change averaged from the eruption period (536–541 AD) relative to Figure 3a. The ensemble model indicates a clear decrease in precipitation following volcanic eruptions, particularly in Scandinavia, where negative change of up to -25 mm/year are observed. Some areas in Norway have precipitation change ranging from -25 to -50 mm/year, indicating dryness post-eruption. This reduction in precipitation is attributed to a decrease in short-wave radiation reaching the surface due to the eruption (Figure S3: Supplemental information), which leads to reduced evaporation and atmospheric stabilization (Cao et al., 2012). Additionally, a cooler atmosphere undergoes less radiative cooling to space, allowing less condensation and precipitation (Allen and Ingram, 2002; O’Gorman et al., 2012).

Volcanic response in different regions

Figure 4 shows the temperature evolution in our selected study regions, including all 10 ensemble members and their ensemble mean for the model simulations from 500 to 600 AD with volcanic eruption. In Dalarna, the results indicate an immediate cooling at 537 and 541 AD after the eruption, with the mean ensemble temperature declining from 5.2°C to 4.5°C and 4.1°C , respectively,

following the eruption at 536. The model ensemble means change at 537 AD was -1.2°C and -1.6°C at 541 AD compared to the no volcanic ensemble mean for this inland Sweden region (Figure S2: Figure in Supplemental Material). The temperatures started to rise again after the eruption in 543 AD.

The southern Sweden (Coastal) study region (Figure 4) also shows a temperature decrease following a pattern similar to Dalarna but with different changes and recovery periods in response to the volcanic eruption. The volcanic signals are significant and clearly shown, with maximum cooling observed in the first (537 AD) and second year (541 AD) after the eruption, followed by a gradual rise after 543 AD for over 30 years.

We utilized a student *t*-test to establish the statistical significance of the volcanic eruption’s impact on the ensemble simulations. By comparing the change in temperature of the ensemble mean during the volcanic period (536–541 AD) to the average ensemble mean temperature without the volcanic eruption period (536–541 AD) for all study regions, we determined *p*-values. Southern Sweden showed *p*-values below 0.05 (Table S2, Supplemental Material), indicating a significant cooling at 95%. Norway and Dalarna had *p*-values below 0.1, indicating substantial cooling at 90%. This statistical test is crucial to validate the confidence in our results. Our test gives us confidence that the volcanic eruption during the 536–541 AD had an impact in the regions we studied in Scandinavia, showing that the change in temperature between the two experiments was due to the impact of the volcanic forcings prescribed in the simulations.

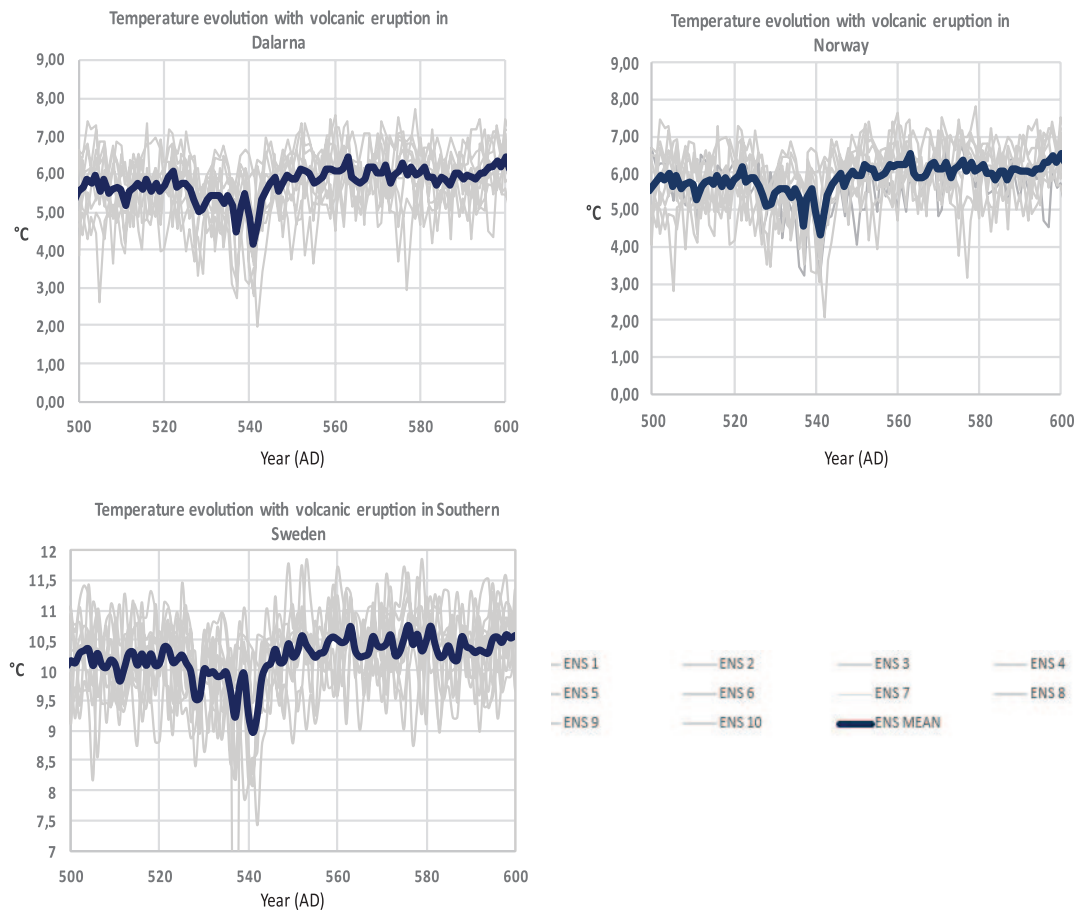


Figure 4. Time series of the temperature ensemble runs simulated by the climate model (iLOVECLIM) with volcanic eruption applied in our study regions (Dalarna, Norway, and South Sweden). All the 10 ensemble members are shown in gray with the ensemble mean in deep blue color.

Growing degree days (GDD0)

The simulated ensemble mean temperature changes are similar across the study areas after the 536 and 540 eruptions. However, the impact of climate variability on society and society's response depends on its effect on agriculture in different regions. To understand agricultural vulnerability, we analyzed changes in simulated growing degree days (GDD0), the sum of daily mean temperatures above a given threshold (in our case, 0°C) to provide GDD0 during the growing season.

The simulated GDD0 index changes during the eruption (relative to NOVOLC_1000) showed a substantial reduction in plant growing conditions in Scandinavia and the rest of Europe (Figure 3d). The GDD0 anomalies were between -400 and -500 degree days in the coastal regions of Norway and Sweden, while the GDD0 anomalies of Sweden and Norway's inland were between -200 and -400 degree days, which indicates a larger limiting impact on plant growing conditions on the coast than the inland.

Figure 5 displays localized Scandinavian temporal trends in the growing degree days index following the volcanic eruption. The results show southern Sweden experienced the most negligible impact on the growing season compared to the inland areas in Norway and Dalarna, with coastal Norway having the most drop in GDD0 during the eruption period.

The trends in GDD0 follow similar patterns in all regions, but the degree index and percentage change magnitude differ. In Dalarna, GDD0 decreased by approximately 27% during the eruption but later recovered (Figure 5). Before the eruption, in 535AD, GDD0 was around 2452°C-days but declined to 2138°C-days in 537AD, then 1818°C-days to 540AD, with its lowest level of 1794°C-days occurring in 542AD. However, the

GDD0 started rising again in 543AD, reaching a peak of 2803°C-days in 560AD (Figure 5). Norway experienced about 29% reduction in the length of the growing season after the eruption, with GDD0 declining from 2461°C-days (535AD) to 1752°C-days (542AD) (Figure 8). Southern Sweden also had a 20% reduction in growing degree days, decreasing from 3101 (535AD) to 2477°C-days (540AD). Coastal Norway showed the most significant reduction during the event, with a drop of almost 500°C-days, while the inland experienced a reduction of 400°C-days as shown in (Figure 3d).

Null model hypothesis testing of 14C datasets

The logistical growth model analysis of our data set as whole reveals a significant negative departure from the null occurring just after the 536/540AD event (Figure 6). The observed SPD's lack of fit within much of the 95% confidence envelope, coupled with a global p -value of 0.001, suggests an effect on demographic growth at this time. Similar significant negative deviations after the 536/540AD event are observed in coastal and inland Sweden. However, while growth in these regions falls below the null's expectations, the observed SPDs still reflect increasing growth. In both of Norway's regions, the observed SPD begins a downward trend close to the 536/540AD eruptions, but there is an approximate 10 to 20-year lag before a significant negative deviation from the null.

Mark permutation test

The initial permutation test results (Figure 7) reveal significant divergences in demographic patterns between Norway and

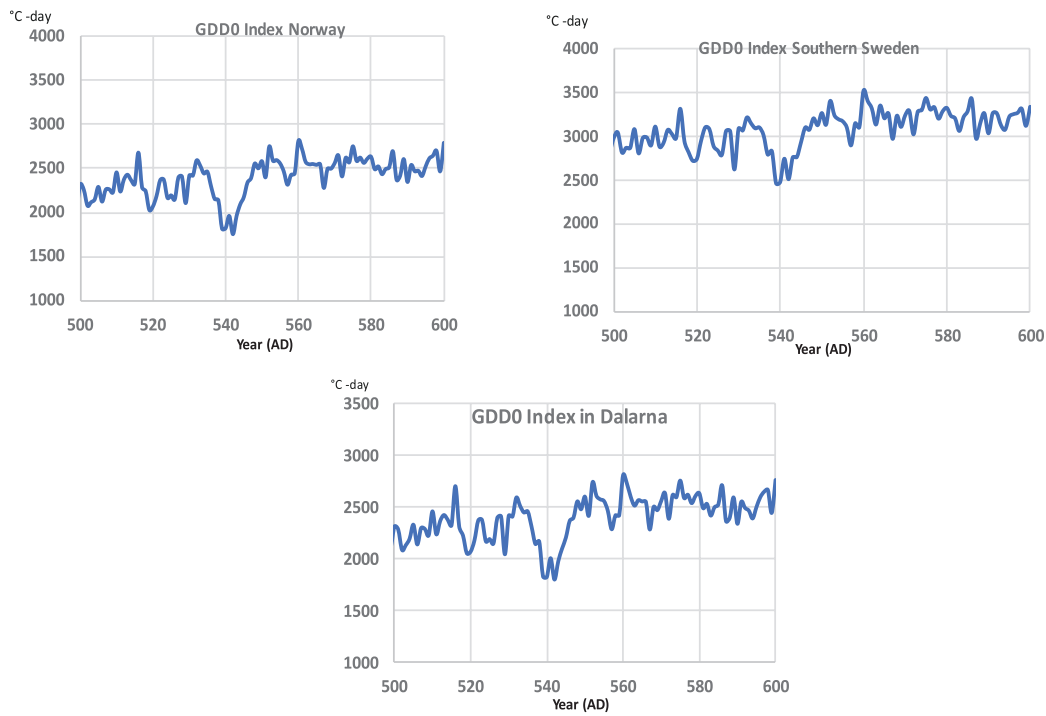


Figure 5. Time series of the Growing Degree Days index simulated with volcanic eruption applied in the iLOVECLIM model in our study regions (Dalarna, Norway, and Southern Sweden).

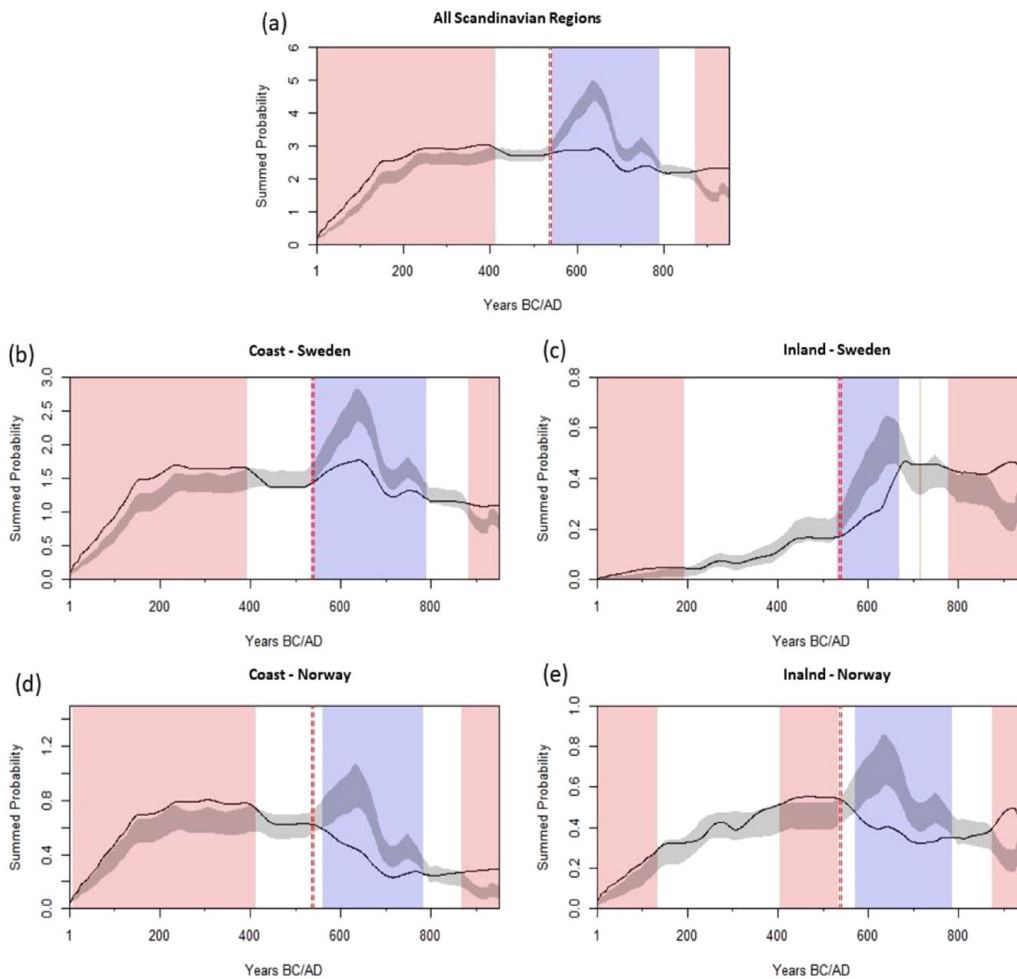


Figure 6. Logistical growth models for (a) all Scandinavian regions ($n_{\text{dates}} = 4016$, $n_{\text{sites}} = 1898$, $n_{\text{bins}} = 2583$, $p\text{-value} = 0.001$); (b) Coastal Sweden ($n_{\text{dates}} = 2093$, $n_{\text{sites}} = 755$, $n_{\text{bins}} = 1389$, $p\text{-value} = 0.001$); (c) Inland Sweden ($n_{\text{dates}} = 368$, $n_{\text{sites}} = 280$, $n_{\text{bins}} = 254$, $p\text{-value} = 0.001$); (d) Coastal Norway ($n_{\text{dates}} = 879$, $n_{\text{sites}} = 435$, $n_{\text{bins}} = 508$, $p\text{-value} = 0.001$); (e) Inland Norway ($n_{\text{dates}} = 676$, $n_{\text{sites}} = 428$, $n_{\text{bins}} = 432$, $p\text{-value} = 0.001$). Gray area represents the 95% confidence envelope of the fitted logistical growth model. Black line represents the observed SPD with red areas showing periods exceeding the expected growth and blue areas showing periods below the expected growth. The dashed red line represents the 536/540 AD event.

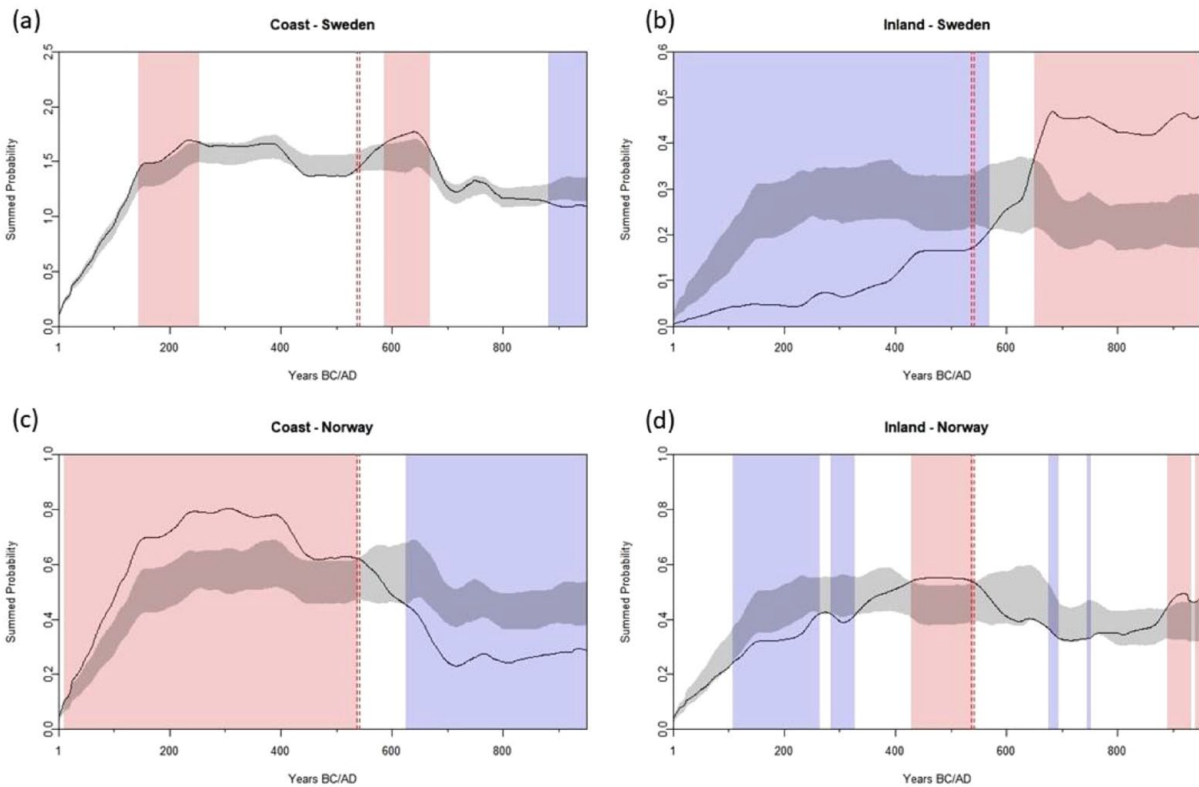


Figure 7. Permutation test comparing (a) Coastal Sweden ($n_{\text{dates}} = 2093$, $n_{\text{sites}} = 755$, $n_{\text{bins}} = 1389$, $p\text{-value} = 0.001$); (b) Inland Sweden ($n_{\text{dates}} = 368$, $n_{\text{sites}} = 280$, $n_{\text{bins}} = 254$, $p\text{-value} = 0.001$); (c) Coastal Norway ($n_{\text{dates}} = 879$, $n_{\text{sites}} = 435$, $n_{\text{bins}} = 508$, $p\text{-value} = 0.001$); (d) Inland Norway ($n_{\text{dates}} = 676$, $n_{\text{sites}} = 428$, $n_{\text{bins}} = 432$, $p\text{-value} = 0.001$). Gray area represents the 95% confidence envelope of the permutation null model (i.e. where the distribution is calculated from a rearrangement or permutation of the observed ^{14}C records). Black line represents the observed SPD with red areas showing periods exceeding the expected growth and blue areas showing periods below. The dashed red line represents the 536/540 AD event.

Sweden in the first millennium AD (Crema and Bevan, 2021). In Sweden's inland region ($p\text{-value} = 0.001$), significant deviations below the permuted null persist until shortly after the volcanic event. Following 536/540 AD, regional growth recovers, meeting the confidence envelope before exceeding expectations around 650 AD. Meanwhile, coastal Sweden's observed SPD ($p\text{-value} = 0.008$) closely adheres to the confidence envelope but trends upwards just before the *Fimbulwinter*, deviating positively from the null approximately 50 years after the event.

Conversely, Norway's regions positively deviate from the null leading up to the 536/540 eruptions, but then experience a decline. This reduction may have started before the volcanic event (Figure 7), raising the curiosity as to whether the eruption triggered a demographic and social restructuring or intensified an ongoing societal transformation. These results will be further discussing in the following discussion section.

Spatial permutation tests

Using the spatial permutation method provided by the *rcarbon* package, we analyzed the geographical intensity of population and land use activity in the Scandinavian region over two centuries (450–650 AD) (see SI and Crema et al., 2017 for an in-depth explanation of this approach; Brown and Crema, 2021; Crema et al., 2017). Our findings indicate an increased dependence on the inland regions of Sweden and Norway, a substantial decline in the Norwegian coastal area, a heterogeneous results for the southern coast of Sweden (Figure 8; Figure S5–S9, Supplemental Material).

The results for the Swedish inland align with our previous permutation analysis, showing a significant positive deviation after the *Fimbulwinter*. However, this spatial permutation test revealed

a Norwegian inland hotspot not detected in the earlier analysis, highlighting how region-specific nuances can be obscured with a solely temporal permutation approach (Figure 8a).

Across the 200-year time block, pronounced growth is observed in the inland regions and the southernmost tip of Sweden, while Norway's Oslo fjord coastal region shows decline (Figure 8). Southern Sweden's coast displays variation, with the northern portion experiencing a decline in growth and less fluctuation at the southernmost border. In the third transition, a geographic shift in land use intensity is evident, with an expansion southward in inland Norway and eastward in inland Sweden, possibly indicating recovery and a return to areas previously utilized before the *Fimbulwinter* (Figure 8b).

Land use tests

We analyzed regional land utilization to extend the investigation of the overarching demographic patterns, which had previously suggested an increased dependence on the boreal inland following the 536/540 AD event. Thus, we employed a spatial permutation test to examine specific spatial alterations in land use over a 200-year timeframe, which revealed notable changes in several land use categories (see Figure S5–S9, Supplemental Material).

During the three transitions, settlement activity deviated negatively, especially along the Norwegian coast (Figure S5a, Supplemental Material). However, southern Sweden exhibited only a slight decline in growth rates (Figure S5b) across transitions I–III, still surpassing the expectations of the null model (Figure S5a). Meanwhile, the inland region of Norway experienced pockets of considerable positive settlement growth, exceeding the expectations of the null model, whereas settlement in inland Sweden only trended positively in transition III.

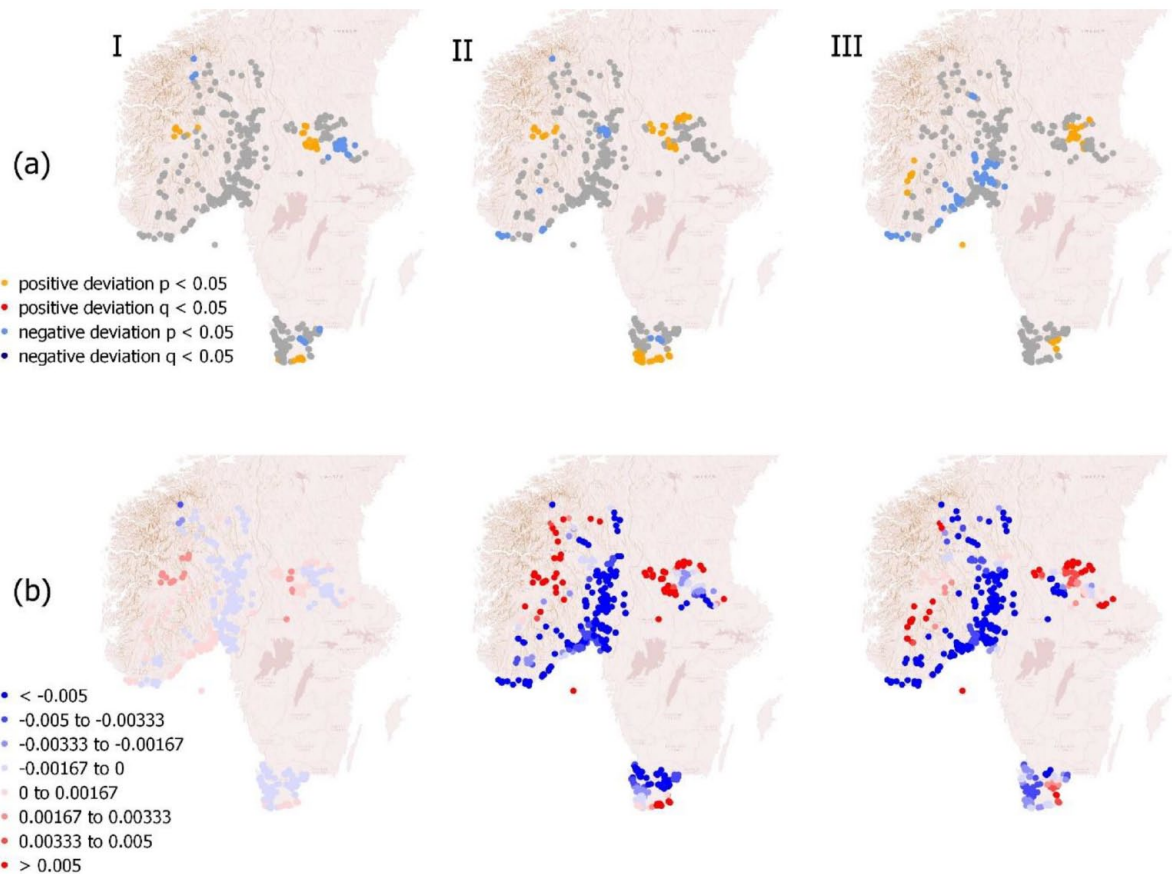


Figure 8. (a) r_{carbon} spstest () (i.e. spatial permutation test) for all radiocarbon dated sites in Scandinavian study regions across three transitions: (I) 450–500 to 500–550 AD, (II) 500–550 to 550–600 AD, (III) 550–600 to 650 AD, depicting “hot and cold” spots of growth with p -value and q -value deviations. (b) Local geometric growth rates across transitions I–III.

Limited ^{14}C records hindered a prominent agricultural signal, but local growth rates indicate increased activity around the Oslo fjord and inland Sweden in the first two transitions (Figure S7a). Transition III witnessed a decline in coastal growth rates and Sweden’s inland region exhibited heterogeneity (Figure S7b).

Similarly, our datasets contained limited hunting records for these periods, but hunting appeared more prevalent in the inland regions, with Norway’s hunting declining across transitions and Sweden’s increasing (Figure S8).

Iron production significantly grew in the inland areas of Norway and Sweden over the transitions (Figure S6b). Inland Norway presents as an iron production hotspot during the first two transitions, while Sweden’s iron production rising notably during transition II, or the *fimbulwinter* event period, and thereafter (Figure S6a). Moreover, as observed in the overall demographic activity, the same geographical shift eastward in inland Sweden is reflected in the third transition, or climate recovery period (Figure S6b).

Discussion

Summary of results

The iLOVECLIM climate simulations reveal distinct patterns of temperature, precipitation and GDD changes during the volcanic period, with variations observed between our coastal and inland regions. Temperature results show an overall regional decrease in mean ensemble (-1°C), yet the inland areas see a larger reduction in temperature, with ensemble 7 yielding a more regionally varied difference in temperature (-1°C to -1.5°C inland and -0.25°C to -0.5°C coastally) compared to the mean and ensemble 1 (-1.5°C). Precipitation results are generally homogenous between

regions, with negative changes of up to -25mm/year observed and a few areas in Norway with changes of up to -50mm/year . Simulations of GDD for regional coastal areas show changes between -400 and -500 degrees days, while the inland regions changes were between -200 and -400 degree days.

Our spatial-temporal analysis of ^{14}C archeological data also reveals distinct regional patterns in the demographic chronology and land use activities surrounding the 536/540 event. All regions negatively deviate from the logistical null either during or closely after the volcanic event. Notably, the Swedish regions’ observed SPDs trend positively around 536/540 AD, while Norway’s observed SPDs trend negatively. However, results from the mark permutation test somewhat alter these findings, as significant deviations in the demographics of coastal Norway and both inland regions end just before or around 536/540 AD (Figure 7b–d). Additionally, the coastal Sweden region shows significant deviations approximately 50 years after the event and then trends positively (Figure 7a). The spatial permutations findings indicate an increased spatial intensity occurring in the inland regions of Sweden and Norway, a substantial decline in the Norwegian coastal area, a heterogeneous results for the southern coast of Sweden during the modeled volcanic event period (500–550 to 550–600 AD) (Figures S5–S9).

Moreover, the land use mark permutation tests highlight regional variations occurring around Transition II (500–550 to 550–600 AD). Coastal Norway emerges as a cold spot for settlement, with specific local growth rates indicating declines in settlement and iron production, an uptick in agriculture, and a decline in the other category sites. Inland Norway maintains two small hotspots of settlement before, during, and after the volcanic event, with local growth rates increasing during transition II. Similarly, the region experiences positive trends in iron production

during Transition II. Coastal Sweden is a minor hotspot for settlement during Transition II, mixed cold and hotspots for agriculture and hunting, and declining sites in the “other” category. Inland Sweden also emerges as a minor hotspot for settlement, becoming an iron production hotspot after the volcanic event (550–600 to 600–650AD). However, local growth rates in this region indicate an increase in iron production, agriculture, hunting, and other activities during Transition II.

Regional societal response to the 536/540AD volcanic event

During the volcanic event, Norway’s coast experienced the largest decrease in GDD0 among all four regions, reaching –500-degree days (see Figure 3d). This decline in GDD0 can be attributed to a combination of temperature and precipitation factors, although individually, these variable changes were not as drastic as compared to other regions. The significant decrease in GDD0 suggests that crop growth and production were more severely affected in this region, particularly in the Oslo fjord area, which relied more heavily on domestic crops compared to the mixed farming inland areas (Bevan et al., 2017; Eriksson et al., 2021; see Figures 3d and 5, Figure S7). The GDD0 values can be compared to specific crops relevant to the study area (Table S2). Figure 5 indicates that the volcanic eruption may have limited wheat and buckwheat growth but not barley, which dominated crops in Norway and Sweden during the first millennium BC (Widgren and Pedersen, 2011). The ¹⁴C land use tests reveal a slight increasing trend in agriculture leading up to and during the 536/540AD event, followed by a decline during the climate recovery period, raising questions about the lag time between a climate event and societal change, and the significance of crop diversification as a coping strategy.

The trend in the archeological ¹⁴C results for Norway’s coast during the same period indicates general decreased spatial-temporal intensity in demography and land use, suggesting region’s specific environmental risks, such as its latitude and topography, may have pushed it past a critical threshold, contributing to unavoidable activity declines. However, our land use analysis of the region shows a reduction in the diversity of activities had begun prior to the *Fimbulwinter* period (Figures S10, S13), possibly affecting the region’s ability to quickly adapt to the 536/540AD event. Additionally, the evidence of prior land use change suggests that social influences, possibly the Migration period upheaval (400–800AD), were already affecting the region before 536/540AD. The volcanic event may have augmented this ongoing change (Eriksson et al., 2021; Gjerpe, 2017; Iversen, 2016; Loftsgarden and Solheim, 2023).

Norway’s inland, also experienced quite drastic declines in GDD0 (–400-degree days), temperature (–1 to –1.5°C) and precipitation (up to –50 mm/year). However, this region’s permutation results show hotspots of demographic intensity before, during and after the 536/540 event. ¹⁴C records of land use also present as more robustly diverse, both in intensity and in number, than its coastal counterpart prior to the volcanic event (Figure S10, S14). Specifically, there is an increase in iron production after the volcanic event and agricultural activity remains stable for a period. The trends observed imply that in challenging environments, where diverse economic strategies like iron production and agripastoral farming are necessary, trade continued to be a valuable adaptive response to uncertainties. These economic pursuits provided communities with added resilience, ensuring their ability to cope with sudden environmental adversities.

The iLOVECLIM model simulated similar climate effects of the volcanic event on coastal Sweden as coastal Norway, presenting decreasing temperatures (–0.25°C to –0.5°C), precipitation

(–25 mm/year) and GDD0 (–400-degree days). This implies a potential impact on agricultural productivity due to a shortened growing season, with increased frost days and higher likelihood of drought. Though similar climatic variability occurs here as on the Norwegian coast, demographic and land use trends present as generally stable and within expected critical envelope ranges (S10, S11) in the face of the volcanic event. Unlike the Norwegian coast, the land use intensity levels in coastal Sweden prior to the volcanic event were generally stable and, in some cases, even displayed positive trends. This finding reinforces the idea that stability is resilient and difficult to disrupt. It also highlights the importance of creating diverse resources and strategies to withstand and adapt to abrupt events effectively.

Inland Sweden experienced a relatively minimal climatological impact during the 536/540AD event, with decreases of approximately –200-degree days in GDD0, –1.2°C and –1.6°C in temperature, and –0.25 mm/year in precipitation compared to other regions. Despite this, the spatial-temporal analysis of inland Sweden’s ¹⁴C records shows some degree of growth across all five land-use categories in the aftermath of the volcanic eruption (Figures S10, S12). The region’s unique geographical location, possible favorable microclimates, diversified land uses, and the creation of new grazing space for livestock resulting from forest clearance for iron production likely preconditioned the area for success during the *Fimbulwinter* (Eriksson et al., 2021; Eriksson, 2023; Hatlestad et al., 2021; Löwenborg, 2023; Oinonen et al., 2020). Just like in inland Norway, the fact that iron production continued in inland Sweden after the *Fimbulwinter* indicates that trade remained a viable strategy for coping with environmental risk.

Uncertainties and future extensions

Most climate models confirm cooling effects following Northern Hemisphere volcanic eruptions, aligning with our dynamically downscaled iLOVECLIM model ensemble setup, which reveals surface cooling during the *fimbulwinter* in Scandinavia. Recent work by van Dijk et al. (2022) utilizing the Max Planck Institute Earth System Model and identical PMIP4 volcanic forcing as our study, demonstrates significant cooling in mean Northern Hemisphere surface climate for up to two decades post the major eruptions of 536, 540, 574, and 626AD. Earlier research on volcanic eruption effects within the last millennium, such as Timmreck et al. (2009) and Guillet et al. (2020), indicated a decade-long cooling period following exceptionally large eruptions. Notably, Earth System Model simulations around 536 and 540AD by Toohey et al. (2016), driven by volcanic forcings, displayed Northern Hemisphere mean temperature anomalies exceeding –2°C, implying substantial crop production reductions across Scandinavia. In agreement with the findings of Toohey et al. (2016), iLOVECLIM simulations also demonstrate a decrease in the GDD0 index across our study areas, lending support to the hypothesis linking the mid-sixth-century social crisis to the volcanic eruptions of 536 and 540AD.

Divergent ¹⁴C results observed in these studies may be influenced by other concurrent factors, such as famine and plague, which themselves may be a cascading result of sudden perturbations that destabilize the climate and further impact a society’s ability to cope (Bondeson and Bondesson, 2014; Harbeck et al., 2013; Iversen, 2016; Solheim and Iversen, 2019). This underscores the complexity of human-environment dynamics. Nevertheless, our comparative analysis provides strong evidence that mid-sixth century societal transformations in our study regions were influenced by the 536/540AD volcanic event.

Another issue is a lack of terrestrial hunting data for the Norwegian coast, which can be attributed to its marine geography, indicating a greater dependence on aquatic sources. Unfortunately, there are few archeological sites reflecting the exploitation

of marine resources. As a result, our understanding of land use diversification opportunities in this area may be skewed.

Consideration of lag time is crucial when comparing the climate and societal records. Changes in human societies do not often present in the archeological record immediately, resulting in a time delay before responses to environmental influences become evident. Several researchers have developed and employed methods to address this issue. The methods used include running significance tests on the correlation between climate events and differences in population development, to identify “trigger” events or measure temporal lags between population decline and change in environmental proxy age depth models (Donges et al., 2016; Siegmund, Siegmund and Donner, 2017; Heitz et al., 2021; Riris and de Souza, 2021; Kim et al., 2021; Kintigh and Ingram, 2018). By considering these lag time factors and employing rigorous statistical methods, researchers can gain a more nuanced understanding of the relationship between climate events and societal changes.

Conclusion

In this study, we conducted a spatial-temporal analysis of ^{14}C records from Sweden and Norway compared to the downscaled iLOVECLIM climate model. Our results revealed distinct regional capabilities in maintaining land-use systems during the climate variability of the *Fimbulwinter*. Our investigation concludes with the insights we have gained into our original research questions:

- (i) *What is the impact of the 536/540 volcanic event on Scandinavian society?* Our analysis of the simulated ensemble mean changes and the changes of Ensembles 1 and 7 during the volcanic event, in comparison to the NOVOLC_1000 simulations, revealed abrupt declines in temperature, precipitation, and GDD0 index across all regions during 536 and 540AD. However, our findings indicate that the impact of these changes varied across regions, with Norway experiencing more severe climatic changes after the event, while Sweden with milder climatic effects, showed fewer indications of societal decline during the same period.
- (ii) *Can we see evidence for a relationship between patterns of climate and ^{14}C records? Can we identify the volcanic event as a leading signal to change in the archeological record?* Again, we observed pronounced regional disparities in the correlation between the climate simulations and the archeological data. Specifically, while the climate deteriorated in Scandinavia as a whole following the volcanic event, we noted that land use and demography in Sweden remained relatively stable, and even increased in its inland, while the coast of Norway experienced a decline. However, we were not able to definitively identify the 536/540AD event as a “trigger” for these regions’ changes in demography and land use.
- (iii) *Did changes in land use or regional spatial intensity occur following the event? If so, what does that indicate about regional capacities to cope with abrupt climate risk?*

The spatial permutation tests performed on the ^{14}C samples allowed us to track regional trends before, during and after the volcanic eruptions. The results reveal that trade, mobility and land use diversification were adaptive societal responses to abrupt environmental risks.

The study enhances our comprehension of the multifaceted relationship between society and the environment and sheds light on the adaptive mechanisms of humans in response to environmental

stressors. The outcomes of our investigation emphasize the need for a region-specific approach when evaluating the impact of climate change on societal response. Furthermore, our results point to diversification and mobility as resilient societal adaptations.

Acknowledgements

We wish to thank our many colleagues for providing their insights, technical assistance and reviews throughout this process, notably Marco Hostettler and Eugene Costello. We are also grateful to Joakim Wehlin for sharing his ^{14}C database (originally published in Hatlestad et al., 2021) as well as Friman and Lagerås (2023) whose database we have accessed thanks to FAIR principles. And many thanks to our co-authors Kjetil Loftsgarden and Steiner Solheim for the reuse of their comprehensive Norwegian ^{14}C database.

Authors contribution

All authors designed the study. FA and KH performed the climate simulations and the archeological analysis and wrote the manuscript with contributions of HR, K-JL, KL, DL, SS, and DMR. The results were analyzed and interpreted by all authors.






Data and code availability

The iLOVECLIM source code is accessible at <https://www.elic.ucl.ac.be/modx/elic/index.php?id=289> (UCL, 2021). The developments on the iLOVECLIM source code are hosted at <https://forge.ipsl.jussieu.fr/ludus> (IPSL, 2021); due to copyright restrictions they cannot be publicly accessed. Request for access can be made by contacting Didier M. Roche (didier.roche@lscce.ipsl.fr). For this study, we used the model at revision 1147. S1 File. Supporting information and figures [DOCX]. S2 File. R Scripts and Data [ZIP].

Funding

The author(s) disclosed receipt of the following financial support for the research, authorship, and/or publication of this article: The research is financed through the European Union’s Horizon 2020 research and innovation program within the TERRANOVA project, no. 813904. The paper only reflects the views of the authors, and the European Union cannot be held responsible for any use which may be made of the information contained therein.

ORCID iDs

Frank Arthur  <https://orcid.org/0000-0002-9217-2058>
 Kailin Hatlestad  <https://orcid.org/0000-0003-4423-7379>
 Kjetil Loftsgarden  <https://orcid.org/0000-0002-0739-3084>
 Steinar Solheim  <https://orcid.org/0000-0001-8293-8147>
 Hans Renssen  <https://orcid.org/0000-0002-5104-0526>

Supplemental material

Supplemental material for this article is available online.

References

- Allen MR and Ingram WJ (2002) Constraints on future changes in climate and the hydrologic cycle. *Nature* 419(6903): 224–232. DOI: 10.1038/nature01092
- Arjava A (2005) The Mystery Cloud of 536 CE in the Mediterranean sources. *Dumbarton Oaks Papers* 59: 73.
- Arrhenius B (2013) Helgö in the shadow of the dust veil 536–37. *Journal of Ancient History and Archeology* 5: 1–15.
- Arthur F, Roche DM, Fyfe R et al. (2023) Simulations of the Holocene climate in Europe using an interactive downscaling within the ILOVECLIM model (version 1.1). *Climate of the Past* 19(1): 87–106.
- Axboe M (1999) The year 536 and the Scandinavian gold hoards. *Medieval Archaeology* 43: 186–188.

- Axboe M (2001) Amulet pendants and a darkened sun. On the function of the gold bracteates and a possible motivation for the large gold hoards. In: Magnus B (ed.) *Roman Gold and the Development of the Early Germanic Kingdoms*, vol. 51, pp.119–136.
- Baillie MGL (1994) Dendrochronology raises questions about the nature of the AD 536 dust-veil event. *Holocene* 4(2): 212–217.
- Baillie MGL (1999) *Exodus to Arthur: Catastrophic Encounters with Comets*. London: BT Batsford Ltd.
- Bellows HA (2004) *The Poetic Eddas: The Mythological Poems*. Mineola, NY: Dover Publishers.
- Berger A (1978) Long-term variations of daily insolation and quaternary climatic changes. *Journal of the Atmospheric Sciences* 35(12): 2362–2367.
- Bevan A, Colledge S, Fuller D et al. (2017) Holocene fluctuations in human population demonstrate repeated links to food production and climate. *Proceedings of the National Academy of Sciences* 114(49): E10524–E10531. DOI: 10.1073/pnas.1709190114
- Bondeson L and Bondesson T (2014) On the mystery cloud of AD 536, a crisis in dispute and epidemic ergotism: A linking hypothesis. *Danish Journal of Archaeology* 3(1): 61–67.
- Brovkin V, Ganopolski A and Svirezhev Y (1997) A continuous climate-vegetation classification for use in climate-biosphere studies. *Ecological Modelling* 101(2–3): 251–261.
- Brown AA and Crema ER (2021) Māori population growth in pre-contact New Zealand: Regional population dynamics inferred from summed probability distributions of radiocarbon dates. *Journal of Island and Coastal Archaeology* 16(2–4): 572–590.
- Brown WA (2015) Through a filter, darkly: Population size estimation, systematic error, and random error in radiocarbon-supported demographic temporal frequency analysis. *Journal of Archaeological Science* 53: 133–147.
- Büntgen U, Arseneault D, Boucher et al. (2020) Prominent role of volcanism in Common Era climate variability and human history. *Dendrochronologia* 64: 1125–7865.
- Büntgen U, Myglan VS, Ljungqvist FC et al. (2016) Cooling and societal change during the Late Antique Little Ice Age from 536 to around 660 AD. *Nature Geoscience* 9(3): 231–236.
- Cao L, Bala G and Caldeira K (2012) Climate response to changes in atmospheric carbon dioxide and solar irradiance on the time scale of days to weeks. *Environmental Research Letters* 7(3): 034015.
- Carleton WC and Groucutt HS (2021) Sum things are not what they seem: Problems with point-wise interpretations and quantitative analyses of proxies based on aggregated radiocarbon dates. *Holocene* 31(4): 630–643.
- Claussen M, Mysak LA, Weaver AJ et al. (2002) Earth system models of intermediate complexity: Closing the gap in the spectrum of climate system models. *Climate Dynamics* 18(7): 579–586.
- Crema ER (2022) Statistical inference of prehistoric demography from frequency distributions of radiocarbon dates: A review and a guide for the perplexed. *Journal of Archaeological Method and Theory* 29: 1387–1418.
- Crema ER and Bevan A (2021) Inference from large sets of radiocarbon dates: Software and methods. *Radiocarbon* 63(1): 23–39.
- Crema ER, Bevan A and Shennan S (2017) Spatio-temporal approaches to archaeological radiocarbon dates. *Journal of Archaeological Science* 87: 1–9.
- Crema ER, Habu J, Kobayashi K et al. (2016) Summed probability distribution of ¹⁴C dates suggests regional divergences in the population dynamics of the Jomon period in eastern Japan. *PLoS One* 11(4): e0154809.
- Deacon J (1974) Patterning in the radiocarbon dates for the Wilton/Smithfield Complex in Southern Africa. *South African Archaeological Bulletin* 29(113/114): 3.
- Donges JF, Schleussner C-F, Siegmund JF et al. (2016) ‘Event coincidence analysis for quantifying statistical interrelationships between event time series: On the role of flood events as triggers of epidemic outbreaks’. *European Physical Journal: Special Topics* 225(3): 471–487.
- Dull RA, Southon JR, Kutterolf S et al. (2019) Radiocarbon and geologic evidence reveal Ilopango volcano as source of the colossal ‘mystery’ eruption of 539/40 CE. *Quaternary Science Reviews* 222: 105855.
- Eriksson O (2023) Domesticated forest landscapes in Central Scandinavia during the Iron Age: Resource colonization for iron and subsistence strategies based on livestock. *Journal of Field Archaeology* 48(4): 315–326.
- Eriksson O, Arnell M and Lindholm KJ (2021) ‘Historical ecology of Scandinavian infield systems’. *Sustainability (Switzerland)* 13(2). DOI: 10.3390/su13020817
- Friman B and Lagerås P (2023) From Neolithic Boom-and-Bust to Iron Age Peak and decline: Population and settlement dynamics in southern Sweden inferred from summed radiocarbon dates. *European Journal of Archaeology* 26(2): 168–188.
- Gao C, Robock A and Ammann C (2008) Volcanic forcing of climate over the past 1500 years: An improved ice core-based index for climate models. *Journal of Geophysical Research* 113(D23). DOI: 10.1029/2008jd010239
- Geyh MA (1980) Holocene sea-level history: Case study of the statistical evaluation of ¹⁴C dates. *Radiocarbon* 22(3): 695–704.
- Gjerpe LE (2017) *Effektive hus. Bosetning, jord og rettigheter på Østlandet i jernalder*. PhD thesis, University of Oslo, Oslo.
- Goosse H, Brovkin V, Fichefet T et al. (2010) Description of the earth system model of intermediate complexity LOVECLIM version 1.2. *Geoscientific Model Development* 3(2): 603–633.
- Goosse H and Fichefet T (1999) Importance of ice-ocean interactions for the global ocean circulation: A model study. *Journal of Geophysical Research Oceans* 104(C10): 23337–23355.
- Goosse H and Renssen H (2004) Exciting natural modes of variability by solar and volcanic forcing: Idealized and realistic experiments. *Climate Dynamics* 23(2): 153–163.
- Gräslund B (2007) Fimbulvintern, Ragnarök och klimatkrisen år 536-537 e. Kr. *Saga och sed: Kungl. Gustav Adolfs akademis årsbok* 93–123.
- Gräslund B and Price N (2012) Twilight of the gods? The ‘dust veil event’ of AD 536 in critical perspective. *Antiquity* 86(332): 428–443.
- Guillet S, Corona C, Ludlow F et al. (2020) Climatic and societal impacts of a “forgotten” cluster of volcanic eruptions in 1108–1110 CE. *Scientific Reports* 10(1): 6715.
- Gundersen I, Mørkestøl CL, Rødsrud J et al. (2019) Kokegroper som massemateriale. Regional variasjon i en kulturhistorisk brytningstid. Christian Løchsen Rødsrud og Axel Mjærum (red.): Ingen vei utenom – Arkeologiske undersøkelser i forbindelse med etablering av ny rv.3/25 i Løten og Elverum kommuner, Innlandet. *Viking* 85(1): 187–199. DOI: 10.5617/viking.9093
- Gundersen IM (1970) The Fimbulwinter theory and the 6th century crisis in the light of Norwegian archaeology: Towards a human-environmental approach. *Primitive Tider* (21): 101–120. DOI: 10.5617/pt.7538
- Gunn JD (ed.) (2000) *AD 536 and Its 300-Year Aftermath - the Years Without Summer: Tracing AD 536 and Its Aftermath*. (BAR, International Series 872). Oxford, pp.5–20.
- Harbeck M, Seifert L, Hänsch S et al. (2013) ‘Yersinia pestis’ DNA from skeletal remains from the 6th century AD reveals insights into Justinianic plague’. *PLoS Pathogens* 9(5): e1003349.
- Hatlestad K, Wehlin J and Lindholm K-J (2021) Coping with risk. A deep-time perspective on societal responses to ecological

- uncertainty in the river Dalälven catchment area in Sweden. *Land* 10(8): 883.
- Hegerl GC, Crowley TJ, Hyde WT et al. (2006) Climate sensitivity constrained by temperature reconstructions over the past seven centuries. *Nature* 440(7087): 1029–1032.
- Heitz C, Laabs J, Hinz M et al. (2021) Collapse and Resilience in Prehistoric Archaeology: Questioning Concepts and Causalities in Models of Climate-Induced Societal Transformations. In: Erdkamp P, Manning JG and Verboven K (eds) *Climate Change and Ancient Societies in Europe and the Near East. Palgrave Studies in Ancient Economies*. Cham: Palgrave Macmillan, pp.127–199.
- Helama S, Arppe L, Uusitalo J et al. (2018) Volcanic dust veils from sixth century tree-ring isotopes linked to reduced irradiance, primary production and human health. *Scientific Reports* 8(1): 1339.
- Herschend F (2009) *The Early Iron Age in South Scandinavia: Social Order in Settlement and Landscape*. Uppsala: Department of Archaeology and Ancient History, Uppsala University.
- Holm I, Innselset SM and Øye I (eds) (2005) *Utmark: he Outfield as Industry and Ideology in the Iron Age and the Middle Ages*. Bergen: UBAS. University of Bergen Archaeological Series International. Available at: <http://opac.regesta-imperii.de/id/1024317> (accessed 20 July 2023).
- Holm O (2012) *Självägarområdenas egenart: Jämtland och andra områden i Skandinavien med småskaligt jordägande 900-1500*. Diss. Stockholm: Stockholm University.
- Høiland-Nielsen K (2006) "Abundant gold and bad harvests: changes in southern Scandinavian society during the 5th to 7th centuries". In: Mindaugas B (ed.) *Transformatio mundi: The Transition from the Late Migration Period to the Early Viking Age in the East Baltic*. Kaunas: Lithuania Kaunas University, pp.41–50.
- Iversen F (2016) Estate Division: Social Cohesion in the aftermath of AD 536-7. In: Iversen FRODE and Petersson H (eds) *The Agrarian Life of the North 2000 BC-AD 1000. Studies in Rural Settlement and Farming in Norway. Portal*. Kristiansand: Portal Academic, pp.41–75.
- Jones GS, Gregory JM, Stott PA et al. (2005) An AOGCM simulation of the climate response to a volcanic super-eruption. *Climate Dynamics* 25(7-8): 725–738.
- Jungclaus JH, Bard E, Baroni M et al. (2017) The PMIP4 contribution to CMIP6 – Part 3: The last millennium, scientific objective, and experimental design for the PMIP4 *past1000* simulations. *Geoscientific Model Development* 10(11): 4005–4033.
- Keller M, Spyrou MA, Scheib CL et al. (2019) Ancient Yersinia pestis genomes from across Western Europe reveal early diversification during the first pandemic (541–750). *Proceedings of the National Academy of Sciences* 116(25): 12363–12372.
- Keys D (2000) *Catastrophe: A Quest for the Origins of the Modern World*. New York: Ballantine Pub.
- Kim H, Lee GA and Crema ER (2021) Bayesian analyses question the role of climate in Chulmun demography. *Scientific Reports* 11(1): 23797–23810.
- Kintigh KW and Ingram SE (2018) Was the drought really responsible? Assessing statistical relationships between climate extremes and cultural transitions. *Journal of Archaeological Science* 89: 25–31.
- Kitover DC, van Balen R, Roche DM et al. (2015) Advancement toward coupling of the VAMPER permafrost model within the Earth system model iLOVECLIM (version 1.0): Description and validation. *Geoscientific Model Development* 8(5): 1445–1460.
- Larsen JH (2009) *Jernvinneundersøkelser*. Seksjonen. Available at: https://urn.nb.no/URN:NBN:no-nb_digibok_2012071705208.
- Larsen LB, Vinther BM, Briffa KR et al. (2008) New ice core evidence for a volcanic cause of the A.D. 536 dust veil. *Geophysical Research Letters* 35. DOI: 10.1029/2007GL032450
- Loftsgarden K (2019) The Prime Movers of iron production in the Norwegian Viking and Middle Ages. *Fornvannen-Journal of Swedish Antiquarian Research* 114(2): 75–87.
- Loftsgarden K (2020) Mass production and mountain market-places in Norway in the Viking and Middle Ages. *Medieval Archaeology* 64(1): 94–115.
- Loftsgarden K and Solheim S (2023) Uncovering population dynamics in Southeast Norway from 99 1300 BC to AD 800 using summed radiocarbon probability distributions. In: Ødegaard M and Ystgaard I (eds) *Complexity and Dynamics. Settlement and Landscape From the Bronze Age to the Renaissance in the Nordic Countries (1700 BC–AD 1600)*. Leiden: Sidestone Press, pp.99–112.
- Löwenborg D (2023) An Iron Age shock doctrine. *Journal of Ancient History and Archeology* (4): 1–29. DOI: 10.33063/jaah.vi4.120
- Mairese A (2013) *Analysis of the Holocene climate variability using a data assimilation method in the model LOVECLIM*. Dissertation, Université catholique de Louvain. <http://hdl.handle.net/2078.1/154845>
- Masson-Delmotte V, Schulz M, Abe-Ouchi A et al. (2013) Information from Paleoclimate archives. In: Stocker TF, Qin D, Plattner G-K et al. (eds) *Climate Change (2013): The Physical Science Basis: Contribution of Working Group I to the Fifth Assessment Report of the Intergovernmental Panel on Climate Change*. Cambridge: Cambridge University Press, pp.383–464.
- McGregor S and Timmermann A (2011) The effect of explosive tropical volcanism on ENSO. *Journal of Climate* 24(8): 2178–2191.
- Oinonen M, Alenius T, Arppe L et al. (2020) Buried in water, burdened by nature—Resilience carried the iron Age people through Fimbulvinter. *Plos One* 15(4): e0231787.
- Oman L, Robock A, Stenchikov GL et al. (2006) High-latitude eruptions cast shadow over the African monsoon and the flow of the Nile. *Geophysical Research Letters* 33(18): L18711. DOI: 10.1029/2006gl027665
- Opsteegh JD, Haarsma RJ, Selten FM et al. (1998) ECBILT: A dynamic alternative to mixed boundary conditions in ocean models. *Tellus A* 50(3): 348.
- O’Gorman PA, Allan RP, Byrne MP et al. (2012) Energetic constraints on precipitation under climate change. *Surveys in Geophysics* 33(3–4): 585–608.
- Persson G, Sjöqvist E, Åström S et al. (2012) *Klimatanalys för Skåne län*. SMHI rapport Nr 2011-52.
- Pfister C (2010) The vulnerability of past societies to climatic variation: A new focus for historical climatology in the twenty-first century. *Climatic Change* 100(1): 25–31.
- Price N and Gräslund B (2015) Excavating the Fimbulvinter? Archaeology, geomorphology and the climate event(s) of AD 536. In: Riede F (ed.) *Past Vulnerability, Volcanic Eruptions and Human Vulnerability in Traditional Societies Past and Present*. Aarhus: Aarhus University Press, pp.109–320.
- Quiquet A, Roche DM, Dumas C et al. (2018) Online dynamical downscaling of temperature and precipitation within the iLOVECLIM model (version 1.1). *Geoscientific Model Development* 11(1): 453–466.
- Raynaud D, Barnola J-M, Chappellaz J et al. (2000) The ice record of greenhouse gases: A view in the context of future changes. *Quaternary Science Reviews* 19(1-5): 9–17.
- Rick JW (1987) Dates as data: An examination of the Peruvian preceramic radiocarbon record. *American Antiquity* 52(1): 55.
- Riris P and Arroyo-Kalin M (2019) Widespread population decline in South America correlates with mid-Holocene climate change. *Scientific Reports* 9(1): 6850.

- Riris P and de Souza JG (2021) 'Formal Tests for *Resistance-Resilience in Archaeological Time Series*'. *Frontiers in Ecology and Evolution* 9(December): 1–16. DOI: 10.3389/fevo.2021.740629
- Robock A (2000) Volcanic eruptions and climate. *Reviews of Geophysics* 38(2): 191–219.
- Rundberget B (2013) *Jernets dunkle dimensjon: jernvinna i sørlige Hedmark, sentral økonomisk faktor og premiss for samfunnsutvikling c. AD700–1300*. PhD dissertation, Oslo University, Oslo.
- Schmidt GA, Shindell DT, Miller RL et al. (2004) General circulation modelling of Holocene climate variability. *Quaternary Science Reviews* 23(20–22): 2167–2181.
- Schneider DP, Ammann CM, Otto-Bliesner BL et al. (2009) Climate response to large, high-latitude and low-latitude volcanic eruptions in the community climate system model. *Journal of Geophysical Research* 114(D15). DOI: 10.1029/2008jd011222
- Schurer AP, Tett SFB and Hegerl GC (2014) Small influence of solar variability on climate over the past Millennium. *Nature Geoscience* 7(2): 104–108.
- Shennan S, Downey SS, Timpson A et al. (2013) Regional population collapse followed initial agriculture booms in mid-Holocene Europe. *Nature Communications* 4: 31–34.
- Siegmund JF, Siegmund N and Donner RV (2017) 'CoinCalc—A new R package for quantifying simultaneities of event series'. *Computers and Geosciences* 98: 64–72. DOI:10.1016/j.cageo.2016.10.004
- Sigl M, McConnell JR, Layman L et al. (2013) A new bipolar ice core record of volcanism from Wais Divide and neem and implications for climate forcing of the last 2000 years. *Journal of Geophysical Research Atmospheres* 118(3): 1151–1169.
- Sigl M, Winstrup M, McConnell JR et al. (2015) Timing and climate forcing of volcanic eruptions for the past 2,500 years. *Nature* 523(7562): 543–549.
- Skoglund MK (2022) Climate variability and grain production in Scania, 1702–1911. *Climate of the Past* 18(3): 405–433.
- Solheim S and Iversen F (2019) The mid-6th century crises and their impacts on human activity and settlements in south-eastern Norway. In: Brady N and Theune C (eds) *Settlement change Across Medieval Europe: Old paradigms and new vistas*. Leiden: Sidestone Press, pp.423–434
- Stothers R (1999) Volcanic dry fogs, climate cooling, and plague pandemics in Europe and the Middle East. *Climatic Change* 42(4): 713–723.
- Stothers RB (1984) Mystery cloud of AD 536. *Nature* 307(5949): 344–345.
- Stothers RB and Rampino MR (1983) Historic volcanism, European dry fogs, and Greenland acid precipitation, 1500 B.C. to A.D. 1500. *Science* 222(4622): 411–413.
- Svensson E (1998) Människor i utmark. *Lund Studies in Medieval Archaeology* 21: 221–231.
- Timmreck C (2012) Modeling the climatic effects of large explosive volcanic eruptions. *WIREs Climate Change* 3(6): 545–564.
- Timmreck C, Graf H, Lorenz SJ et al. (2010) Aerosol size confines climate response to volcanic super-eruptions. *Geophysical Research Letters* 37(24): L24705. DOI: 10.1029/2010gl045464
- Timmreck C, Lorenz SJ, Crowley TJ et al. (2009) Limited temperature response to the very large AD 1258 volcanic eruption. *Geophysical Research Letters* 36: L21708. DOI: 10.1029/2009gl040083
- Timpson A, Colledge S, Crema E et al. (2014) Reconstructing regional population fluctuations in the European Neolithic using radiocarbon dates: A new case-study using an improved method. *Journal of Archaeological Science* 52: 549–557.
- Toohey M, Krüger K, Schmidt H et al. (2019) Disproportionately strong climate forcing from extratropical explosive volcanic eruptions. *Nature Geoscience* 12(2): 100–107.
- Toohey M, Krüger K, Sigl M et al. (2016) Climatic and societal impacts of a volcanic double event at the dawn of the Middle Ages. *Climatic Change* 136(3–4): 401–412.
- Toohey M, Krüger K and Timmreck C (2013) Volcanic sulfate deposition to Greenland and Antarctica: A modeling sensitivity study. *Journal of Geophysical Research Atmospheres* 118(10): 4788–4800.
- Toohey M and Sigl M (2017) Volcanic stratospheric sulfur injections and aerosol optical depth from 500 BCE to 1900 CE. *Earth System Science Data* 9(2): 809–831.
- Tvauri A (2013) The impact of the Climate Catastrophe of 536–537 AD in Estonia and neighbouring areas. *Estonian Journal of Archaeology* 18(1): 30.
- van Dijk E, Jungclaus J, Lorenz S et al. (2022) Was there a volcanic-induced long-lasting cooling over the northern hemisphere in the mid-6th–7th century? *Climate of the Past* 18(7): 1601–1623.
- van Dijk E, Mørkestø I, Gundersen I, de Bode A et al. (2023) Climatic and societal impacts in Scandinavia following the 536 and 540 CE volcanic double event. *Climate of the Past* 19(2): 357–398.
- Widgren M and Pedersen EA (2011) Agriculture in Sweden: 800 BC–1000 ad. In: Janken M and Orell MM (eds) *The Agrarian History of Sweden: From 4000 BC to AD*. Lund: Nordic Academic Press, pp.46–71.
- Wilkinson MD, Dumontier M, Aalbersberg IJ et al. (2016) The FAIR guiding principles for scientific data management and stewardship. *Scientific Data* 3(1): 160018. DOI: 10.1038/sdata.2016.18
- Williams AN (2012) The use of summed radiocarbon probability distributions in archaeology: A review of methods. *Journal of Archaeological Science* 39(3): 578–589.
- Zachrisson T (2011) Property and honour - social change in Central Sweden, 200–700 AD mirrored in the area around Old Uppsala. In: *Det 61. Internationale Sachsensymposium 2010*, Haderslev, pp.141–156. Available at: <http://opac.regesta-imperii.de/id/1935636>.
- Zhuo Z, Kirchner I, Pfahl S et al. (2021) Climate impact of volcanic eruptions: The sensitivity to eruption season and latitude in MPI-ESM ensemble experiments. *Atmospheric Chemistry and Physics* 21(17): 13425–13442.

Paper 4

Zapolska, A., Vrac, M., Quiquet, A., Extier, T., **Arthur, F.**, Renssen, H., & Roche, D. M. (2023). Improving biome and climate modelling for a set of past climate conditions: evaluating bias correction using the CDF-t approach. *Environmental Research: Climate*, 2(2), 025004. <https://doi.org/10.1088/2752-5295/accbe2>

PAPER • OPEN ACCESS

Improving biome and climate modelling for a set of past climate conditions: evaluating bias correction using the CDF-t approach

To cite this article: Anhelina Zapolska *et al* 2023 *Environ. Res.: Climate* **2** 025004

View the [article online](#) for updates and enhancements.

You may also like

- [A novel energy-motion model for continuous sEMG decoding: from muscle energy to motor pattern](#)
Gang Liu, Lu Wang and Jing Wang
- [Head and neck tumor segmentation convolutional neural network robust to missing PET/CT modalities using channel dropout](#)
Lin-mei Zhao, Helen Zhang, Daniel D Kim et al.
- [Prediction of cortical responses to simultaneous electrical stimulation of the retina](#)
Kerry J Halupka, Mohit N Shivdasani, Shaun L Cloherty et al.

ENVIRONMENTAL RESEARCH CLIMATE



PAPER

OPEN ACCESS

RECEIVED
4 July 2022

REVISED
29 March 2023

ACCEPTED FOR PUBLICATION
11 April 2023








PUBLISHED
25 April 2023

Original content from
this work may be used
under the terms of the
Creative Commons
Attribution 4.0 licence.

Any further distribution
of this work must
maintain attribution to
the author(s) and the title
of the work, journal
citation and DOI.



Improving biome and climate modelling for a set of past climate conditions: evaluating bias correction using the CDF-t approach

Anhelina Zapolska^{1,*} , Mathieu Vrac² , Aurélien Quiquet^{2,3} , Thomas Extier⁴ , Frank Arthur⁵ ,
Hans Renssen⁵  and Didier M Roche^{1,2} 

¹ Earth and Climate Cluster, Faculty of Science, Vrije Universiteit Amsterdam, Amsterdam, The Netherlands

² Laboratoire des Sciences du Climat et de l'Environnement, LSCE/IPSL, CEA-CNRS-UVSQ, Université Paris-Saclay, Gif-sur-Yvette, France

³ University Grenoble Alpes, CNRS, IRD, Grenoble INP, IGE, 38000 Grenoble, France

⁴ University Bordeaux, CNRS, Bordeaux INP, EPOC, UMR 5805, F-33600 Pessac, France

⁵ Department of Natural Sciences and Environmental Health, University of South-Eastern Norway, Bø, Norway

* Author to whom any correspondence should be addressed.

E-mail: zapolskaanhelina@gmail.com

Keywords: bias correction, palaeoclimate modelling, climate downscaling, model-data comparison

Supplementary material for this article is available [online](#)

Abstract

Climate model simulations are inherently biased. It is a notably difficult problem when dealing with climate impact assessments and model-data integration. This is especially true when looking at derived quantities such as biomes, where not only climate but also vegetation dynamics biases come into play. To overcome such difficulties, we evaluate the performance of an existing methodology to correct climate model outputs, applied here for the first time to long past climate conditions. The proposed methodology relies on the 'Cumulative Distribution Function-transform' (CDF-t) technique, which allows to account for climate change within the bias-correction procedure. The results are evaluated in two independent ways: (i) using forward modelling, so that model results are directly comparable to reconstructed vegetation distribution; (ii) using climatic reconstructions based on an inverse modelling approach. The modelling is performed using the intermediate complexity model iLOVECLIM in the standard global and interactively downscaled over the Europe version. The combined effects of dynamical downscaling and bias correction resulted in significantly stronger agreement between the simulated results and pollen-based biome reconstructions (BIOME6000) for the pre-industrial (0.18 versus 0.44) and mid-Holocene (MH) (0.31 versus 0.40). Higher correlation is also observed between statistically modelled global gridded potential natural distribution and modelled biomes (0.36 versus 0.41). Similarly, we find higher correlation between the reconstructed and the modelled temperatures for the MH (0.02 versus 0.21). No significant difference is found for the Last Glacial Maximum when using temperature reconstructions, due to the low number of data points available. Our findings show that the application of the CDF-t method on simulated climate variables enables us to simulate palaeoclimate and vegetation distribution in better agreement with independent reconstructions.

1. Introduction

Earth's palaeoclimate research is a prominent source of knowledge about the climate system, its functions and interactions, as well as a tool for investigating potential human-made climate effects (Hansen and Sato 2012). Nowadays, various tools and methods allow us to assess the state of past climates based on a set of climate proxies (Guiot *et al* 1993, Peyron *et al* 1998, Mauri *et al* 2015, Kaufman *et al* 2020). Proxy-based climate reconstructions provide knowledge of past climatic conditions but do not readily give access to the

underlying mechanisms behind them. In addition, they are often spatially discontinuous and temporally limited. This brings the need for a methodology to physically interpolate them at a regional scale. In this view, climate modelling is a complementary approach that is both flexible in terms of spatial and temporal variability, and can be adapted to a wide range of studies (Haywood *et al* 2019). Data and models play a complementary role in understanding climate change. Models offer mechanisms to explain the data, while proxy data provides a knowledge base for evaluating the models.

Palaeoclimate model simulations using Earth system models of intermediate complexity (EMICs) can be widely used to improve the understanding of the mechanisms and dynamics of the climate system (Claussen *et al* 2002, Keery *et al* 2016). However, EMICs have very limited simulation power at finer geographical scales and need alternative methods to be compared to small-scale proxies (over land in particular).

To achieve higher spatial resolution, we can use downscaling approaches. In our approach, we rely on the interactive physical downscaling approach introduced by Quiquet *et al* (2018) within the model of intermediate complexity iLOVECLIM (Claussen *et al* 2002, Goosse *et al* 2010, Roche *et al* 2014). The downscaling technique significantly improved spatial resolution and overall performance of the model, including correction of several topography-related biases (Arthur *et al* 2023). However, large-scale model biases remain present in the outputs of the downscaled version of iLOVECLIM, considering that the downscaling technique was not designed to correct broader, regional scale, model biases (Quiquet *et al* 2018). Broad-scale iLOVECLIM biases, linked to the model formulation and underlying assumptions, were described by Goosse *et al* (2010), and include, among others: overestimation of temperatures in low latitudes and precipitations in subtropics (in particular in South America and West Africa), biases in atmospheric circulation, and too symmetric distribution of precipitation between the Northern and the Southern hemisphere.

Vrac *et al* (2012) have developed a bias correction methodology, based on cumulative distribution function transformations (CDF-t), aimed to reduce large-scale model biases. The findings indicate a significant improvement in the results of regional climate models with respect to observations for wind speed, temperature, and precipitation distributions (Vrac *et al* 2012). The CDF-t method is an advancement of the quantile mapping (QM) bias correction method (Guo *et al* 2020). The QM method was shown to have the potential to reduce biases in palaeoclimate simulations (Beyer *et al* 2020). The CDF-t method was previously applied as a downscaling technique (Michelangeli *et al* 2009, Lavaysse *et al* 2012, Vigaud *et al* 2013, Noël *et al* 2021) and as a bias correction methodology (Luu *et al* 2018, Mesta and Kentel 2022) to correct regional climate model outputs, used as an input for impact models. However, this methodology has not yet been tested for past time periods with available paleoenvironmental data synthesis, which is the goal of the present study. We are, therefore, assessing the performance of CDF-t as a bias correction technique only over three periods of the past with contrasting climatic conditions: pre-industrial (PI, 0 ka BP), mid-Holocene (MH, 6 ka BP or climatic optimum), and Last Glacial Maximum (LGM, 21 ka BP). These periods have been a focus for the synthesis of paleoenvironmental data (Prentice and Webb 1998, Prentice *et al* 2000, Harrison *et al* 2016, Harrison 2017), for intercomparison modelling exercises (Kageyama *et al* 2018), and to evaluate the climate models with data (Kohfeld and Harrison 2000, Bartlein *et al* 2011, Cleator *et al* 2020, Kaufman *et al* 2020), which created a basis for model evaluation and established them as key periods in palaeoclimate modelling (Brierley *et al* 2020).

The assessment of the performance of palaeoclimate modelling is typically done using proxy-based reconstructions as a reference (e.g. Ramstein *et al* 2007, Goosse *et al* 2010). This can be done in two ways, using a forward or an inverse approach. The forward approach implies modelling of observables (e.g. biomes, oxygen isotopes of water and air) directly within the climate model (Haywood *et al* 2019). During the inverse approach, proxies are processed to reconstruct physical climatic variables, analogous to typical climate model outputs (Haywood *et al* 2019). For example, applying reverse vegetation modelling or statistical modelling approaches (e.g. response surface and modern analogue approaches) to pollen data to estimate temperature and precipitation values (Guiot *et al* 2000, Chevalier *et al* 2020). The inverse approach was previously used to evaluate the performance of bias correction methods (the delta method, generalized additive models, and QM) for palaeoclimate simulations by Beyer *et al* (2020). To provide an in-depth analysis of the potential of the CDF-t bias correction method, we estimate its accuracy using the forward and inverse approaches of data-model comparison. Both approaches have considerable limitations. In the forward approach, data-model biome comparison is qualitative, and it is challenging to evaluate the similarity between data and model results. While, the inverse approach strongly depends on the vegetation model used. The use of both methods in combination provides an advantage of independent evaluation of the featured bias correction with two different methods. We will analyse the bias correction performance with a specific focus on terrestrial biomes at the global scale and over the European area at high resolution. If

the CDF-t method results in a better representation of the distributions of the tested variables (temperature and precipitation) in past climate contexts than non-corrected model results, we can be more confident that the biomes simulated by the model for these past periods are also more realistic. This allows potentially for a more accurate analysis of the climate dynamics, contributing to a better understanding of the conditions during these crucial benchmark periods in the past.

The main objectives of our study are: (i) to apply the CDF-t methodology for correcting climatic biases in the context of palaeoclimate modelling; (ii) to test the robustness of the developed technique on three time periods of the past with contrasting climatic conditions, using proxy-based climate and vegetation reconstructions; and (iii) to evaluate the advantages and shortcomings of the proposed approach.

2. Methodology

2.1. Climate input

2.1.1. *iLOVECLIM* model description and online dynamical downscaling

The climate simulations were performed with the *iLOVECLIM* model, version 1.1.5. This model is a code fork of the original *LOVECLIM* 1.2 model (Goosse *et al* 2010), revised by Roche (2013) and further expanded by Quiquet *et al* (2018). The applied version of *iLOVECLIM* includes an atmospheric component (ECBilt), an oceanic general circulation model (CLIO), and a simple land vegetation model (VECODE) (Roche *et al* 2014). ECBilt is a three-level, quasi-geostrophic model that consists of three vertical layers at T21 horizontal resolution, corresponding to $\sim 5.625^\circ \times \sim 5.625^\circ$ latitude–longitude (Opsteegh *et al* 1998). CLIO is an oceanic GCM with 20 unevenly spaced vertical layers at $3^\circ \times 3^\circ$ latitude–longitude horizontal resolution (Goosse and Fichefet 1999). VECODE is a reduced-form dynamic global vegetation model (DGVM), which describes vegetation dynamics using two plant functional types (PFTs): trees and grass (Brovkin *et al* 1997). *iLOVECLIM* has been previously successfully applied to simulate the climate of the Holocene (Arthur *et al* 2023, 2016, Zhang *et al* 2018, Li *et al* 2019), the LGM (Lhardy *et al* 2021), the last deglaciation (Quiquet *et al* 2021) and the last interglacial (Li *et al* 2020).

In order to obtain higher spatial resolution climate model outputs, we make use of the online interactive downscaling method embedded in *iLOVECLIM*, first described by Quiquet *et al* (2018). It is a physical downscaling procedure that replicates the processes governing the computation of climatic parameters on a spatially refined grid to explicitly take into account the sub-grid topography in the computation of heat and precipitation. Here we use a global climatic simulation with a zoom at high spatial resolution grid of $0.25^\circ \times 0.25^\circ$ over Europe. The downscaled segment is extracted and used for the analysis. This downscaling procedure is interactive in the sense that the large-scale temperature and precipitation are directly impacted by the sub-grid computations. This means that the large-scale climate outputs are different when using the downscaling or not.

2.1.2. Numerical experiments

To explore the performance of the CDF-t bias correction method under different climatic conditions, we carried out experiments for four distinct periods (present day (PD), PI, MH, and LGM) for the two *iLOVECLIM* grids: T21 (5.625° resolution, global simulations) and hi-res (0.25° resolution, simulations over Europe). In our simulations we used standardized boundary conditions for palaeoclimate simulations, provided by the Palaeoclimate Modelling Intercomparison Project Phase 4 (PMIP-4) (Kageyama *et al* 2017), using the forcings presented in table 1. The astronomic conditions in the simulations were derived from Berger (1978). Three equilibrium simulations were performed with a spinup of 3000 years: LGM, MH, and PI (taken at 1750 A.D.). From the PI, a transient PD simulation was then run transiently covering 1750–2014. During the transient simulations of 1750–2014 astronomical parameters were kept constant, under the assumption that at this time scale the changes were so minor that there was no significant effect on the climate. The concentrations of the atmospheric trace gases were derived from the consolidated datasets of historical atmospheric concentrations for the Climate Model Intercomparison Project (CMIP6) (Meinshausen *et al* 2017).

To be consistent with the length of the observation dataset, 38 years were extracted from each simulation: 1976–2014 for the transient PD simulation and 38 years at the end of the spin-up for each of the equilibrium simulations. For the analysis, we used climatological mean of the simulations. To ensure that the selection of a 38 year average does not distort our analysis, we tested sensitivity of our method to low-frequency climate variability within the *iLOVECLIM* model. The results (data not shown) indicated no significant impact of low-frequency climate variability in *iLOVECLIM* on studied variables following the CDF-t application.

Table 1. Experimental set-up. The name of each experiment consists of an abbreviation of a studied period (PI, MH, LGM), and a grid name (T21, hi-res). T21 simulations are performed globally (g), hi-res simulations—over Europe (EU). For the LGM experiment, the ice-sheet forcing is the GLAC-1D reconstruction taken from the PMIP-4 protocol (Kageyama et al 2017). For a complete description of the experimental setup of the LGM simulation, the reader is referred to Lhardy et al (2021). For equilibrium (E) simulations, 3000 years of spinup were performed, and the last 38 years have been used for the analysis. For transient (T) simulations, 3000 years of spinup were performed, and then transient simulations for 264 years were performed, of which the last 38 years have been used for the analysis.

Simulation name	Resolution (°)	Simulation type	Astronomical parameters	Concentration of greenhouse gases
PD—T21 (g)	5.625	T	Eccentricity = 0.016 724	CO ₂ = 333.3–395.5 ppm
PD—hi-res (EU)	0.25	T	Obliquity = 23.446° Perihelion-180° = 102.04°	CH ₄ = 1527.7–1831.5 ppb N ₂ O = 299.3–326.9 ppb
PI—T21 (g)	5.625	E		CO ₂ = 280 ppm
PI—hi-res (EU)	0.25	E		CH ₄ = 760 ppb N ₂ O = 270 ppb
MH—T21 (g)	5.625	E	Eccentricity = 0.018 682	CO ₂ = 264.4 ppm
MH—hi-res (EU)	0.25	E	Obliquity = 24.105° Perihelion-180° = 0.87°	CH ₄ = 597 ppb N ₂ O = 262 ppb
LGM—T21 (g)	5.625	E	Eccentricity = 0.018 994 Obliquity = 22.949° Perihelion-180° = 114.42°	CO ₂ = 190 ppm CH ₄ = 375 ppb N ₂ O = 200 ppb

2.1.3. Reference observation dataset

The observational reference dataset used for bias correction is the Earth2Observe, WFDEI and ERA-Interim data Merged and Bias-corrected for the InterSectoral Impact Model Intercomparison Project (Lange 2018). The EWEMBI data covers the entire globe at 0.5° horizontal and daily temporal resolution from 1979 to 2014.

For consistency with the EWEMBI dataset, for bias correction we have extracted the 1979–2014 timespan from the 1750–2014 model simulation, both at T21 and on the high-resolution grid. The EWEMBI dataset grid has been regridded to the iLOVECLIM T21 and hi-res grids using the first-order conservative remapping approach (Jones 1999) to ensure that each iLOVECLIM grid cell time series corresponds to an EWEMBI grid cell. This approach allowed us to perform bias correction on a gridcell-by-gridcell basis.

2.2. CDF-t method

2.2.1. CDF-t description

The method we used for bias correction is the ‘cumulative distribution function-transform’ (CDF-t) (Vrac et al 2012). The CDF-t method is an extension of a widely-applied univariate bias-correction method, the ‘quantile-quantile’ (QQ) method (e.g. Haddad and Rosenfeld 1997, Déqué 2007). In contrast to the QQ method, the CDF-t approach allows accounting for the climate change signal provided by the climate simulations that need to be corrected. This allows for the transformation (i.e. correction) of the simulations by modifying its underlying statistical distribution while maintaining the modelled climate change signal (Vrac et al 2012). The QQ method performs a QM between the CDF F_{Sh} of the simulated data (subscript S) and the CDF F_{Rh} of the reference data (subscript R), both under a historical period (subscript h). Hence, when a simulated value, say x_p , over a projection period (subscript p) has to be bias-corrected, QQ first estimates its probability value in terms of CDF from historical simulations, before associating a quantile, say y_{QQ} , with the same probability in the ‘observations’ world:

$$F_{Rh}(y_{QQ}) = F_{Sh}(x_p) \Leftrightarrow y_{QQ} = F_{Rh}^{-1}(F_{Sh}(x_p)),$$

where F_{Rh}^{-1} is the inverse CDF function of F_{Rh} . Thus, even though x_p does not follow the distribution F_{Sh} , the associated probability $F_{Sh}(x_p)$ is computed anyway, which is problematic (Vrac et al 2012). The CDF-t approach avoids this potential mismatch between simulated values and their associated CDFs by considering the CDF change between observed and simulated climatic variables, in order to estimate the reference CDF F_{Rp} under the projection period, and then perform a QM between F_{Sp} and F_{Rp} . The transformation T from F_{Sh} to F_{Rh} is modelled as:

$$T(F_{Sh}(x)) = F_{Rh}(x), \quad (1)$$

which, by substituting x with $F_{Sh}^{-1}(u)$, where u represents any probability in $[0, 1]$, is estimated as:

$$T(u) = F_{Rh}(F_{Sh}^{-1}(u)). \quad (2)$$

Based on this definition of T , and assuming that it is time-invariant, the transformation can be applied to F_{Sp} , the CDF of the variable of interest during a (future or past) projection period p , to estimate F_{Rp} , the CDF of the same variable during the projection period p :

$$T(F_{Sp}(x)) = F_{Rp}(x), \quad (3)$$

that is

$$F_{Rp}(x) = F_{Rh}(F_{Sh}^{-1}(F_{Sp}(x))). \quad (4)$$

After obtaining F_{Rp} using equation (4), a QM can then be performed between F_{Sp} and F_{Rp} to obtain local bias-corrected time series. Unlike the QQ method that is applied directly between F_{Sh} and F_{Rh} (Déqué 2007), the CDF-t method corresponds to a QM between F_{Sp} and F_{Rp} . Subsequently, the values are generated based on the F_{Rp} in chronological agreement with simulated climate data. Previous studies with BIOME models (Prentice et al 1998, Harrison and Prentice 2003, Wohlfahrt et al 2004) had proposed an anomaly procedure to remove the inherent model biases for diagnostic purposes. In the anomaly procedure, the vegetation models are run using modern (baseline) climatology (e.g. CRU) with the added modelled climate change (anomaly) between the past and PI periods. Both CDF-t and anomaly methodologies preserve the climate change between two time periods. The main difference between CDF-t and the anomaly procedure is that using CDF-t, the temporal chronology (i.e. the sequence of events in its own variability) simulated by a climate model is preserved while in the anomaly procedure, chronology remains identical to reference (baseline) climate dataset variability. This is a fundamental advantage of CDF-t: a change in the temporal properties of the climate simulations is not accounted for in the anomaly procedure while it is also preserved by CDF-t.

A full description of the method can be found in Vrac et al (2012).

2.2.2. Application

In this study, we used CDF-t to correct three climatic variables simulated by iLOVECLIM and needed for the vegetation computations: near-surface air temperature, precipitation, and relative humidity. The calibration of the bias correction was based on these variables from the PD simulations 1979–2014 and the observation dataset for the same period. This bias correction was then applied to PI, MH, and LGM.

Seasonality of the geological past of the Earth differs from modern seasonality (Guiot et al 2000, Wu et al 2007, Koutavas and Joanides 2012) due to the change in the solar input's to the Earth over the year following long-term change of its orbit around the sun. Therefore, we tested our methodology by applying bias correction both on a monthly and yearly basis to evaluate the consequence of the choice made. For the monthly-based bias correction, we applied CDF-t, on a monthly basis, to the daily data ensemble of each grid cell, given that the days belong to the same month. During the yearly-corrected bias correction, we applied CDF-t to the full data ensemble of each grid cell, regardless of the month. Within the two options for bias correction with CDF-t (on a monthly or yearly basis) there is potential to test if one or the other methodology has a significant impact on the result. It must be recognized that bias correcting on a per month basis does not guarantee to maintain the seasonality changes at a period where the orbital configuration is significantly different. The performance of the bias correction was analysed by calculating the root-mean-square error (RMSE), Pearson's correlation coefficient (R), and standard deviation (SD) between the values of the bias-corrected iLOVECLIM simulations and the EWEMBI values.

An additional complexity arises for the LGM simulations: the land-sea distribution was different during that time period (supplementary figure 1), owing to a sea-level difference of about 125 m lower than that of the PD (e.g. Lambeck et al 2014). Hence, there are regions that were land 21 ka ago and that are oceans or seas today. Applying the CDF-t methodology on LGM land grid cells that are oceans or seas today would be inconsistent. Hence, we decided to restrict the bias correction of variables on locations that are land both during the LGM and today.

2.3. Method evaluation

2.3.1. Inverse approach: comparison with climate reconstructions

The inverse approach entails the comparison of modelled temperature and proxy-based reconstructions. The CDF-t approach preserves the evolutions of the input climate, and thus the anomalies (differences) with respect to the PD are constant before and after the CDF-t bias correction. These anomalies for the Holocene were previously analysed by Arthur et al (2023) with respect to proxy-based reconstructions from the Italian Alps (Harrison et al 1996, Mauri et al 2015, Furlanetto et al 2018), Scandinavia (Harrison et al 1996, Mauri et al 2015, Bjune et al 2005, Seppä and Birks 2001), and Mediterranean region (Kuhnt et al 2008, Bartlein et al 2011, Guiot and Kaniewski 2015, Mauri et al 2015, Peyron et al 2017, Finné et al 2019). Their findings

indicated that dynamically downscaled iLOVECLIM simulations result in a better agreement with proxy-based reconstructions and other climate model studies, compared to the coarse resolution grid, particularly in the Mediterranean and complex mountainous terrain. In the current study, the dataset used for the data-model comparison was extracted from the global database of Holocene paleotemperature records Temperature 12k at version 1.0.0 (Kaufman *et al* 2020), where data is represented as absolute temperature values, rather than anomalies. It consists of reconstructed through the inverse modelling absolute near-surface air temperature data points derived from lake sediment, marine sediment, peat, glacier ice, and other natural archives. Temperature reconstructions were done by numerous independent studies using a wide variety of proxy data (i.e. alkenones, $\delta^{18}O$), associated with several uncertainties (see section 4.1). The design of the Temperature 12k database is further described by Kaufman *et al* (2020), while the sources of each data point are included in the metadata of the database.

For the purpose of this study, we extracted the Temperature 12k terrestrial mean annual values dated between 5.5–6.5 ka (MH), and 20.5–21.5 ka (LGM). For the sake of comparing with the iLOVECLIM model outputs, we resampled the Temperature 12k data points to T21 and hi-res grid, using the aggregated average resampling method. This method assigns to the new output cell the most common values of the cells in the input map within the limits of the output cell (Díaz-Pacheco *et al* 2018). We then analysed the differences between the modelled and reconstructed near-surface air temperatures before and after the CDF-t application at corresponding grid cells.

2.3.2. Forward approach: comparison with pollen-based vegetation reconstructions

As the second step of the evaluation, we used a forward approach to directly simulate the reconstructed vegetation from pollen proxies, so that we are not dependent on ‘transfer functions’, as in the inverse method. To evaluate the performance of the bias correction in palaeoclimate modelling with the forward evaluation approach, we performed a set of simulations of biome distribution of the studied periods. The embedded reduced-form DGVM in iLOVECLIM describes vegetation dynamics using only 2 PFTs (Brovkin *et al* 1997). Thus, for the current study, we use the more complex CARbon Assimilation In the Biosphere (CARAIB) dynamic vegetation model (Warnant *et al* 1994, François *et al* 1998, Otto *et al* 2002, Laurent *et al* 2008, Dury *et al* 2011), forced offline using iLOVECLIM climatic outputs. The CARAIB model is made of five modules: hydrological, canopy photosynthesis and stomatal regulation, carbon allocation-growth-respiration, heterotrophic respiration, and plant competition and biogeography. Vegetation is distributed in 26 PFTs, which, with respect to climatic parameters, are classified into 20 biomes. As an input, CARAIB requires six variables with a daily frequency: near-surface air temperature, precipitation, relative humidity, wind speed, sunshine hours and daily temperature amplitude. In all simulations of this study, wind speed was taken from the EWEMBI dataset, and sunshine hours were used directly from iLOVECLIM. The iLOVECLIM model does not have a daily cycle, thus daily temperature amplitudes were taken from observations (Climatic Research Unit (CRU) data, mean over 1901–2015) and kept constant for all time periods.

To assess the effect of the CDF-t application on the accuracy of simulated biome distribution, we used different sets of surface temperature, precipitations, and relative humidity taken (a) from the EWEMBI observation dataset (b) from the iLOVECLIM model, and (c) from the iLOVECLIM model after the CDF-t application to the outputs. The observation-enforced simulation was used as a control for the PI simulations.

The resulting computed biome distribution was compared to the BIOME6000 reconstruction (Harrison 2017). This reconstruction is based on the Paleovegetation Mapping Project (Prentice *et al* 1998, 2000). In BIOME6000, biomes are represented based on degrees of affinity of PFTs with each biome (Prentice *et al* 1996). In this work, we used megabiomes from BIOME6000, described by Harrison and Bartlein (2012). The 20 biomes in CARAIB were then reclassified into the nine megabiomes used in the BIOME6000 pollen database using the methodology of Extier (2019) (supplementary table 1).

Similarly to the inverse approach, we resampled BIOME6000 data points to the T21 and hi-res grids, using the majority resampling method (figure 6). The agreement was tested by calculating matching ratios between the resampled BIOME6000 and CARAIB-derived biomes before and after the CDF-t application. To account for the discrepancies in biome classification and spatial incoherency we also present the biome distribution in data and model in a form of contingency tables (supplementary tables 2–11), that outline frequency for particular combinations of biomes.

We found that the spatial irregularity of the data distribution of BIOME6000 and its absence in certain bioclimatic zones led to major regional inconsistencies. To overcome this data scarcity and irregularity across different regions and biomes (see section 4.1), we thus further compared our results with the statistically modelled gridded potential natural vegetation (PNV) distribution of Levvasseur *et al* (2012). The PNV is relying on BIOME6000 at the PI period as a predictand for a multinomial logistic regression on a high-resolution grid worldwide. Besides its regular grid spacing without missing data, it also has the

advantage of including a prediction of climatic zones where biomes remain are scarce or non-existent such as desertic areas (see section 4.1).

To test differences between the matching ratios before and after correction, we used the generalized Pearson chi-squared test of independence.

3. Results

In this section, we present the results of the bias correction of palaeoclimate modelling, starting with the outcomes of the test of monthly-based against yearly-based bias correction approach. These results are used to show the methodology for the bias correction. The test is followed by the results of inverse and forward accuracy evaluation approaches, which are used to assess the robustness of the developed technique.

3.1. Monthly-based and yearly-based bias correction approach

In order to evaluate the impact of methodological choices on our final result, we first apply both the monthly and yearly based CDF-t approaches, as highlighted above, to the PI climate. For the comparison, we used mean values of the temporal data ensemble for a grid cell, to evaluate the properties of the data ensemble in terms of spatial structure. The monthly-based approach results in higher Pearson correlation of precipitation to the observations. The SD of the monthly-based approach is also slightly better for the temperature and relative humidity than for yearly-based approach (figure 1). Additionally, the monthly-based approach allows for a better preservation of the raw monthly differences for temperature and precipitation between the different climate states (e.g. MH versus PI, not shown). We further tested monthly- and yearly-based approaches using the forward mode evaluation by comparison with pollen-based biome reconstructions (not included in the paper), and found consistently higher matching ratios using the monthly-based approach. Hence in the following, we report on results using the monthly-based approach.

3.2. Inverse mode. Comparison with paleotemperature record

The results of the comparison between the modelled climate parameters and proxy-reconstructed values from the Temperature 12k dataset are represented as scatterplots (figure 2). We observe significant improvement after the CDF-t application for the MH on the hi-res grid over Europe and on a T21 grid globally. No statistical difference was detected for the LGM.

In supplementary figures 2–7 we can observe a reduction in known large-scale iLOVECLIM biases, outlined in the literature (Goosse *et al* 2010). After the CDF-t application, North America is getting colder (supplementary figure 2) and, in parts, dryer (supplementary figures 3 and 4), which corrects the overestimation of temperatures in low latitudes in iLOVECLIM. Similarly, we observed a decrease in precipitations in subtropics, in particular in Asia and Australia (supplementary figure 3). The region of high precipitations is moved westward in Tropical Africa (supplementary figure 3), thus improving the representation of the recorded patterns of precipitations in these regions. Symmetry in the distribution of precipitation between the hemispheres is corrected with the increase in precipitations over the Northern hemisphere (supplementary figures 3 and 6).

The performance of the bias correction was further analysed using the RMSE, R , and SD of the modelled data with respect to Temperature 12k reconstructions, combined in Taylor diagrams (figure 3). Similarly to the figure 1, we used mean values of the temporal data ensemble for each grid cell.

We observe better R and RMSE in bias-corrected values for MH on a T21 grid globally ($R = 0.88$, RMSE = 6.32, SD = 9.37 before correction; $R = 0.91$, RMSE = 4.71, SD = 10.05 after correction) and on the hi-res grid over Europe ($R = 0.15$, RMSE = 4.13, SD = 3.46 before correction; $R = 0.46$, RMSE = 2.79, SD = 1.97 after correction). This indicates that temperatures after correction are closer to proxy-derived temperatures of Kaufman *et al* (2020), and thus confirms improvement of the temperature predictions after CDF-t bias correction for MH. The downscaled results show that after correction most of the data points of the simulated climate became colder than before correction (figure 4). These data points represent pollen data location, clustered in Scandinavia (the data points in figure 4 and supplementary figure 9 represent temperature values at site of the pollen reconstruction). Pollen-based reconstructions feature higher temperatures in Scandinavia than in our model and observations, which indicates one of the limitations of the proposed approach (see section 4.1). However, after correction, there are no more extreme outliers (8° and 9° warmer) relative to the reconstruction. The highest difference value after the correction is reduced to 5° . At the LGM, we observe no significant differences in R and an increased RMSE (figures 2 and 3), which indicates low similarity of the corrected model to the point reconstructions. The results are highly influenced by a low number of points with extremely negative values located in Greenland (figure 5, supplementary figure 9).

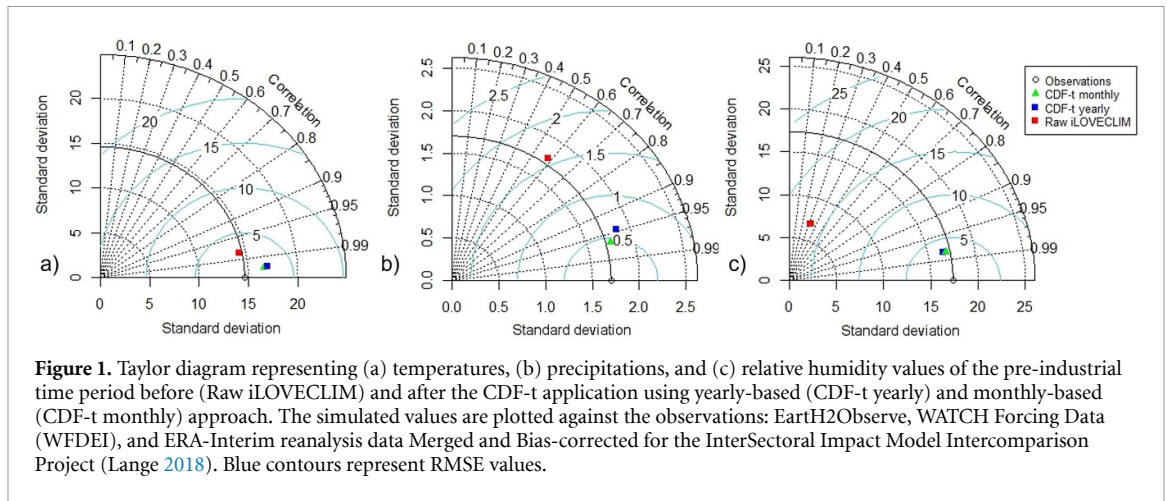


Figure 1. Taylor diagram representing (a) temperatures, (b) precipitations, and (c) relative humidity values of the pre-industrial time period before (Raw iLOVECLIM) and after the CDF-t application using yearly-based (CDF-t yearly) and monthly-based (CDF-t monthly) approach. The simulated values are plotted against the observations: Earth2Observe, WATCH Forcing Data (WFDEI), and ERA-Interim reanalysis data Merged and Bias-corrected for the InterSectoral Impact Model Intercomparison Project (Lange 2018). Blue contours represent RMSE values.

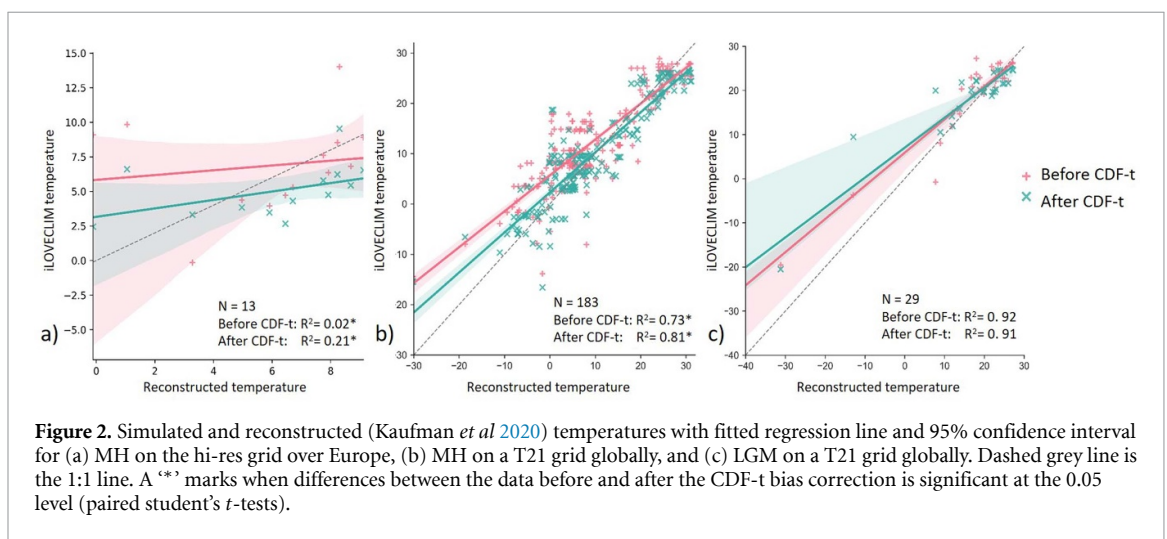


Figure 2. Simulated and reconstructed (Kaufman et al 2020) temperatures with fitted regression line and 95% confidence interval for (a) MH on the hi-res grid over Europe, (b) MH on a T21 grid globally, and (c) LGM on a T21 grid globally. Dashed grey line is the 1:1 line. A “*” marks when differences between the data before and after the CDF-t bias correction is significant at the 0.05 level (paired student’s *t*-tests).

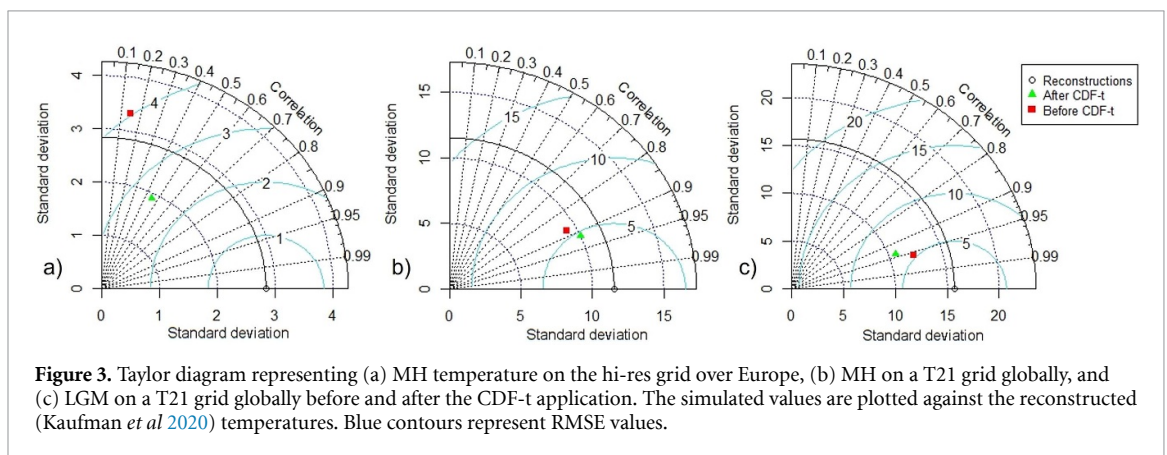


Figure 3. Taylor diagram representing (a) MH temperature on the hi-res grid over Europe, (b) MH on a T21 grid globally, and (c) LGM on a T21 grid globally before and after the CDF-t application. The simulated values are plotted against the reconstructed (Kaufman et al 2020) temperatures. Blue contours represent RMSE values.

3.3. Forward mode. Comparison with pollen-based vegetation reconstructions

To quantify the performance of the CDF-t bias correction method to simulate the global biome distribution, we compare the resulting biome maps with biome reconstructions provided by the BIOME6000 project (Harrison 2017). Since there is an inherent bias related to the use of the CARAIB model as well as the reconstruction dataset, we first compute biomes from CARAIB vegetation output using the EWEMBI observations (control) as an input. This biome output represents the best attainable fields using the bias correction. The difference between that reference field and the other biome fields is indicative of the remaining error in the climatic field.

Table 2 shows that after the CDF-t correction, the modelled biomes better match the BIOME6000 pollen data in all experiments except for the T21 PI, as opposed to non-corrected values. The improvement is

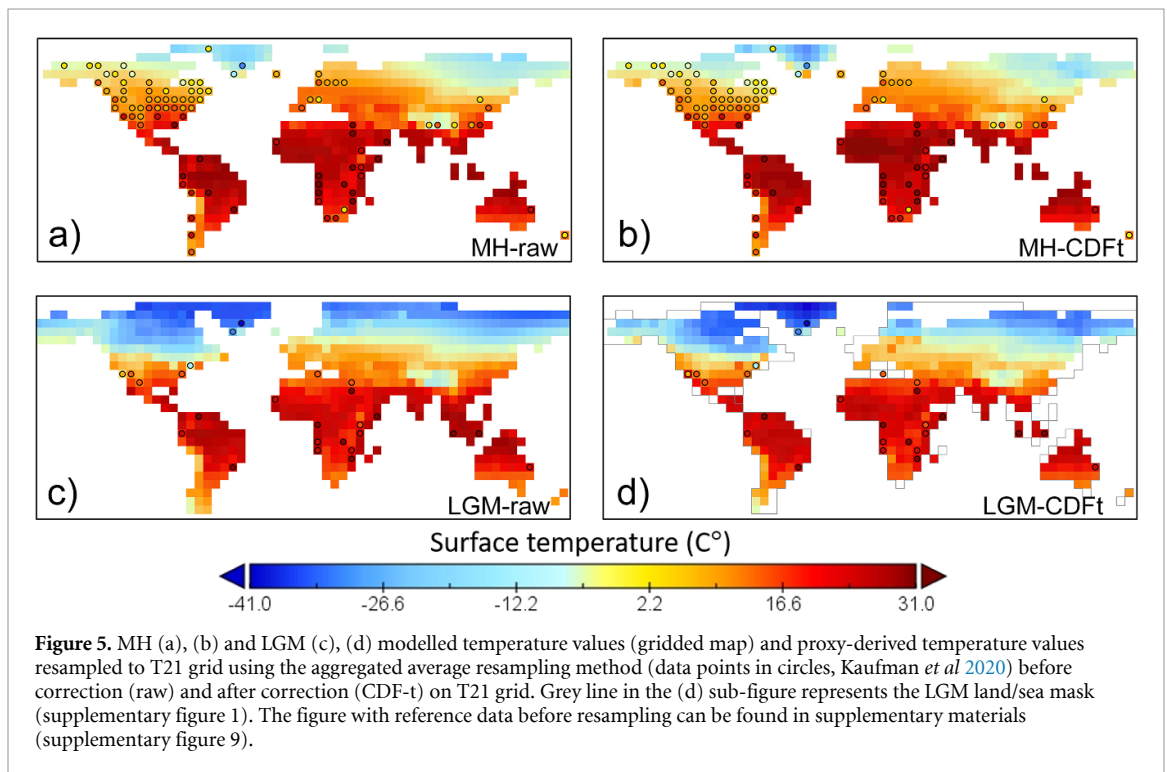
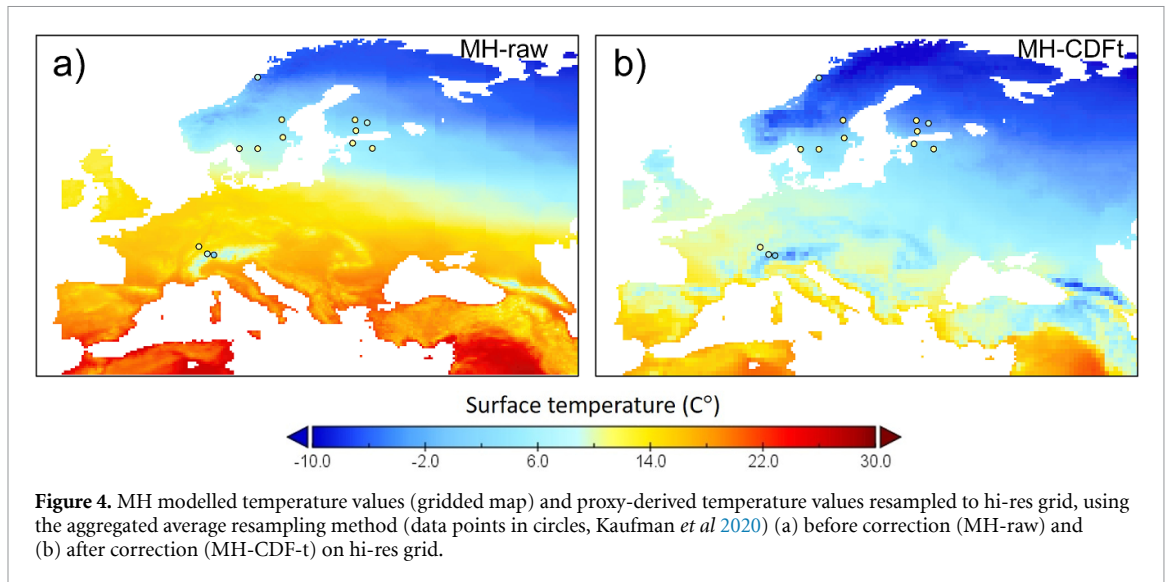


Table 2. Matching ratios between megabiomes in pollen reconstructions (BIOME6000) and biomes predicted by the CARAIB model using: unaltered iLOVECLIM climatic variables (before correction); bias-corrected iLOVECLIM climatic variables using the CDF-t method on a monthly basis (after correction); and EWEMBI climatic variables (control). Hi-res: downscaled simulation over Europe; T21: standard global simulation. The megabiome classification consists of 9 biomes. A ‘*’ marks when differences between the data before and after the CDF-t bias correction is statistically significant at the 0.05 level with a chi-squared test.

	hi-res EWEMBI (control)	T21 EWEMBI (control)	hi-res PI	hi-res MH	T21 PI	T21 MH	T21 LGM
Before CDF-t correction	0.39	0.47	0.18	0.31	0.36	0.38	0.22
After CDF-t correction	—	—	0.44*	0.40*	0.36	0.44*	0.25
N of grid cells	941	333	941	389	333	286	130

significant on the hi-res grid over Europe for PI and MH, and for MH on a T21 grid globally. Comparison with the PNV of Levvasseur *et al* (2012) (table 3) also indicates significant improvement at T21 grid globally and in Europe on the hi-res grid. Since the coverage in pollen samples and their accuracy varies widely among different continents (Harrison 2017, Chevalier *et al* 2020, Li *et al* 2022), we compare our results with

Table 3. Matching ratios per continent between megabiomes in Levvasseur *et al* (2012) pollen reconstructions (BIOME6000) and biomes predicted by the CARAIB model forced with: unaltered iLOVECLIM climatic variables (before correction); bias-corrected iLOVECLIM climatic variables using the CDF-t method on a monthly basis (after correction). A ‘**’ marks when differences between the data before and after the CDF-t bias correction is statistically significant at the 0.05 level with a chi-squared test.

	Before CDF-t correction	After CDF-t correction	N of grid cells
Global	0.36	0.41*	286
North America	0.51	0.40	81
Australia	0.22	0.26	8
Asia	0.35	0.44*	94
South America	0.16	0.14	27
Africa	0.25	0.58*	34
Europe	0.51	0.39	42
Europe hi-res	0.39	0.49*	389

biome reconstructions for each continent separately (figures 6–8). The matching ratios for individual biomes can be found in supplementary tables 2–11.

3.3.1. North America

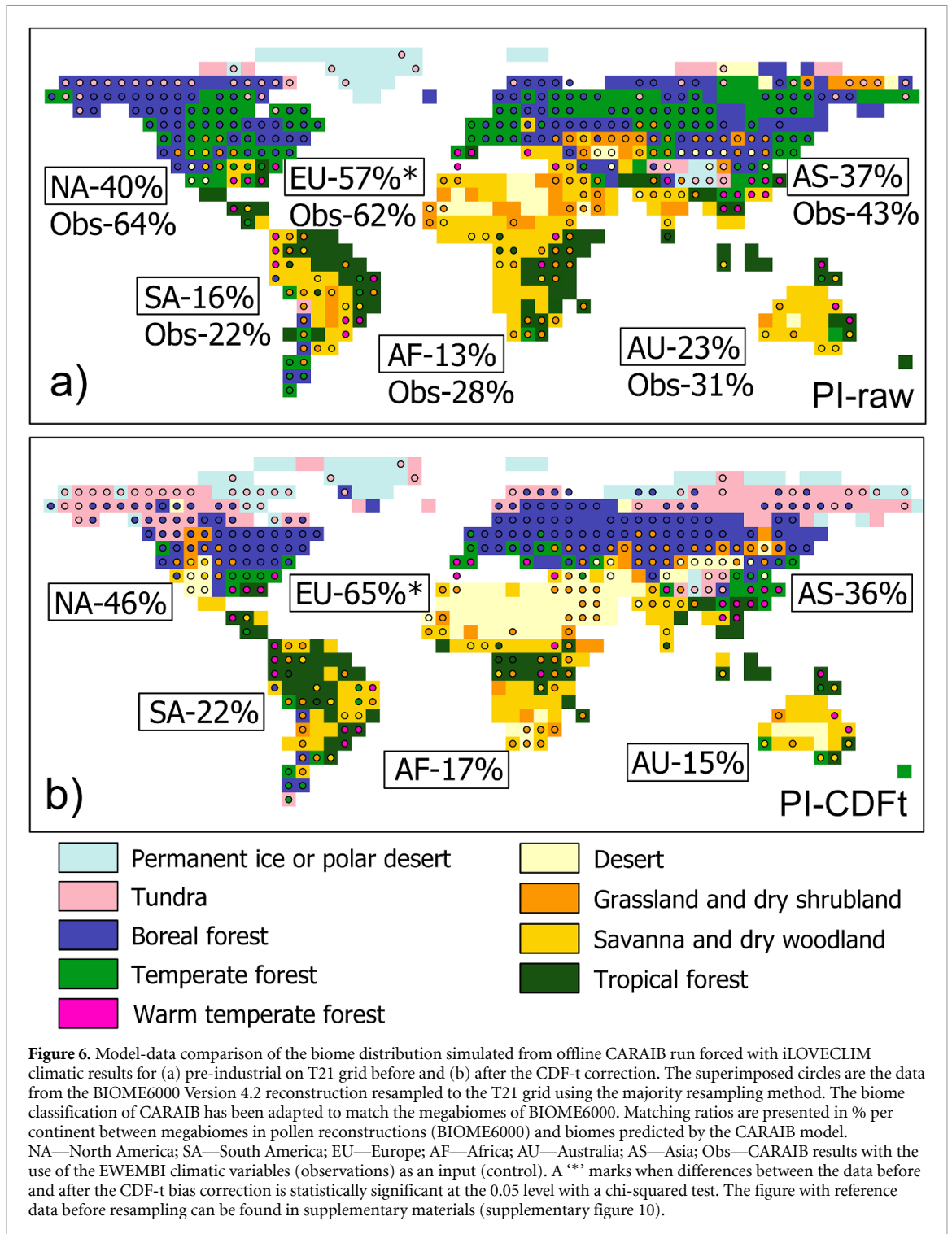
This continent is well represented by high-quality pollen samples (Harrison 2017, Chevalier *et al* 2020, Li *et al* 2022), and thus has an exceptionally large number of BIOME6000 records. The matching ratios show an increase in agreement between the modelled and the reconstructed biomes of all three time periods post CDF-t application, which is significant for the MH (40 *versus* 53%). Figures 6 and 7 demonstrate a better representation of the southern extent of tundra over the continent for the PI and MH. The South-Western part of the continent became dryer after correction (supplementary figures 3 and 4), which led to a better representation of the biomes over the region.

3.3.2. Europe

The area is also well-represented in the BIOME6000 database. However, the number of records for LGM is quite low, and mostly represented by the grassland and dry shrubland data points near PD coastal areas, generally clustered around the Mediterranean. This lack of diversity in the reconstructions hampers obtaining a full picture for other biomes. At PI, in the Mediterranean region CARAIB simulates temperate (before CDF-t) and boreal forest (after CDF-t), thus no significant improvement in matching ratios is observed. However, the results indicate a significant improvement in biome representation for PI (57 *versus* 65%) and MH (50 *versus* 85%) after the CDF-t application. The lack of improvement in comparison with Levvasseur *et al* (2012) on a T21 grid (matching ratio 51% before and 39% after CDF-t) could be attributed to the coarse resolution of the model, since the downscaled simulation results in a significant increase in the matching ratios between the models after the CDF-t application (39 and 49% correspondingly) (table 3). Figure 9 indicates a better representation of the boreal forest in Central Europe in the corrected hi-res PI run. However, it still underestimates the Southward expansion of the boreal forest in Eastern Europe, especially under MH climate conditions. The CDF-t application decreases the temperature and increases annual precipitation levels of the Caspian regions (supplementary figures 5 and 6), which creates climatic conditions attributed to temperate forest biome by CARAIB and worsens the representation of biome distribution over the area in PI after bias correction. However, the above-mentioned changes in climate parameters improve the modelled biome distribution over the Balkans and Iberian Peninsula for both studied time periods. The parts of Southern Great Britain, identified as temperate forest in the BIOME6000 records, are classified by CARAIB before correction as tropical rainforest. The decrease in near-surface relative humidity after the CDF-t application (supplementary figure 7) transforms them into savannah and dry woodland in PI, and temperate and boreal forest in MH.

3.3.3. Asia

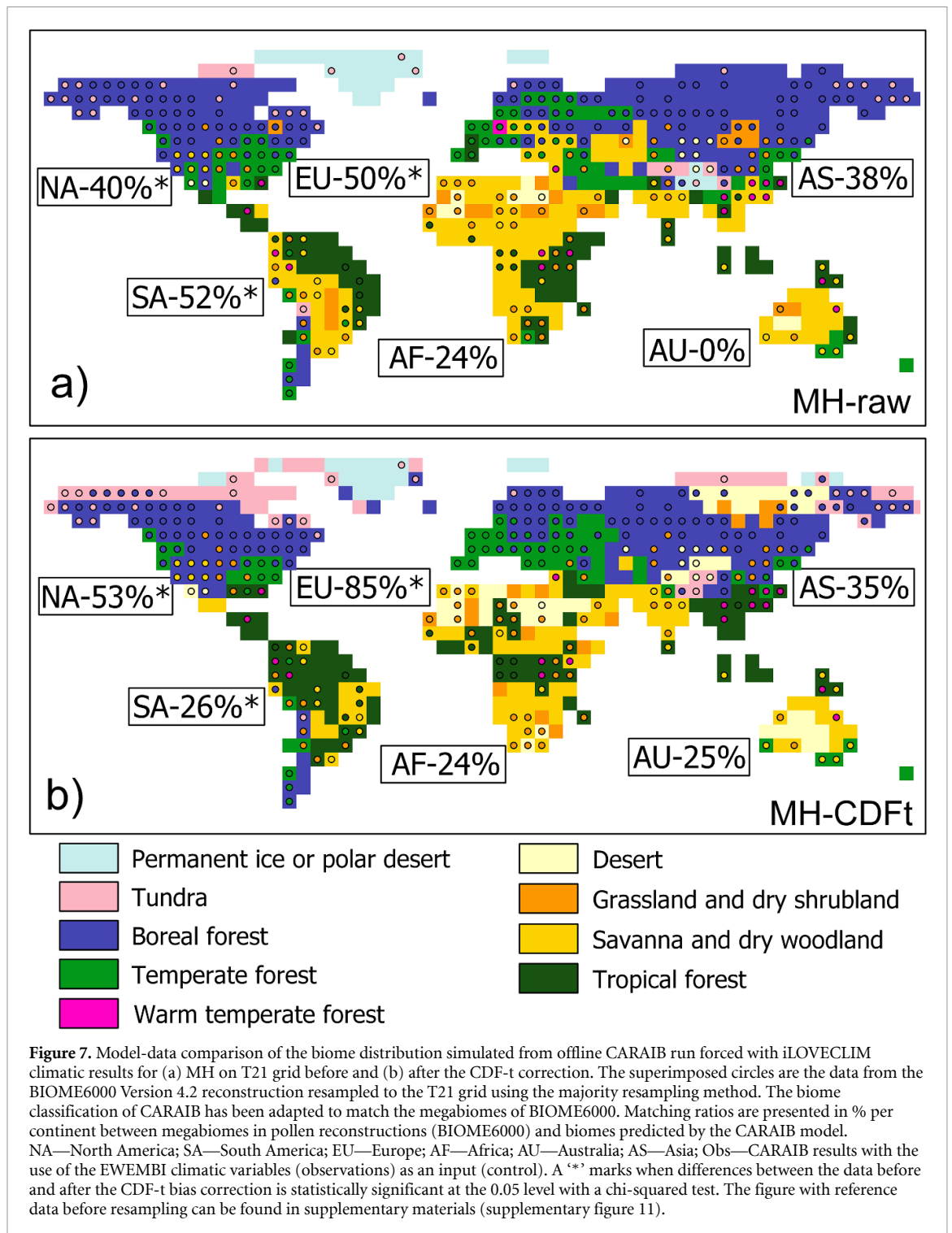
Asia appears to have lower matching ratios after the bias correction for each studied period, compared to non-bias corrected results, but these differences are not statistically significant (PI: 37 *versus* 36%, MH: 38 *versus* 35%, LGM: 33 *versus* 29%). Comparison with the PNV of Levvasseur *et al* (2012), however, indicates significant improvement in matching ratios after correction (35 *versus* 44%). This suggests that the results of comparison with reconstructions are negatively influenced by poor BIOME6000 data spatial coverage in Siberia, and highlights the role of spatial distribution and continuity of the reconstructions. CARAIB classifies cold desert as ‘desert’, and therefore, large areas of Siberia are assigned to this distribution. This negatively reflects on matching ratios for the region of Asia. Another aspect that contributes to the decrease in matching ratios over the entire continent, is the fact that the conditions of warm temperate forest are



attributed to temperate forest in CARAIB. After CDF-t correction, the model overestimates the extent of tundra compared to reconstructions for all the studied time periods. However, the southern extent of the boreal forest after the CDF-t application is in better agreement with the BIOME6000 records and PNV of Levvasseur *et al* (2012).

3.3.4. South America

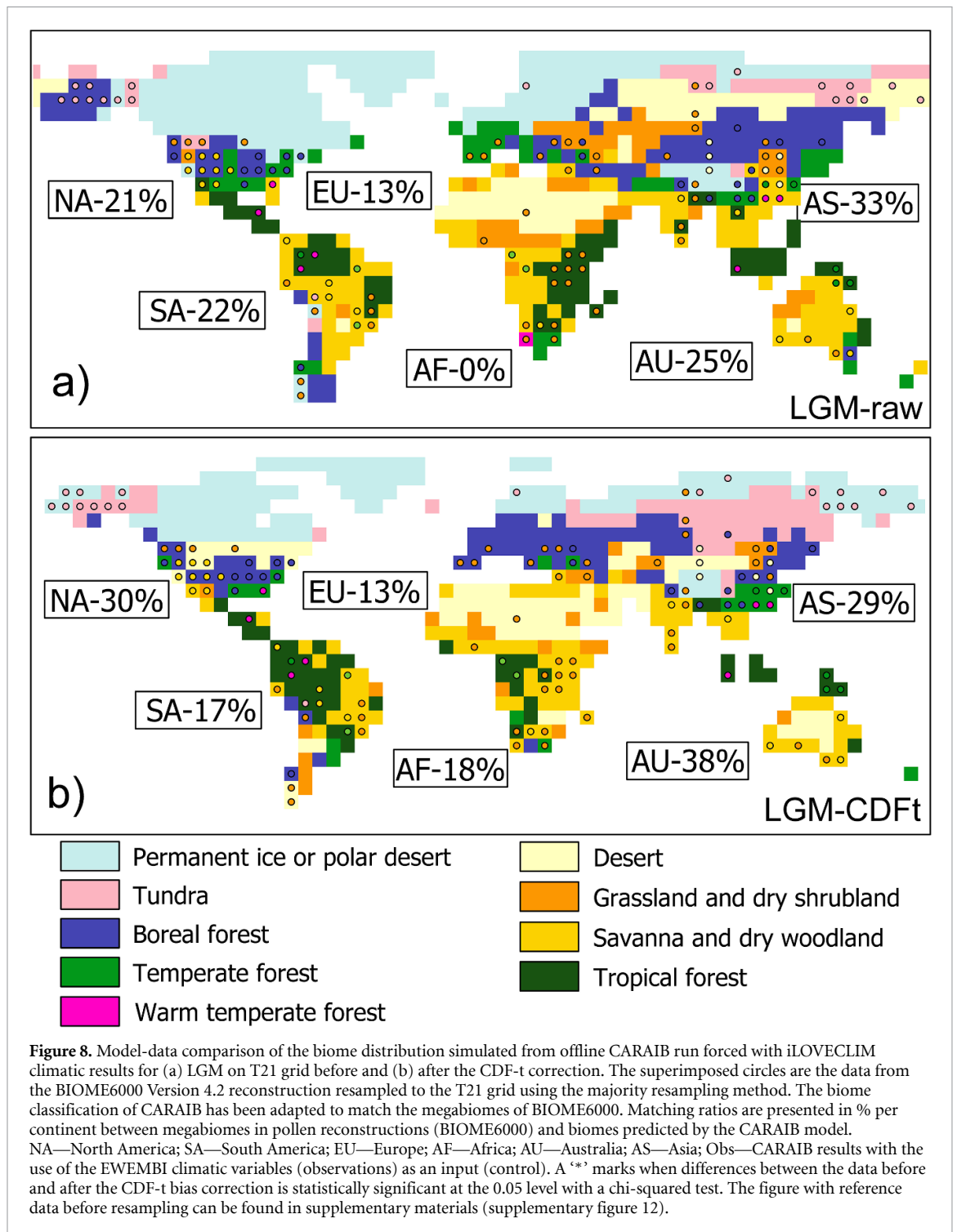
The extent and location of the Amazon rainforest after correction seem visually better represented (supplementary tables 3–7). However, this is not supported by the matching ratios. We observe a significant decrease in accuracy after bias correction for the MH (52 *versus* 26%). This is probably a consequence of the low number of pollen samples in the rainforest. The vast majority of data points from the region are found on the borders of the rainforest with other biomes and are, due to the coarse spatial resolution of our



simulations, attributed to temperate, warm temperate forest, savannah, and dry woodland. Comparison with Levvasseur *et al* (2012) indicated no significant improvement (table 3), since the PNV of Levvasseur *et al* (2012) is based on BIOME6000 data, and thus tropical forest is largely replaced by warm-temperate forests in both datasets.

3.3.5. Australia

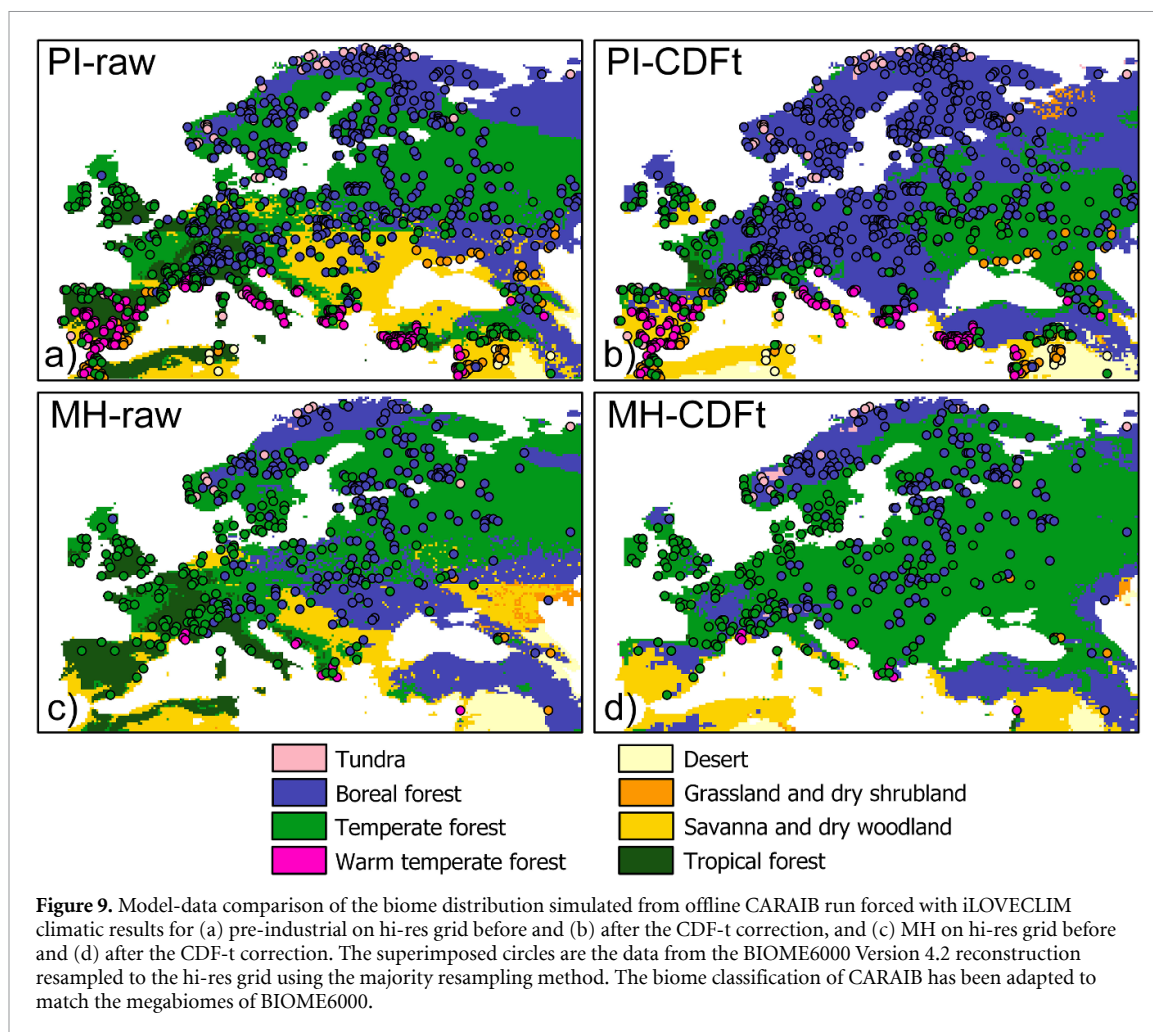
Due to the low number of BIOME6000 data points and model resolution, CDF-t has no significant impact on the matching ratios on the continent compared both to reconstructions and to PNV of Levvasseur *et al* (2012). Due to the lack of representation of biomes, not specific to pollen-based climate reconstructions, the desert is not reflected in the BIOME6000 dataset. Thus, here, as well as in North Africa and the Himalayas, the matching ratios are negatively biased by the absence of an important biome class in one of the compared



datasets. Taking this aspect into account, it is evident from figure 6 and supplementary figure 10 that the expansion of the Australian desert resulting from the bias correction in the model leads to a spatial distribution in better agreement with its PD size and location, and the biome distribution modelled by Levvasseur *et al* (2012) (supplementary figure 8).

3.3.6. Africa

The accuracy of modelled biome distribution increases with the CDF-t application for all three studied periods, but the improvement is not statistically significant (figures 6–8). The location of the Congo rainforest before correction is conditioned by the precipitation patterns of the region. In iLOVECLIM, the African precipitation bias is one of the large-scale biases, described by Goosse *et al* (2010). The CDF-t method reduces the bias over this region (supplementary figure 3, section 3.2), which results in a shift of the African rainforest to a location that is more consistent with its PD position and maps of Levvasseur *et al*



(2012). Similarly to the Amazon rainforest, a large number of data points are located in the bordering regions with other biomes, which contributes to a decrease in matching ratios due to the model resolution. As previously described, the desert range is marked by the absence of pollen data and thus does not contribute to the matching ratios displayed in the figure 6. Similarly to the observation made for the Australian desert, an observation of the PD extent of the desertic areas in the Sahara and in our bias-corrected result shows that the desert is better represented overall. This is confirmed by comparing our biome distribution with the gridded PNV maps of Levavasseur *et al* (2012), which resulted in significantly better matching ratios after bias correction (25 versus 58%).

4. Discussion

By simulating the climate and the biome distributions for different past conditions and comparing outcomes before and after bias correction, our goal is to evaluate whether the CDF-t approach can significantly improve modelled fields with respect to reconstructions and field data. We additionally test the robustness of the method on different time periods and resolution grids. As within any modelling approach, the models used in our study (iLOVECLIM and CARAIB) entail biases that we do not try to evaluate since this has been done elsewhere (Warnant *et al* 1994, Otto *et al* 2002, Laurent *et al* 2008, Goosse *et al* 2010, Dury *et al* 2011). For the method to work, we also assume a form of stationarity of the biases that are being corrected relative to the PD. For the time periods analysed, the significant improvement in representing the PNV distribution across regions and climate regimes (see table 3) seems to indicate it is a valid assumption. There are however a number of limitations that are worth discussing in the following.

4.1. Uncertainty of CDF-t approach application and evaluation

While analysing our results, it is essential to understand the potential drawbacks and shortcomings of the methodology. Among the important limitations to consider when using this approach are those related to (1)

vegetation modelling procedure, (2) uncertainties of paleovegetation reconstructions, (3) uncertainties of biomization procedure, and (4) uncertainties of paleotemperature reconstructions.

4.1.1. Limitations related to multivariate correlations in vegetation modelling

As an input, CARAIB model requires six variables: near-surface air temperature, precipitation, relative humidity, wind speed, sunshine hours, and daily temperature amplitude. However, due to data availability of the observational dataset, we were only able to apply the CDF-t method to three of them (surface temperature, precipitation, relative humidity). CDF-t bias correction has been applied independently for each of the three variables. However, the application of univariate calibrations by CDF-t should not disrupt existing spatial coherency and dependence among variables. Indeed, as it is a QQ-based technique, CDF-t respects the dependence (i.e. coherency) between the variables of the simulations to be corrected. This means that a high (or low) simulated value is transformed to a high (respectively, low) corrected value and, more generally, that a simulation value corresponding to the p% percentile is transformed to the p% percentile of the correction values. As a consequence, the separate applications of CDF-t to various variables and gridcells do not modify the Spearman (i.e. rank) correlations from the simulations (Vrac 2018, François *et al* 2020). Therefore, the statistical spatial coherence and inter-variable dependencies are mostly preserved and come from the model simulations.

4.1.2. Limitations related to paleovegetation reconstructions

While being a quantitative approach to denote a similarity between datasets, there are several limitations to consider while interpreting paleovegetation reconstructions. Firstly, the BIOME6000 is an amalgamation of multiple data sets, each containing significant reconstruction uncertainties (Hengl *et al* 2018) related to pollen sampling and analysis methods (Prentice and Webb 1998, Harrison 2017). There are relatively little data for tropical South America, Africa, and Asia (Hengl *et al* 2018), where lower confidence in the results is expected. This is also true for other regions for the LGM because of the very few data points. BIOME6000 is a point-based dataset, which represents biomes of specific locations, often influenced by the local micro-climate and geo-environmental parameters. In this study, we resampled the BIOME6000 dataset to match the native grid of iLOVECLIM, which led to the loss of spatial detail in the reconstructions. Additionally, it created a bias in the regions, poorly represented in the BIOME6000 database, since scarcely located data points were considered representative of entire grid cells. This bias is particularly strong on a coarser resolution T21 grid, at bordering regions between the biomes, and in cases where the BIOME6000 data points were located near an edge of a grid cell. An example of such bias can be seen on the Western border of the Sahara desert at PI (figure 6, supplementary figure 10), where several reconstruction data points associate the region with grassland and dry woodland. While being in close vicinity with the corresponding biome class in CARAIB, a few of them fall at the edge of a desert grid cell, and therefore, do not contribute to the increase in matching ratios. This brings to our attention another limitation: a lack of representation of biomes, not specific to pollen-based climate reconstructions, i.e. desert and permanent ice or polar desert. Thus, the grid cells of the mentioned biomes in CARAIB are often attributed to BIOME6000 grassland and dry woodland, and tundra data points respectively (supplementary tables 2–11). To overcome this limitation, we used the gridded PNV distribution of Levvasseur *et al* (2012) which is constrained by biome reconstructions but is also providing biomes in regions where no pollen data is available such as desert. The analysis of the results alongside the PNV is, therefore, a promising approach, which provides an added benefit to interpretation of the modelled vegetation distribution.

4.1.3. Limitations related to biomization

As expected, a large caveat of the methodology arises due to differences in biomization procedures, as no universally acknowledged guidelines regulate the biomization of PFTs (Dallmeyer *et al* 2019). To further investigate the relationship between BIOME6000 and modelled biomes we analysed contingency tables of data distribution across different biomes (supplementary tables 2–11). The analysis revealed that the majority of data points of BIOME6000 were attributed to biomes with similar ternary coordinates (Pierce *et al* 2017) by the CARAIB model, and are, therefore, attributed to similar environmental and climatic conditions. For example, the megabiome of the warm temperate forest is not well reproduced by CARAIB under the applied biomization procedure. It is often misclassified as savanna and dry woodland, or tropical forest, with which it shares similar key species on a genus or family level (Ni *et al* 2010). The functional diversity of savannas (fire tolerance, functional ecology shade intolerance) is also not usually well-represented in DGVMs (Ratnam *et al* 2011, Dallmeyer *et al* 2019). This biome is unstable and vulnerable to grazing, fire regime, and climate, which transform savannas into forests or grasslands (Franco *et al* 2014). This feature is reflected in our findings since BIOME6000 savannas are largely represented by grasslands, dry shrublands, and tropical forests in CARAIB (supplementary tables 2–11). The limitations of

confinement of warm temperate forest and savanna biomes via PFT mixtures are further discussed by Dallmeyer *et al* (2019). Moreover, the biomization procedure is based on PD bioclimatic limits, which may not be applicable to glacial vegetation (Dallmeyer *et al* 2019). The biomization technique has been applied for the LGM but the conversion from PFT to biomes based on bioclimatic limits for the PI is considered constant over time which may not be the case. This may contribute to lower matching ratios at LGM compared to PI and MH (tables 2 and 3). The abovementioned patterns persist after the CDF-t application, as well as for the control simulation, which indicates that differences in biomization methods of BIOME6000 compared to CARAIB significantly influenced the inter-comparison of the two datasets.

4.1.4. Limitations related to paleotemperature reconstructions

Most published studies present the reconstructed, as well as modelled climate data in a form of anomalies (differences) to modern values (Mauri *et al* 2015, Cleator *et al* 2020). The CDF-t approach, however, preserves the evolutions of the input climate values by design, since the CDF-t corrects stationary biases under different mean states and preserves simulated by climate models anomalies. Therefore, useful data for the evaluation of the CDF-t methodology are scarce. Among the few available options, we selected the Temperature 12k dataset (Kaufman *et al* 2020) as a reference dataset for paleotemperature reconstructions. While being a compilation of non-continuous point data and featuring exclusively temperatures, it presents the data in a form of absolute values, which allows direct comparison with the modelled values prior to and following the CDF-t correction. In addition, the Temperature 12k is composed of consistent, quality-controlled paleotemperature records derived from the lake and marine sediments, peat, glacier ice, and other natural archives (Kaufman *et al* 2020). High standards of quality control of the featured data and consistency throughout a large number of records allow the use of the dataset as a reference in the context of the current study. Being largely based on pollen samples, the Temperature 12k dataset shares a similar spatial bias as the BIOME6000 dataset regarding quantification of deserts and other not specific to pollen-based reconstructions biomes (Chevalier *et al* 2020). Other uncertainties of the dataset are related to calibration and proxy biases, chronology, and spatiotemporal coverage (Kaufman *et al* 2020). In addition, a vast majority of the Temperature 12k data points were derived from marine proxies and thus were not used in this study, which is focused on the land surface. The effect of the limitations of the reconstruction datasets is more likely to be significant when the number of data points is low. This can be seen in the example of the downscaled MH. In figure 3, we compare the results of our simulations to the observation-based simulation. Temperature 12k indicates higher temperatures in Scandinavia than iLOVECLIM. This was also noted in comparison between the temperature reconstructions and PMIP4-CMIP6 simulations, where annual mean temperatures of the reconstructions for the MH were warmer at most latitudes, with maximum warming in the Arctic (Brierley *et al* 2020). However, the EWEMBI data show that this region is colder than in iLOVECLIM at the PD, thus it further lowers the temperatures over the region when applying the CDF-t. A similar phenomenon is observed in the Northern Hemisphere for the LGM. This indicates the significance of the impact of sampling biases in the data compilations used as a reference for calibration and evaluation of our methodology and contributes to the worsening of *R* and RMSE values for downscaled MH and LGM (figures 2 and 3).

4.2. Benefit of bias correction

Despite the above-mentioned limitations, the forward approach indicated significant improvement in the representation of biomes across different timesteps (tables 2 and 3), as well as across different regions (figures 6–8) and model resolutions (tables 2 and 3, figures 6–9). A lower matching ratio after CDF-t is systematically associated with non-significant results. This means that the correction is in fact not significantly deteriorating the results although the matching ratio is sometimes decreasing. Furthermore, we observe statistically significant improvement in bias-corrected biome representation of well-studied regions with high confidence in pollen reconstructions—Europe and North America (Harrison 2017, Chevalier *et al* 2020, Li *et al* 2022) (figures 6–8). Better representation of these regions in pollen databases, compared to rather poorly-covered South America, Africa, and Asia (Hengl *et al* 2018), attributes to higher confidence in the results of the comparison for the aforementioned regions. The T21 coarse grid is rather disadvantageous for capturing regionally confined biomes (i.e. savannah and dry woodland), which are better represented at finer downscaled resolution. However, large biome belts (such as tropical forest) are well captured following the bias correction procedure on both studied resolution grids (figures 6–9).

The use of the CDF-t bias correction improves the agreement for the PI with predicted PNV distribution based on multinomial logistic models (Levvasseur *et al* 2012) and the BIOME1 model results (Dallmeyer *et al* 2019).

Taylor diagrams (figures 1 and 3) indicate that the climatic parameters after the CDF-t application are statistically closer to observations and reconstructions in most cases, compared to non-corrected model

outputs. Moreover, they better agree with the temperature and precipitation patterns from the palaeoclimate simulations included in the current phase of PMIP for MH (Brierley *et al* 2020) and LGM (Kageyama *et al* 2017).

The results of the inverse accuracy evaluation approach indicated no major increase in accuracy in the PI period on the T21 grid after the CDF-t application since the iLOVECLIM model was calibrated with observations at PI (table 2). However, the downscaled simulations for this time period indicate a significant improvement in the agreement with the reconstructed data following the bias correction procedure. Thus, by combining the CDF-t method with the interactive downscaling, we can observe the added value of CDF-t. While acting as bias correction methods, they both target principally different biases. The design of interactive downscaling highly relies on topography, and thus it reduces biases related to topographic forcing (Quiquet *et al* 2018). The CDF-t method, when used for bias correction purposes, is designed to correct large-scale systemic model biases from one time period to another in a consistent manner (Vrac *et al* 2012). Combining the two methods into a joined workflow synthesises the aforementioned increase in large-scale model biases with the reduction in topography-related biases, provided by the embedded downscaling (Quiquet *et al* 2018).

5. Conclusions

This study was aimed: (i) to establish a methodology for correcting climatic biases in the context of palaeoclimate modelling; (ii) to test the robustness of the developed technique on three time periods of the past with contrasting climatic conditions, using proxy-based climate and vegetation reconstructions; and (iii) to evaluate the advantages and shortcomings of the proposed approach. We presented a CDF-t methodology for correcting biases of palaeoclimate modelling and evaluated its ability to perform bias correction of the modelled palaeoclimate variables of the iLOVECLIM climate model. The robustness of the developed technique was tested on three time periods (PI, MH, and LGM) and two spatial resolutions (5.625° and 0.25°).

Despite both forward (comparison with paleovegetation reconstructions) and inverse (comparison with paleotemperature reconstructions) accuracy evaluation approaches having limitations, we achieved a significant improvement in the agreement between the modelled and reconstructed data by the application of CDF-t to the modelled values. We have demonstrated that placing the CDF-t technique as an additional post-processing step of modelled data is a clear advantage to correct palaeoclimate model data for systematic biases. Our conclusion is supported by a set of statistical parameters (matching ratios, R , RMSE) showing better agreement between the models and the reconstruction datasets for the PI and MH. We found higher correlation between the reconstructed (Kaufman *et al* 2020) and the modelled temperatures after bias correction on both 5.625° ($R = 0.88$, RMSE = 6.32, SD = 9.37 before correction; $R = 0.91$, RMSE = 4.71, SD = 10.05 after correction) and 0.25° grid ($R = 0.15$, RMSE = 4.13, SD = 3.46 before correction; $R = 0.46$, RMSE = 2.79, SD = 1.97 after correction). Comparison with BIOME6000 reconstructions resulted in significant increase in matching ratios after bias correction for the MH at T21 grid at the 0.05 level (0.38 before and 0.44 after CDF-t).

The application of the proposed methodology to the downscaled climate variables further improved the accuracy and the level of detail captured by the model (matching ratios 0.31 before and 0.40 after CDF-t for the MH, and 0.18 and 0.44 for the PI respectively) and outlined an added value of the combination of the embedded downscaling with the bias correction that could be further extended to other regions.

At the LGM we observed no significant improvement in comparison with pollen-based reconstructions, which may suggest limitations in the use of the PD bioclimatic limits to describe a glacial environment. However, the results are largely determined by a low number of data points in the reconstructions, so further research is needed.

Our study reports the first attempt of bias correcting palaeoclimate model outputs using the CDF-t approach. To further assess the usefulness of the CDF-t application in palaeoclimate modelling the proposed methodology remains to be tested on more time periods, using climate models of different complexity and conducting perfect model experiments.

Data availability statement

All data that support the findings of this study are included within the article (and any supplementary information files).

Acknowledgments

The authors would like to thank Louis M François for providing the CARAIB global dynamic vegetation model and his help in running it, Bastien François for his valuable assistance in experiment preparation, as well as two anonymous reviewers and a subject editor for comments that improved the manuscript.

Funding

The research is financed through the European Union's Horizon 2020 research and innovation programme within the TERRANOVA project, Grant Agreement No. 813904, and supported by the Vrije Universiteit Amsterdam. The paper reflects the views only of the authors, and the European Union cannot be held responsible for any use which may be made of the information contained therein.

ORCID iDs

Anhelina Zapolska  <https://orcid.org/0000-0002-8045-8016>

Mathieu Vrac  <https://orcid.org/0000-0002-6176-0439>

Aurélien Quiquet  <https://orcid.org/0000-0001-6207-3043>

Thomas Extier  <https://orcid.org/0000-0002-9531-8753>

Frank Arthur  <https://orcid.org/0000-0002-9217-2058>

Hans Renssen  <https://orcid.org/0000-0002-5104-0526>

Didier M Roche  <https://orcid.org/0000-0001-6272-9428>

References

- Arthur F, Roche D M, Fyfe R, Quiquet A and Renssen H 2023 Simulations of the Holocene climate in Europe using an interactive downscaling within the iLOVECLIM model (version 1.1) *Clim. Past* **19** 87–106
- Bartlein P J et al 2011 Pollen-based continental climate reconstructions at 6 and 21 ka: a global synthesis *Clim. Dyn.* **37** 775–802
- Berger A L 1978 Long-term variations of daily insolation and Quaternary climatic changes *J. Atmos. Sci.* **35** 2361–7
- Beyer R, Krapp M and Manica A 2020 An empirical evaluation of bias correction methods for palaeoclimate simulations *Clim. Past* **16** 1493–508
- Bjune A E, Bakke J, Nesje A and Birks H J B 2005 Holocene mean July temperature and winter precipitation in western Norway inferred from palynological and glaciological lake-sediment proxies *The Holocene* **15** 177–89
- Brierley C M et al 2020 Large-scale features and evaluation of the PMIP4-CMIP6 mid Holocene simulations *Clim. Past* **16** 1847–72
- Brovkin V, Ganopolski A and Svirezhev Y 1997 A continuous climate-vegetation classification for use in climate-biosphere studies *Ecol. Modell.* **101** 251–61
- Chevalier M et al 2020 Pollen-based climate reconstruction techniques for late Quaternary studies *Earth-Sci. Rev.* **210** 103384
- Claussen M et al 2002 Earth system models of intermediate complexity: closing the gap in the spectrum of climate system models *Clim. Dyn.* **18** 579–86
- Cleator S F, Harrison S P, Nichols N K, Colin Prentice I and Roulstone I 2020 A new multivariable benchmark for Last Glacial Maximum climate simulations *Clim. Past* **16** 699–712
- Dallmeyer A, Claussen M and Brovkin V 2019 Harmonising plant functional type distributions for evaluating Earth system models *Clim. Past* **15** 335–66
- Déqué M 2007 Frequency of precipitation and temperature extremes over France in an anthropogenic scenario: model results and statistical correction according to observed values *Glob. Planet. Change* **57** 16–26
- Díaz-Pacheco J, van Delden H and Hewitt R 2018 The importance of scale in land use models: experiments in data conversion, data resampling, resolution and neighborhood extent *Geomatic Approaches for Modeling Land Change Scenarios* (Cham: Springer) pp 163–86
- Dury M, Hambuckers A, Warnant P, Henrot A, Favre E, Ouberdous M and François L 2011 Responses of European forest ecosystems to 21st century climate: assessing changes in interannual variability and fire intensity *IForest* **4** 82–99
- Extier T 2019 Variations climatiques et variations du cycle hydrologique aux basses latitudes au cours du Quaternaire : une approche combinant modèle et données *PhD Thesis* Université Paris-Saclay (available at: www.theses.fr/2019SACL056)
- Finné M, Woodbridge J, Labuhn I and Roberts C N 2019 Holocene hydro-climatic variability in the Mediterranean: a synthetic multi-proxy reconstruction *The Holocene* **29** 847–63
- Franco A C, Rossatto D R, de Carvalho Ramos Silva L and da Silva Ferreira C 2014 Cerrado vegetation and global change: the role of functional types, resource availability and disturbance in regulating plant community responses to rising CO₂ levels and climate warming *Theor. Exp. Plant Physiol.* **26** 19–38
- François B, Vrac M, Cannon A J, Robin Y and Allard D 2020 Multivariate bias corrections of climate simulations: which benefits for which losses? *Earth Syst. Dyn.* **11** 537–62
- François L M, Delire C, Warnant P and Munhoven G 1998 Modelling the glacial-interglacial changes in the continental biosphere *Glob. Planet. Change* **16–17** 37–52
- Furlanetto G, Ravazzi C, Pini R, Vallè F, Brunetti M, Comolli R, Novellino M D, Garozzo L and Maggi V 2018 Holocene vegetation history and quantitative climate reconstructions in a high-elevation oceanic district of the Italian Alps. Evidence for a middle to late Holocene precipitation increase *Quat. Sci. Rev.* **200** 212–36
- Goosse H et al 2010 Description of the Earth system model of intermediate complexity LOVECLIM version 1.2 *Geosci. Model Dev.* **3** 603–33

- Goosse H and Fichefet T 1999 Importance of ice-ocean interactions for the global ocean circulation: a model study *J. Geophys. Res. Ocean* **104** 23337–55
- Guiot J, Harrison S P and Colin Prentice I 1993 Reconstruction of Holocene precipitation patterns in Europe using pollen and lake-level data *Quat. Res.* **40** 139–49
- Guiot J and Kaniewski D 2015 The Mediterranean Basin and Southern Europe in a warmer world: what can we learn from the past? *Front. Earth Sci.* **3** 28
- Guiot J, Torre F, Jolly D, Peyron O, Boreux J J and Cheddadi R 2000 Inverse vegetation modeling by Monte Carlo sampling to reconstruct palaeoclimates under changed precipitation seasonality and CO₂ conditions: application to glacial climate in Mediterranean region *Ecol. Modell.* **127** 119–40
- Guo L, Jiang Z, Chen D, Le Treut H and Li L 2020 Projected precipitation changes over China for global warming levels at 1.5 °C and 2 °C in an ensemble of regional climate simulations: impact of bias correction methods *Clim. Change* **162** 623–43
- Haddad Z S and Rosenfeld D 1997 Optimality of empirical Z-R relations *Q. J. R. Meteorol. Soc.* **123** 1283–93
- Hansen J E and Sato M 2012 Paleoclimate implications for human-made climate change *Climate Change: Inferences from Paleoclimate and Regional Aspects* (Vienna: Springer) pp 21–47
- Harrison S P 2017 BIOME 6000 DB classified plotfile version 1 *Univ. Reading Dataset* (<https://doi.org/10.17864/1947.99>)
- Harrison S P, Bartlein P J and Prentice I C 2016 What have we learnt from palaeoclimate simulations? *J. Quat. Sci.* **31** 363–85
- Harrison S P and Bartlein P 2012 Records from the past, lessons for the future: what the palaeorecord implies about mechanisms of global change *Future World's Climate* (Amsterdam: Elsevier) pp 403–36 (available at: <https://researchers.mq.edu.au/en/publications/records-from-the-past-lessons-for-the-future-what-the-palaeorecor>)
- Harrison S P and Prentice C I 2003 Climate and CO₂ controls on global vegetation distribution at the last glacial maximum: Analysis based on palaeovegetation data, biome modelling and palaeoclimate simulations *Glob. Change Biol.* **9** 983–1004
- Harrison S P, Yu G E and Tarasov P E 1996 Late Quaternary lake-level record from northern Eurasia *Quat. Res.* **45** 138–59
- Haywood A M et al 2019 What can Palaeoclimate modelling do for you? *Earth Syst. Environ.* **3** 1–18
- Hengl T, Walsh M G, Sanderman J, Wheeler I, Harrison S P and Prentice I C 2018 Global mapping of potential natural vegetation: an assessment of machine learning algorithms for estimating land potential *Peer J.* **6** e5457
- Jones P W 1999 First- and second-order conservative remapping schemes for grids in spherical coordinates *Mon. Weather Rev.* **127** 2204–10
- Kageyama M et al 2017 The PMIP4 contribution to CMIP6—part 4: scientific objectives and experimental design of the PMIP4-CMIP6 Last Glacial Maximum experiments and PMIP4 sensitivity experiments *Geosci. Model Dev.* **10** 4035–55
- Kageyama M et al 2018 The PMIP4 contribution to CMIP6—part 1: overview and over-arching analysis plan *Geosci. Model Dev.* **11** 1033–57
- Kaufman D et al 2020 A global database of Holocene paleotemperature records *Sci. Data* **7** 1–34
- Keery J, Holden P, Edwards N, Monteiro F, Ridgwell A, Keery J, Holden P, Edwards N, Monteiro F and Ridgwell A 2016 Insights into the paleoclimate of the PETM from an ensemble of EMIC simulations *EGU General Assembly* vol 18 pp EPSC2016–13948 (available at: <https://ui.adsabs.harvard.edu/abs/2016EGUGA.1813948K/abstract>)
- Kohfeld K E and Harrison S P 2000 How well can we simulate past climates? Evaluating the models using global palaeoenvironmental datasets *Quat. Sci. Rev.* **19** 321–46
- Koutavas A and Joanides S 2012 El Niño-Southern oscillation extrema in the Holocene and Last Glacial Maximum *Paleoceanography* **27** 4208
- Kuhnt T, Schmiedl G, Ehrmann W, Hamann Y and Andersen N 2008 Stable isotopic composition of Holocene benthic foraminifers from the Eastern Mediterranean Sea: past changes in productivity and deep water oxygenation *Palaeogeogr. Palaeoclimatol. Palaeoecol.* **268** 106–15
- Lambeck K, Rouby H, Purcell A, Sun Y and Sambridge M 2014 Sea level and global ice volumes from the Last Glacial Maximum to the Holocene *Proc. Natl Acad. Sci. USA* **111** 15296–303
- Lange S 2018 Bias correction of surface downwelling longwave and shortwave radiation for the EWEMBI dataset *Earth Syst. Dyn.* **9** 627–45
- Laurent J M, François L, Bar-Hen A, Bel L and Cheddadi R 2008 European bioclimatic affinity groups: data-model comparisons *Glob. Planet. Change* **61** 28–40
- Lavaysse C, Vrac M, Drobinski P, Lengaigne M and Vischel T 2012 Statistical downscaling of the French Mediterranean climate: assessment for present and projection in an anthropogenic scenario *Nat. Hazards Earth Syst. Sci.* **12** 651–70
- Levasseur G, Vrac M, Roche D M and Paillard D 2012 Statistical modelling of a new global potential vegetation distribution *Environ. Res. Lett.* **7** 44019–30
- Lhardy F et al 2021 A first intercomparison of the simulated LGM carbon results within PMIP-Carbon: role of the Ocean boundary conditions *Paleoceanogr. Palaeoclimatol.* **36** e2021PA004302
- Li C, Postl A K, Böhmer T, Cao X, Dolman A M and Herzschuh U 2022 Harmonized chronologies of a global late Quaternary pollen dataset (LegacyAge 1.0) *Earth Syst. Sci. Data* **14** 1331–43
- Li H, Renssen H and Roche D M 2019 Global vegetation distribution driving factors in two dynamic global vegetation models of contrasting complexities *Glob. Planet. Change* **180** 51–65
- Li H, Renssen H and Roche D M 2020 Modeling climate-vegetation interactions during the last interglacial: The impact of biogeophysical feedbacks in North Africa *Quat. Sci. Rev.* **249** 106609
- Luu L N, Vautard R, Yiou P, van Oldenborgh G J and Lenderink G 2018 Attribution of extreme rainfall events in the South of France using EURO-CORDEX simulations *Geophys. Res. Lett.* **45** 6242–50
- M R D 2013 Delta O-18 water isotope in the iLOVECLIM model (version 1.0)—part 1: implementation and verification *Geosci. Model Dev.* **6** 1481–91
- Mauri A, Davis B A S, Collins P M and Kaplan J O 2015 The climate of Europe during the Holocene: a gridded pollen-based reconstruction and its multi-proxy evaluation *Quat. Sci. Rev.* **112** 109–27
- Meinshausen M et al 2017 Historical greenhouse gas concentrations for climate modelling (CMIP6) *Geosci. Model Dev.* **10** 2057–116
- Mesta B and Kentel E 2022 Superensembles of raw and bias-adjusted regional climate models for Mediterranean region, Turkey *Int. J. Climatol.* **42** 2566–85
- Michelangeli P A, Vrac M and Loukos H 2009 Probabilistic downscaling approaches: application to wind cumulative distribution functions *Geophys. Res. Lett.* **36** L11708
- Ni J, Yu G, Harrison S P and Prentice I C 2010 Palaeovegetation in China during the late Quaternary: biome reconstructions based on a global scheme of plant functional types *Palaeogeogr. Palaeoclimatol. Palaeoecol.* **289** 44–61

- Noël T, Loukos H, Defrance D, Vrac M and Levvasseur G 2021 A high-resolution downscaled CMIP5 projections dataset of essential surface climate variables over the globe coherent with the ERA5 reanalysis for climate change impact assessments *Data Brief* **35** 106900
- Opsteegh J D, Haarsma R J, Selten F M and Kattenberg A 1998 ECBILT: a dynamic alternative to mixed boundary conditions in ocean models *Tellus A* **50** 348–67
- Otto D, Rasse D, Kaplan J, Warnant P and François L 2002 Biospheric carbon stocks reconstructed at the Last Glacial Maximum: comparison between general circulation models using prescribed and computed sea surface temperatures *Glob. Planet. Change* **33** 117–38
- Peyron O et al 2017 Precipitation changes in the Mediterranean basin during the Holocene from terrestrial and marine pollen records: a model-data comparison *Clim. Past* **13** 249–65
- Peyron O, Guiot J, Cheddadi R, Tarasov P, Reille M, De Beaulieu J L, Bottema S and Andrieu V 1998 Climatic reconstruction in Europe for 18,000 YR B.P. from pollen data *Quat. Res.* **49** 183–96
- Pierce S et al 2017 A global method for calculating plant CSR ecological strategies applied across biomes world-wide *Funct. Ecol.* **31** 444–57
- Prentice C I, Guiot J, Huntley B, Jolly D and Cheddadi R 1996 Reconstructing biomes from palaeoecological data: a general method and its application to European pollen data at 0 and 6 ka *Clim. Dyn.* **12** 185–94
- Prentice C I and Webb T 1998 BIOME 6000: reconstructing global mid-Holocene vegetation patterns from palaeoecological records *J. Biogeogr.* **25** 997–1005
- Prentice I C et al 2000 Mid-Holocene and glacial-maximum vegetation geography of the northern continents and Africa *J. Biogeogr.* **27** 507–19
- Prentice I C, Harrison S P, Jolly D and Guiot J 1998 The climate and biomes of Europe at 6000 yr BP: comparison of model simulations and pollen-based reconstructions *Quat. Sci. Rev.* **17** 659–68
- Quiquet A, Dumas C, Paillard D, Ramstein G, Ritz C and Roche D M 2021 Deglacial ice sheet instabilities induced by proglacial lakes *Geophys. Res. Lett.* **48** e2020GL092141
- Quiquet A, Roche D, Dumas C, Paillard D and Roche D M 2018 Online dynamical downscaling of temperature and precipitation within the iLOVECLIM model (version 1.1) *Geosci. Model Dev.* **11** 453–66
- Ramstein G, Kageyama M, Guiot J, Wu H, Hély C, Krinner G and Brewer S 2007 How cold was Europe at the Last Glacial Maximum? A synthesis of the progress achieved since the first PMIP model-data comparison *Clim. Past* **3** 331–9
- Ratnam J, Bond W J, Fensham R J, Hoffmann W A, Archibald S, Lehmann C E R, Anderson M T, Higgins S I and Sankaran M 2011 When is a “forest” a savanna, and why does it matter? *Glob. Ecol. Biogeogr.* **20** 653–60
- Roche D M, Dumas C, Bügelmayer M, Charbit S and Ritz C 2014 Adding a dynamical cryosphere to iLOVECLIM (version 1.0): coupling with the GRISLI ice-sheet model *Geosci. Model Dev.* **7** 1377–94
- Seppä H and Birks H J B 2001 July mean temperature and annual precipitation trends during the Holocene in the Fennoscandian tree-line area: pollen-based climate reconstructions *The Holocene* **11** 527–39
- Vigaud N, Vrac M and Caballero Y 2013 Probabilistic downscaling of GCM scenarios over southern India *Int. J. Climatol.* **33** 1248–63
- Vrac M 2018 Multivariate bias adjustment of high-dimensional climate simulations: the rank resampling for distributions and dependences (R2D2) bias correction *Hydrol. Earth Syst. Sci.* **22** 3175–96
- Vrac M, Drobinski P, Merlo A, Herrmann M, Lavaysse C, Li L and Somot S 2012 Dynamical and statistical downscaling of the French Mediterranean climate: uncertainty assessment *Nat. Hazards Earth Syst. Sci.* **12** 2769–84
- Warnant P, François L, Strivay D and Gérard J-C 1994 CARAIB: a global model of terrestrial biological productivity *Glob. Biogeochem. Cycles* **8** 255–70
- Wohlfahrt J, Harrison S P and Braconnot P 2004 Synergistic feedbacks between ocean and vegetation on mid- and high-latitude climates during the mid-Holocene *Clim. Dyn.* **22** 223–38
- Wu H, Guiot J, Brewer S and Guo Z 2007 Climatic changes in Eurasia and Africa at the last glacial maximum and mid-Holocene: reconstruction from pollen data using inverse vegetation modelling *Clim. Dyn.* **29** 211–29
- Zhang Y, Renssen H and Seppä H 2016 Effects of melting ice sheets and orbital forcing on the early Holocene warming in the extratropical Northern Hemisphere *Clim. Past* **12** 1119–35
- Zhang Y, Renssen H, Seppä H and Valdes P J 2018 Holocene temperature trends in the extratropical Northern Hemisphere based on inter-model comparisons *J. Quat. Sci.* **33** 464–76

**Modelling and characterization
of climate, environment,
and human impact during
the Holocene and Eemian
using an Interactive Physical
Downscaling**

Frank Arthur

**Doctoral dissertations at the
University of South-Eastern
Norway no. 199**

ISBN 978-82-7206-868-3 (print)
ISBN 978-82-7206-869-0 (online)

usn.no